EXPERIMENTAL AND STATISTICAL REQUIREMENTS FOR DEVELOPING A WELL-DEFINED K_{IR} CURVE

EPRI NP-372
(Research Project 696-1)

Final Report

May 1977

Prepared by

Fracture Control Corporation
330 South Kellogg Avenue, Suite E.
Goleta, California 93017

Principal Investigators
W. L. Server
W. Oldfield*
R. A. Wullaert

*Material Research and Computer Simulation
Goleta, California 93017

Prepared for

Electric Power Research Institute
3412 Hillview Avenue
Palo Alto, California 94304

Project Manager
Karl Stahlkopf

LEGAL NOTICE

This report was prepared by Fracture Control Corporation (FCC), as an account of work sponsored by the Electric Power Research Institute (EPRI). Neither EPRI, members of EPRI, FCC, nor any person acting on behalf of either: (a) makes any warranty or representation, express or implied, with respect to the accuracy, completeness, or usefulness of the information contained in this report, or that the use of any information, apparatus, method, or process disclosed in this report may not infringe privately owned rights; or (b) assumes any liabilities with respect to the use of, or for damages resulting from the use of, any information, apparatus, method or process disclosed in this report.

ABSTRACT

The objective of the current program has been to further the development of a statistically well-defined reference fracture toughness curve to verify and compliment the K_{IR} curve presently specified in Appendix G, Section III of the ASME Code. This objective was accomplished by performing critical experiments in small specimen fracture mechanics and improving techniques for statistical analysis of the data.

Existing EPRI test and data analysis procedures and acceptance criteria were revised to include the current requirements for elastic-plastic fracture toughness measurements. Except for cleavage initiated fracture, crack initiation was observed to occur prior to maximum load for all of the materials investigated. Thus, initiation fracture toughness values (K_{Jc}) based on R-curve heat-tinting studies were up to 50 percent less than the previously reported equivalent energy values (K_d^*). At upper shelf temperatures, the initiation fracture toughness (K_{Jc}) generally increased with stress intensification rate. Both K_{Jc}-Charpy V-notch and K_{Ic}-specimen strength ratio correlations are promising methods for predicting thick-section behavior from small specimens.

The results of the small specimen fracture mechanics study were used to requalify the existing EPRI fracture toughness data base prior to an advanced statistical analysis to establish a lower bound fracture toughness curve. The previously developed tanh curve fitting procedure was improved to permit estimates of the variances and covariances of the regression coefficients to be computed. The distribution of the fracture toughness data was determined as a function of temperature. Instrumented precracked Charpy results were used to normalize (remove heat-to-heat differences) the larger specimen fracture toughness data. The transformed large specimen fracture toughness data are used to generate statistically-based lower bound reference fracture toughness curves for either static or dynamic test results. Using the precracked Charpy normalized reference fracture toughness lower bound curves, the lower bounds for a specific heat of material can be generated. A comparison of these lower bound curves with the K_{IR} curve shows that the K_{IR} curve is more conservative over most of its range.

CONTENTS

CONTENTS (Contd.)

LIST OF FIGURES

LIST OF FIGURES (Contd.)

LIST OF FIGURES (Contd.)

LIST OF FIGURES (Contd.)

LIST OF FIGURES (Contd.)

LIST OF FIGURES (Contd.)

LIST OF FIGURES (Contd.)

LIST OF TABLES

LIST OF TABLES (Contd.)

FOREWORD

In October 1972, the Atomic Energy Commission (now Nuclear Regulatory Commission), in a meeting with utilities and reactor vendors, stated its belief that additional research was needed to demonstrate that toughness requirements for ferritic materials in nuclear reactor pressure vessels, as published in the K_{IR} curve of the ASME Boiler and Pressure Vessel Code, were representative of actual production heats of materials used in vessel construction. A task group under the joint sponsorship of the Pressure Vessel Research Committee (PVRC) and the Metal Properties Council (MPC) was formed in response to this meeting to define required research. The joint PVRC/MPC Task Group formulated a program which addressed these needs and recommended the program to EPRI in the summer of 1973. EPRI modified and expanded the program and work began in March 1974 under RP232. The objective of this research project was to measure the fracture toughness of 50 heats and weldments of reactor pressure vessel steel and bolting material, including: A533B Class 1 plate, A508 Class 2 forging, A302B modified plate, and A540 bolting material. RP232 was completed in late 1975. At that time it became apparent that the K_{IR} curve, as formulated in the ASME Code, was in need of revision. This curve represented the lower bounding value of fracture toughness values of principally one heat of steel.

In January of 1976 the present project, RP696, was begun with the objectives of using the large data base developed under RP232 to develop a statistically well defined reference toughness curve (K_{IR}) as a potential replacement for the K_{IR} curve presently specified in Appendix G of Section III of the ASME Boiler and Pressure Vessel Code. The documentation of the development of this curve, along with an alternate temperature indexing procedure for reduction of data scatter is presented in this report.

Karl Stahlkopf
Program Manager

PROGRAM SUMMARY

This final report covers the work performed by Fracture Control Corporation during a one-year program with the Electric Power Research Institute (Contract No. RP 696-1). Progress during the first two quarters was reported in FCC 76-6 (March 15, 1976)[1] and FCC 76-9 (June 15, 1976)[2]. Since the program was completed shortly after the end of the third quarter the progress during the third quarter is covered in the final report.

Dr. R.A. Wullaert, President, Fracture Control Corporation, was responsible for overall management of the program, and W.L. Server, Vice President, was the principal investigator. Dr. W. Oldfield performed the statistical analysis and developed novel statistical aspects for the program, and Dr. T.R. Wilshaw provided a review of the current analyses of the instrumented impact test. The performance of the experimental testing program was the responsibility of J.W. Sheckherd.

The program consisted of four major tasks which are discussed in the following paragraphs.

SMALL SPECIMEN FRACTURE MECHANICS

The previous EPRI fracture toughness programs did not verify that elastic-plastic toughness values from small specimens, such as the precracked Charpy specimen, gave conservative predictions of thick section behavior. Several areas of fracture safe design and operation of nuclear pressure vessels are heavily dependent upon establishing a correlation between small and large fracture mechanics specimens. For example, surveillance programs must use small specimens to predict the degree of radiation embrittlement of thick-section pressure vessels. Additional experimental and analytical studies were performed in the current program to evaluate the potential of small specimens for obtaining meaningful fracture toughness data.

The EPRI acceptance criteria and test and data analysis procedures were reviewed and updated as necessary particularly with respect to

elastic-plastic measurements. The acceptability of using a static analysis for calculating dynamic fracture toughness was justified by evaluating recently proposed dynamic solutions with respect to the existing EPRI procedures. The influence of fracture mode on elastic-plastic toughness calculations was studied. Determining the mode of crack initiation (cleavage or fibrous) was found to be very useful in determining the validity of the elastic-plastic toughness data. The error associated with using maximum load for crack initiation was established by reviewing current research programs in this area and by determining J integral initiation values from R-curve heat-tinting measurements. The influence of stress intensity rate ($\dot{K}$) and specimen thickness on elastic-plastic fracture toughness (J) was determined for HSST Plate 02 (A533B-1 steel) over the temperature range of -20°F (-29°C) to 160°F (71°C).

UPPER SHELF FRACTURE TOUGHNESS TESTING

The upper shelf temperature region corresponds to the normal operating temperature for nuclear pressure vessels. In the past EPRI programs, upper shelf elastic-plastic fracture mechanics data were only obtained from the precracked Charpy test (except for some of the A540 results). The static and dynamic 1-in. (25 mm) compact fracture and dynamic 1-in. (25 mm) bend tests were limited to temperatures below NDTT + 180°F (NDTT + 100°C). These results were further complicated by the fact that fracture initiation was assumed to occur at maximum load. R-curve heat-tinting tests were performed in the upper shelf region to permit a proper comparison of equivalent energy (maximum load) and J-integral initiation fracture parameters. For each type of material tested in the previous EPRI program (except the A540), the heat with the lowest upper shelf fracture toughness based upon the precracked Charpy equivalent energy toughness results was selected. In addition, a heat of A302B steel supplied by NRL was also chosen as a low upper shelf material. J-integral initiation fracture toughness tests (1-in., 25 mm) were performed in the upper shelf temperature region (350°F, 177°C) at stress intensity rates corresponding

to those used to obtain the previous equivalent energy results (~3 and either 10^3 or 10^5 MN-m$^{-3/2}$/s). For all of the materials investigated, crack initiation occurred prior to maximum load. Initiation fracture toughness values (K_{Jc}) were up to 50% less than the previously reported equivalent energy values (K_d^*). Initiation fracture toughness increased with stress intensity rate for all but one material.

The use of upper shelf empirical correlations to predict thick section fracture toughness behaviour from small specimen data was examined. Relationships were developed between elastic-plastic toughness data (maximum load and initiation) and Charpy V-notch upper shelf energy. A relationship was also developed between fracture toughness and specimen strength ratio. Both the J_{Ic} - Charpy V-notch and K_{Ic} - strength ratio correlations are promising methods for predicting thick section behaviour from small specimens.

DEVELOPMENT OF PREDICTION LIMITS FROM THE TANH CURVE FIT

The procedures originally developed to fit the tanh curve (Figure 1) to test data had to be revised when the curve was used to develop prediction limits. The original procedure did not provide as precise a fit as was needed, nor did it compute estimates of the variances and covariances of the coefficients of the curve. Hence, the accuracy of a prediction based on the tanh curve fit could not be defined. The software procedures to develop the tanh coefficients have been completely revised. Upper limits for the variances and covariances of the coefficients are now computed, and the coefficients A, B, T_0, and C (Figure 1) are now found with greater precision.

Using the revised tanh curve fitting procedures, it was now possible to develop a revised K_{IR} curve using the data bank from past EPRI-funded programs.

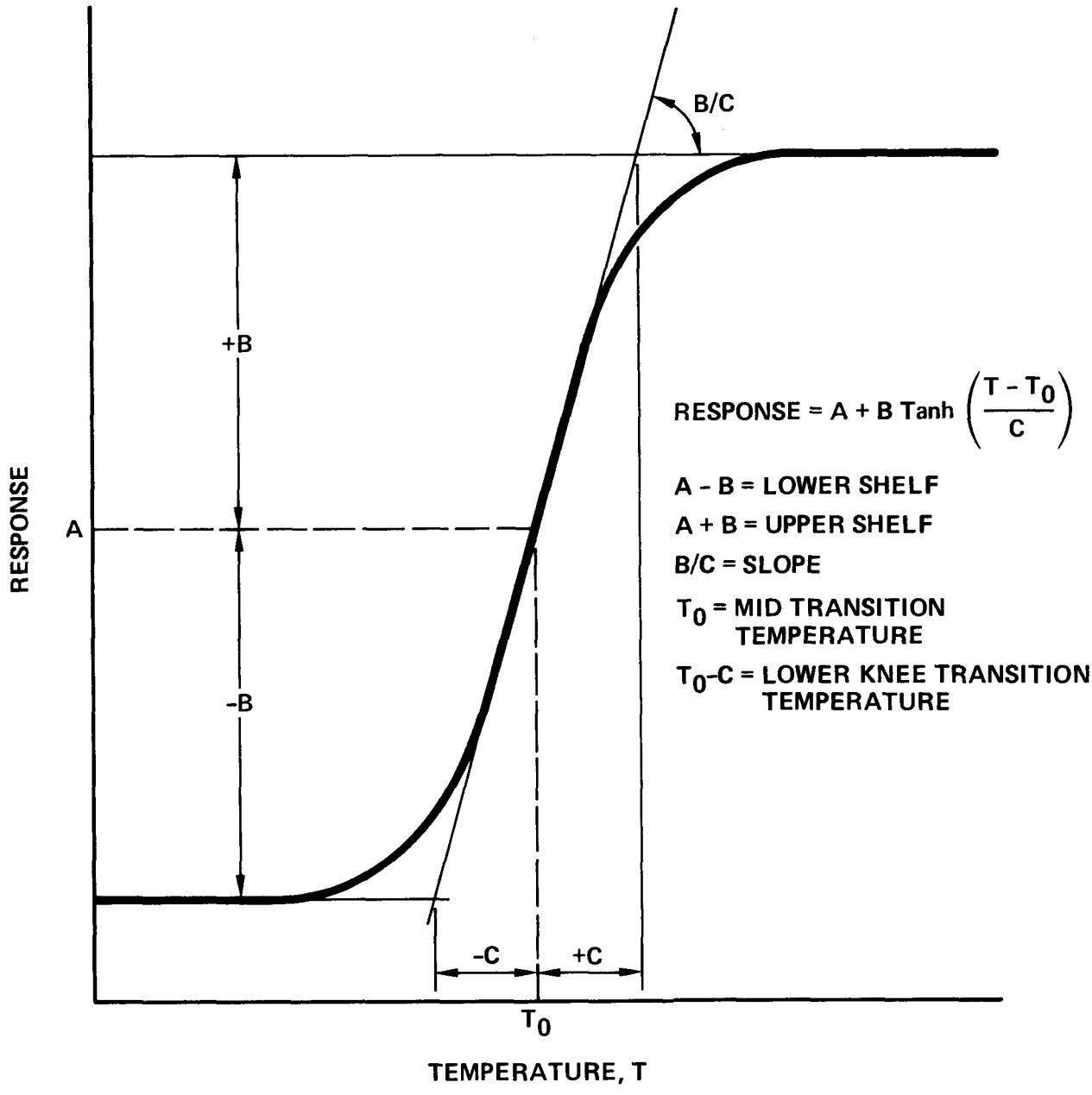

Figure 1. Interpretation of the Tanh Curve

DEVELOPMENT OF A REVISED K_{IR} CURVE

The development of a revised lower bound curve required the computation of the variance, and the characterization of the data distribution as a function of temperature.

For the instrumented precracked Charpy test, the fracture toughness data could be analyzed directly because of the large number of test results. Three classes of behavior were isolated; a lower shelf behavior, transition (between shelf) behavior, and upper shelf behavior. Since the data on the upper shelf could not be used for reasons already mentioned, a lower bound was developed only for the remainder of the curve. At the lower shelf, the data were found to be skewed high and to have a lower variance than the transition results. A lower bound can be set using the Pearson distributions; this bound, because of the form of the distribution, never passes below zero toughness. In the property transition range, the distribution is very close to the Normal distribution. There are many techniques which can be used to set the lower bound; the t - distribution was preferred.

There were too few large specimen (static and dynamic) test results to allow a direct analysis. Data from all heats of each material had to be combined to provide a useful data base. To perform this analysis, normalizing procedures were developed. These procedures use the instrumented precracked Charpy test to reveal heat-to-heat differences. The normalized fracture toughness (large specimen) is expressed in terms relative to the instrumented precracked Charpy test estimates of the lower and upper shelf, i.e., A and B. Similarly, the test temperature is expressed as a deviation from T_0, in units of the temperature range over which the property transition takes place, i.e.,

$$f = \frac{F - A}{B} \quad ; \quad t = \frac{T - T_0}{C} \quad ;$$

f and t are the transformed fracture toughness and temperature values, respectively, F is the measured fracture toughness, T is the

temperature, and A, B, T_0 and C are the coefficients of the instrumented precracked Charpy test data curve.

Using the normalized data, f and t, for each material, the heat-to-heat variability was substantially removed in most cases. The transformed data could then be fitted to a tanh curve, and the deviations from the curve treated in the same manner as the instrumented precracked Charpy test results. Much the same result was found: the lower shelf had a smaller variance than the transition test data, and the lower shelf data were skewed high, while the transition data were quite close to a Normal distribution about the curve. The Pearson distributions and the t - distribution were used to define lower bounds for each material, for both static and dynamic test results. The lower bound curves were then used to demonstrate the development of bounds for specific heats of material which had been characterized by the instrumented precracked Charpy test. These curves (in toughness - temperature coordinates) were then compared to the K_{IR} curve. As might be expected, the K_{IR} curve was more conservative over most of its range.

TECHNICAL BACKGROUND

The Electric Power Research Institute (EPRI) funded two research programs (RP 232 and RP 312) that had the common objectives of (1) measuring the fracture toughness properties of 50 production heats and weldments of light water reactor (LWR) pressure vessel steels and (2) evaluating the applicability of using small test samples to measure meaningful fracture toughness data[3-7]. A third program (RP 337) with similar objectives involved 5 production heats and weldments of high temperature gas-cooled reactor (HTGR) pressure boundary steels[8]. The focus of these research programs was to demonstrate that the toughness requirements for ferritic materials in nuclear power plant components, as specified by the reference toughness curves (K_{IR}) in Appendix G of the ASME Code, Section III, is representative of actual production heats of materials used in reactor pressure vessel construction.

The technical approach used in the EPRI fracture toughness programs was to perform standard and non-standard fracture toughness tests over a wide range of temperatures and loading rates. A sound basis for performing a proper statistical analysis of the test data was achieved by performing a round robin test program[9], employing uniform test and data analysis procedures[10], by determining the statistical distribution of the test data[11], and by developing a statistical curve fitting technique[12]. A statistically sound presentation of the data base generated in the recent EPRI programs should provide a rational basis for establishing a statistically significant lower bound (K_{IR}) curve[13].

All fracture toughness data obtained in EPRI programs RP 232 and RP 337 have been analyzed using the tanh fit statistical analysis developed in the round robin study[7,8]. The results indicated that the criteria for acceptable fracture toughness data (EPRI acceptance criteria) had no significant effect on the results and may actually be too conservative in some cases. Impact tests using strain gaged specimens have confirmed that the EPRI instrumented impact test procedures are adequate[14,15]. A modi-

fication of the tanh statistical analysis has been used to express the initiation toughness data used to generate the Code K_{IR} curve in a statistically meaningful manner with approximate scatter limits[9].

Although a great deal of progress has been made toward achieving the objectives of the EPRI fracture toughness programs, some problems and uncertainties must still be resolved to assure an unconditional acceptance of a revised K_{IR} curve (and perhaps concept) by the technical and Codemaking community. The objective of the current program was to further the development of a statistically well-defined K_{IR} curve. This task was achieved by performing critical experiments to resolve uncertainties in small specimen fracture mechanics and by further developing the tanh curve fit statistical analysis.

PROGRAM RESULTS

SMALL SPECIMEN FRACTURE MECHANICS

The main emphasis in this phase of the program was to resolve some of the uncertainties associated with obtaining fracture toughness values from small specimens. Since most of the small specimen fracture toughness data were obtained from instrumented precracked Charpy tests, initial efforts were directed towards a review of the EPRI test and data analysis procedures for this test. The EPRI acceptance criteria were also reviewed and updated to include criteria for acceptable elastic-plastic fracture toughness values. Critical J-integral initiation experiments on selected EPRI archive materials were performed to identify the potential error associated with assuming that crack initiation occurs at maximum load. The prediction of thick section fracture toughness behavior from both direct measurements on small fracture mechanics specimens (elastic-plastic analysis) and empirical correlations with other small specimen parameters (energy, strength ratio) was examined.

Review of EPRI Procedures and Criteria

Even though the EPRI procedures for dynamic fracture toughness testing have been experimentally verified[14,15], they have not been fully accepted by the technical community because (1) the procedures are somewhat complicated, (2) they have a semi-empirical basis, and (3) a static analysis is used to calculate dynamic toughness. Justification of the use of a static analysis and efforts to simplify the procedures are presented in this section. The original EPRI acceptance criteria were primarily based on the requirements of linear elastic fracture mechanics. These criteria are updated in this section to include requirements for acceptable elastic-plastic fracture toughness data.

Test and Analysis Data Procedures

The EPRI criteria for acceptable impact load-time data were centered

around the apparent period of the specimen oscillations (τ) and the response time (T_R) of the electronics used to measure the striker signal[10]. Since the load signal measured from an instrumented tup oscillates about the actual load required to deform the sample, the signal analysis procedure should minimize the deviation of these two loads. A simplistic view of the impact event allows identification of three major areas for test specification: inertial loading, limited frequency response (response time), and electronic curve fitting.

The impact of a sample results in inertial oscillations in the contact load between the striker and the sample. A time approximately equal to 2τ is required for the load to be dissipated to a reasonable level. To avoid inertial loading problems, specification of loading times greater than 2τ is necessary which requires control of the impacting velocity. The potential problem of limited frequency response of the transducer amplifier system is avoided by specifying the minimum response time for the electronics in relation to the first time measurement required (t), i.e., either time to fracture or time to general yield. The curve-fitting problem can be achieved by either controlling the velocity such that $t \geq 3\tau$, or by letting $t \geq 2.3\tau$ with the added restriction that the signal must be electronically filtered at a controlled level. Since the requirements for obtaining reliable load-time measurements result in the need to control the impact velocity, a corresponding control of the total available energy (E_o) is inherent. The reduction in velocity should be minimized to less than 20 percent through initiation (maximum load).

A detailed discussion of the current impact testing requirements is presented in Appendix B. The purpose of this procedures review was to resolve some of the semi-empirical parameters used in the specification and to simplify the requirements as much as possible. The following equations represent the most concise form to state the requirements for obtaining reliable load-time data:

$$t \geq 3\tau \qquad \text{(Inertial Loading)}, \qquad (1)$$

and

$$t \geq 1.1\ T_R \qquad \text{(Limited Response)}. \qquad (2)$$

When the requirements related to Equation 1 cannot be met, the minimum requirements would include electronic curve-fitting:

$$t \geq 2.3\tau \qquad \text{(Inertial Loading)}, \qquad (3)$$

$$t \geq 1.1\ T_R \qquad \text{(Limited Response)}, \qquad (2)$$

and

$$T_R \geq 1.4\,\tau \qquad \text{(Electronic Curve-Fitting)}. \qquad (4)$$

Furthermore, the conservative constant velocity requirement (less than 20 percent change) for both cases above is simply

$$E_o \geq 3\ W_M \qquad \text{(Energy)} \qquad , \qquad (5)$$

where W_M is the total energy to maximum load.

In addition to the review of the testing procedures, a review of the analysis technique for a machine compliance energy correction[10] was also performed in Appendix B. The outcome of the review was that the current procedure for correcting the initiation energy is adequate and that the assumptions made result in offsetting corrections (resulting in a negligible change to slightly higher values). Thus, the current analysis technique is slightly conservative and need not be changed.

Recent analyses of the mechanics of impact fracture testing have been reviewed in Appendix A by T.R. Wilshaw. These recent analyses for small precracked bars in bending support the empirically based EPRI impact procedures. The EPRI procedures ensure that the inertial effects are not excessive and that the load-time curve is a reasonable analog of the central bending moment (and stress intensity factor) -- see Equations 1 - 5.

Even under the most severe permissible conditions where the inertial effects are greatest, the errors in fracture toughness using Equations 1 - 5 are never greater than 10 percent. In fact, experimental data generated to substantiate the EPRI procedures indicate much less than a 10 percent increase[14] in linear elastic toughness results.

Elastic-Plastic Acceptance Criteria

The acceptance criteria used in the previous EPRI fracture toughness programs are listed under the linear elastic column in Table 1. A statistical analysis of the EPRI RP 232 program data revealed that these acceptance criteria had no significant effect on the fracture toughness results. It should be noted, however, that the original acceptance criteria were primarily concerned with obtaining accurate data at high loading rates and obtaining acceptable linear elastic fracture toughness values using ASTM method requirements. At present there are no ASTM test methods for measuring valid elastic-plastic fracture toughness, although ASMT subcommittees generated some preliminary procedures after the EPRI RP 232 program was initiated. Thus, only the elastic criteria were applied to the data analysis procedure. However, when the statistics related to the elastic data alone were analyzed, there was still no significant influence of the unacceptable data points on the scatter (variance) about the tanh curve fit[7,11]. This effect on the elastic data is probably due to the fact that most of the criteria relate to crack depth and shape, and these criteria are conservative.

The validity criteria developed by ASTM subcommittees are essentially the same for both the equivalent energy and J-integral techniques[16]:

$$a,\ b,\ B \geq 50\ J/\sigma_f = 50\ \frac{\sigma_f}{E}\left(\frac{K_J}{\sigma_f}\right)^2 \qquad (6)$$

or

Table 1. Revised EPRI Acceptance Criteria

Linear Elastic	Elastic-Plastic
a. E399 Thickness Criterion (when $P_M/P_Q \leq 1.10$); $B \geq 2.5 \left(\frac{K_Q}{\sigma_y}\right)^2$; also true for a and b.	a. Dimensional Criterion (when $P_M/P_Q > 1.10$ or $P_M > P_{GY}$); a, b, $B \geq \frac{50J}{\sigma_f}$; also, the mode of fracture initiation must be determined by examining the fracture surface immediately below the fatigue crack.
b. $0.45 \leq a/w \leq 0.55$ (E399)	b. $0.50 \leq a/w \leq 0.70$
c. Crack front must not be skewed or out of plane (E399)	c. Same
d. K_f (max) over last 2.5% of $a \leq 0.6\ K_Q$ (E399)	d. K_f (max) over last 2.5% of $a \leq 0.6\ K_{Jc}$
e. $t_M \geq 3\tau$, or $t_M \geq 2.3\tau$ when $T_R \geq 1.4\tau$ (t_M is the time to maximum load)	e. $t_{GY} \geq 3\tau$, or $t_{GY} \geq 2.3\tau$ when $T_R \geq 1.4\tau$ (t_{GY} is the time to (general yield)
f. $t_M \geq 1.1\ T_R$	f. $t_{GY} \geq 1.1\ T_R$
g. $E_o \geq 3\ W_M$	g. Same

$$a,\ b,\ B \geq 50\ \frac{\sigma_y}{E}\left(\frac{K^*}{\sigma_y}\right)^2 \quad , \tag{7}$$

where J is the J-integral value, σ_y is the yield stress, σ_f is the flow stress (half of the sum of ultimate and yield stress), E is Young's Modulus, K_J is the J-integral fracture toughness, K^* is the equivalent energy fracture toughness, and a, b, and B are sample dimensions (crack length, ligament depth, and thickness, respectively). There is some question as to the value of 50 in Equations 6 and 7; some investigators suggest the use of 25 rather than 50. As seen from Equations 6 and 7 the real difference between the two criteria (since K_J and K^* are approximately equal)[†] is the use of the flow stress versus the yield stress. The elastic-plastic ASTM criteria also specify the crack depth be greater than an a/w of 0.5, and the crack depth can exceed an a/w > 0.55. The recommended additions to the EPRI acceptance criteria for elastic-plastic toughness measurements are listed in Table 1.

These elastic-plastic criteria were evaluated for the round robin material as a function of temperature and are shown in Figures 2-5 for the different sample geometries (a/w = 0.5) and strain rates. The tensile test results from the round robin program were used to obtain a temperature (T, degrees Fahrenheit) dependence of the static yield stress (σ_{ys}) and flow stress (σ_{fs}) needed to calculate the static criteria:

$$\sigma_{ys} = 73.62 - 6.03 \times 10^{-2}T + 1.32 \times 10^{-4}T^2 - 1.16 \times 10^{-7}T^3 \tag{8}$$

$$\sigma_{fs} = 85.90 - 6.71 \times 10^{-2}T + 5.09 \times 10^{-4}T^2 - 4.26 \times 10^{-8}T^3 \quad . \tag{9}$$

The σ_{ys} and σ_{fs} values are in units of ksi; to convert to metric units, 1 ksi = 6.8948 MPa. The dynamic yield and flow stress data required to establish limits for the precracked Charpy and dynamic bend results were obtained from an analysis of standard Charpy V-notch instrumented test records[10]. The relationship used for ultimate strength (using the same

[†]When the same measurement point is used for crack initiation.

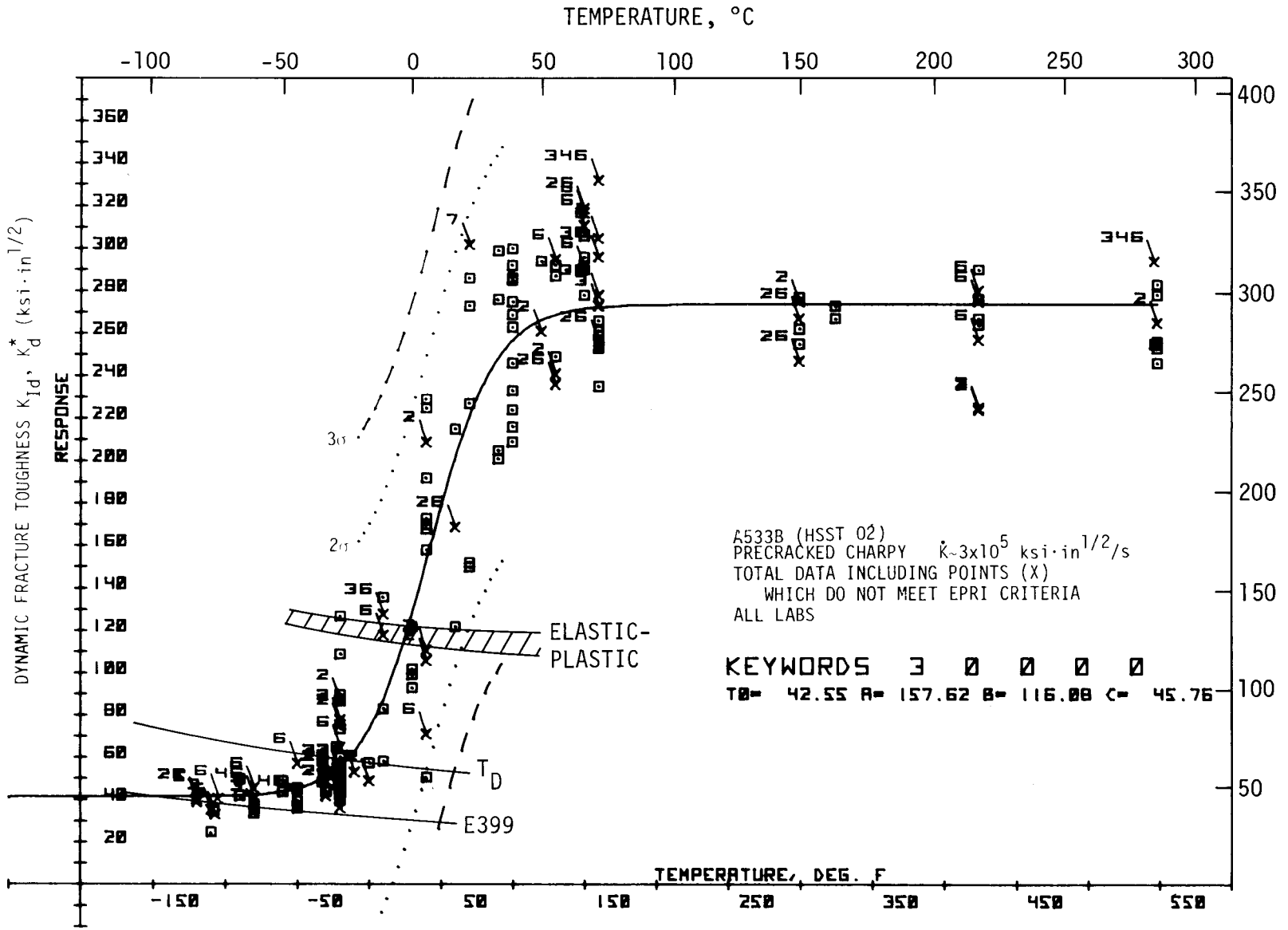

Figure 2. Summary of Total Precracked Charpy Dynamic Fracture Toughness Results Obtained by the Interlaboratory Test Program Participants

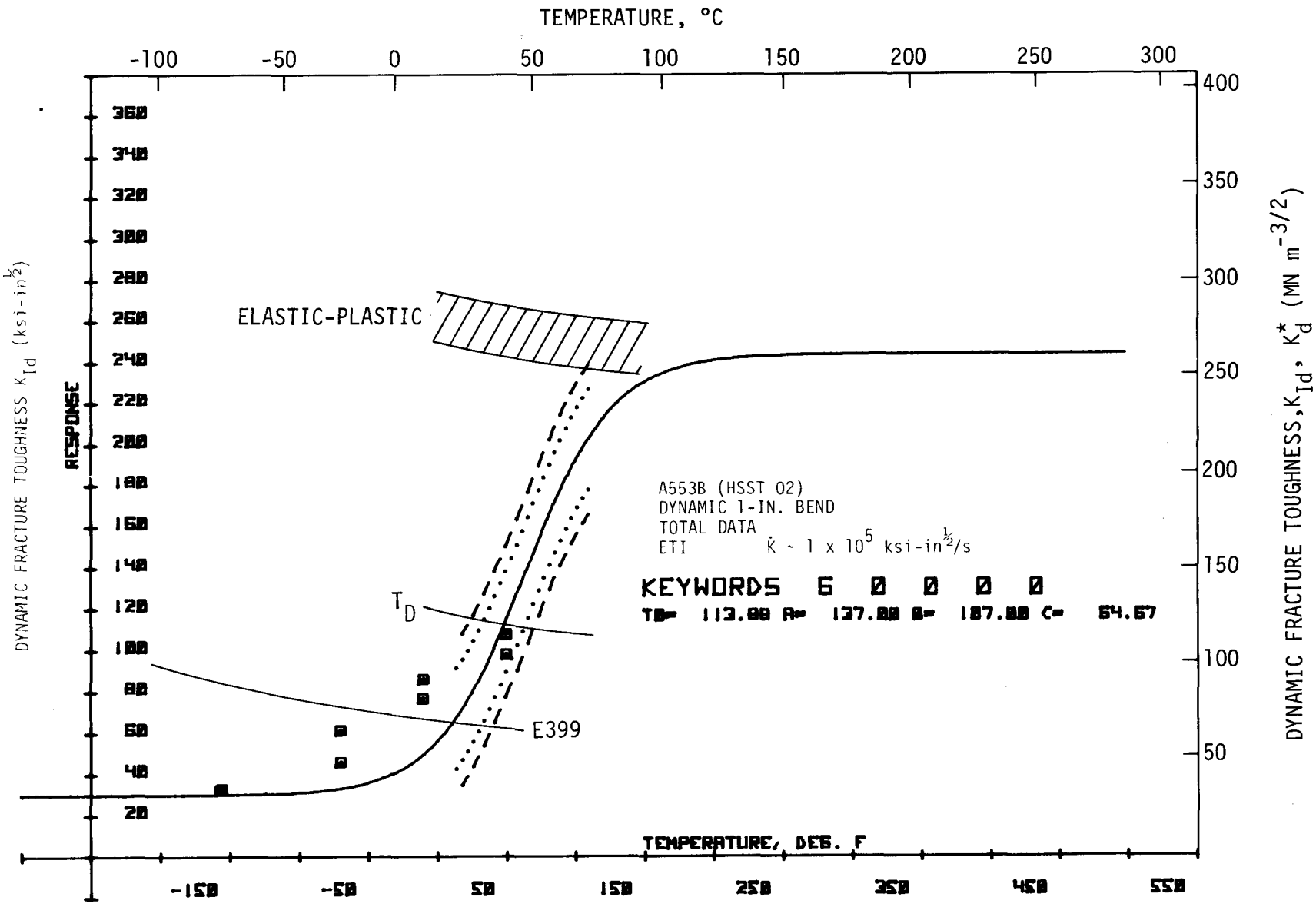

Figure 3. Tahn Model Fit to Dynamic 1-in. (25 mm) Bend Fracture Toughness Results (Upper and Lower Shelf Predetermined)

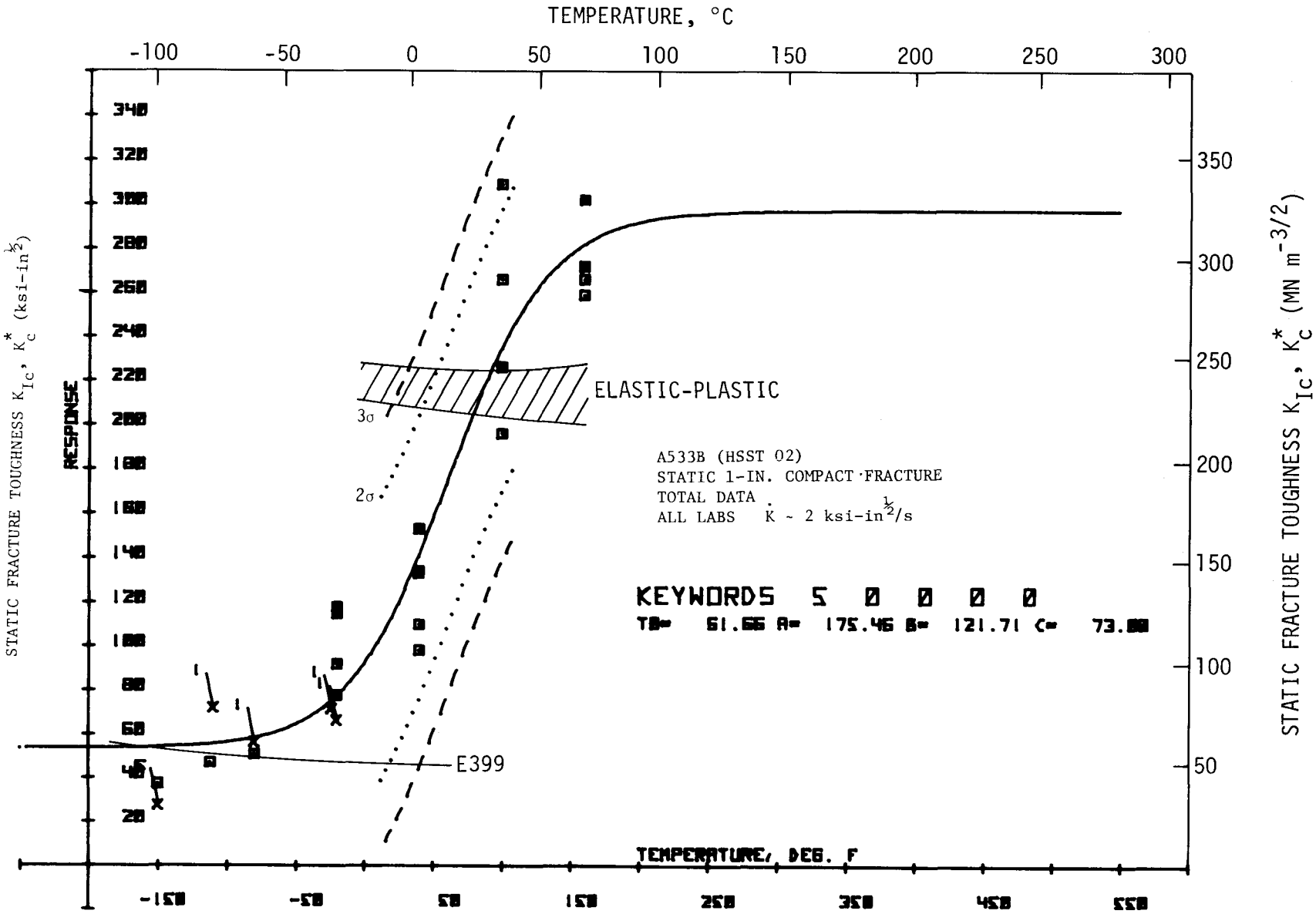

Figure 4. Tanh Model Fit to Static 1-in. (25 mm) Compact Fracture Toughness Results

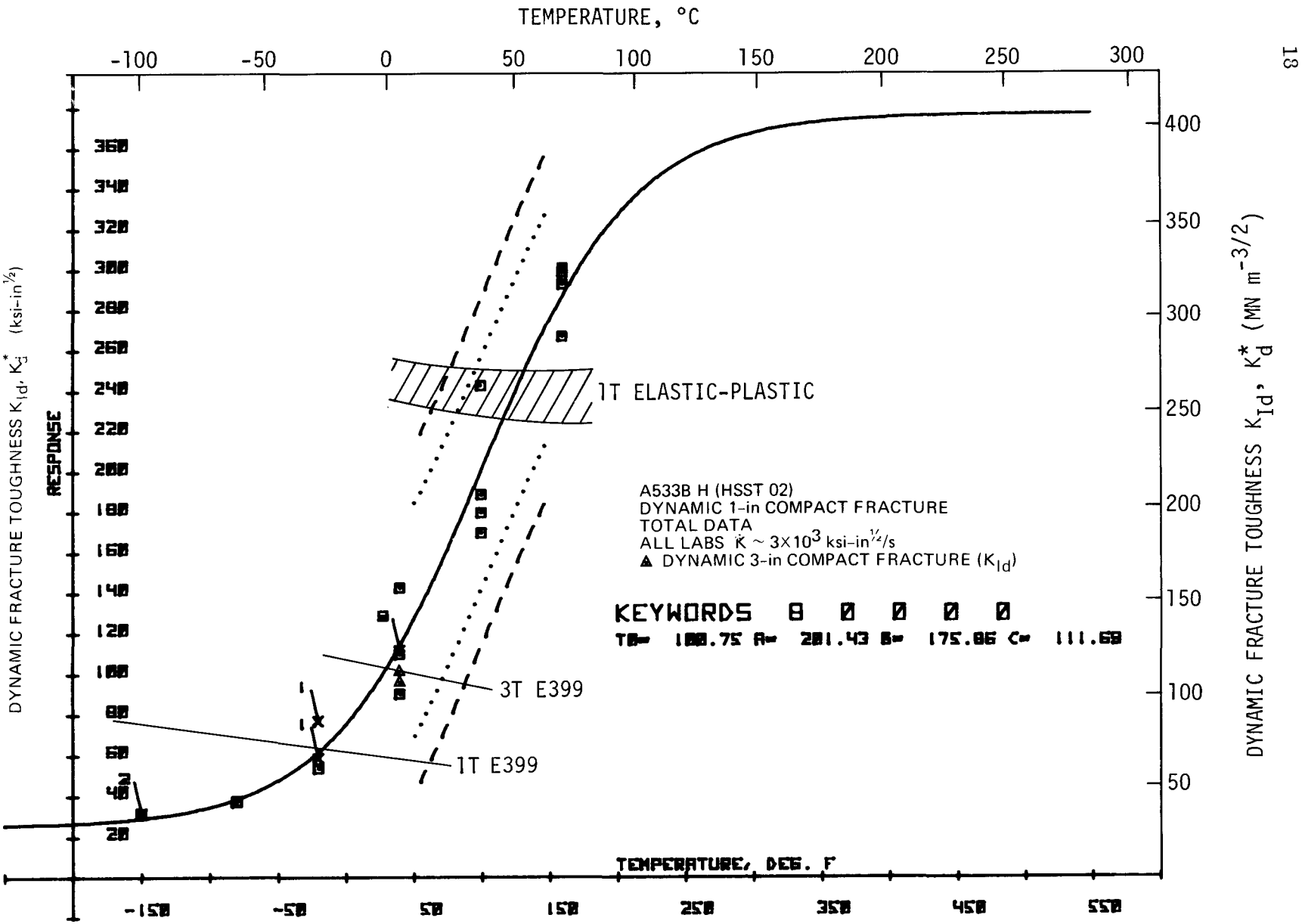

Figure 5. Tanh Model Fit to Dynamic 1-in. (25 mm) and 3-in. (76 mm) Compact Fracture Toughness Results

conversion as yield stress) for temperatures greater than $-20^{o}F$ ($-29^{o}C$) was extrapolated back to lower temperatures. The dynamic yield stress (σ_{yd}) and dynamic flow stress (σ_{fd}) temperature dependencies are:

$$\sigma_{yd} = 112.95 - 1.58 \times 10^{-2}T + 3.78 \times 10^{-4}T^2 - 3.96 \times 10^{-7}T^3 \quad (10)$$

$$\sigma_{fd} = 131.53 - 1.32 \times 10^{-2}T + 2.68 \times 10^{-4}T^2 - 2.68 \times 10^{-7}T^3 \quad . \quad (11)$$

The intermediate loading rate data required for the dynamic compact specimens were obtained by a linear interpolation between the quasi-static loading rate and the dynamic impact loading rate to give the following relationship for intermediate yield stress (σ_{yi}) and flow stress (σ_{fi}):

$$\sigma_{yi} = 0.6\ \sigma_{yd} + 0.4\ \sigma_{ys} \quad (12)$$

$$\sigma_{fi} = 0.6\ \sigma_{fd} + 0.4\ \sigma_{fs} \quad . \quad (13)$$

The temperature dependence (T, degrees Fahrenheit) of the elastic modulus (psi $\times 10^6$) was used,

$$E = 30.2 - 0.0046T \quad . \quad (14)$$

Also shown in Figures 2-5 are the ASTM E399 elastic toughness criteria; i.e.,

$$a,\ b,\ B \geq 2.5 \left(\frac{K_Q}{\sigma_y}\right)^2 \quad , \quad (15)$$

where K_Q is the linear elastic toughness value. For the impact test results there is also shown in Figures 2 and 3 the limit at which fracture occurs at general yield (which corresponds to a transition temperature T_D). For the precracked Charpy geometry

$$K/\sigma_{yd} = 0.504 \quad , \tag{16}$$

and for the 1.00 in (25.4 mm) bend geometry

$$K/\sigma_{yd} = 1.135 \quad . \tag{17}$$

It will be shown later that for the dynamic tests, the limits of elastic behavior specified in Equations 16 and 17 have more meaning than the E399 criteria in Equation 15.

Fracture Mode and Initiation Studies

It was observed that (in Figures 4 and 5) the data above the validity criteria specified in Equations 6 and 7 correspond to fully ductile behavior, while the points falling below the limits correspond to cleavage initiation at maximum load with no ductile tearing. Thus, it appears that the limits for the 1T* compact test results correspond approximately to the change in fracture mode. However, for the precracked Charpy test results the validity line corresponding to Equations 6 and 7 is lower than the fracture mode transition; using a value of 25 in Equations 6 and 7 corresponds to the limit more closely approximating the fracture mode change ($K_d^* \simeq 160$ ksi-in$^{1/2}$ [176 MN-m$^{-3/2}$]). Since there is a fracture mode transition, there tends to be a high degree of scatter in the corresponding transition temperature region. This effect can be seen in the data analyzed in the verification experiments[14]. Figure 6 is a curve taken from that study with the addition of the limits imposed by Equations 6 and 7. The striking features in this figure are the large shift in toughness for precracked Charpy tests to very high values, and the validity lines which fall in an area of very little data. Post-test examination of the test records and broken samples show again that all results below the validity lines exhibited cleavage at maximum load (indicating that

*1T designates a standard 1-in. (25 mm) thickness sample: this abbreviated form will be used throughout the rest of the report.

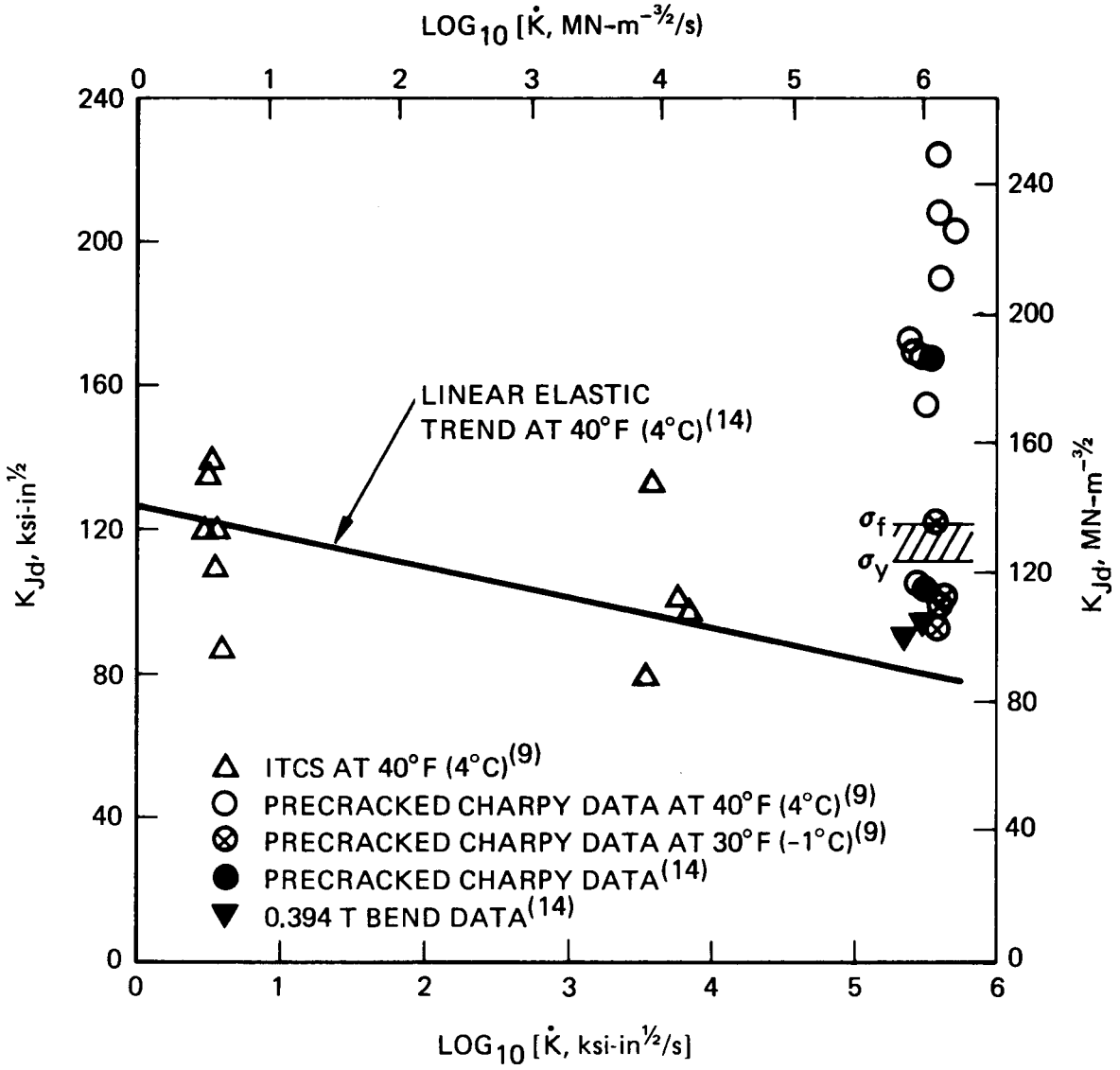

Figure 6. Comparison of Elastic-Plastic Results with Large Specimen Linear Elastic Trend Line(14)

maximum load corresponded to the initiation of fracture), and all results above the lines showed only ductile (no cleavage) behavior. Had the validity criteria corresponding to a value of 25 (rather than 50) been drawn, the ductile results would still have fallen above the limit. The results from the experimental program to follow will attempt to clarify these observations.

The effect of sample dimensions with respect to validity is somewhat more confusing. The work of Griffis[17] shown in Figure 7 illustrates the comparison of actual fibrous initiation values of J with maximum load values for various thickness (and ligament depth) samples. For Charpy thickness samples of the HY 80 steel (B = 10 mm), the difference between maximum load values and the J-initiation value (J_{Ic}) is rather small. Consider that a larger specimen valid K_{Ic} test could allow up to 2 percent crack growth which would raise the equivalent J_{Ic} value closer to the small specimen maximum load results. However, an alternate argument can be made against obtaining a higher valid elastic K_{Ic} result by considering the scatter resulting from a Weibull-type size effects. The argument postulates that larger samples are more likely to contain weak toughness areas leading to a lower measured fracture toughness in the absence of any stress state effects (which is probably appropriate for most initiation fracture results). These conflicting arguments plus the idea that initiation values from small samples (b, B < 10 mm, fibrous initiation) underestimate the true J_{Ic} value are a bit confusing. To further complicate matters, some recent data suggest a continuous increase in J_{Ic} with increasing specimen thickness[18].

A test matrix utilizing the results already obtained in the round robin[9] and verification experiments[14] was designed. The material tested was A533B-1 steel from HSST Plate 02. The effects of sample thickness and ligament depth, fracture mode, and loading rate on initiation J values were investigated. Tests were performed at four temperatures: $-20^{o}F$ ($-29^{o}C$), $40^{o}F$ ($4^{o}C$), room temperature, and $160^{o}F$ ($71^{o}C$); and four

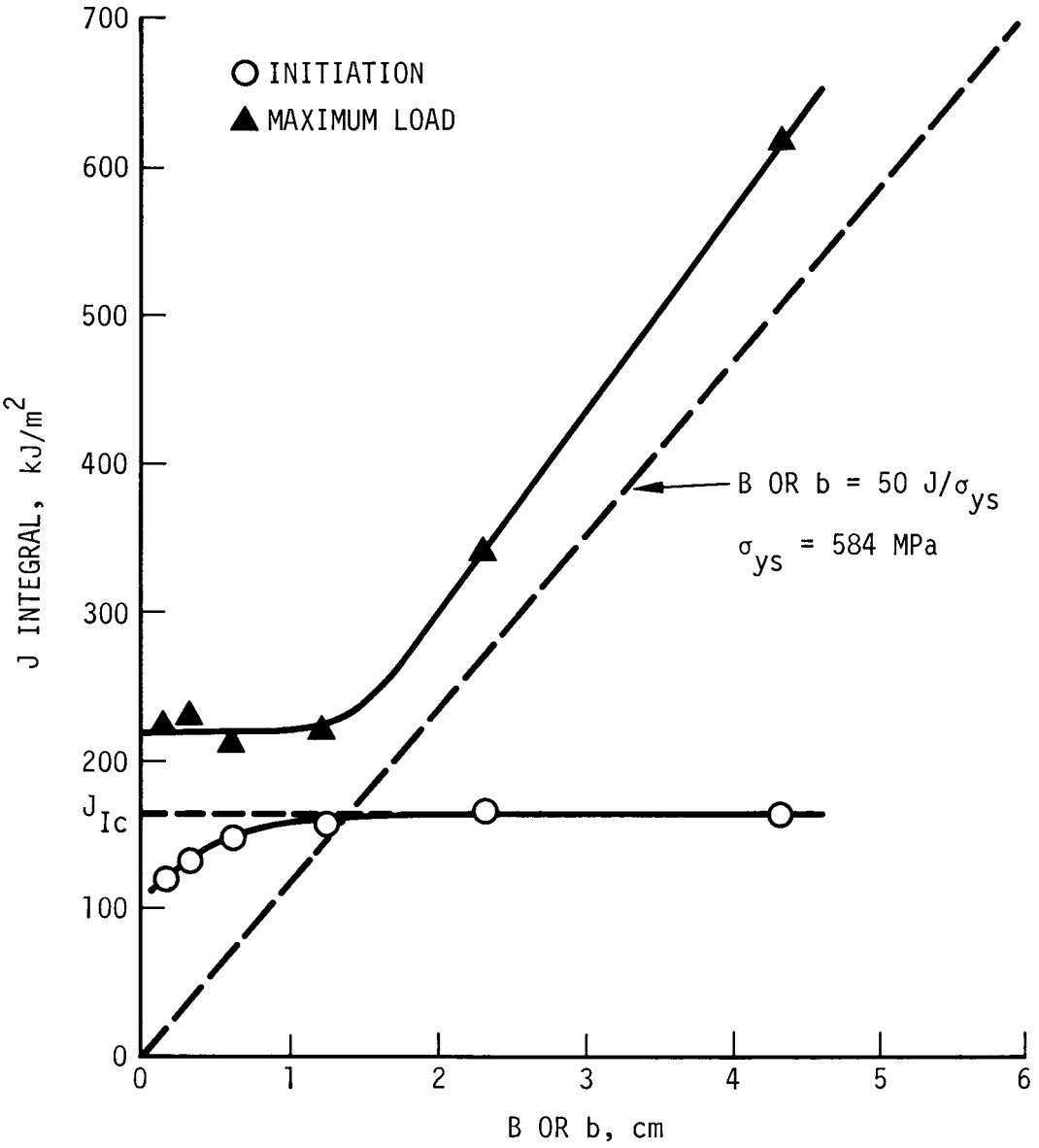

Figure 7. Effect of Specimen Size on Static J-integral at Initial Crack Extension and at Maximum Load for an HY-80 Steel at Room Temperature[17].

sample sizes were used: precracked Charpy, 0.394 T bend (10 mm thickness E399 bend sample), 1T bend (25 mm thickness), and 1T compact (25 mm thickness). The loading rates were quasi-static ($\dot{K} < 3$ ksi-in$^{1/2}$/s [3.3 MN-m$^{-3/2}$/s]), closed loop dynamic ($\dot{K} \simeq 10^3$ ksi-in$^{1/2}$/s [10^3 MN-m$^{-3/2}$/s]), and impact dynamic ($\dot{K} \simeq 10^5$ ksi-in$^{1/2}$/s [10^5 MN-m$^{-3/2}$/s]). The results from these tests will be presented after a brief discussion of the J (R-curve)testing procedure.

Testing Procedures

A general procedure for J initiation testing following the guidelines of the ASTM Elastic-Plastic Fracture Mechanics Task Group[16] was followed. The general procedure (with dynamic testing considerations added) in outline form is:

1. Each specimen is loaded to different displacement values in a closed loop test machine in displacement control or with deflection stops in a drop tower impact machine (see Figures 8a and 9).

2. Each specimen is unloaded and the crack marked utilizing a heat tinting procedure (550°F, 30 minutes). Note that when unstable cleavage crack extension occurs it is often better to complete the fracture without heat-tinting since any fibrous growth will be marked by the change to cleavage fracture.

3. Each specimen is then broken, usually at low temperature (approximately -100°F [-73°C]), and the amount of crack extension is measured. The crack extension measured is taken to include all crack extension from the end of the fatigue precrack to the end of the heat-tinted marking (thus including the stretch zone). An average of the extension at the thickness quarter points and center is used since the amount of extension is usually not uniform (see Figure 8b).

4. J values are calculated from the load versus centerline of loading displacement records using the formula developed by Rice, et al., for calculating J from single specimen tests[19]

$$J = \frac{2E_i}{Bb} \quad , \tag{18}$$

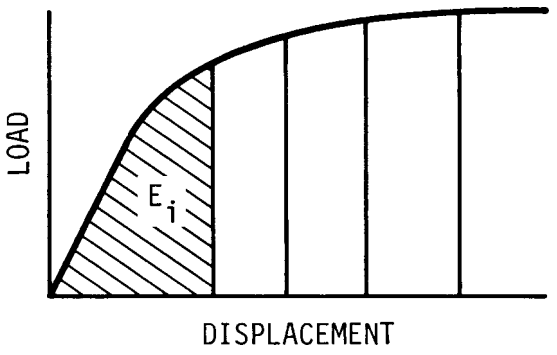

a. Load Specimens to Various Displacments

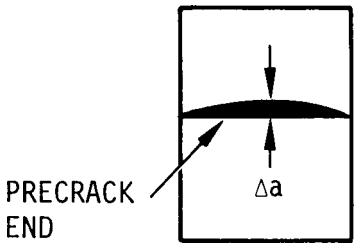

b. Measure Crack Extension

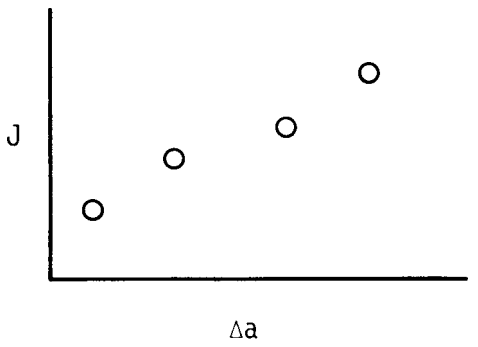

c. Calculate J for Each Specimen and Plot Versus Δa

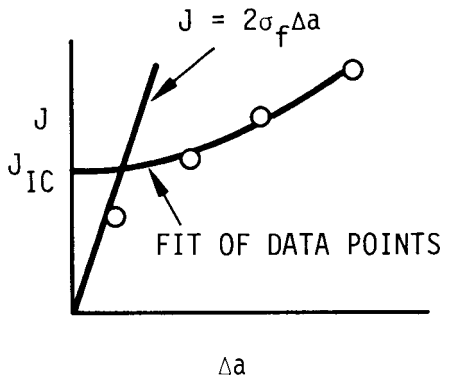

d. Construct Two Curves for J_{IC} Measurement

Figure 8. Procedure for J_{IC} Measurement

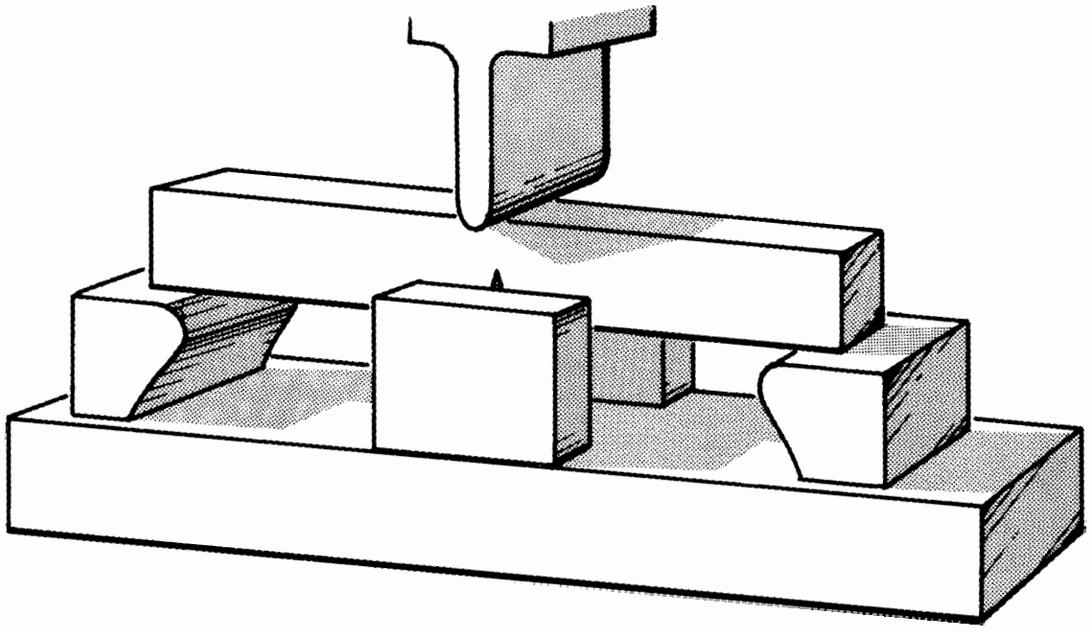

Figure 9. Schematic Diagram of the Drop Tower Stop Block Arrangement

where E_i is the area (energy) under the load-displacement curve taken at the displacement of interest, B is the specimen thickness and b is the remaining uncracked ligament.

5. A plot of J versus crack extension is constructed (Figure 8c).

6. The straight line representing stretch zone formation, $J = 2\sigma_f \Delta a$, is constructed where σ_f is a flow stress indicative of the sample loading rate equal to half the yield plus ultimate stresses (see Equations 8 -13). In addition, a best fit line is constructed through the J versus crack extension points (Figure 8d). The critical value of J (J_{Ic}) is the J value which occurs at the intersection of these two lines. Corresponding K_{Jc} values are calculated from the relationship between elastic-plastic and linear elastic fracture mechanics parameters

$$K_{Jc} = (EJ_{Ic})^{1/2} \quad . \tag{19}$$

The additional term $(1 - \nu^2)$ is sometimes used as a denominator in the square root quantity in Equation 19 to account for plane strain conditions, but was not used in the current study.

The center load-line displacement of the compact samples was monitored directly using a clip gage located at the loading pin centerline. The displacement of the closed loop bend test was monitored by using the ram displacement. A machine compliance term was determined (similar to the procedure for obtaining the impact testing compliance term[10]), and the corresponding energy attributed to the machine was subtracted to get the correct value of E_i. This technique appears to be accurate within 1-2% for both bend testing and compact testing (i.e., applicable to high temperature testing above the normal capability of standard clip gages)[20]. A correlation for compact data obtained in this program will be presented later.

The dynamic initiation technique developed for the bend tests on the Fracture Control drop tower is shown schematically in Figure 9. Hardened steel deflection stops were used to stop the falling tup at differing

amounts of deflection. When the tup strikes the deflection block, an instantaneous increase in load occurs marking the stopping event. It should be noted that a few millimeters of deflection can still occur due to the elastics in the stop blocks; therefore, the value of J (energy) calculated is slightly conservative (low). The drop tower weight for the 1T bend tests was 2115 lbf (9408 N), and the impact velocity was 55.4 in/s (1.41 m/s). The weight used for the 0.394 T bend and the pre-cracked Charpy testing was 610 lbf (2713 N), and an impact velocity of 48.0 in/s (1.22 m/s) was maintained. The load cells used for testing were calibrated statically and dynamically in the same manner as specified in the EPRI RP 232 program[4,10].

The static and dynamic closed loop initiation testing was performed on an MTS 20 kip (89 kN) machine. The tests were programmed under stroke control, and the dynamic tests were program halted at various amounts of deflection. There was no overshoot in load or deflection, but a change in rate occurred during the last millisecond of loading. The real effect of this decrease in loading rate on the actual stress intensification rate is unknown, but there is definitely a difference in results due to the dynamic rate of loading as will be shown later. The MTS load cell and the Fracture Control clip gages were calibrated in accordance with previous EPRI procedures[4,10].

HSST Plate 02 Results

The material chosen for this portion of the testing program was HSST Plate 02 (A533B-1 steel). This same material was used in the EPRI round robin program[9] and the verification experiments program[14]. The J results obtained from the testing are presented in Tables C.1 - C.4 in Appendix C and are shown graphically in Figures 10 - 17. The data shown in Figures 10 - 13 lead to an observation related to unstable cleavage extension. Three of the 1T compact specimens in Figure 12 and two in Figure 13 exhibited an unstable extension (filled triangles). Had the

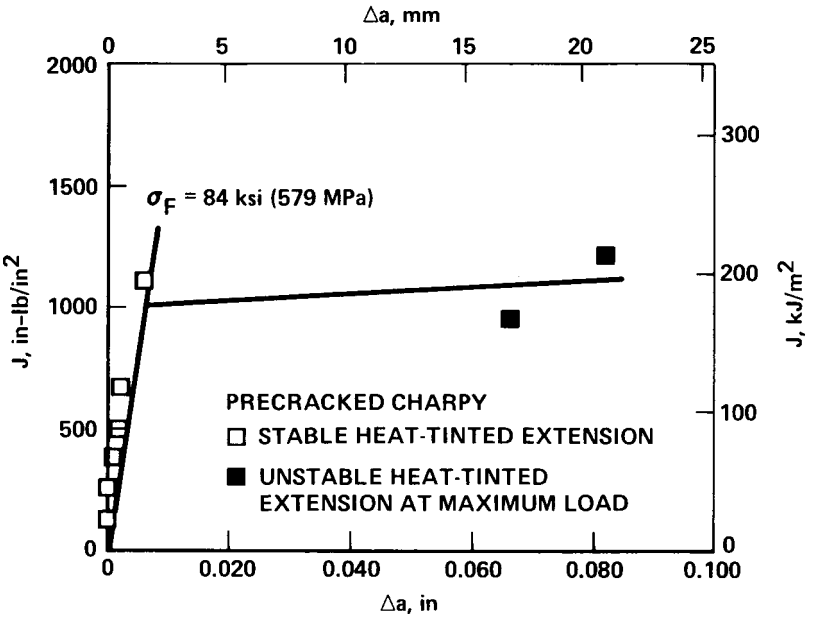

Figure 10. Quasi-Static Precracked Charpy J-Initiation at 40°F (4°C)

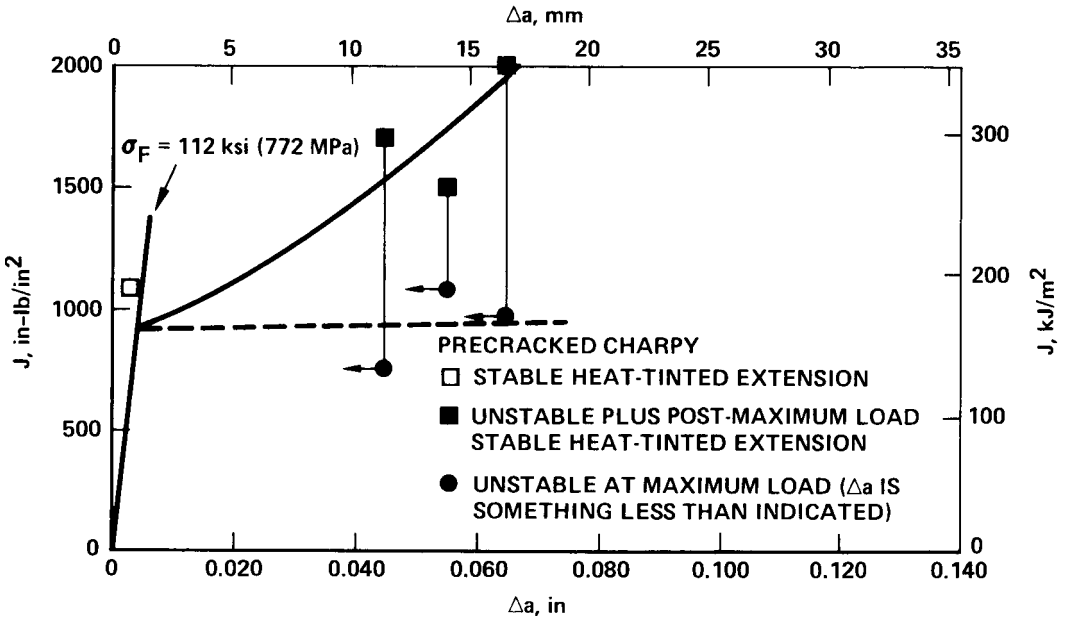

Figure 11. Intermediate Rate Dynamic Precracked Charpy J-Initiation at 40°F (4°C)

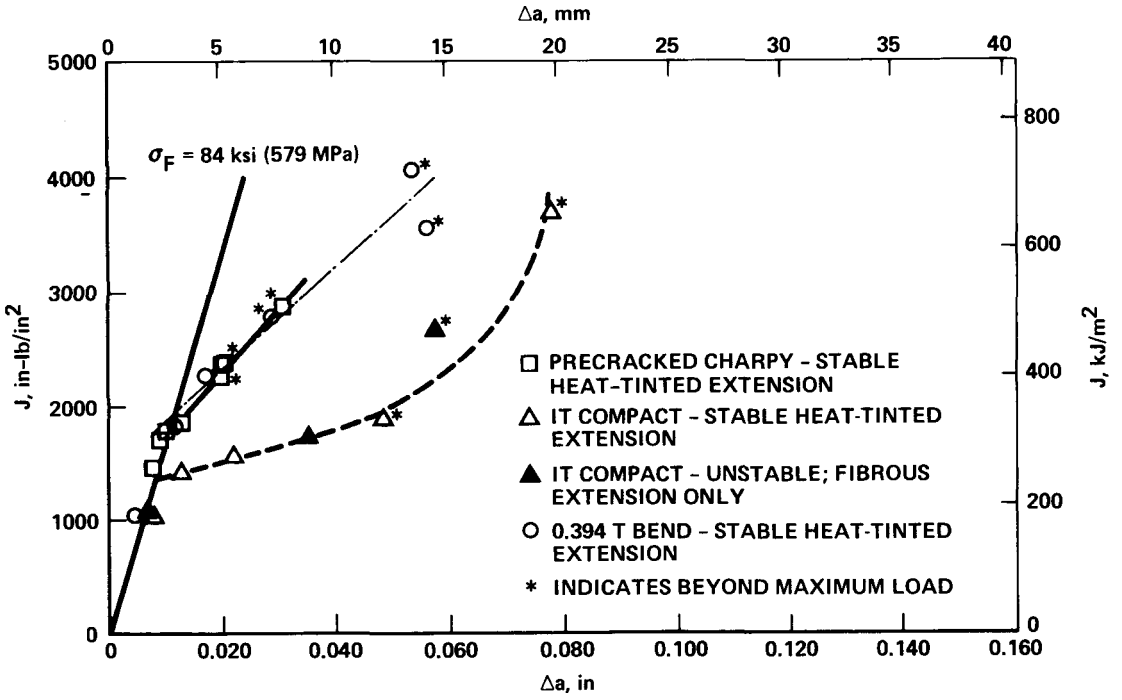

Figure 12. Quasi-Static J-Initiation at Room Temperature

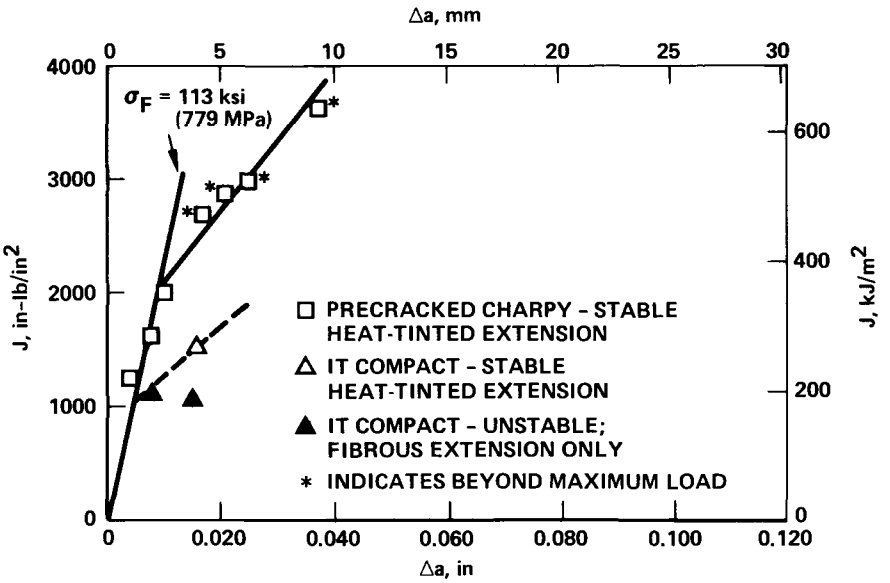

Figure 13. Intermediate Rate Dynamic J-Initiation at Room Temperature

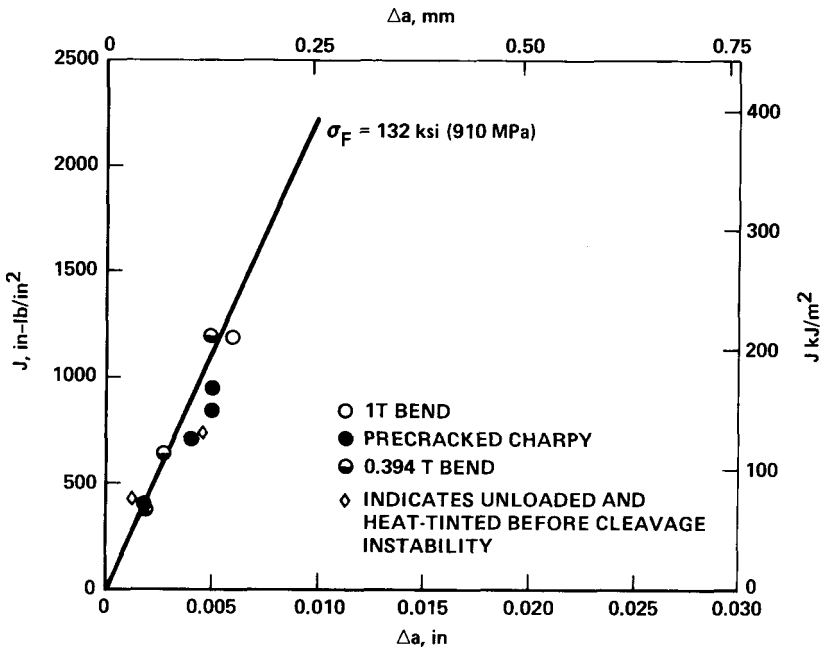

Figure 14. Impact Dynamic J-Initiation at Room Temperature

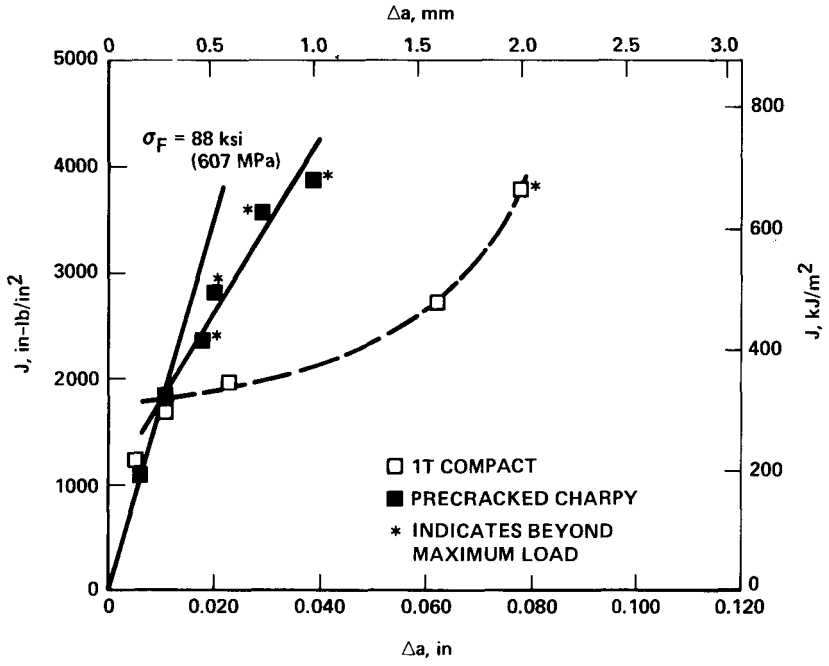

Figure 15. Quasi-Static J-Initiation at 160°F (71°C)

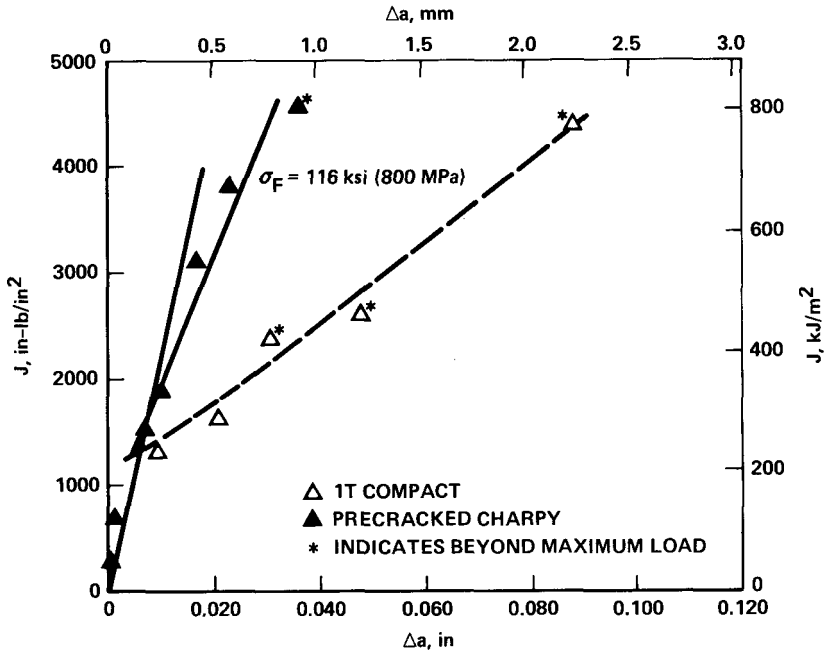

Figure 16. Intermediate Rate Dynamic J-Initiation at 160°F (71°C)

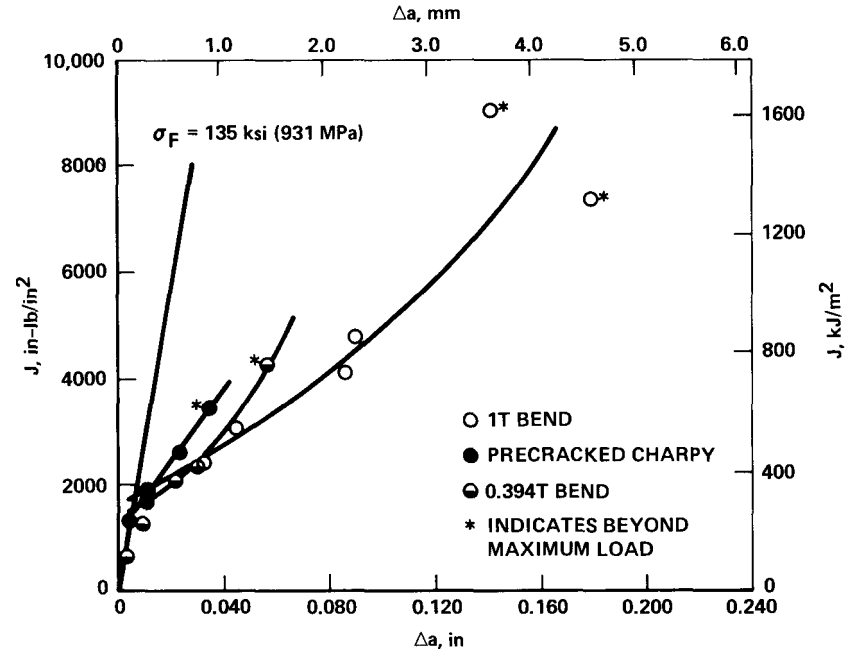

Figure 17. Impact Dynamic J-Initiation at 160°F (71°C)

samples been heat-tinted the extension seen would have corresponded to fibrous tearing plus flat cleavage fracture. Therefore these samples were not heat-tinted and the fibrous tearing measured directly since it can be seen macroscopically. The work on precracked Charpy specimens at 40°F (4°C) was not treated in this manner (see Figures 10 and 11). All other unstable cleavage tests were not heat-tinted. It is obvious from the R-curves that decreasing size increases the slope of the R-curve. Also, the effect of increased loading rate also appears to increase the slope of the R-curve.

To assess the effects of validity limits on specimen size, fracture mode changes, loading rate, and temperature, the J-initiation values obtained were compared with previous work on the same material in the EPRI programs[9,14] and the HSST program[21]. The J-initiation results from this program are tabulated in Table 2. Also listed in Table 2 is the validity criterion of Equation 6 using both a value of 50 and 25. The results of Table 2 are plotted and compared to the previous work on this material in Figures 18 - 21.

Figure 18 shows the comparison of results at -20°F (-29°C); note that all fractures are cleavage initiation. Only the validity line using the constant 50 in Equation 6 is indicated on this figure when it is on scale, i.e., if no validity point is indicated all results are "valid". It is readily apparent that the averaged slow bend precracked Charpy value is "invalid" and significantly higher than the larger sample linear elastic results. The three linear elastic 1T compact results did not meet the E399 thickness requirements, but agree favorably with larger specimen valid data. The 1T compact intermediate rate results do not agree as favorably with the valid linear elastic data although the 1T results are most likely acceptable elastic-plastic results due to elevation in yield strength. The elastic-plastic impact data tend to be higher than the linear elastic results for the same thickness sample (as would be expected). This tendency dictates the inherent material property scatter; thicker

Table 2. Initiation Toughness Results for HSST Plate 02

TEST TYPE	Temperature ^{o}F (^{o}C)	$\dot{K}$ ksi-in$^{\frac{1}{2}}$/s (MN-m$^{-3/2}$/s)	J_{Ic} in-lb/in^2 (kJ/m^2)	$\frac{50J}{\sigma_f}$ in (mm)	$\frac{25J}{\sigma_f}$ in (mm)	K_{JC} ksi-in$^{\frac{1}{2}}$ (MN-m$^{-3/2}$)
PCCV*	-20 (-29)	<3 (3.3)	738 (129)	0.42^{I}(10.7)	0.21^{I}(5.3)	150 (165)
0.394T Bend	-20 (-29)	~10^5 (10^5)	---	---	---	38^{e,a}(42)
PCCV	40 (4)	<3 (3.3)	1000 (175)	0.60^{I}(15.2)	0.30^{I}(7.6)	173 (190)
PCCV	40 (4)	~10^4 (10^4)	850 (149)	0.38^{I}(9.7)	0.19 (4.8)	160 (176)
PCCV	75-80 (24-27)	<3 (3.3)	1750 (306)	1.04^{I}(26.4)	0.52^{I}(13.2)	229 (252)
0.394T Bend	78 (26)	<3 (3.3)	1900 (333)	1.13^{I}(28.7)	0.57^{I}(14.4)	239 (263)
1T Compact	75-80 (24-27)	<3 (3.3)	1350 (236)	0.80 (20.3)	0.40 (10.2)	201 (221)
PCCV	75-80 (24-27)	~10^4 (10^4)	2000 (350)	0.88^{I}(22.4)	0.44^{I}(11.2)	245 (269)
1T Compact	80-85 (27-29)	~10^3 (10^3)	1000 (175)	0.44 (11.2)	0.22 (5.6)	173 (190)
PCCV	75 (24)	~10^5 (10^5)	900 (158)	0.34^{I}(8.6)	0.17 (4.3)	159 (175)
0.394T Bend	75 (24)	~10^5 (10^5)	748^{a}(131)	0.28 (7.1)	0.14 (3.6)	150 (165)
1T Bend	72 (22)	~10^5 (10^5)	1214 (213)	0.46 (11.7)	0.23 (5.8)	191 (210)
PCCV	160 (71)	<3 (3.3)	1800 (315)	1.02^{I}(25.9)	0.51^{I}(13.0)	230 (253)
1T Compact	160 (71)	<3 (3.3)	1790 (313)	1.02^{I}(25.9)	0.51 (13.0)	230 (253)
PCCV	160 (71)	~10^4 (10^4)	1500 (262)	0.65^{I}(16.5)	0.32^{I}(8.3)	210 (231)
1T Compact	160 (71)	~10^3 (10^3)	1320 (231)	0.57 (14.5)	0.28 (7.2)	197 (216)
PCCV	160 (71)	~10^5 (10^5)	1550 (271)	0.57^{I}(14.5)	0.29^{I}(7.2)	214 (235)
0.394T Bend	160 (71)	~10^5 (10^5)	1550 (271)	0.57^{I}(14.5)	0.29 (7.2)	214 (235)
1T Bend	160 (71)	~10^5 (10^5)	1800 (315)	0.67 (17.0)	0.33 (8.5)	230 (253)

* PCCV is the precracked Charpy sample

I Does not meet indicated validity criteria for B, b, and/or a

e Linear elastic values

a Averaged value

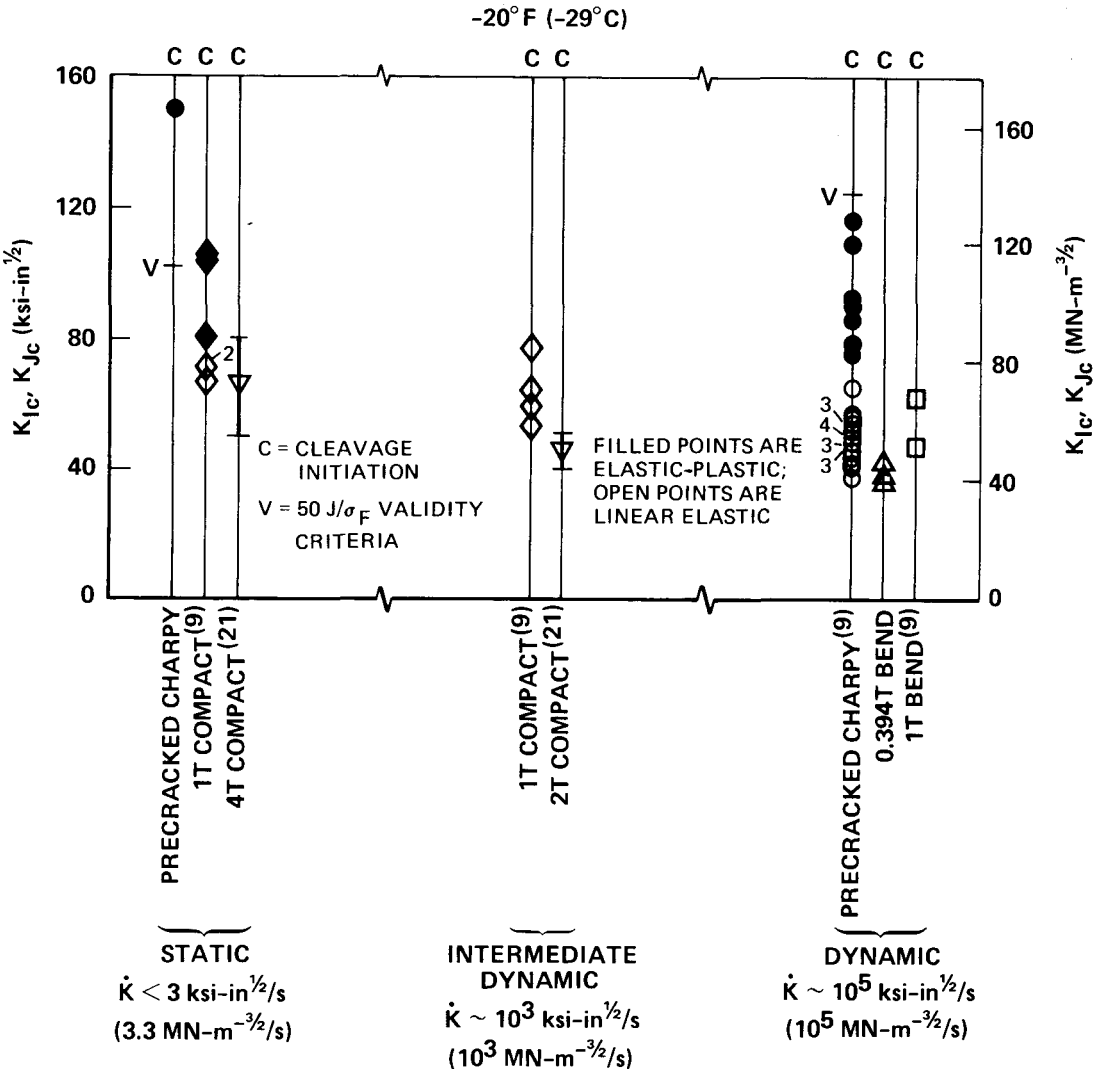

Figure 18. Comparison of Initiation Toughness Results at -20°F (-29°C)

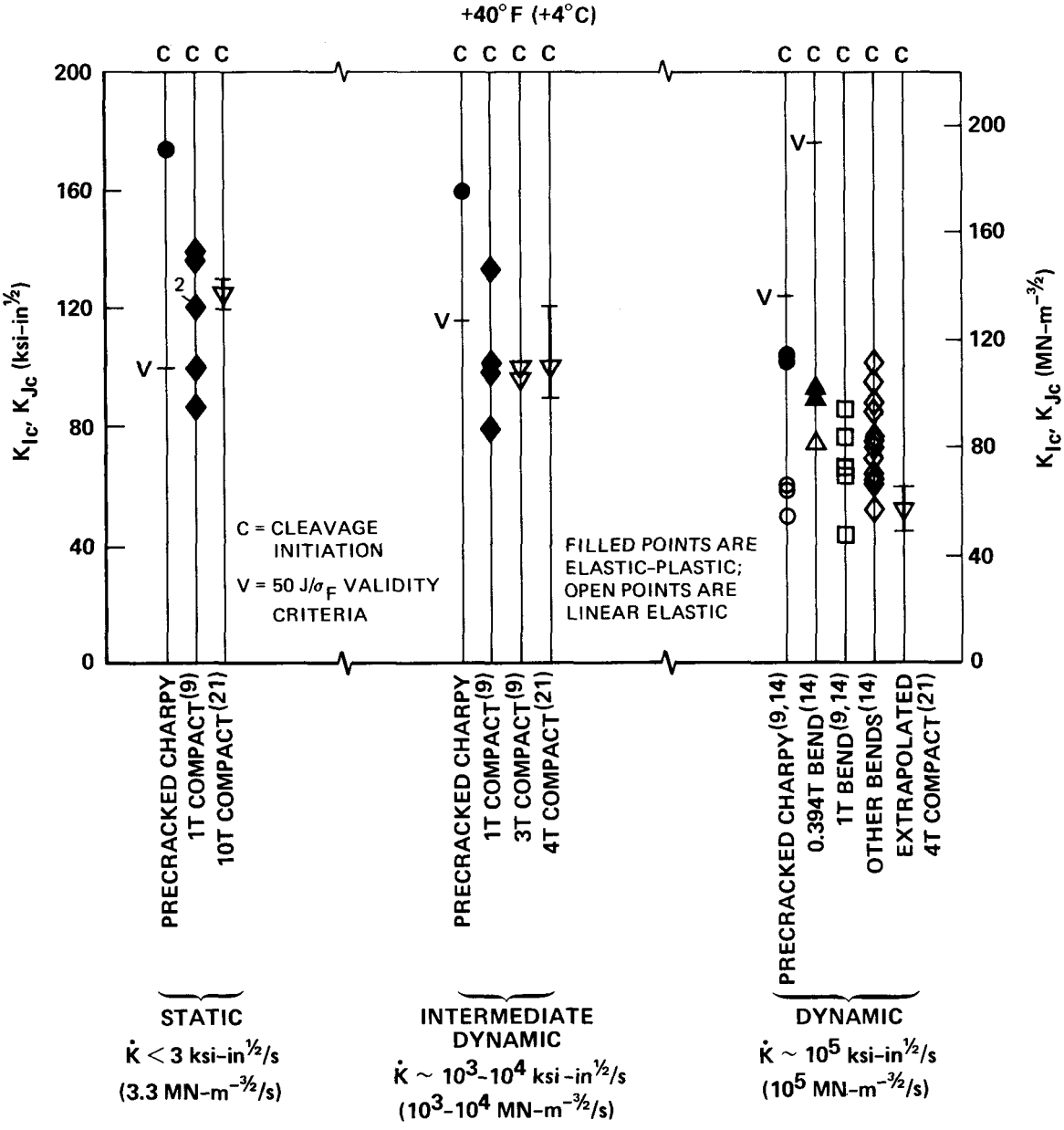

Figure 19. Comparison of Initiation Toughness Results at 40°F (4°C)

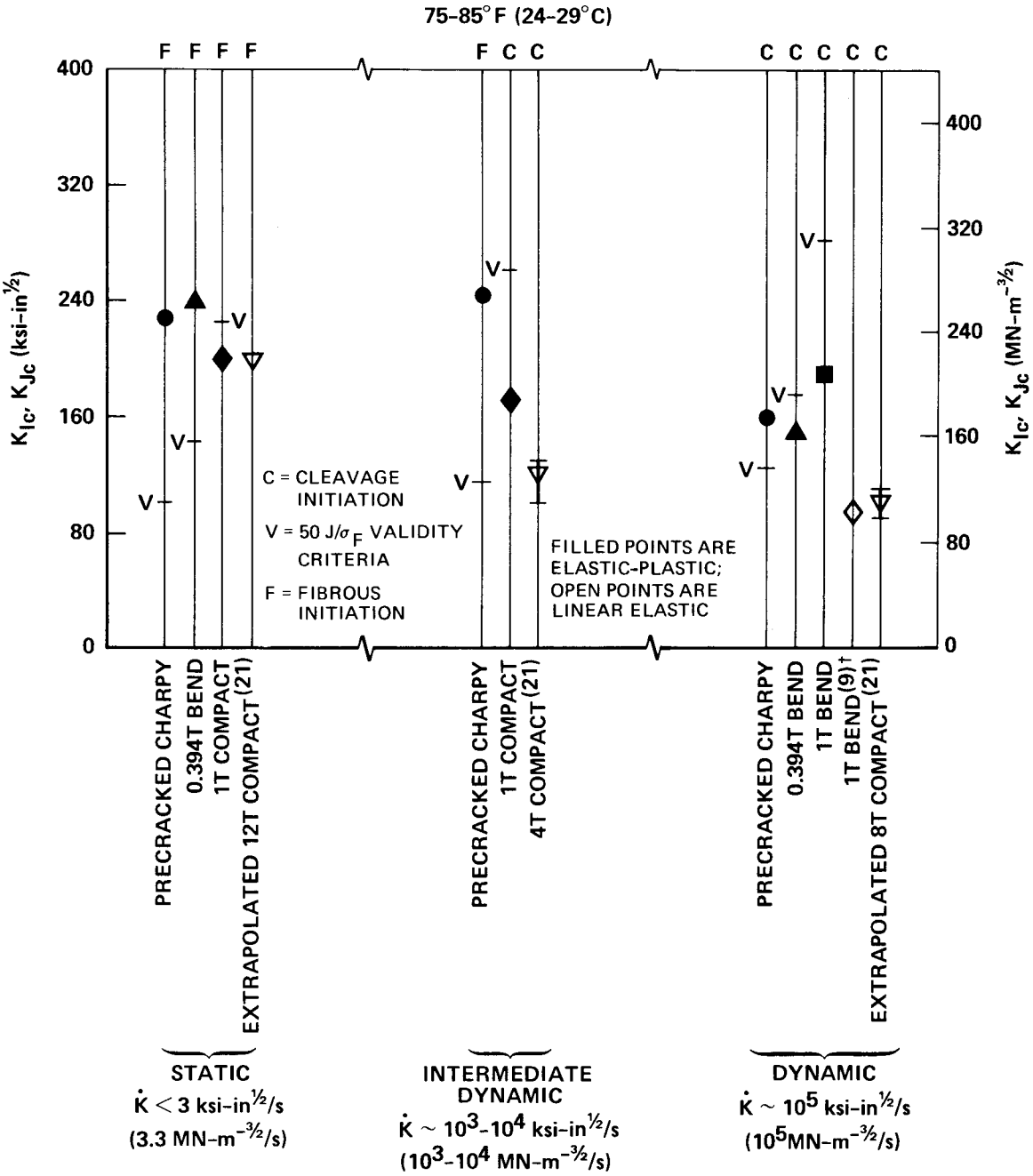

† INTERPOLATED FROM ELASTIC RESULTS AT 40°F (4°C) AND 100°F (38°C)

Figure 20. Comparison of Initiation Toughness Results at Room Temperature

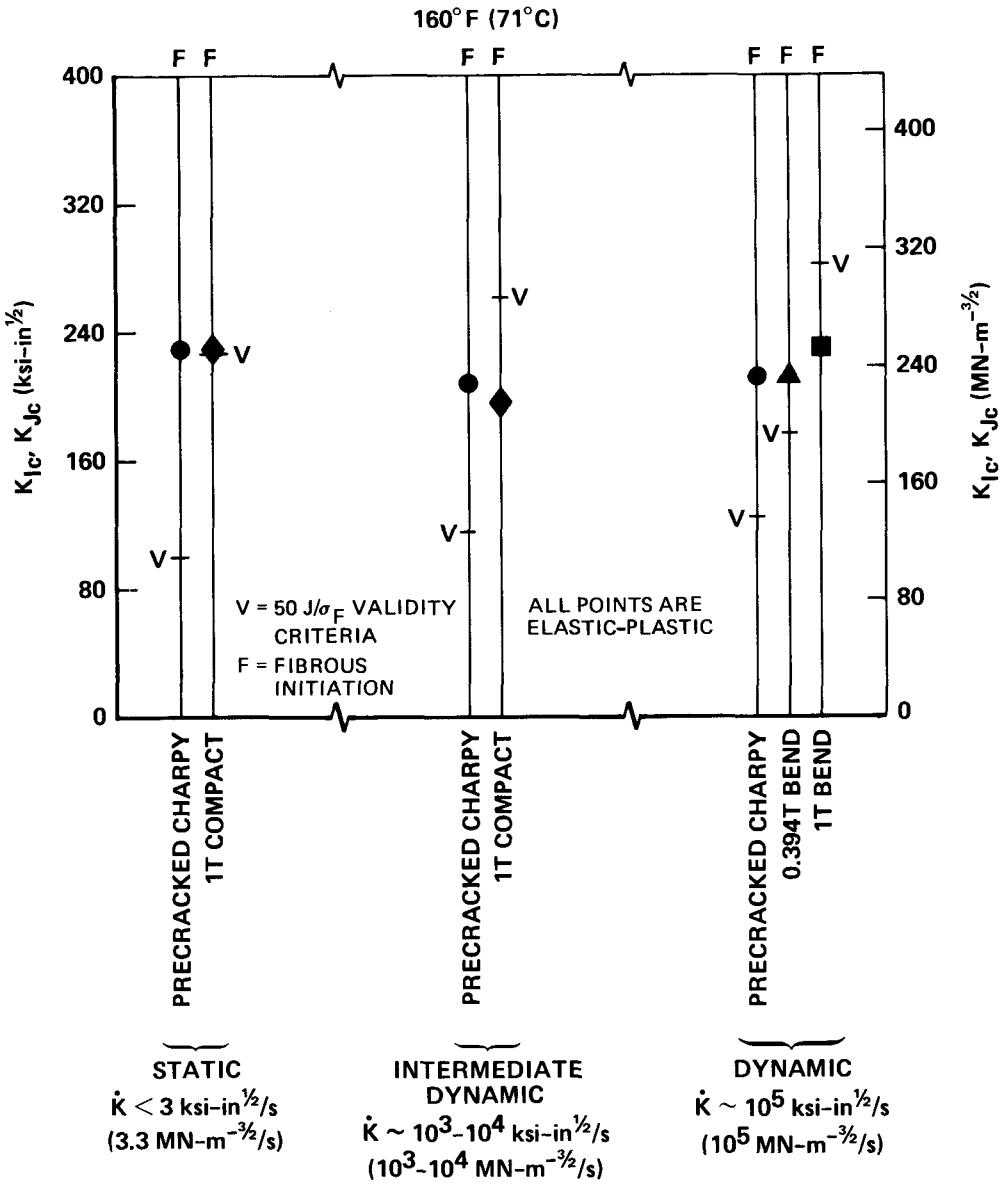

Figure 21. Comparison of Initiation Toughness Results at 160°F (71°C)

samples will not have this same degree of scatter since a larger volume of material is being tested at one time and the lowest level of toughness within this volume of material should result in the measured value of toughness.

The data in Figure 19 illustrate the toughness trends at 40°F (4°C). Again all results shown are for cleavage initiation. However, it should be noted that many additional precracked Charpy impact tests (shown in Figure 6) resulted in ductile initiation and extremely high levels of toughness (for maximum load). Thus, a fracture mode transition is being approached at this temperature with the smallest specimens, although it is unusual that this transition showed up at the highest rate of loading (many more tests were performed at this rate, however). Values of toughness which fall above the validity line are very high (precracked Charpy slow bend and intermediate rate results). The agreement with the other linear elastic and elastic-plastic results is within the data scatter to be expected.

The room temperature results in Figure 20 show a slightly different trend since some of the initiation results are for fibrous initiation and others for cleavage initiation. It appears from the static data that for fibrous initiation there is little difference between "valid" elastic-plastic and linear elastic results and "invalid" elastic-plastic results. However, when the smaller specimen has a mode of fracture different from larger samples, the "invalid" data are substantially higher as evidenced by the intermediate rate results. The impact dynamic results are a bit confusing since the 1T bend test result was elastic-plastic while the round robin data[9] showed two elastic results at 100°F (38°C). However, the remaining impact data are similar to that shown in Figures 18 and 19. The comparison between precracked Charpy and 0.394T bend data suggests that the 0.394T bend sample maintains elastic constraint only slightly more than the precracked Charpy.

The results in Figure 21 are for fibrous initiation at 160°F (71°C). It is interesting that there is little difference between "valid" and "invalid" results and between different loading rates. In fact, the intermediate rate initiation results look to be slightly lower. There also appears to be no effect on ligament depth when fibrous initiation occurs; however, this comparison of precracked Charpy and 0.394T bend results at the impact rate of loading may be obscured since both sets of results do not meet the validity criterion if it should indeed apply.

In summary, the comparison of the initiation toughness results obtained lead to the following observations:

1. For cleavage initiation, the $50J/\sigma_f$ specimen size criterion appears to separate out high ("invalid") results.

2. For fibrous initiation, the $50J/\sigma_f$ specimen size criterion does not appear to apply. Small specimen results violating this criterion agree quite favorably with "valid" data.

3. A fracture mode transition occurs near room temperature, but the absolute temperature at which this transition occurs appears to be a function of loading rate, specimen size, and statistics.

4. There appears to be only a slight positive effect of doubling the ligament depth and span (still 4w, however) on the precracked Charpy sample to increase elastic constraint.

5. Small specimen data may reflect the true material property variability throughout the material, whereas large specimen data reflects the lowest level of toughness due to the total volume of material being tested.

6. The R-curves obtained indicate that decreased specimen size and increased loading rate increase the slope of the R-curve.

Single Specimen Initiation Techniques

There exist several single specimen techniques for measuring the initiation point for fibrous stable crack growth. However, none of these techniques has been perfected to allow uniform and precise measures of

this initiation point. Work in the technical community is being performed using compliance difference[22], ultrasonics[23], resonant frequency[24], ultra-sensitive piezoelectric load cell[25], and electric-potential[26,27] techniques. A cursory investigation of the electric potential method was initiated in this program.

A one-specimen initiation approach using a DC electric-potential method was tried on several of the 1T static compact specimen tests at room temperature. The electric-potential method entails passing a current through a cracked test specimen under load and measuring the electric potential difference across the crack. As the crack extends the uncracked cross-sectional area of the specimen decreases, the electrical resistance increases, and the potential difference between two points on either side of the crack increases. The crack length to width ratio (a/w) may be determined by monitoring this potential increase and comparing it with a reference potential measured elsewhere on the specimen (in a region not affected by crack growth or on a separate sample). The technique does show a definite increase in potential as loading continues past yielding and P_Q, but no distinct discontinuity occurs which marks the onset of fibrous tearing. The increase in potential is the result of plasticity and tearing (when it does occur). Figure 22 illustrates the shape of the DC potential change curves obtained.

The initial rise in the curve is due to contact of the fatigue precracked surfaces at the beginning of the test (closure). The decrease in output after the initial increase is described in Reference 27 as due to an inverse magnetostriction phenomenon for an AC system. However, this effect is not applicable to a DC current and, therefore, does not explain the decrease observed here. Bachmann and Munz[28] suggest that the start of the decrease occurs as plastic deformation begins (i.e., above the precracking K_f(max)) due to lateral shear displacements when rough surfaces are present. Ritchie[29] has found, however, that this closure-type phenomenon does not occur for high strength steels

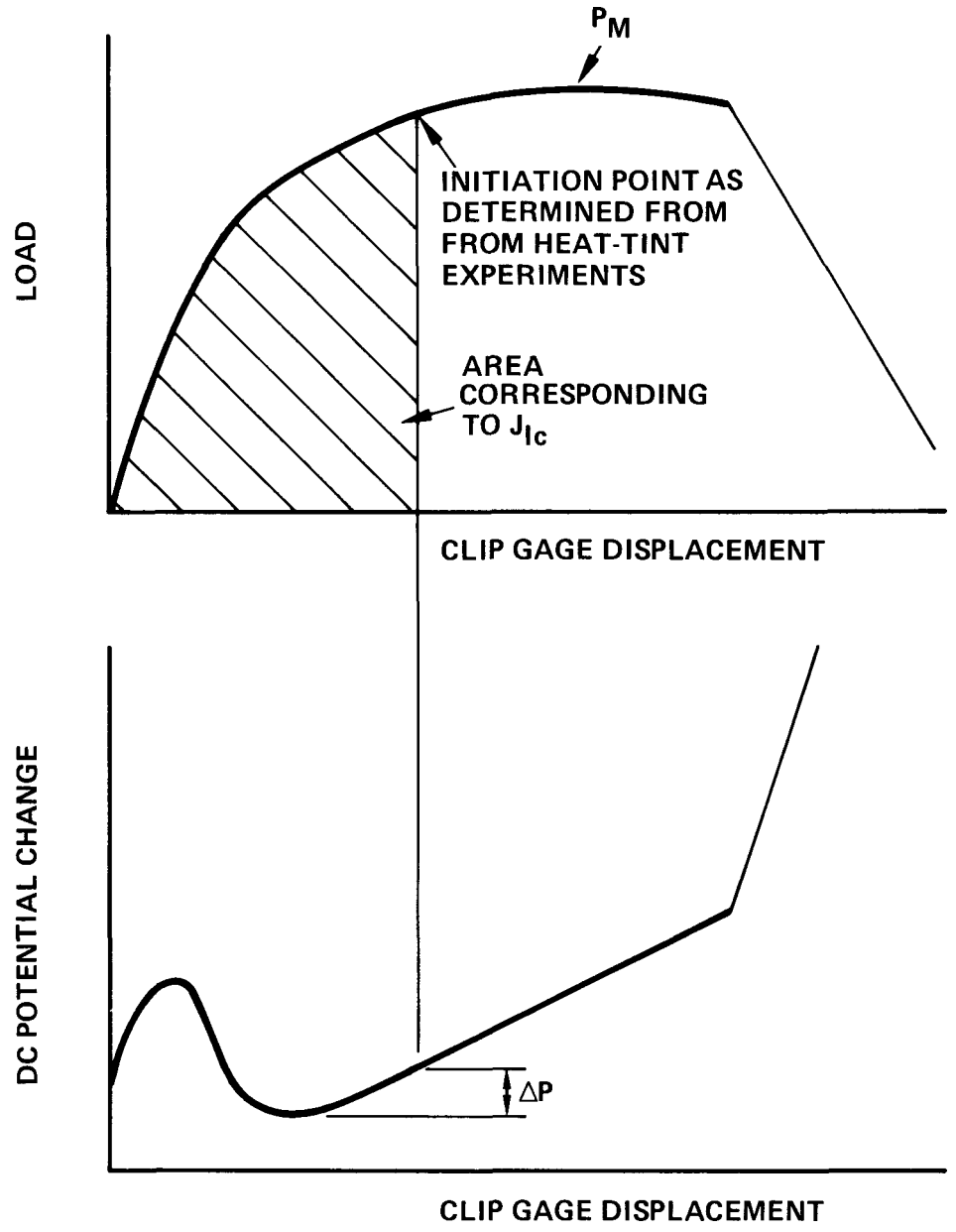

Figure 22. Electric-Potential Procedure for Obtaining Initiation of Fibrous Growth

(σ_y > 150 ksi [1034 MPa]) regardless of the crack roughness. Whatever the effect is that causes the decrease, when substantial plasticity and stable tearing become predominant, the potential curve starts to increase.

Marandet and Sanz[27] indicate that initiation occurs at the minimum point of the curve. The results from our experiments suggest that there is an increase in potential before initiation; this increase is designated as ΔP in Figure 22. For the conditions used in our experiments (30 amps current and measurement across the front edge of the specimen), the ΔP approach gives a value of J_{Ic} = 1315 $\pm$ 200 in-lb/in^2 as compared to the J_{Ic} = 1350 in-lb/in^2 obtained from the heat-tinting approach (see Table 2 and Figure 12). Further work in this area is required to validate a ΔP approach.

UPPER SHELF FRACTURE TOUGHNESS RESULTS

The upper shelf materials were selected on the basis of having a low precracked Charpy upper shelf toughness level (based on maximum load). The EPRI materials selected are listed in Table 3. Initiation toughness tests were performed both statically and dynamically at 350°F (177°C). The NRL A302B heat[30] was chosen as an additional heat of low upper shelf toughness.

Discussion of Results

The toughness results are tabulated in Table C.5 in Appendix C and are illustrates in Figures 23-38. The line $J = 2\sigma_f \Delta a$ was obtained by using values of σ_f indicative of the loading rate as described previously (see Equations 8-13). All compact results were obtained using a clip gage designed by Fracture Control to operate at temperatures up to 450°F (232°C). However, the clip gage did fail on the one sample noted in Table C.5, and a machine compliance corrected energy (from the ram LVDT*)

*Linear Voltage Displacement Transducer

Table 3. Materials Selected for Upper Shelf Toughness Testing

MATERIAL	HEAT	STRESS INTENSIFICATION RATES ($MN\text{-}m^{-3/2}/s$) STATIC	DYNAMIC CT	DYNAMIC BEND
A533B-1	ETI-G (EG)	2.7	---	1×10^5
A508-2	B&W-B (BBB)	2.7	3×10^3	---
A302B	ETI-N (EN)	2.7	---	1×10^5
	NRL (NA)	2.7	---	1×10^5
MMA Weld Metal A533B-1 Base	ETI-K (EK)	2.7	---	1×10^5
MMA Weld Metal A508-2 Base	B&W-K (BKM)	2.7	3×10^3	---
SA Weld Metal A533B-1 Base	CE-J (CJ)	2.7	3×10^3	---
SA Weld Metal A508-2 Base*	B&W-A* (BAS)	2.7	3×10^3	---

*This weldment did not have any archive material. However, the weld filler material was archived and a new weldment was fabricated with the heat A filler material and matching the original heat input.

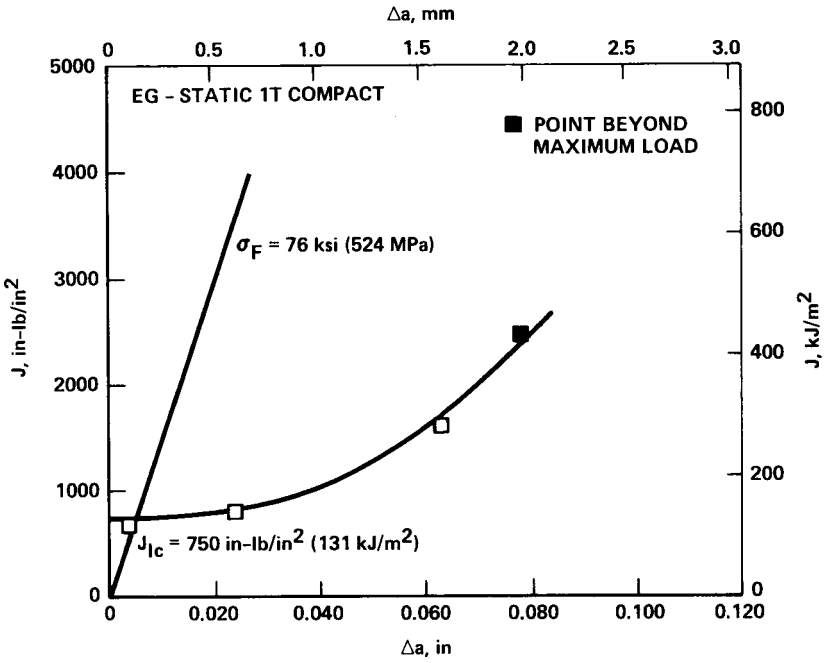

Figure 23. Quasi-Static 1T Compact J-Initiation for Heat EG at 350°F (177°C)

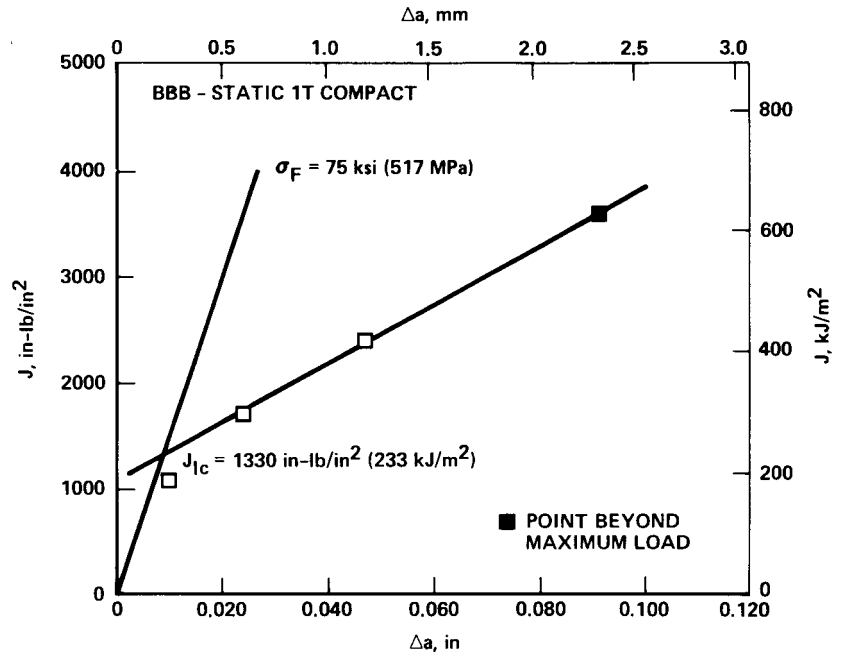

Figure 24. Quasi-Static 1T Compact J-Initiation for Heat BBB at 350°F (177°C)

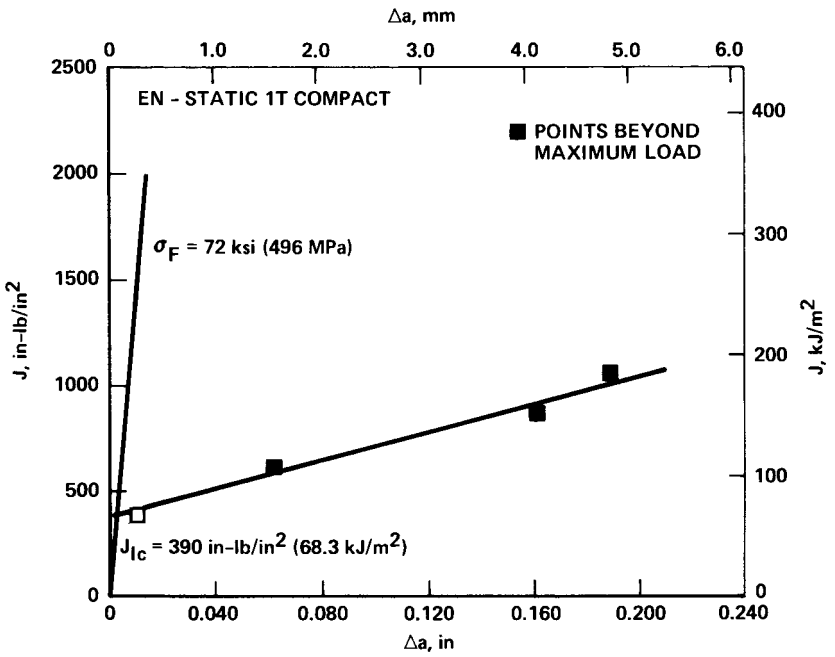

Figure 25. Quasi-Static 1T Compact J-Initiation for Heat EN at 350°F (177°C)

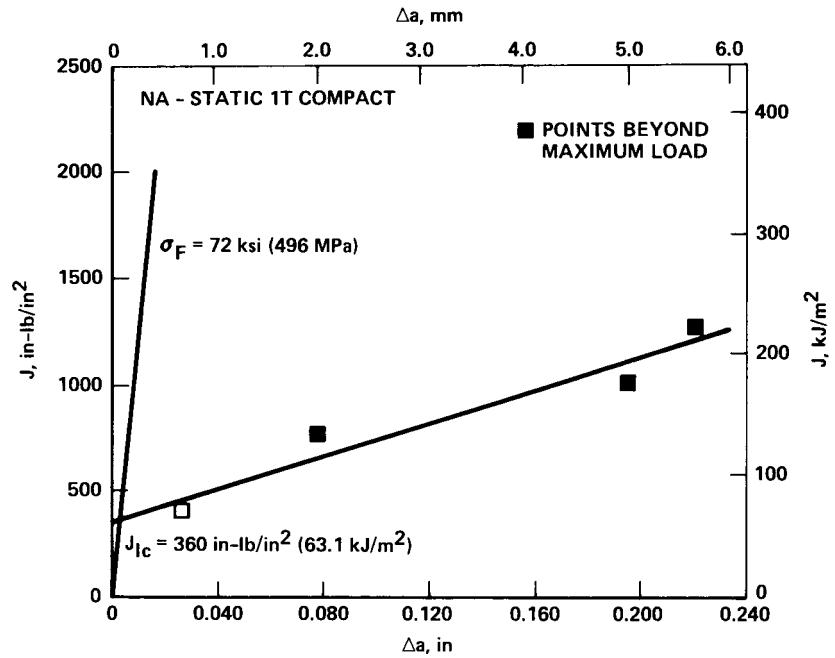

Figure 26. Quasi-Static 1T Compact J-Initiation for Heat NA at 350°F (177°C)

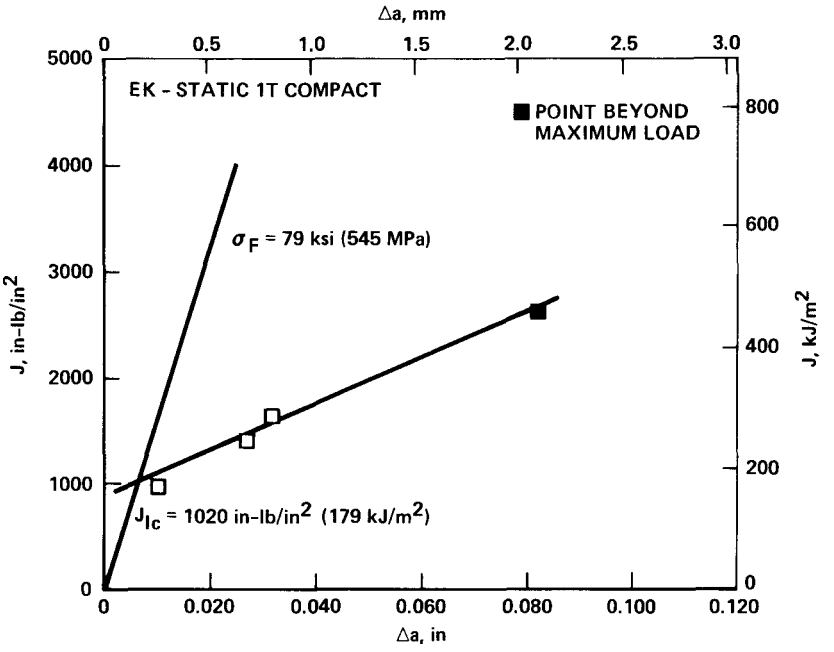

Figure 27. Quasi-Static 1T Compact J-Initiation for Heat EK at 350°F (177°C)

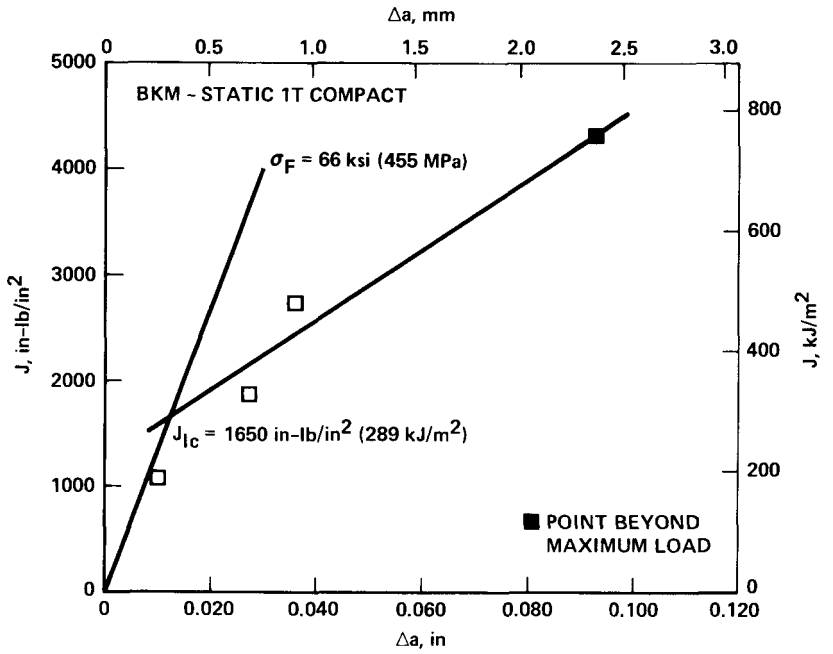

Figure 28. Quasi-Static 1T Compact J-Initiation for Heat BKM at 350°F (177°C)

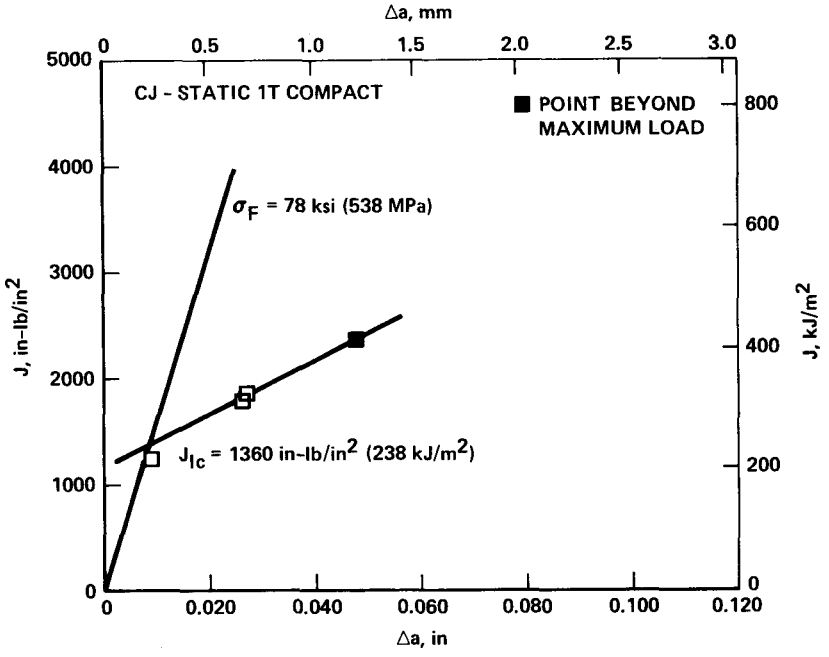

Figure 29. Quasi-Static 1T Compact J-Initiation for Heat CJ at 350°F (177°C)

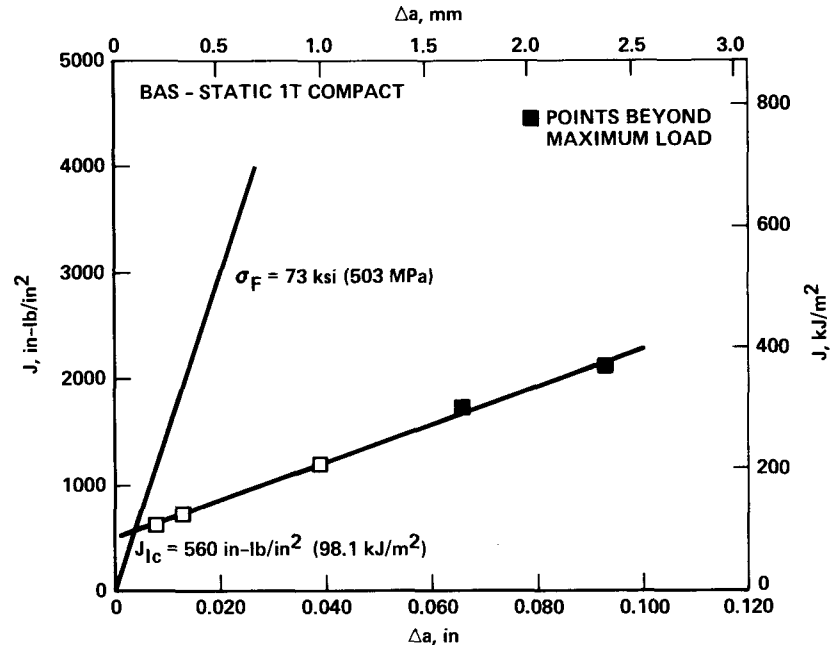

Figure 30. Quasi-Static 1T Compact J-Initiation for Heat BAS at 350°F (177°C)

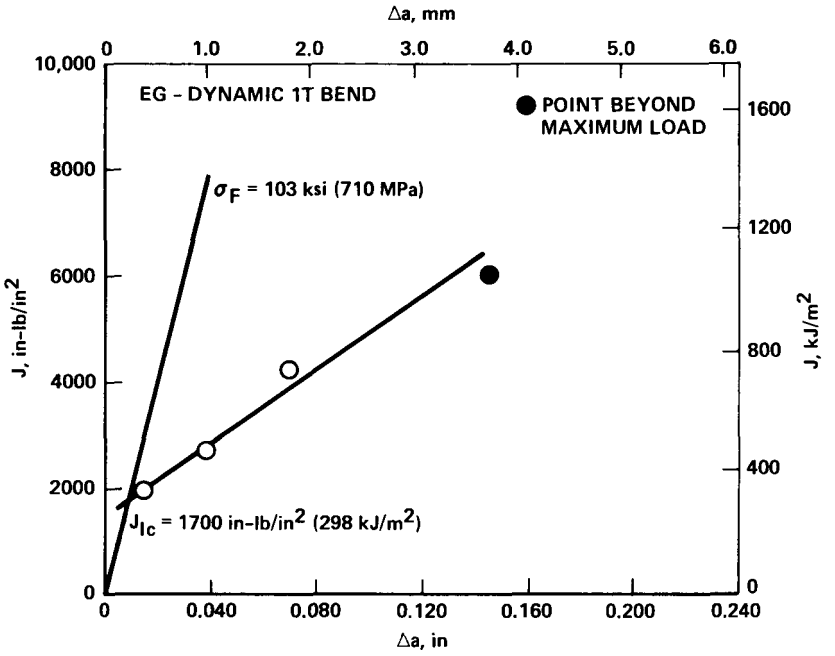

Figure 31. Impact Dynamic 1T Bend J-Initiation for Heat EG at 350°F (177°C)

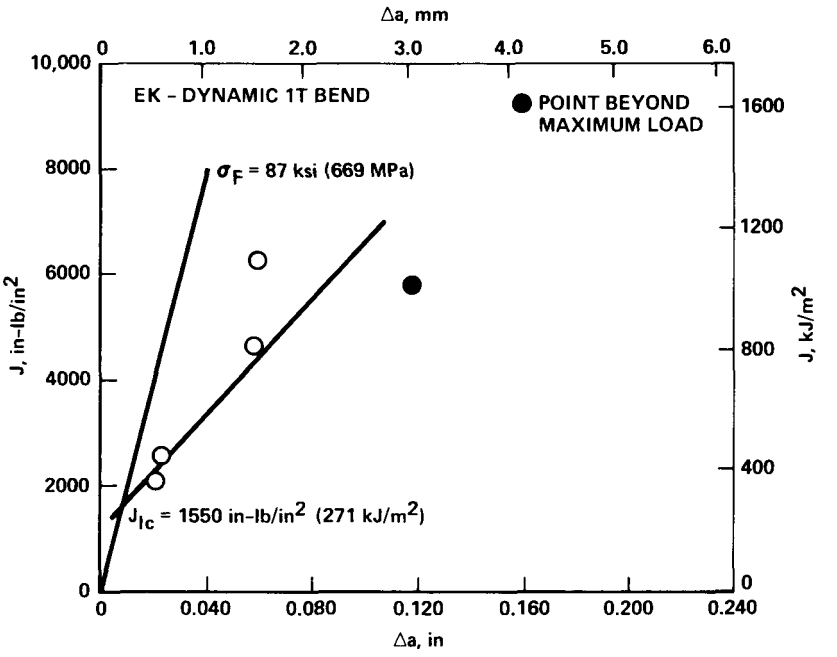

Figure 32. Impact Dynamic 1T Bend J-Initiation for Heat EK at 350°F (177°C)

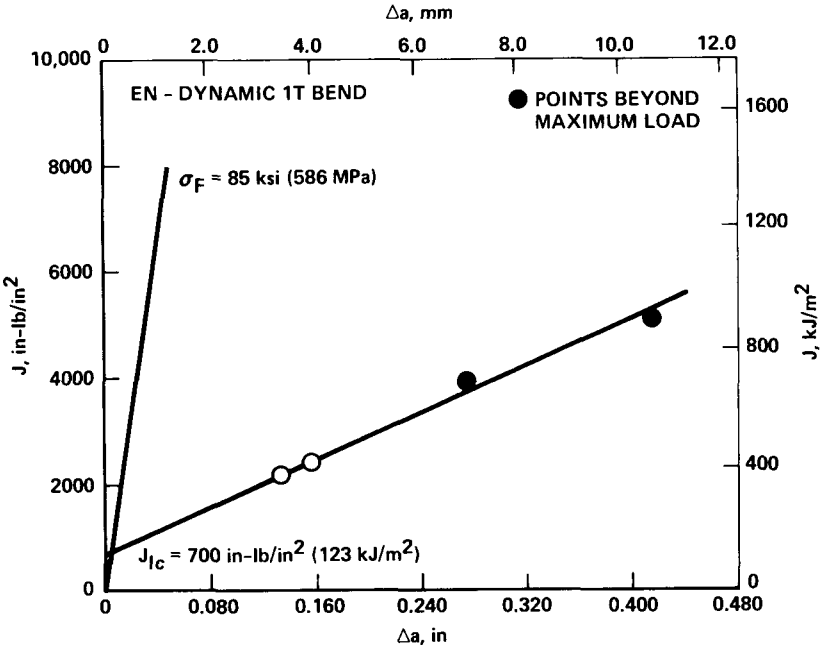

Figure 33. Impact Dynamic 1T Bend J-Initiation for Heat EN at 350°F (177°C)

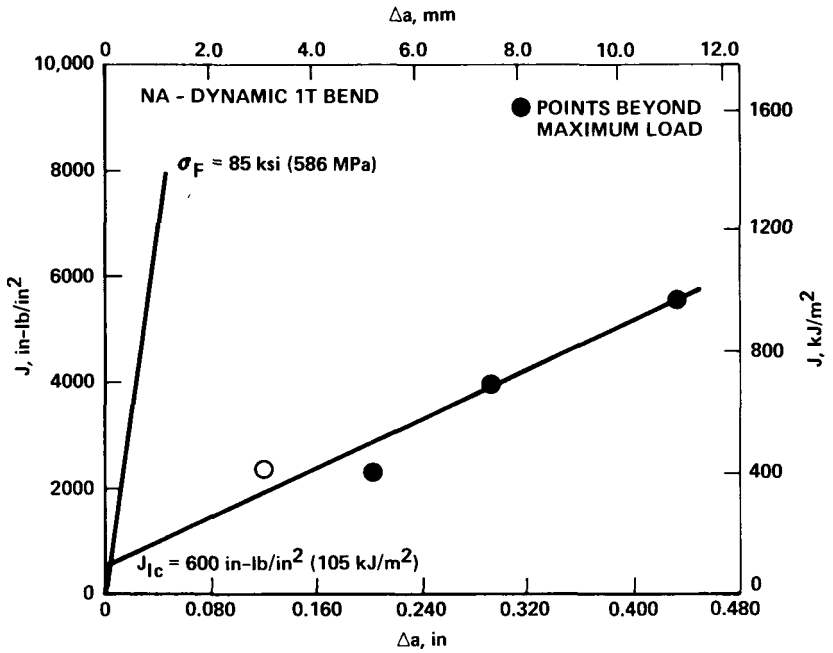

Figure 34. Impact Dynamic 1T Bend J-Initiation for Heat NA at 350°F (177°C)

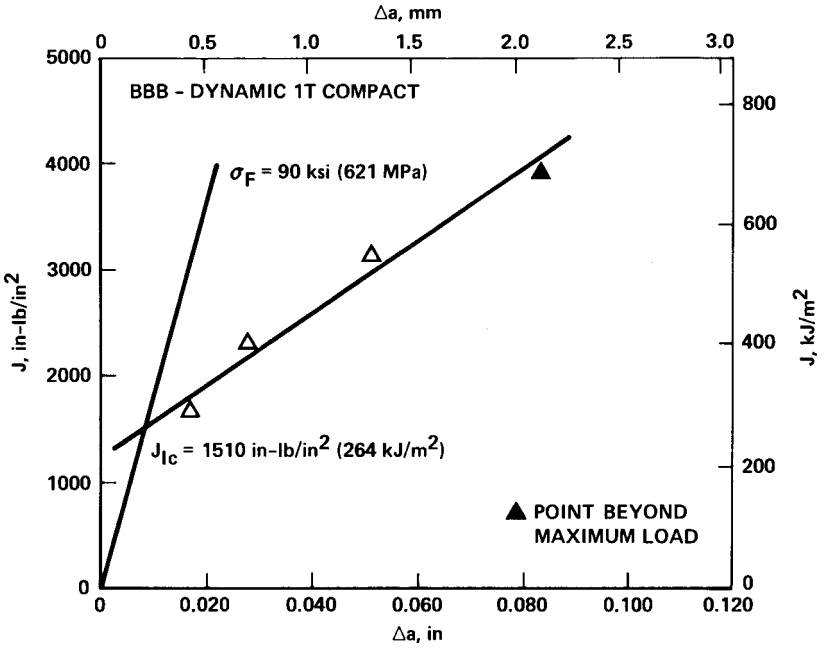

Figure 35. Intermediate Dynamic 1T Compact J-Initiation for Heat BBB at 350°F (177°C)

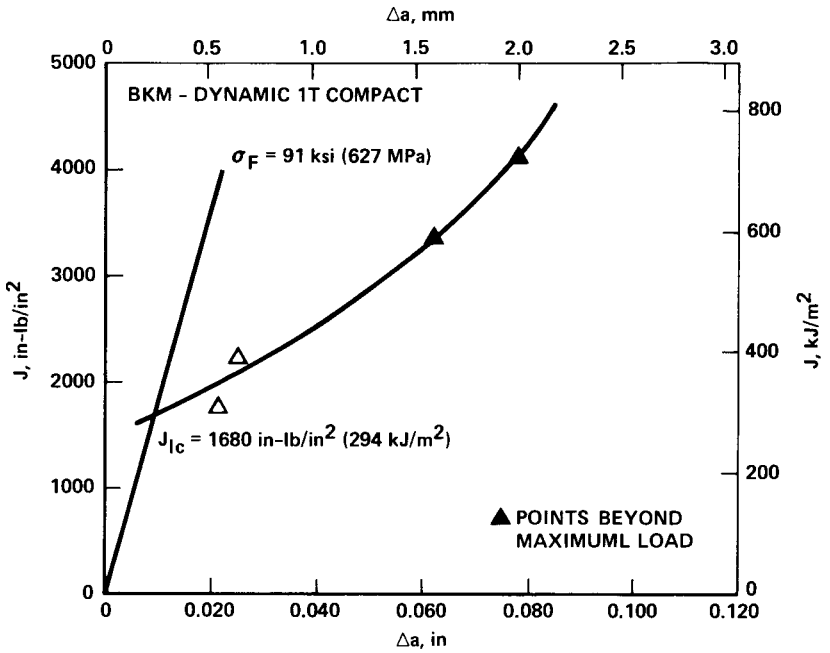

Figure 36. Intermediate Dynamic 1T Compact J-Initiation for Heat BKM at 350°F (177°C)

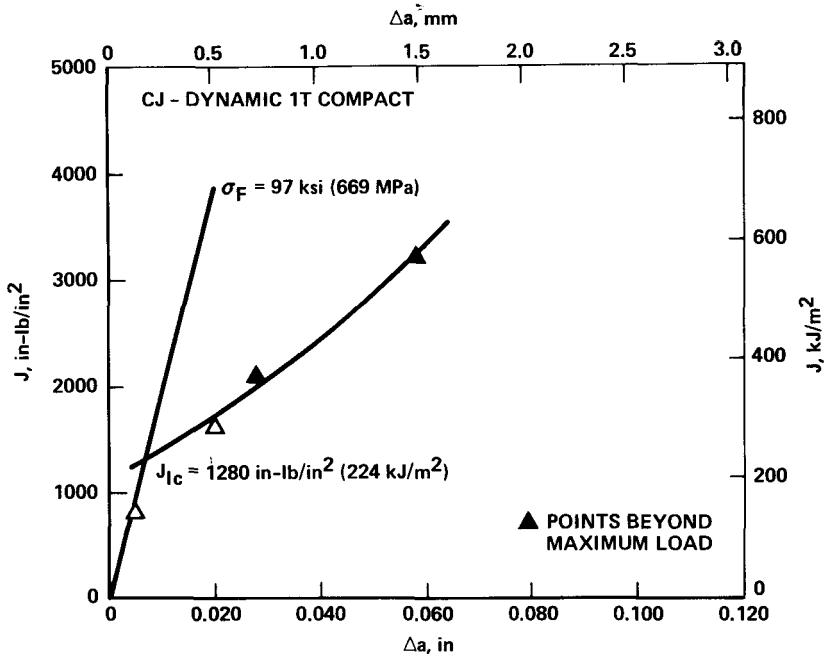

Figure 37. Intermediate Dynamic 1T Compact J-Initiation for Heat CJ at 350°F (177°C)

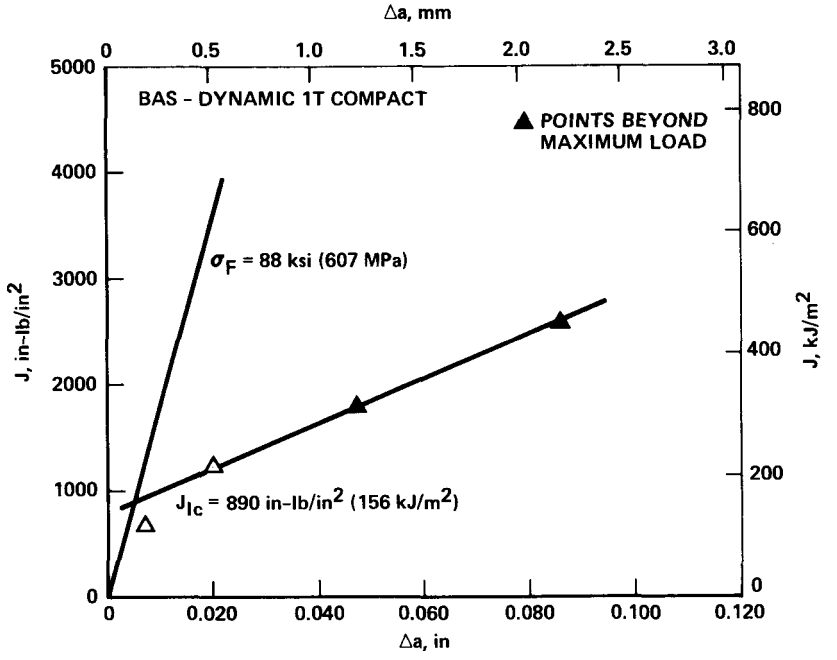

Figure 38. Intermediate Dynamic 1T Compact J-Initiation for Heat BAS at 350°F (177°C)

was used to calculate J. The credibility of using a corrected energy term (E_I') is shown in Figure 39 in which all of the upper shelf compact data and most of the compact data from the HSST Plate 02 tests are plotted. Note that the agreement is quite good and reproducible at all levels of energy. This agreement also adds credibility to the impact bend procedure in which a clip gage cannot be used. This technique may prove valuable for high temperature testing in which very expensive clip gages would be necessary.

The J_{Ic} results obtained in Figures 23-38 are tabulated in Table 4 and converted to K_{Jc} values. All of the values obtained meet the 50 J/σ_f (and therefore 25 J/σ_f) criterion except the BKM static result; the BKM static result does meet the 25 J/σ_f criterion, however. The upper shelf results are shown in comparison with previous data from the EPRI fracture toughness programs in Figures 40-47. The data for all but heat NA are from the original EPRI RP 232 program[7]. The data for heat NA was supplied by NRL[30,31]. In addition, J_{Ic} data from an adjunct EPRI program on heat CJ[32] are shown in Figure 46. Also shown in Figures 40-47 are the precracked Charpy upper shelf levels based upon initiation at maximum load (equivalent energy). Table 5 compares the precracked Charpy upper shelf levels (K_{PCCV}) with the initiation toughness values obtained in the current program. Also, Table 5 compares the difference in static toughness $K_{Jc}(s)$, and dynamic toughness, $K_{Jc}(d)$.

The results indicate that the dynamic R-curves are steeper than the static, and in all but two cases are substantially higher in magnitude than the static. The dynamic bend tests also tend to give slightly higher values than the dynamic compact (lower $\dot{K}$) tests, but this trend is difficult to assess quantitatively since different materials are involved in the comparison. The precracked Charpy level of toughness (initiation assumed at maximum load) is in all cases higher than the R-curve initiation toughness results obtained. However, as a very conservative approximation, the initiation level of toughness in the upper shelf region could

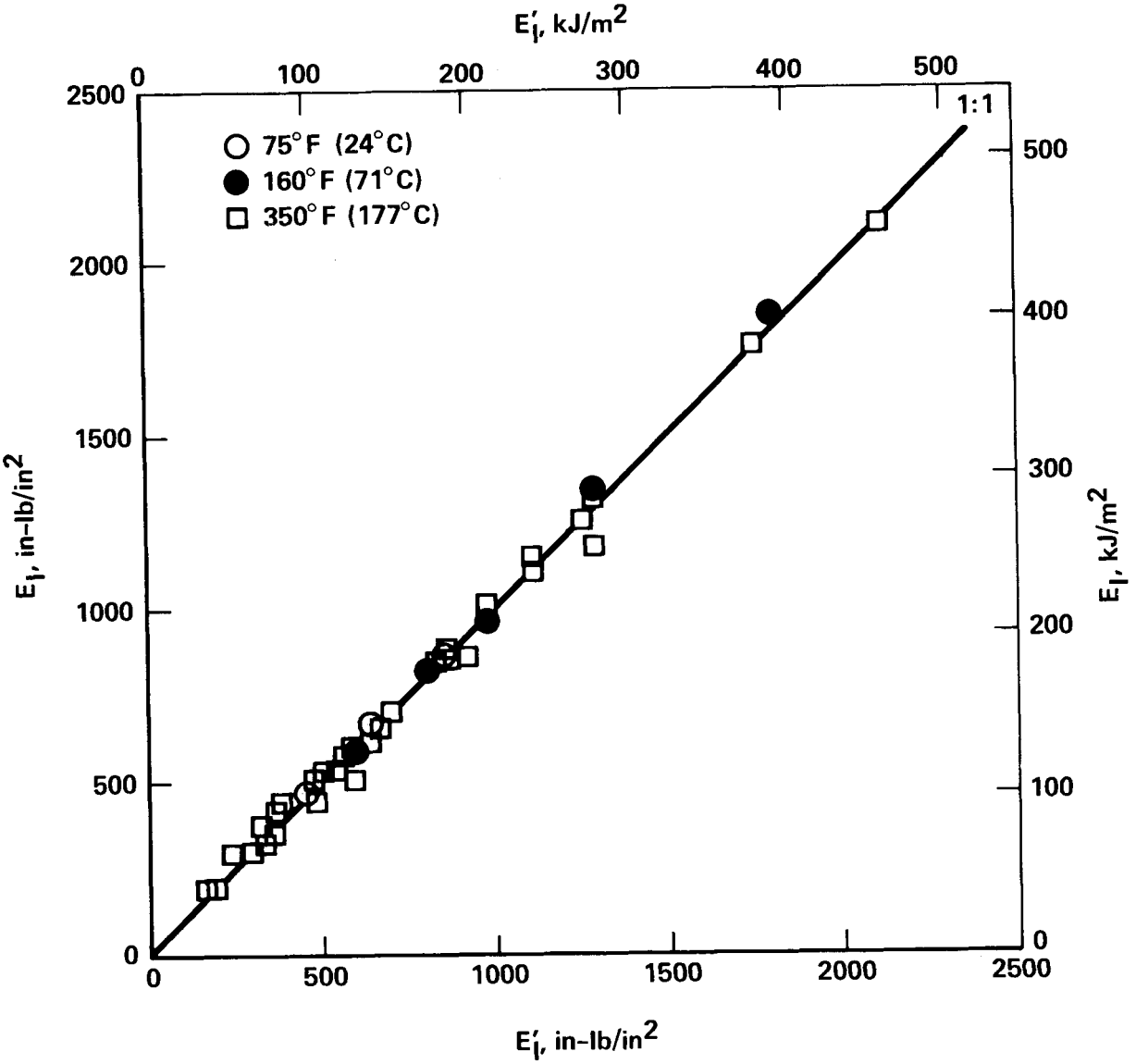

Figure 39. Correlation Between True Load-Line Energy and Ram LVDT-Corrected Energy

Table 4. J_{Ic} Results for Eight Heats Tested at 350°F (177°C)

HEAT	MATERIAL	$\dot{K}$ ksi-in$^{\frac{1}{2}}$/s (MN-m$^{-3/2}$/s)	J_{Ic} in-lb/in^2 (kJ/m^2)	K_{Jc} ksi-in$^{\frac{1}{2}}$ (MN-m$^{-3/2}$)
EG	A533B-1	<3 (3.3)	750 (131)	146 (160)
		~ 10^5 (10^5)	1700 (298)	220 (242)
BBB	A508-2	<3 (3.3)	1330 (233)	195 (214)
		~ 10^3 (10^3)	1510 (264)	208 (229)
EN	A302B	<3 (3.3)	390 (68.3)	106 (116)
		~ 10^5 (10^5)	700 (123)	141 (155)
NA	A302B	<3 (3.3)	360 (63.1)	101 (111)
		~ 10^5 (10^5)	600 (105)	131 (144)
EK	MMA Weld Metal (A533B-1 Base)	<3 (3.3)	1020 (179)	171 (188)
		~ 10^5 (10^5)	1550 (271)	211 (232)
BKM	MMA Weld Metal (A508-2 Base)	<3 (3.3)	1650* (289)	217 (238)
		~ 10^3 (10^3)	1680 (294)	219 (241)
CJ	SA Weld Metal (A533B01 Base)	<3 (3.3)	1360 (238)	197 (216)
		~ 10^3 (10^3)	1280 (224)	191 (210)
BAS	SA Weld Metal (A508-2 Base)	<3 (3.3)	560 (98.1)	127 (140)
		~ 10^3 (10^3)	890 (156)	160 (176)

* Does not meet a, b, $B \geq \frac{50J}{\sigma_f}$ validity criteria

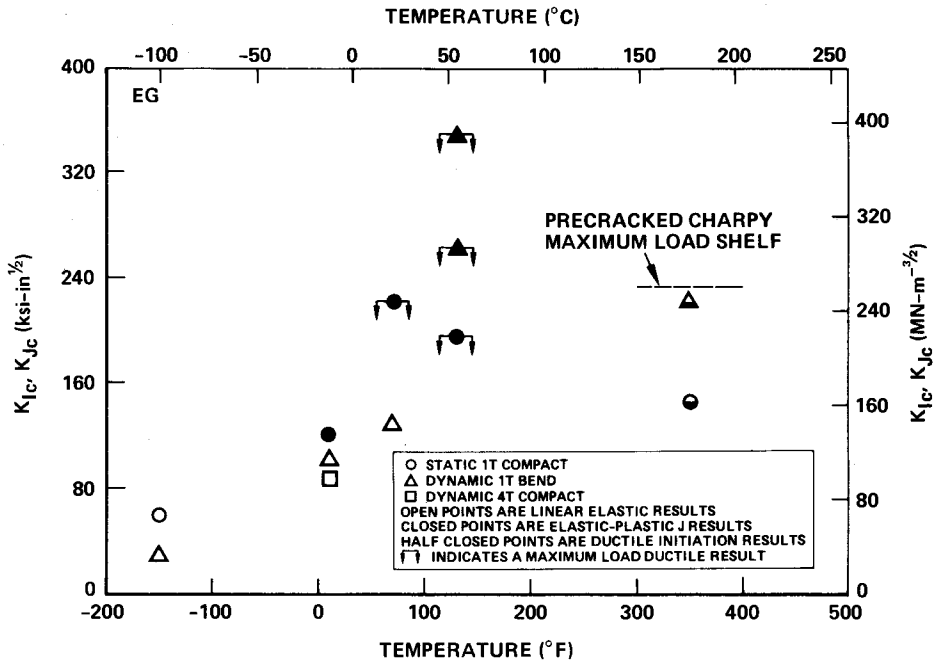

Figure 40. Comparison of Upper Shelf Initiation Results with Previous Results for Heat EG

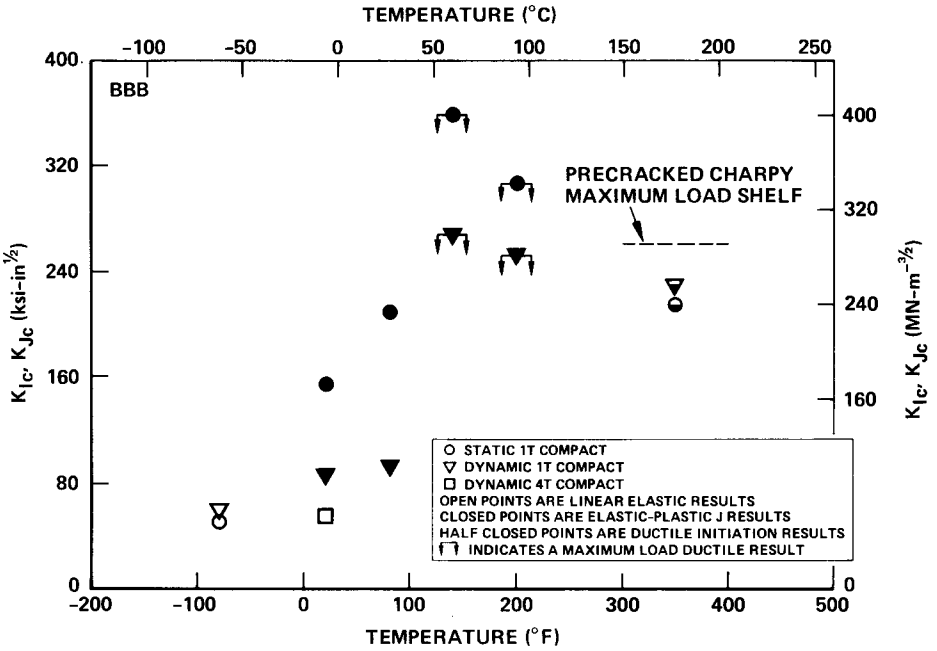

Figure 41. Comparison of Upper Shelf Initiation Results with Previous Results for Heat BBB

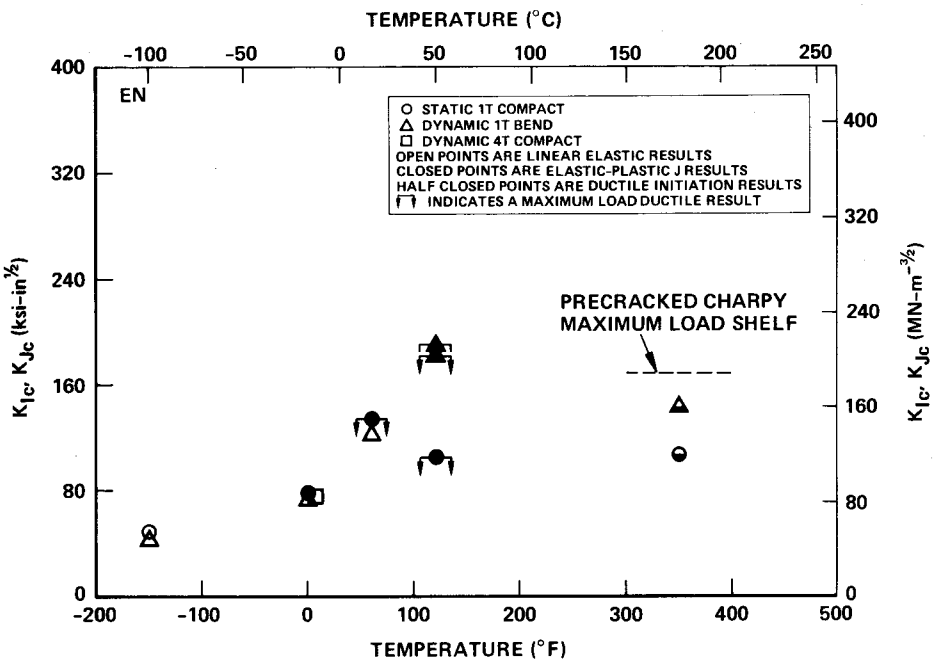

Figure 42. Comparison of Upper Shelf Initiation Results with Previous Results for Heat EN

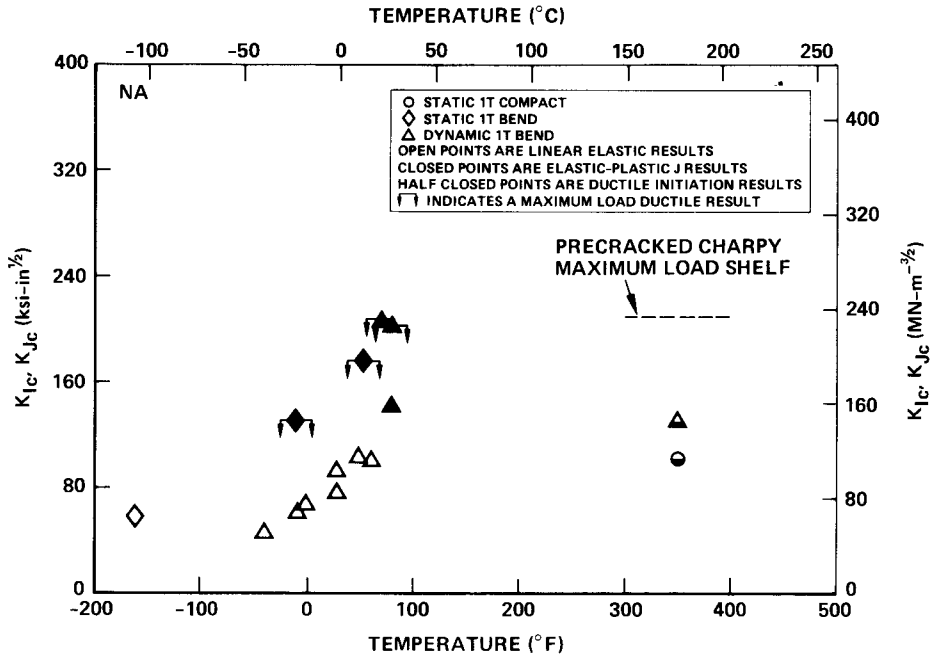

Figure 43. Comparison of Upper Shelf Initiation Results with Previous Results for Heat NA

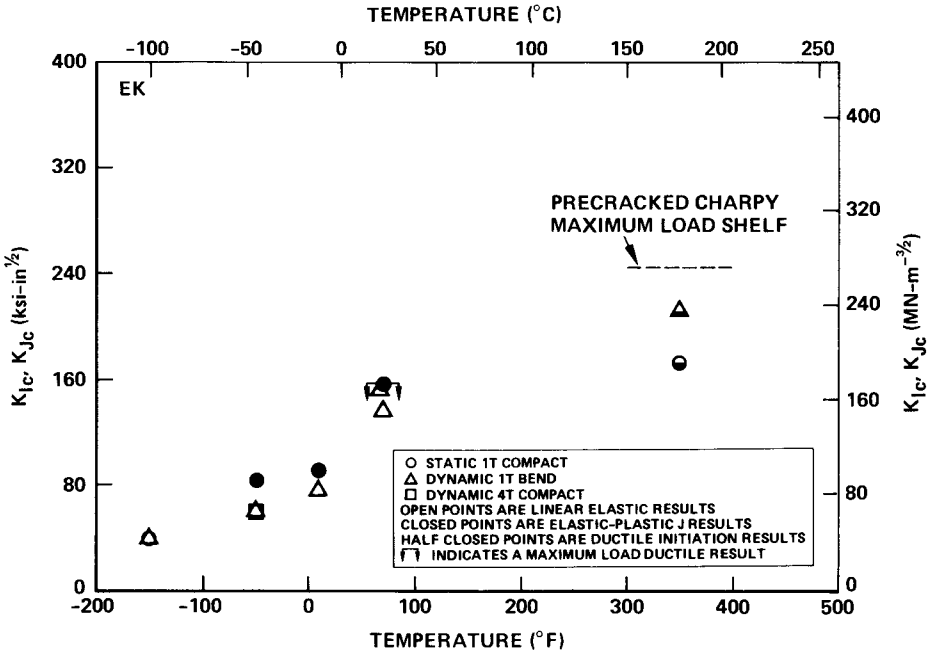

Figure 44. Comparison of Upper Shelf Initiation Results with Previous Results for Heat EK

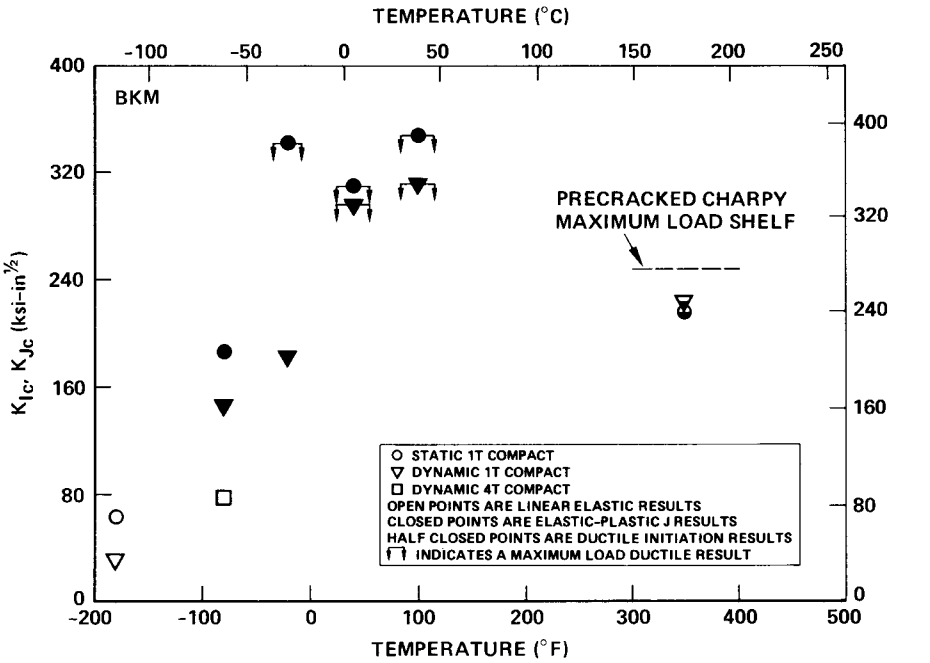

Figure 45. Comparison of Upper Shelf Initiation Results with Previous Results for Heat BKM

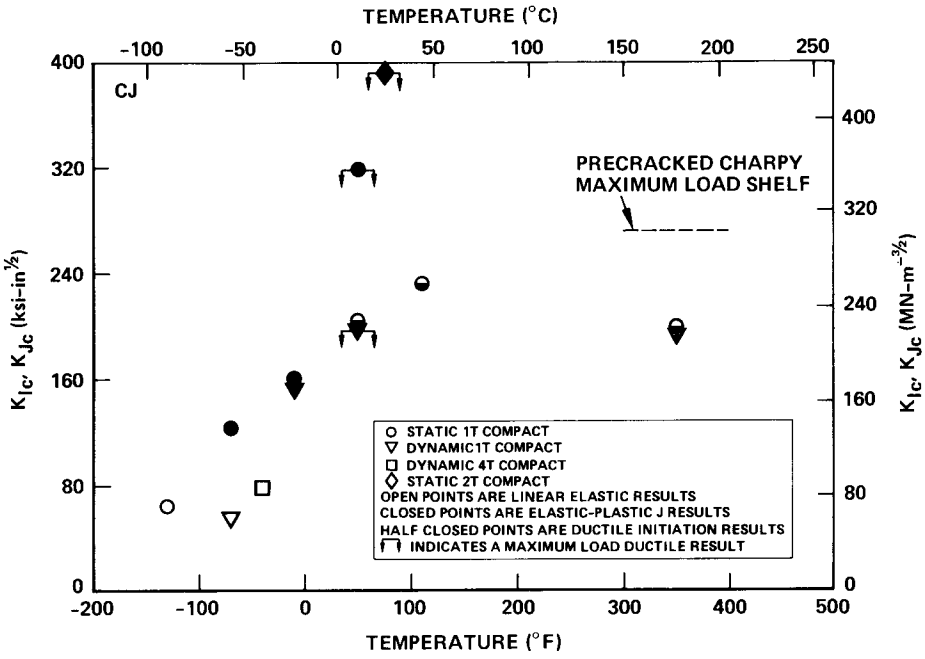

Figure 46. Comparison of Upper Shelf Initiation Results with Previous Results for Heat CJ

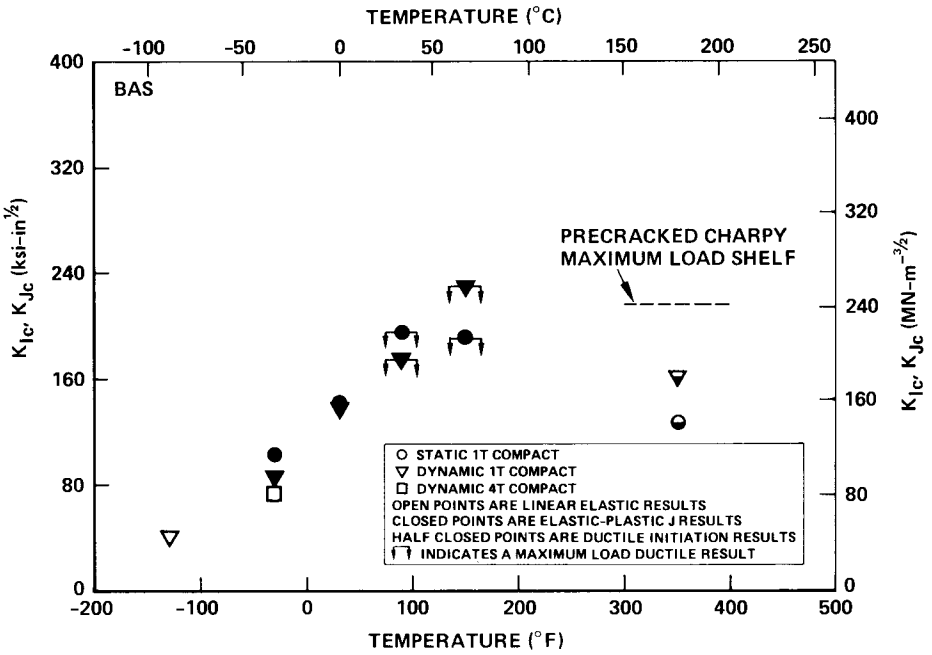

Figure 47. Comparison of Upper Shelf Initiation Results with Previous Results for Heat BAS

Table 5. Comparison of K_{Jc} Initiation Values With Charpy and Precracked Charpy Upper Shelf Levels

HEAT	TEST TYPE	K_{Jc} ksi-in$^{1/2}$ (MN-m$^{-3/2}$)	Charpy Upper Shelf ft-lbf (J)	$K_{PCCV_{1/2}}$ ksi-in$^{1/2}$ (MN-m$^{-3/2}$)	$K_{PCCV} - K_{Jc}$ ksi-in$^{1/2}$ (MN-m$^{-3/2}$)	$K_{Jc}(d)-K_{Jc}(s)$ ksi-in$^{1/2}$ (MN-m$^{-3/2}$)
EG	Static Compact Dynamic Bend	146 (160) 220 (242)	92 (125)	233 (256)	87 (96) 13 (14)	74 (82)
BBB	Static Compact Dynamic Compact	195 (214) 208 (229)	112 (152)	262 (288)	67 (74) 54 (59)	13 (15)
EN	Static Compact Dynamic Bend	106 (116) 141 (155)	44 (60)	169 (186)	63 (70) 28 (31)	35 (39)
NA	Static Compact Dynamic Bend	101 (111) 131 (144)	52 (71)	210 (231)	109 (120) 79 (87)	30 (33)
EK	Static Compact Dynamic Bend	171 (188) 211 (232)	101 (137)	244 (268)	73 (80) 33 (36)	40 (44)
BKM	Static Compact Dynamic Compact	217 (238) 219 (241)	142 (193)	247 (271)	30 (33) 28 (30)	2 (3)
CJ	Static Compact Dynamic Compact	197 (216) 191 (210)	128 (174)	272 (299)	75 (83) 81 (89)	-6 (-6)
BAS	Static Compact Dynamic Compact	127 (140)) 160 (176)	77 (104)	216 (237)	89 (98) 56 (61)	33 (37)

be obtained by measuring the precracked Charpy equivalent energy toughness and subtracting 100 ksi-in$^{1/2}$ (110 MN-m$^{-3/2}$) for static initiation toughness and 80 ksi-in$^{1/2}$ (88 MN-m$^{-3/2}$) for dynamic initiation toughness.

Problem Areas in J_{Ic} R-Curve Testing

There is some controversy regarding the use of the value of 2 in Equation 18. Sumpter and Turner[33] and Merkel and Corten[34] have indicated that the energy should be broken into elastic and plastic components when shallow precrack depths are used; i.e., small a/w ratios. However, for a/w $\geq$ 0.5 a single term is adequate when the following items are considered.

First, there is the question of subtracting out the uncracked body energy in the three-point bend test[35]. For an a/w = 0.5, 35% of the total elastic energy is due to the uncracked body. The error associated with including the uncracked body energy becomes very important at low values of E_i, such as those obtained for the A302B steel. The uncracked body energy (U) is equal to

$$U = \frac{10\ p^2}{EB} \quad , \tag{20}$$

and for the typical cases of interest in this program the value of U results in a reduction in energy of approximately 85 in-lb/in^2 (32.4 kJ/m^2) when normalized for B and b, i.e., $\frac{U}{Bb}$. However, the need to separate out the uncracked body energy has not been resolved[36,37]. The effect of reducing the bend J_{Ic} results by 170 in-lb/in^2 (64.8 kJ/m^2) is indicated in Figure 48 by the arrows for the compact specimen results.

The second effect to be considered is the inclusion of axial forces in the compact specimen test[34]. For an a/w between 0.50 and 0.55, Equation 18 becomes

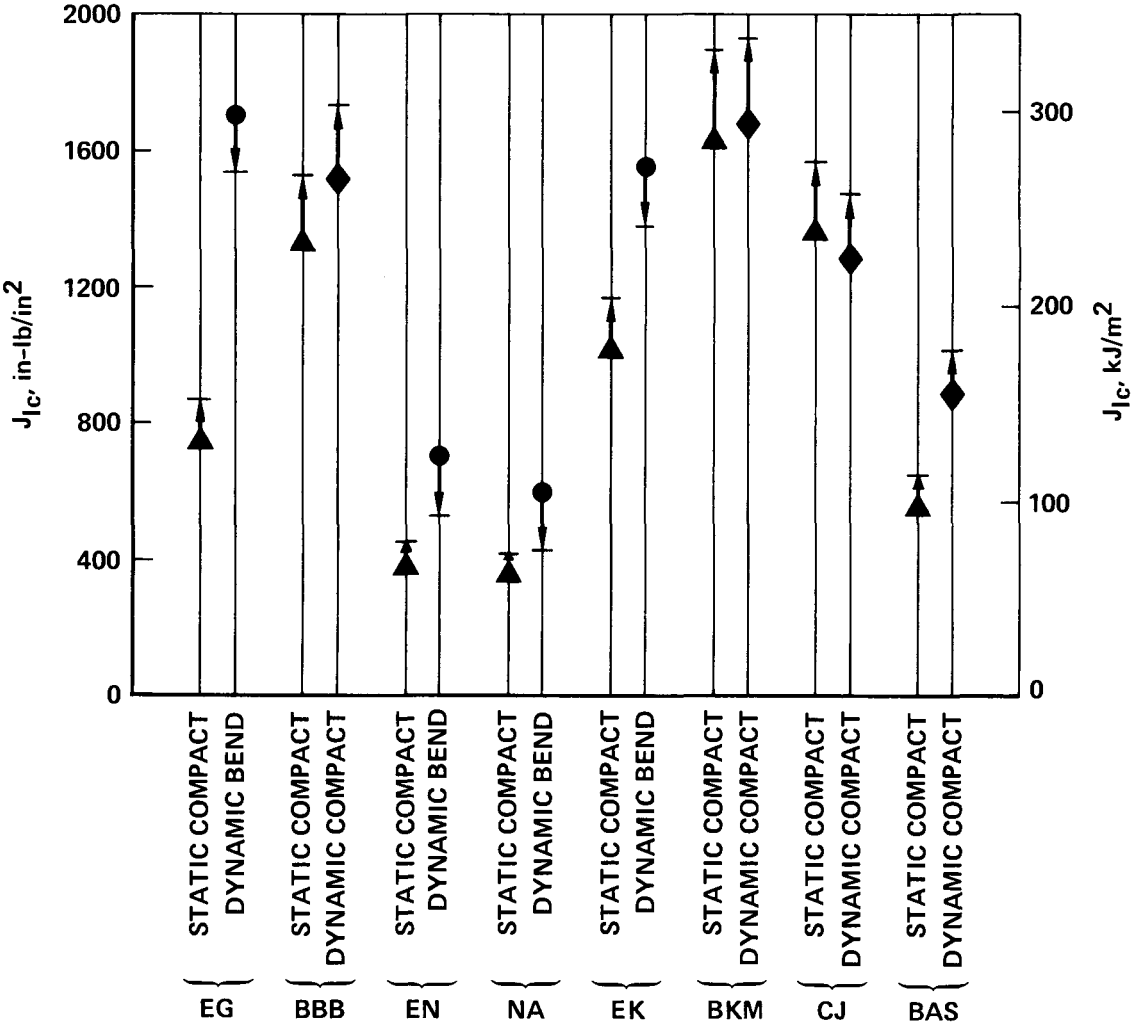

Figure 48. Effect of Correcting the J_{Ic} Values for Uncracked Beam Energy and Axial Forces

$$J = \frac{2.3\ E_i}{bB} \quad . \tag{21}$$

Thus, J increases by approximately 15% for the compact specimen. This increase is also indicated by arrows in Figure 48.

The consequences of including the corrections noted are rather negligible. Except for the heats EN and NA (A302B) the trends in the data remain the same. For the A302B material, the results for static and dynamic tests come together due to the offsetting corrections. Since there is still divided opinion among the technical community concerning these corrections, the original values based on Equation 18 will be considered correct at this point.

There is a further problem related to the statistics of the curve fit to the R-curve data. As a cursory look at the statistics, straight line curve fits were made to the data which were not on the stretch zone (blunting) line. The variance about the linear fit and the number of degrees of freedom are listed in Tables 6 and 7. Note that the number of degrees of freedom is equal to the number of points minus 2. Therefore, in several cases only 1 degree of freedom is possible. The linear fit was then intersected to the blunting line ($J = 2\sigma_f \Delta a$) assuming that this line was known with 100% certainty. The intersection point designated J_i is also listed in Tables 6 and 7 compared to the J_{Ic} values from the manual fits. Any abnormal discrepancy between values of J_i and J_{Ic} are footnoted explaining the difference. Using the t-distribution for 95% confidence, weighted limits of J_i were obtained[38] and are listed in Tables 6 and 7.

It is obvious from Tables 6 and 7 that it is necessary to have as many degrees of freedom as possible and that the variance of the straight line fit should be as low as possible. Therefore, some guidelines related

Table 6. Statistical Analysis of R-Curve Procedure for Eight Heats Tested at 350°F (177°C)

HEAT	TEST TYPE	VARIANCE $[in\text{-}lb/in^2]^2$ ($[kJ/m^2]^2$)	DEGREES OF FREEDOM	J_i $in\text{-}lb/in^2$ (kJ/m^2)	95% CONF. LIMIT $in\text{-}lb/in^2$ (kJ/m^2)	J_{IC} $in\text{-}lb/in^2$ (kJ/m^2)
EG	Static Compact	7.39×10^4 (2.27×10^3)	2	548 (96)	279 (49)	750* (131)
	Dynamic Bend	1.19×10^5 (3.65×10^3)	2	1943 (340)	362 (63)	1700 (298)
BBB	Static Compact	1.83×10^3 (5.61×10^1)	1	1306 (229)	171 (30)	1330 (233)
	Dynamic Compact	3.98×10^4 (1.22×10^3)	2	1578 (276)	202 (35)	1510 (264)
EN	Static Compact	2.89×10^3 (8.86×10^1)	2	383 (67)	57 (10)	390 (68)
	Dynamic Bend	2.90×10^4 (8.89×10^2)	2	853 (149)	180 (32)	700 (123)
NA	Static Compact	1.49×10^4 (4.57×10^2)	2	378 (66)	129 (23)	360 (63)
	Dynamic Bend	3.29×10^5 (1.01×10^4)	2	680 (119)	605 (106)	600 (105)
EK	Static Compact	5.22×10^4 (1.60×10^3)	2	1014 (178)	234 (41)	1020§ (179)
	Dynamic Bend	1.74×10^6 (5.34×10^4)	3	2696 (297)	811 (142)	1550§ (271)
BKM	Static Compact	1.59×10^5 (4.88×10^3)	1	1651 (289)	1609 (282)	1650* (289)
	Dynamic Compact	1.60×10^4 (4.91×10^2)	2	1322 (232)	126 (22)	1680* (294)
CJ	Static Compact	3.65×10^3 (1.12×10^2)	2	1267 (222)	58 (10)	1360† (238)
	Dynamic Compact	1.28×10^4 (3.93×10^2)	1	1076 (188)	426 (75)	1280* (224)
BAS	Static Compact	2.55×10^3 (7.82×10^1)	3	552 (97)	31 (5)	560 (98)
	Dynamic Compact	8.24×10^1 (2.53)	1	939 (164)	36 (6)	890 (156)

* Not a linear curve fit resulting in a higher intersection point

§ Lowest points were weighted heavily lowering the straight line intersection point

† Did not weight lowest points as heavily in the straight line fit resulting in a higher intersection point

Table 7. Statistical Analysis of R-Curve Procedure for HSST Plate 02 Material

TEST TYPE	TEMPERATURE ^{o}F (^{o}C)	$\dot{K}$ ksi-in$^{1/2}$/s (MN-m$^{-3/2}$/s)	VARIANCE [in-lb/in^2]^2 ([kJ/m^2]^2)	DEGREES OF FREEDOM	J_i in-lb/in^2 (kJ/m^2)	95% CONF LIMIT in-lb/in^2 (kJ/m^2)	J_{Ic} in-lb/in^2 (kJ/m^2)
PCCV	75-80 (24-27)	<3 (3.3)	3.94×10^{3} (1.21×10^{2})	4	1889 (331)	25 (4)	1750[§] (306)
	75-80 (24-27)	~10^4 (10^4)	5.02×10^{4} (1.54×10^{3})	3	1893 (332)	122 (21)	2000 (350)
	160 (71)	<3 (3.3)	7.25×10^{5} (2.22×10^{3})	4	1928 (338)	117 (20)	1800 (315)
	160 (71)	~10^3 (10^3)	1.43×10^{3} (4.39×10^{2})	3	1630 (285)	223 (39)	1500[†] (262)
	160 (71)	~10^5 (10^5)	8.29×10^{3} (2.54×10^{2})	3	1326 (232)	52 (9)	1550[†] (271)
0.394T Bend	78 (26)	<3 (3.3)	1.64×10^{5} (5.03×10^{3})	3	1756 (308)	245 (43)	1900[*] (333)
	160 (71)	~10^5 (10^5)	2.76×10^{4} (8.47×10^{2})	2	838 (147)	163 (29)	1550[*] (271)
1T Bend	160 (71)	~10^5 (10^5)	1.53×10^{6} (4.69×10^{4})	4	1373 (240)	554 (97)	1800[*] (315)
1T Compact	75-80 (24-27)	<3 (3.3)	7.94×10^{4} (2.44×10^{3})	6	960 (168)	82 (14)	1350[*] (236)
	160 (71)	<3 (3.3)	9.61×10^{4} (2.95×10^{3})	2	1465 (257)	317 (56)	1790[*] (313)
	160 (71)	~10^3 (10^3)	3.62×10^{4} (1.11×10^{3})	3	1136 (199)	115 (20)	1320[*] (231)

[§] Lowest points were weighted more heavily lowering the straight line intersection point

[†] Lowest point was not weighted as heavily raising the intersection point

[*] Not a linear curve fit resulting in a higher intersection point

to the number of points required and the scatter about the points are necessary. Because of the limited amount of data for each fit, the variance values may be artificially high; if an assumption is made that the scatter about the R-curves for all heats of material is from the same population, the 95% confidence limits about any curve can possibly be reduced. However, the validity in making this assumption must be explored in detail.

Another area needing further work is the use of the blunting line itself. In the preceding statistical analysis, the line was assumed to be known with 100% confidence. If there is any doubt in the slope of this line, the confidence limits about J_i will be enlarged. The J versus Δa curve in reality is probably a smooth curve similar to a tensile stress-strain curve through yielding. The idea of finding a value of J_{Ic} is quite similar to finding the proportional limit. Future work in obtaining a proportional limit-type J_{Ic} may be of benefit.

After the completion of the testing and data analysis phase of the current program, an ASTM Task Group meeting on Elastic-Plastic Fracture Mechanics (E24.01.09) was held in Philadelphia (October, 1976). The main topic of the committee meeting was the development of a new procedure for R-curve J_{Ic} testing. This new procedure would limit the range of crack extension (Δa) used to fit an R-curve and specifies that a linear fit be used. In addition, a minimum of four data points are required to determine the linear extrapolation back to the blunting line. The new procedure allows points to be disallowed if they fall outside certain limits. This new procedure will in general require testing more specimens than have been tested in the past for establishing an R-curve, such as in the current program. However, this new procedure is very preliminary and it may be several years before it is fully documented and accepted by ASTM.

Fracture Toughness Correlations

The primary objective of small specimen fracture mechanics as applied to the nuclear industry is the prediction of thick section behavior. The fracture behavior of large section sizes can be inferred from direct

measurements of elastic-plastic fracture toughness using small fracture mechanics specimens such as the precracked Charpy or 1T compact specimen, as has just been shown. Thick section behavior can also be inferred from empirical correlations between "valid" elastic or elastic-plastic fracture toughness values and data from simple and less expensive tests, such as the Charpy V-notch test. This latter approach is currently being used to determine the continued reliability of operating reactors with respect to radiation embrittlement, since current surveillance programs are almost entirely dependent on Charpy V-notch data. The results of the EPRI RP 232 program and the current program were reviewed with respect to existing empirical fracture toughness correlations with the objective of verifying the existing correlations or developing new correlations to extend the applicability of small specimen fracture mechanics.

The most widely used correlations in the past have been those between fracture toughness (K_{Ic}, K_{Id}) and Charpy V-notch energy (C_V). Empirical correlations have been developed in an attempt to combine the technical merits of the fracture mechanics approach (K_{Ic}) with the economic merits of the transition temperature approach (C_V). The many theoretical objections to the existence of a correlation between a sharp-notched (and sometimes slow) fracture mechanics test and a dynamic, blunt-notched Charpy test have been presented by Wullaert, et al[39] and will not be reviewed here. The existing K_{Ic}, K_{Id} - C_V correlations are listed in Table 8. A graphical presentation of the correlations listed in Table 8 is shown in Figure 49. The solid portion of the curves in Figure 49 represent the range over which data existed to determine the correlation shown. The dashed portion of the curves represents an extrapolation of the original correlation. Note the values of elastic modulus (E) and dynamic yield strength (σ_{yd}) that were assumed for the Barsom, Rolfe and Novak correlations[40]. Dynamic yield strength was used because the curves are being compared to dynamic fracture toughness data. A dynamic yield strength of 90 ksi (620 MPa) is considered a reasonable assumption for all of the EPRI materials except the A540 bolting material, which has a dynamic yield strength of approximately 150 ksi (1034 MPa).

Table 8. Existing Charpy Energy - Fracture Mechanics Correlations for Steels

Barsom, Rolfe, and Novak (Eleven structural steels)[40] --BRN

1. $\frac{K_{Ic}^2}{E} = 2(C_V)^{3/2}$ — Lower shelf and transition region σ_y = 39 to 246 ksi (270 to 1700 MPa)

2. $\left(\frac{K_{Ic}}{\sigma_y}\right)^2 = 5\left[\frac{C_V}{\sigma_y} - 0.05\right]$ — Upper shelf, σ_y = 100 to 246 ksi (690 to 1700 MPa)

Corten and Sailors (USS data plus HSST data)[41] --C&S

3. $K_{Ic} = 15.5\ (C_V)^{1/2}$ — Lower shelf, transition region

4. $K_{Id} = 15.873\ (C_V)^{0.375}$ — Lower shelf, transition region

Note that the constants in the above equations only apply when the English units for the parameters are as follows:

1. $K_{Ic} \equiv$ psi-in$^{\frac{1}{2}}$; $E \equiv$ psi; $C_V \equiv$ ft-lbf
2. $K_{Ic} \equiv$ ksi-in$^{\frac{1}{2}}$; $\sigma_y \equiv$ ksi; $C_V \equiv$ ft-lbf
3&4. $K_{Ic} \equiv$ ksi-in$^{\frac{1}{2}}$; $C_V \equiv$ ft-lbf

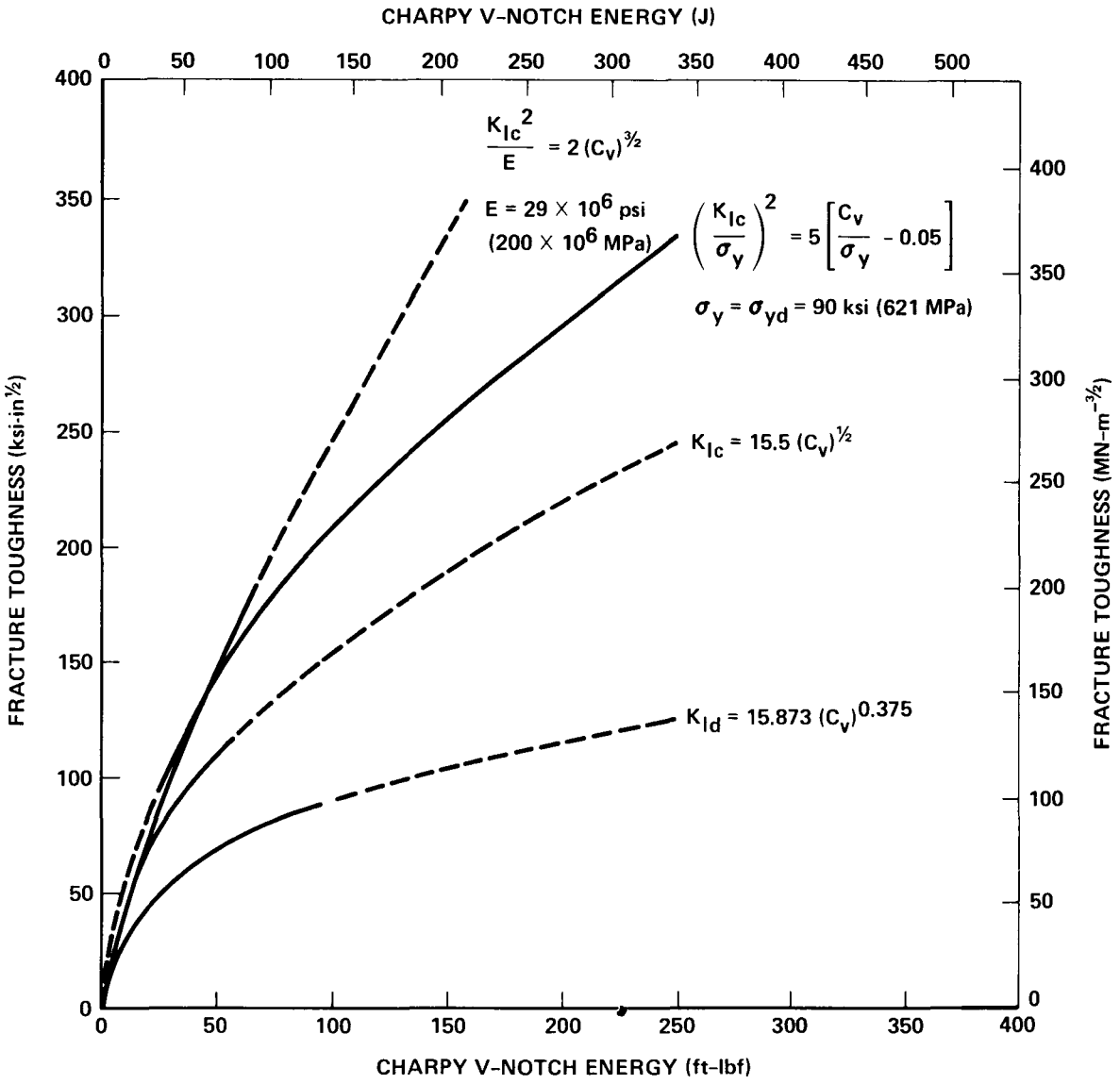

Figure 49. Comparison of Existing Toughness-Energy Correlations

The EPRI fracture toughness data bank was used to extract the pre-cracked Charpy upper shelf fracture toughness (K_d^*) for each heat and the corresponding upper shelf Charpy V-notch energy. Figure 50 shows the relationship between K_d^* (equivalent energy toughness) and Charpy V-notch upper shelf energy for over fifty heats of pressure vessel steels. Note that the equivalent energy toughness values are based on maximum load and may not represent true initiation toughness. All but one of the EPRI data points fall above the Barsom, Rolfe and Novak upper shelf correlation curve. There are two reasons for this trend. One is that dynamic fracture toughness is greater than static fracture toughness in the upper shelf region, as has been shown in the previous section. The other is that the equivalent energy analysis assumes that crack initiation occurs at maximum load. Since the current program has clearly shown that cracks initiate prior to maximum load on the upper shelf, the use of maximum load energy to calculate equivalent energy toughness gives K_d^* values that are too high. It is interesting to note that the extrapolation of the Barsom, Rolfe and Novak transition region correlation fits the EPRI upper shelf K_d^* data better than their upper shelf correlation.

The EPRI data points shown in Figure 50 were fitted with a curve to describe the relationship between dynamic fracture toughness and Charpy V-notch upper shelf energy. The curve can be described in English units by the equation

$$K_d^* = 26\ (C_V)^{0.5} \quad . \tag{22}$$

This relationship represents an "overall" correlation for the EPRI data and may be useful for a rough approximation of upper shelf equivalent energy fracture toughness.

As an attempt to develop a fracture toughness correlation for a specific material, data from the 13 heats of A533B-1 steel in the EPRI program were studied. The correlation between transverse Charpy V-notch energy and transverse dynamic fracture toughness is shown in Figure 51.

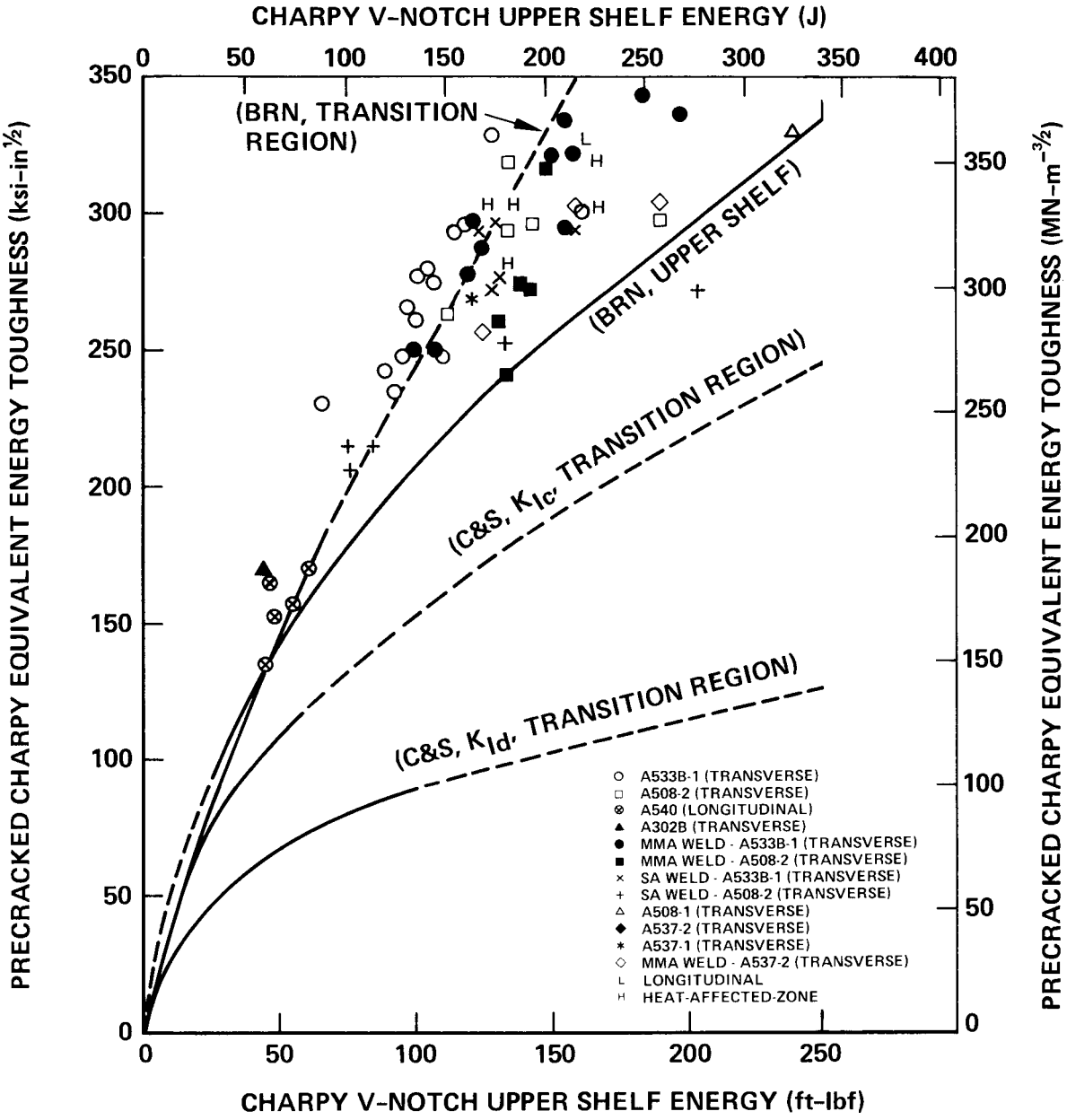

Figure 50. Comparison of EPRI Upper Shelf Data with Existing Correlations

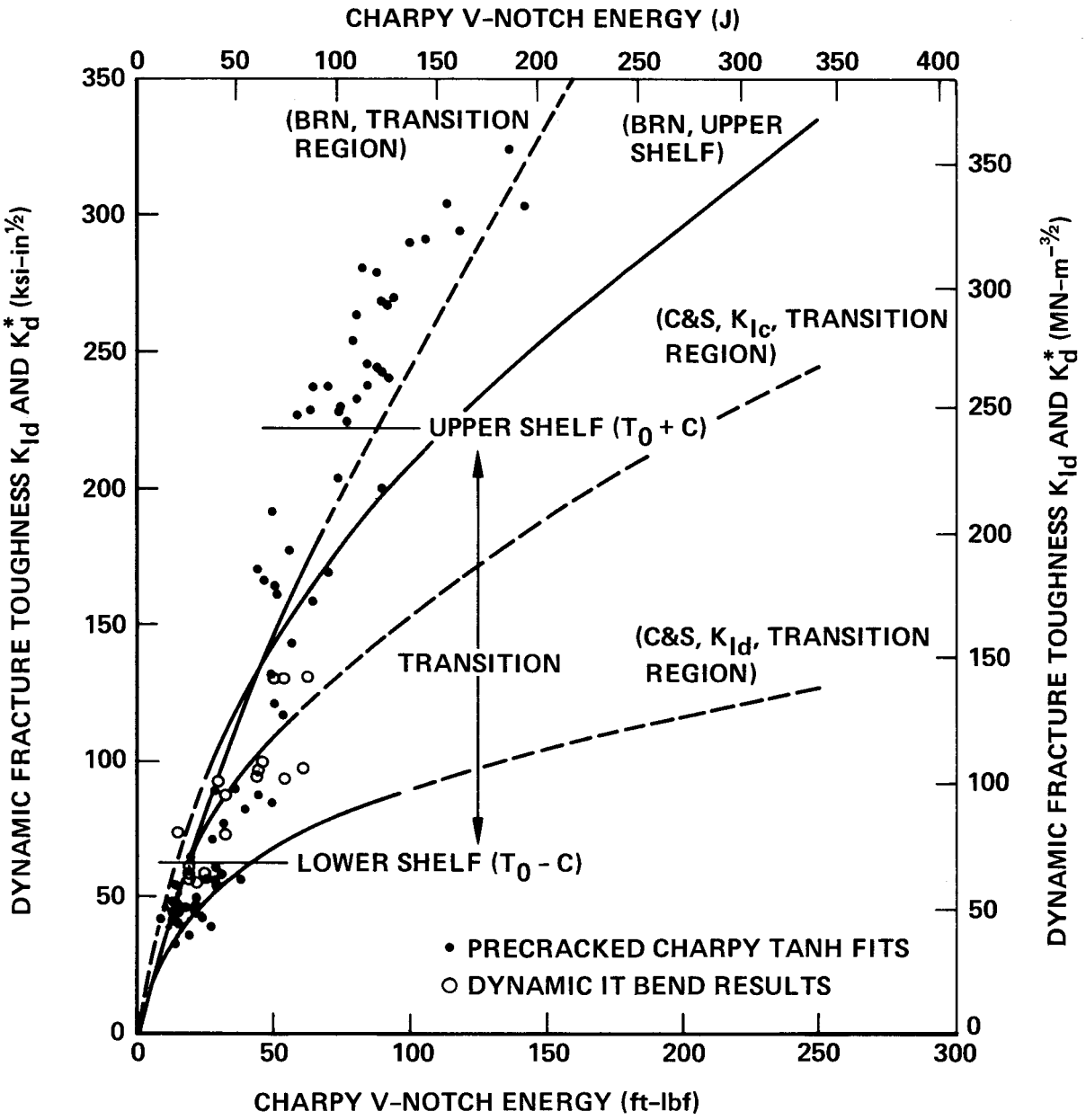

Figure 51. Comparison of EPRI A533B-1 Steel Data with Existing Correlations

Points shown below the lower shelf line are linear elastic K_{Id} values. All points above this line are K_d^* values. Note that both precracked Charpy and dynamic (1T) bend fracture toughness data are used in the figure. Toughness values below the upper shelf (T_0 + C) line are mostly cleavage initiation at maximum load with little or no subcritical ductile tearing. It appears that none of the existing correlations are adequate to describe the EPRI A533B-1 data over the entire range of toughness values. The A533B-1 upper shelf K_d^* values fall well above the "K_{Ic}" values predicted by Barsom, Rolfe and Novak, presumably for the two reasons previously discussed. The K_d^* values in the transition region are much higher than the K_{Id} values predicted by Corten and Sailors. These discrepancies clearly demonstrate the need to better understand the elastic-plastic fracture toughness data in the EPRI data bank.

The new upper shelf K_{Jc} values based on J initiation R-curve data (Table 5) are compared to their corresponding Charpy V-notch upper shelf values in Figure 52. For each of the eight materials studied, both the static and dynamic K_{Jc} values are shown. The Barsom, Rolfe and Novak upper shelf correlation is shown for three different levels of yield strength corresponding to the appropriate strain rate. The Barsom, Rolfe and Novak correlation provides a fairly good approximation of the K_{Jc} values for stress intensity rates ($\dot{K}$) of approximately 10^5 and 10^3 ksi-$in^{1/2}$/s (10^5 and 10^3 MN-$m^{-3/2}$/s), but predicts nonconservative (high) values of K_{Jc} for quasi-static stress intensity rates. The Barsom, Rolfe and Novak correlation is based on valid linear elastic toughness measurements (K_{Ic}), which allow up to two percent crack growth for initiation. If the same amount of crack growth was used to define initiation from the R-curve studies, the J_{Ic} and, therefore, K_{Jc} values would be higher than shown in Figure 52, and a better agreement with the Barsom, Rolfe and Novak correlation would exist. However, there is the counter argument that K_{Jc} values from small specimens overestimate K_{Ic} values (from which K_{Jc} is determined) by not measuring the "weakest link" (Weibull-type size effect previously discussed). These uncertainties, plus the potential complication of a specimen size effect on J_{Ic}[18], do not permit a better resolution of the observations noted in Figure 52.

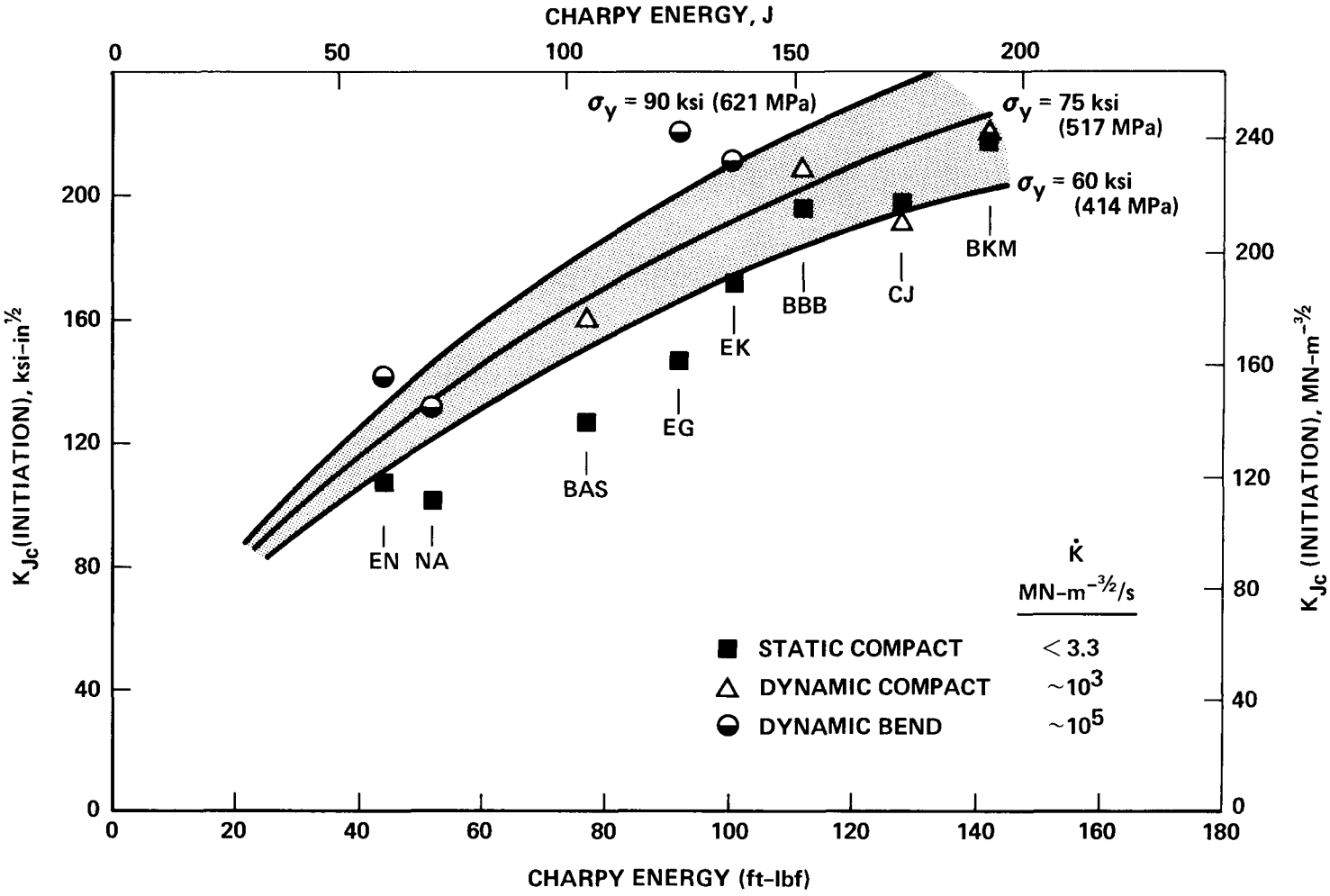

Figure 52. Initiation Toughness Results Compared to the Barsom, Rolfe and Novak Correlation

It should be noted that the data in Figure 52 reflect the worst heat (upper shelf K_d^*) of each of the eight materials (except A540) characterized in the EPRI RP 232 program. For the eight heats studies (seven materials), the two heats of A302B exhibited the lowest upper shelf toughness properties. Heat EN is the old ASTM surveillance correlation heat which is fully described in Reference 42. Heat NA was specially prepared for NRL to simulate the low upper shelf toughness that might result from radiation embrittlement. Thus, neither heat is typical of current pressure vessel steels. However, it is interesting to note that the A302B data indicates that a Charpy V-notch upper shelf energy level of 50 ft-lbf (68 J) corresponds to a static fracture toughness (K_{Jc}) of only 100 ksi-in$^{\frac{1}{2}}$ (110 MN-m$^{-3/2}$). From Table 5 or Figure 50, the dynamic equivalent energy fracture toughness (K_d^*) for heat EN corresponding to 44 ft-lbf (60 J) was 169 ksi-in$^{\frac{1}{2}}$ (186 MN-m$^{-3/2}$). Thus the generally accepted correlation of 150 ksi-in$^{\frac{1}{2}}$ (165 MN-m$^{-3/2}$) with 50 ft-lbf (68 J) is probably based on static and dynamic upper shelf equivalent energy measurements. This study has clearly shown that crack initiation occurs prior to maximum load and, therefore, that true initiation fracture toughness values (K_{Jc}) can be substantially less than equivalent energy fracture toughness (K_d^*). Users of the EPRI fracture toughness data bank[7] must take this into account, along with the previously recommended validity limits for elastic-plastic data.

With regard to the other materials shown in Figure 52, the material with the lowest fracture toughness that is also in current use is heat BAS, which is a submerged arc weldment in A508-2 steel using a Linde 80 flux and a heat input of 102 KJ/in[6]. This weld exhibited an upper shelf static fracture toughness (K_{Jc}) of 127 ksi-in$^{\frac{1}{2}}$ (140 MN-m$^{-3/2}$), which corresponded to a Charpy V-notch upper shelf energy value of 77 ft-lbf (104 J). This weldment also has a high copper content (0.33 percent) and thus may exhibit a rather low upper shelf toughness in service due to the initial low toughness and enhanced radiation sensitivity.

A relatively new approach to extending the fracture toughness measuring capability of small fracture mechanics specimens is through the use of the specimen strength ratio R_s. This ratio for bending is the ratio of the nominal net section bending stress (σ_N) at maximum load (P_M) to the yield stress (σ_y), i.e., for three-point bending and a span to width ratio of 4,

$$R_{sb} = \sigma_N/\sigma_y = \frac{6P_M W}{B(w - a)^2 \sigma_y} \quad . \tag{23}$$

Yukawa[43] and Succop and Brown[44] have reported a correlation between the notch bend strength ratio R_{sb} from slow bend precracked Charpy data and K_{Ic} measurements made on the same high strength steel. Their results are reproduced in Figure 53. Note that there is excellent agreement with the linear elastic fracture mechanics (LEFM) line when the R_{sb} ratio is less than 1.80. It is interesting to substitute the notched bend general yield load (P_{GY}) solution for σ_y (slip line field solution[10]),

$$\sigma_y = \frac{3.3\ P_{GY}\ W}{B(w - a)^2} \quad , \tag{24}$$

in Equation 23 yielding

$$R_{sb} = 1.82\ \frac{P_M}{P_{GY}} \quad . \tag{25}$$

Equation 25 predicts that general yielding occurs at a value of R_{sb} equal to 1.82. Thus, the precracked Charpy sample can predict linear elastic toughness behavior to the point of general yield. This confirms the criteria for elastic fracture used in the EPRI acceptance criteria for dynamic impact tests. That is, Equations 16 and 17 define the upper limit for elastic fracture which occurs when $P_M = P_{GY}$. For the precracked Charpy specimen, the ratio of K to σ_y at general yield is

$$K/\sigma_y = 0.504 \quad , \tag{16}$$

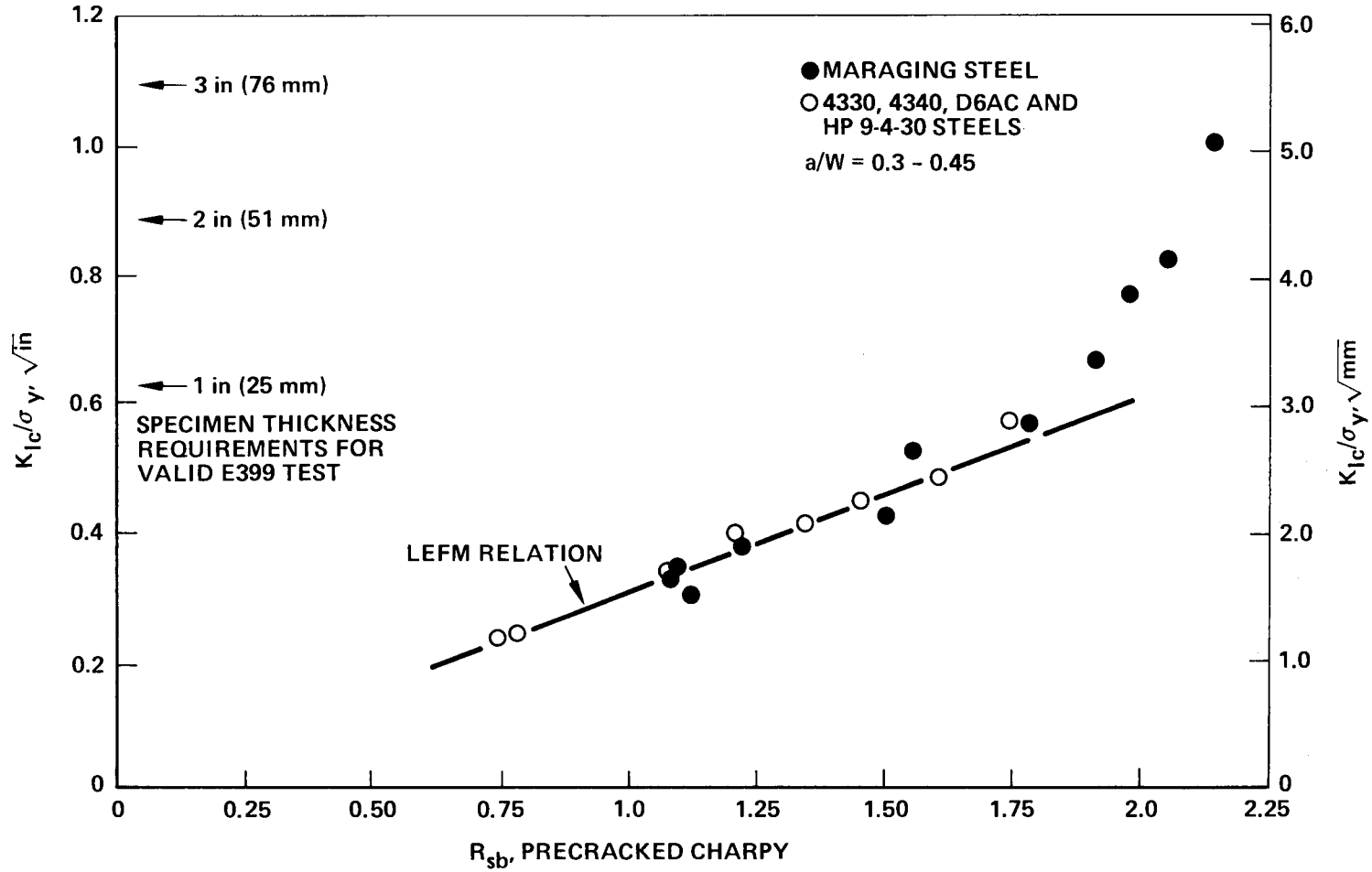

Figure 53. Correlation Between K_{Ic} and Specimen Strength Ratio of Precracked Charpy Slow Bend Data for Several High Strength Steels(43)

which is approximately the same as the value of K/σ_y which corresponds to $R_{sb} = 1.82$ (Figure 53).

The strength ratio can also be applied to compact specimen tests, with the strength ratio R_{sc} being

$$R_{sc} = \frac{2\ P_M\ (2w + a)}{B(w - a)^2\ \sigma_y} \quad . \tag{26}$$

1T compact data from the round robin program[9] and the A533B-1 data from the EPRI fracture toughness program[7] are presented in Figure 54. In this case both valid linear elastic data, invalid linear elastic data (does not meet E399 size requirements), and elastic-plastic data are shown in Figure 54. The temperature dependence of the yield stress (Equation 8) was also used. It is obvious that invalid points fall along the linear elastic line as well as the valid elastic values. This fact indicates that the ASTM thickness requirements are far too restrictive for A533B-1. Figures 53 and 54 indicate that for the ASTM E399 size requirement for elastic fracture

$$a,\ b,\ B \geq 2.5 \left(\frac{K_Q}{\sigma_y}\right)^2 \quad ; \tag{15}$$

the coefficient 2.5 could be reduced to approximately 0.6 for the pre-cracked Charpy (a = b = 0.2 in.) and 0.4 for the 1T compact (a = b = B = 1 in.).

The elastic-plastic results which correspond to cleavage initiation at maximum load (no subcritical tearing) also fall on or slightly above the linear elastic line. The ductile tearing maximum load results deviate substantially from the linear elastic line. Note also that the one true initiation ductile result (K_{Jc}) also falls above the elastic line. However, note that if the linear elastic line was used, conservative values of toughness would be obtained.

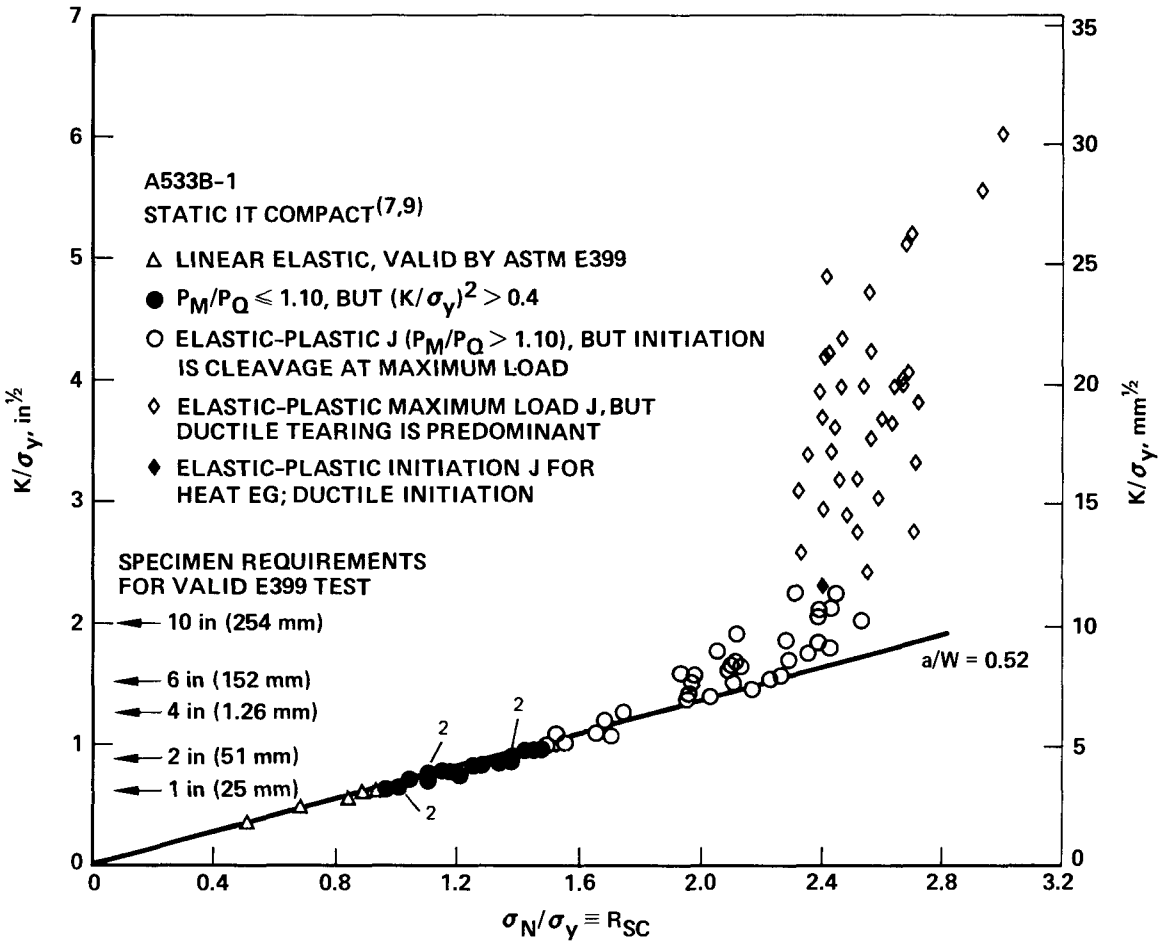

Figure 54. Correlation Between K_{Ic}, K_{Jc} and Specimen Strength Ratio for 1T Compact Specimen Data for Fourteen Heats of A533B-1 Steel

DEVELOPMENT OF PREDICTION LIMITS FOR THE TANH CURVE FIT

Fracture toughness design (or safety analysis) curves are a means by which an analyst uses a practical test (or tests) to determine the lower bound fracture toughness of a pressure vessel steel. The currently used lower bound toughness curve, K_{IR}[45], uses a referencing temperature concept to index nuclear pressure boundary materials to a body of data generated by fracture toughness and crack arrest measurements. The K_{IR} curve is defined as

$$K_{IR} = 26.77 + 1.223 \exp\left\{0.014493\ (T + 160 - RT_{NDT})\right\} \quad , \qquad (27)$$

where RT_{NDT} is the indexing temperature parameter; the units of Equation 27 are English units with temperature (T) expressed in degrees Fahrenheit, and K_{IR} is in ksi-$in^{1/2}$ units.

While recent studies of several heats of each of eight pressure vessel materials[7] have shown the K_{IR} curve to be a lower bound which is rarely transgressed, the work revealed some major difficulties. These may be summarized as follows:

1. The probability that the lower bound will be transgressed needs to to be defined. In general, if a curve has no stated statistical basis, the most secure lower bound curve is the most conservative curve. A practical lower bound curve must have a pre-defined low probability that the fracture toughness of the steel can lie below the curve. To define such a lower bound, a functional relationship must first be found which describes the change in the mean fracture toughness with temperature. Then from an examination of the distribution of the data about the mean the lower bound can be defined for any specified probability.

2. The K_{IR} curve can be seen to be a one-parameter curve, whereby the curve is fitted by normalizing the temperature using RT_{NDT}. There are actually four parameters needed to properly normalize the complete curve. These relate to the physical behavior of fracture toughness as the temperature changes, i.e.,

a. At low temperatures the fracture toughness tends to be a constant value, the lower shelf. One parameter is needed to fix the value of this shelf.

b. At high temperatures there is a corresponding upper shelf, which requires a second parameter.

c. The position of the transition of fracture toughness with temperature must be fixed, needing a third parameter.

d. The rate of transition requires a fourth parameter.

The K_{IR} curve tacitly assumes three of these variables. The lower shelf is bounded at 28 ksi-in$^{\frac{1}{2}}$ (30.8 MN-m$^{-3/2}$). There is assumed to be no upper shelf behavior, and the rate of transition of toughness between the lower and upper shelves is assumed to be increasing continuously at a fixed rate. Thus, the only remaining parameter is the temperature at which the transition occurs which is based upon RT_{NDT}.

3. Assuming that a relationship between the mean fracture toughness and temperature has been derived, there remains the task of defining a lower bound to the curve which will be transgressed with known probability. To derive such a bound the distribution function for the spread of the data about the curve must also be defined. The distribution function is usually defined in terms of a well characterized function such as the Normal distribution and a variance. The form of the distribution may vary with temperature as may the variance.

The Functional Relationship Between Fracture Toughness and Temperature

The four parameters which characterize the fracture toughness changes with temperature can be summarized in the form shown in Figure 1[12]:

$$Y = A + B \tanh \left[\frac{T - T_0}{C} \right] \quad , \tag{28}$$

where Y is the predicted value of fracture toughness, and T is the temperature. The fitted coefficients have the following meaning as also shown in Figure 1:

A is the mean fracture toughness of the lower and upper shelves; B is the $\pm$ deviation of the shelves from the mean; i.e., A + B is the upper shelf fracture toughness, A - B is the lower shelf, and 2B is the difference between the two shelves; T_0 is the temperature at the midpoint of the transition; C is the $\pm$ deviation of the intercepts of the tangent to the transition at T_0 and the lower and upper shelves; and B/C is the slope in the transition range.

While the fracture toughness curve (Equation 28) describes the average fracture toughness as a function of temperature, measuremsnts are scattered in a random fashion about this curve. A simple treatment which is commonly used to set a lower bound for future observations assumes that they are distributed Normally about the curve. Those test results which are available are assumed to be a sample, from which the variance can be estimated. A standard error of a prediction is then developed by combining this estimate with the variance of the mean position of the curve and the variances and covariances of the regression coefficients. This type of analysis is described in Reference 38. Unfortunately, this procedure cannot be applied here. The variance of the EPRI data and the distribution of data about the curve is not uniform over the temperature range of the data, as will be shown by the results which follow. Furthermore, non-linear regression procedures used to fit Equation 28 to the test data do not develop explicit values of the variance and covariance of the coefficients of the curve, A, B, T_0 and C. The procedures provide a conservative upper limit to these variances, which is far too conservative for the generation of lower bounds to the fracture toughness curve. Details of the variance and covariance relationships for the tanh curve fit can be found in Appendix D.

Data Analysis

The recently completed fracture toughness program conducted for EPRI (RP 232) generated a considerable volume of fracture toughness data. The data were generated using static compact, dynamic compact, dynamic bend, and instrumented precracked Charpy tests. For the latter, each group of data (tests performed on a single heat of material) was fitted to a curve of the form shown in Equation 28, so that the deviations about the curve could be studied. There were too few specimens from the larger specimen tests, compact and bend. To allow this data to be analyzed, it had to first be normalized to remove heat-heat variation. This permitted the data from all the heats of each material to be combined, giving a data base which was sufficiently large for analysis. These procedures are described in a later section.

To allow the distribution of data about the curves to be studied in a manner which allowed overall comparisons, a technique was used which related the position of a data point on the curve to be related to the property transition between lower and upper shelves. This technique is the same as the normalization procedure for temperature (to be described later). Instead of using temperature as a reference, normalized temperature, $\frac{T - T_0}{C}$ was used. Data were grouped in the following manner:

Group Number	$t = \frac{T - T_0}{C}$	
1	less than -1	groups 1-6 include linear elastic data.
2	-1 to -0.5	
3	-0.5 to 0	
4	0 to 0.5	
5	0.5 to 1	
6	greater than 1	

As an additional check, to avoid curve-dependent results, deviations were also computed from a regression line fitted to all the data within each temperature range for the heat-heat data sets. This approach was

unsuccessful for two reasons. First, since the lines were independent of adjacent groups of data, they often adopted nonsensical slopes to minimize the variance of the few data points to which the line was being fitted. Second, each line fitted used two degrees of freedom (one for the mean and one for the slope), so that the six groups used 12 degrees of freedom for each data set. This severely restricted the value of the variance estimates.

A group 7 containing only linear elastic data was examined in a preliminary study. This group was found to contain the low toughness data values for group 1, and some low toughness results for group 2. Consequently, the data distributions were found to be highly skewed, and this separation was therefore discontinued.

Variance of Fracture Toughness Data

The deviations of the individual data points from the fitted curves were used to compute the overall variance for each material in each group of data (temperature intervals as defined in the previous section). Because there was no way to allocate the degrees of freedom used to generate the (tanh) curve fitted to the original data, the number of degrees of freedom associated with each group was assumed to be the number of data points within the group.

The results of the analyses are tabulated in the form typified by Table 9. Referring to Table 9, six columns of data are presented. The first column MATERIAL was the material type coded in the way specified in previous work[7]; listed below is the coding scheme:

Code Number	Material
1	A533B-1 base metal
2	A508-2 base metal
3	A540 bolting metal
4	A302B base metal
5	MMA Weld on A533B-1 base
6	MMA Weld on A508-2 base
7	SA Weld on A533B-1 base
8	SA Weld on A508-2 base

Table 9. Variance Analyses for the Precracked Charpy Toughness Results

TABLE OF VALUES

MATERIAL	GROUP	VARIANCE	D.F.	LIMIT	SYMBOL
1	1	78.442	93	23.01	
2	1	86.803	22	52.34	
3	1	27.909	14	21.10	**
4	1	10.183	3	16.63	**
5	1	48.364	54	18.62	**
6	1	63.919	34	31.01	
7	1	116.383	33	57.30	
8	1	184.937	32	92.47	
9	1	228.587	61	82.78	**
1	2	1076.880	15	786.44	
2	2	612.913	8	612.91	
3	2	25.048	8	25.05	**
4	2	141.795	2	283.59	**
5	2	511.895	11	436.55	
6	2	145.546	1	411.67	
7	2	2136.650	7	2284.17	
8	2	2333.420	1	6599.91	
9	2	983.455	8	983.46	
1	3	902.481	11	769.64	
2	3	3498.290	5	4425.03	
3	3	72.249	8	72.25	**
5	3	2557.310	9	2411.05	
6	3	2446.390	3	3994.94	
7	3	2472.990	1	6994.67	
9	3	2884.820	16	2039.88	
1	4	486.292	15	355.14	**
2	4	2057.390	4	2909.59	
3	4	227.372	8	227.37	**
4	4	98.010	1	277.21	**
5	4	4666.740	9	4399.84	
6	4	2941.080	2	5882.16	
7	4	1072.270	6	1238.15	
8	4	1849.280	2	3698.56	
9	4	2414.440	3	3942.76	
1	5	254.511	16	179.97	**
2	5	3414.900	3	5576.51	
3	5	418.547	11	356.94	**
4	5	127.513	2	255.03	**
5	5	3202.930	8	3202.93	
6	5	4614.710	4	6526.19	
7	5	1258.600	6	1453.31	
8	5	478.781	1	1354.20	
9	5	3481.250	6	4019.80	
1	6	439.436	107	120.16	**
2	6	878.865	34	426.31	
3	6	301.355	26	167.16	**
4	6	393.548	9	371.04	
5	6	760.868	80	240.61	
6	6	839.072	38	384.99	
7	6	677.172	46	282.40	
8	6	446.217	47	184.10	
9	6	1068.420	71	358.64	
MEAN VALUES:-					
	1	110.154	346	16.75	
	2	860.237	61	311.53	
	3	2018.525	53	784.23	
	4	1653.985	50	661.59	
	5	1617.124	57	605.83	
	6	674.699	458	89.17	

To avoid confusion, the round robin data (which was actually material 1, A533B-1 base metal) was coded as material 9. When a material is missing, it implies that there were insufficient data points within a particular group to allow the variance to be computed. The second column, GROUP, denotes the temperature group within which $\frac{T - T_0}{C}$ happened to lie, as described earlier. The third column, VARIANCE, shows the computed variance from the quantity $\frac{\Sigma(\text{deviation})^2}{\text{D.F.}}$; VARIANCE is listed in English units for the precracked Charpy results. The fourth column, D.F. (degrees of freedom), shows the number of data points lying within the group. The fifth column, LIMIT, is a measure of the range within which the variance might lie about the mean variance for the group if the data were from a uniform population. LIMIT has qualitative value only, except when there is a large number of data points (a high D.F.) and in which case $\pm$ LIMIT represents the 95% confidence band. LIMIT is also listed in English units for the precracked Charpy results.

Instrumented Precracked Charpy Test

The precracked Charpy variance results for each material are summarized in Table 9 and are shown graphically in Figure 55. A line which represents a mean fit to the variance for all materials is also shown. Figure 56 also shows the combined variance estimate (mean line) for all materials with the ± 2 (standard deviation) range drawn about the mean. To show the results which differed in an important way from the rest, the LIMIT value computed from the estimate of the variance of a variance was used (Table 9). As the number of degrees of freedom increases above about 50, this quantity tends to give 95% limits at ± (LIMIT). Those individual materials which differed from the overall value by more than 1 LIMIT are shown in Figure 56, with the ± range of 1 LIMIT marked on the graph. In addition, they are shown in Table 9 by two asterisks in the SYMBOL column. The materials which showed outliers were materials 1, 3, 4, and 5. All of these deviations were to lower variance. The results for materials 1 - 8 are not too surprising, since materials 1 - 4 are all base materials, which might be expected to be more homogeneous and there-

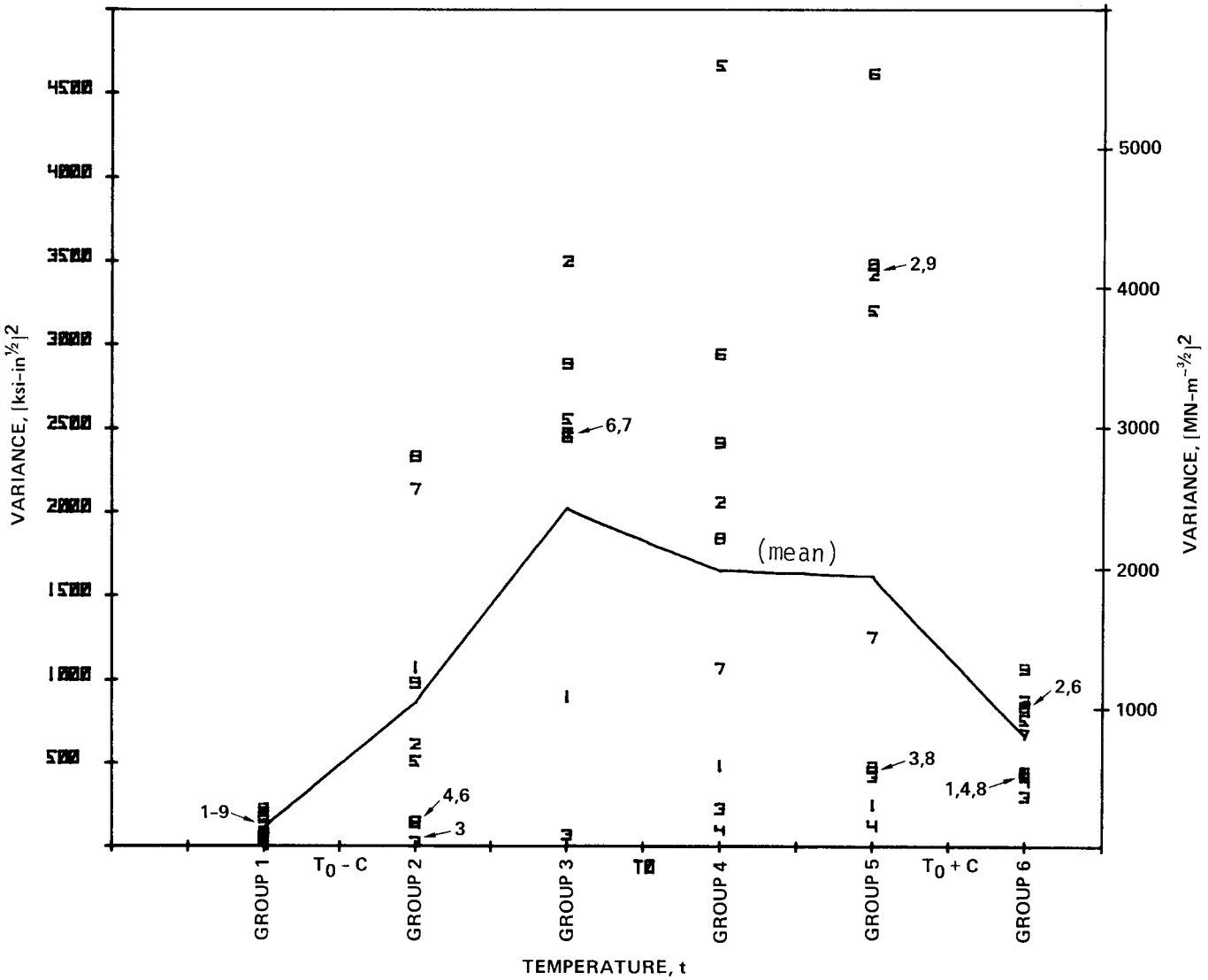

Figure 55. Variance Analyses Results for the Precracked Charpy Test

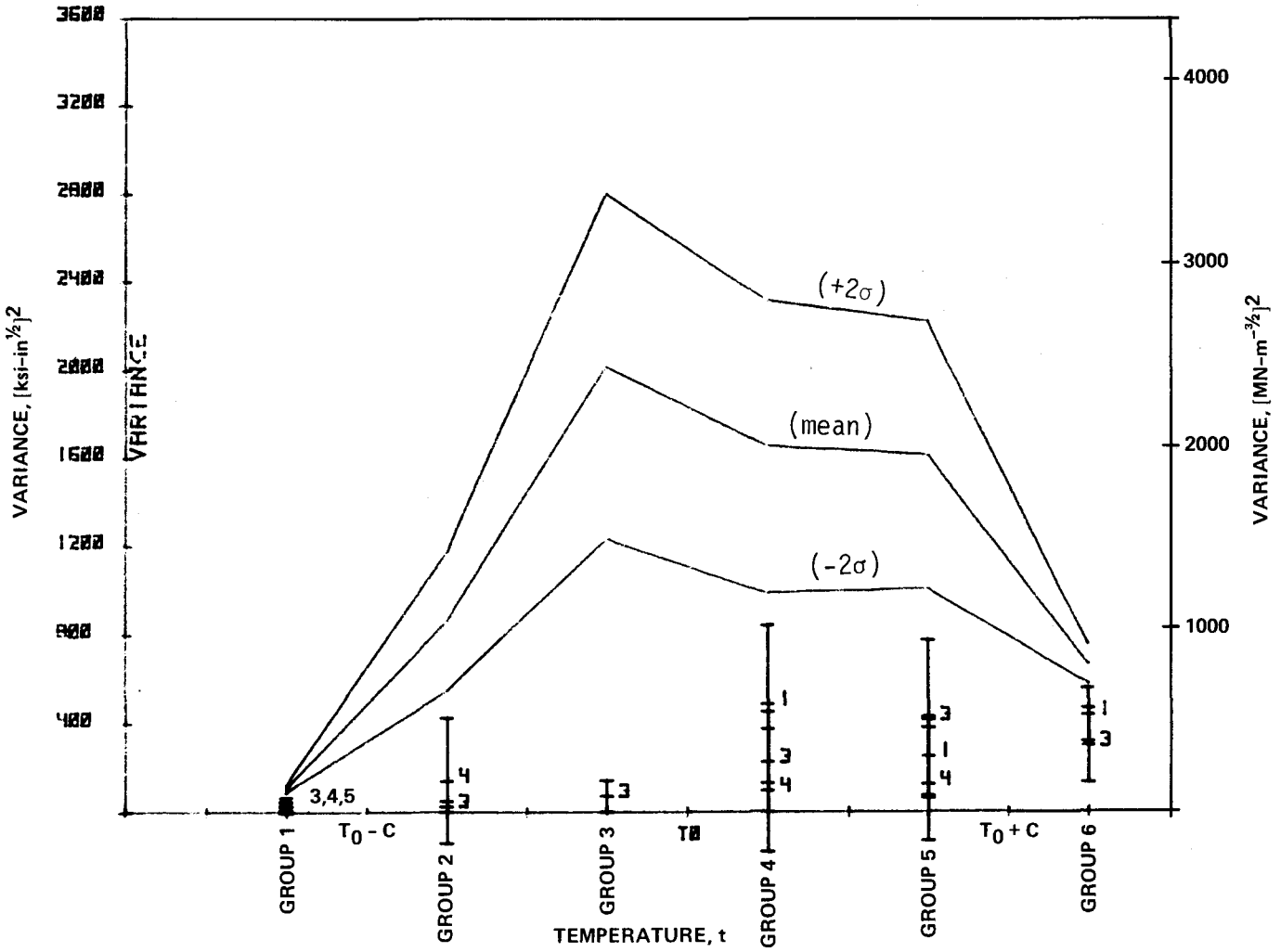

Figure 56. Combined Precracked Charpy Toughness Estimate for All Materials (With ± 2 σ Range Drawn About the Mean)

fore have a lower variability than weld metal. Material 5 was a weld material, so that the marginally low variance in group 1 is somewhat surprising. However, an even greater surprise was provided by the comparison of materials 1 (A533B-1) and 9 (the same material type, but used in the round robin program). A direct comparison is shown on the next page.

Temperature Group:	1	2	3	4	5	6
F Value:*	2.91	0.91	3.20	4.96	13.68	2.43
D.F. (Mat 1):	93	15	11	15	16	107
D.F. (Mat 9):	61	8	16	3	6	71
Significance:†	***	none	**	**	***	***

This comparison shows that highly significant differences exist between the two sets of results for groups 1, 5, and 6. There were significant differences between the results for groups 3 and 4. The differences in variance in group 1 were largely based on results for linear elastic fractures. This result should be considered in the context of the round robin analysis, which showed that certain laboratories had experimental variances which were significantly lower than the other laboratories. One explanation for the results shown here is that the laboratories learned from each other in the round robin program. This learning process indicates that a certain amount of experience is required to follow the testing procedures[10] as they now exist.

As shown by the mean values for each group (Table 9) the variance changed from group to group. Group 1, mainly linear elastic K_{Id} data, had a highly significant lower variance than even the least variable group of elastic-plastic data, group 6. There is no unambiguous statistical

*The F value is the ratio of the two variances, the round robin (material 9) variance divided by the material 1 variance.

†The significance level was determined from tables of the F distribution[46] Two asterisks denote the 95% confidence level and three asterisks the 99% level.

test which would show conclusively that there are significant differences between the other groups of data at this stage, since the most useful tests are dependent upon the assumption that the data is Normally distributed. However, the observed differences are such that we may assert that the variance is approximately constant over the transition temperature range (groups 3-5), but much lower at the lower and upper shelves. The variance apparently increases from the group 1 level in a gradual manner to the middle of the property transition range ($T = T_0$) and then drops at the upper shelf.

Large Specimen Compact and Bend Tests

Attempts to analyze the large specimen test data by the same methods used for the precracked Charpy test data failed. There were usually only four or five data points per heat, barely sufficient to establish a four parameter curve at best, but certainly insufficient to be used to estimate the variance and distribution of the data about the curve.

A procedure was therefore developed to first normalize the data so that all heats could be combined to permit the distribution and variance to be determined. In taking this approach, the heat-heat variability could be removed by the normalization techniques permitting all the data for each material to be combined. The normalization procedure will be discussed prior to the presentation of the large specimen fracture toughness variance distribution studies.

Normalization Procedures

It has already been stated that four parameters are needed to completely normalize a fracture toughness curve. Fewer parameters can be used, but part of the heat-heat variability will be retained and result in an inflation of the variance about the curve. Therefore, in consequence, a lower limit may be obtained than might otherwise be possible. The ideal normalizing parameters have the following properties:

1. They must be conveniently obtained. For example, a Charpy or precracked Charpy test might be appropriate, since it can be performed more easily than large specimen fracture toughness tests; and

2. They must derive from a test which measures the same quantities as the large specimen fracture toughness tests, at least within the limitations of a single material.

When fracture toughness tests are then used in conjunction with the parameters to develop a new, normalized curve, the curve essentially reveals the bias between the actual fracture toughness test and the test used to generate the normalizing parameters.

The precracked Charpy test appears to be an ideal normalizing test, and the tanh curve coefficients (Equation 28) the ideal parameters. On this basis, fracture toughness data can be normalized in the following manner:

$$\underline{\text{Normalized toughness}} = (\text{measured toughness} - A)/B$$

$$\underline{\text{Normalized temperature}} = (\text{measured temperature} - T_0)/C$$

where A, B, T_0 and C are the coefficients from Equation 28 developed for precracked Charpy test data for the same heat used for the larger specimen fracture toughness test. Using normalized test data, heat-heat variation can be substantially removed. A plot of the normalized data can then be developed for all of the heats of a given type of material, allowing variances and data distributions to be computed.

The data for each of the materials (except material 4 for which there was only one heat) were analyzed in this manner. The results are presented in Figures 57 to 72. For materials 1 and 5 the heat numbering is ambiguous, with different heats from the two testing laboratories having the same heat number. To avoid confusion in these cases, the heats tested by Combustion Engineering, Inc. have been marked by a flag. The test types were separated by stress intensity rate ($\dot{K}$) with the

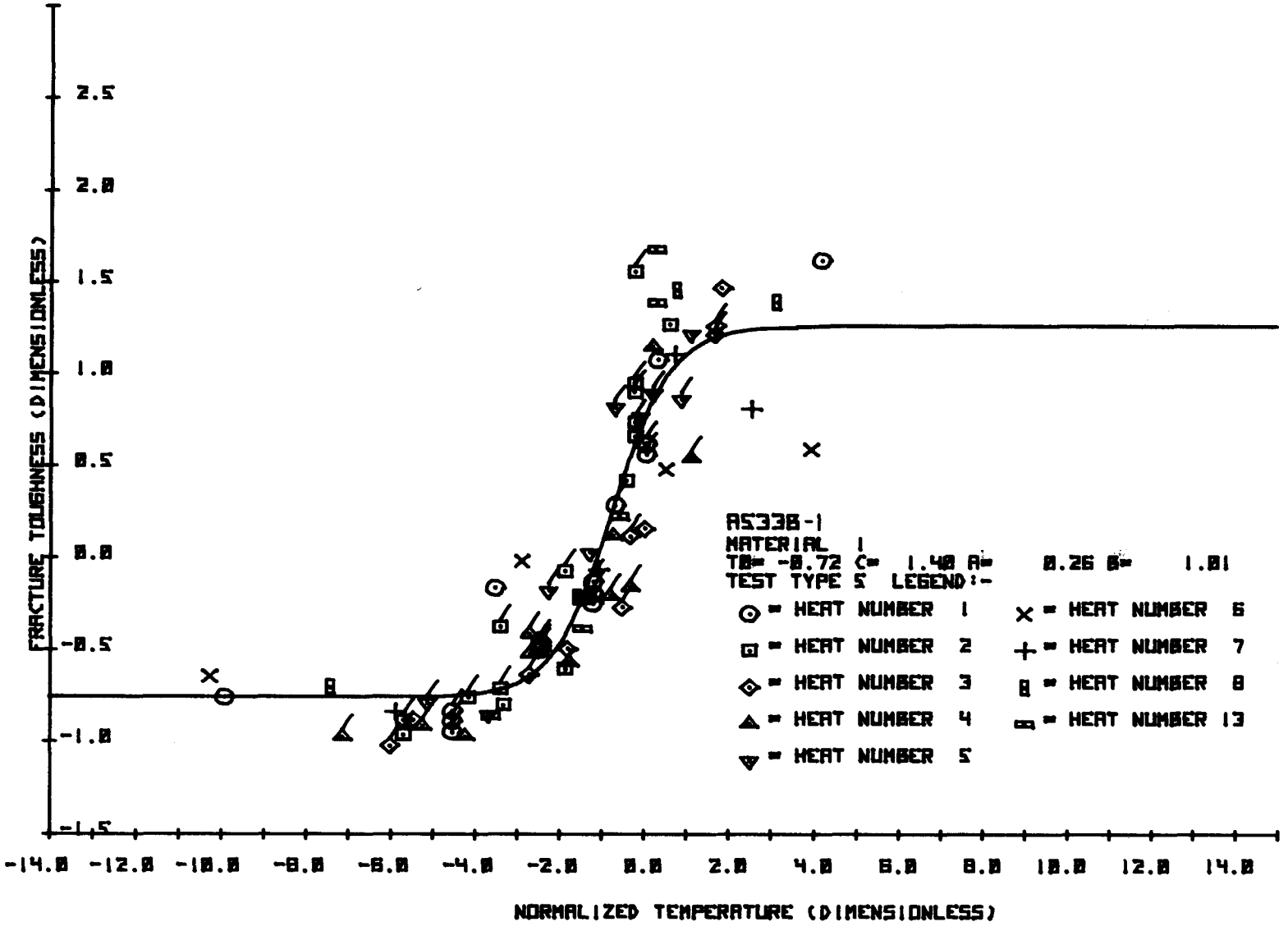

Figure 57. Normalized Fracture Toughness for Material 1, Static Compact

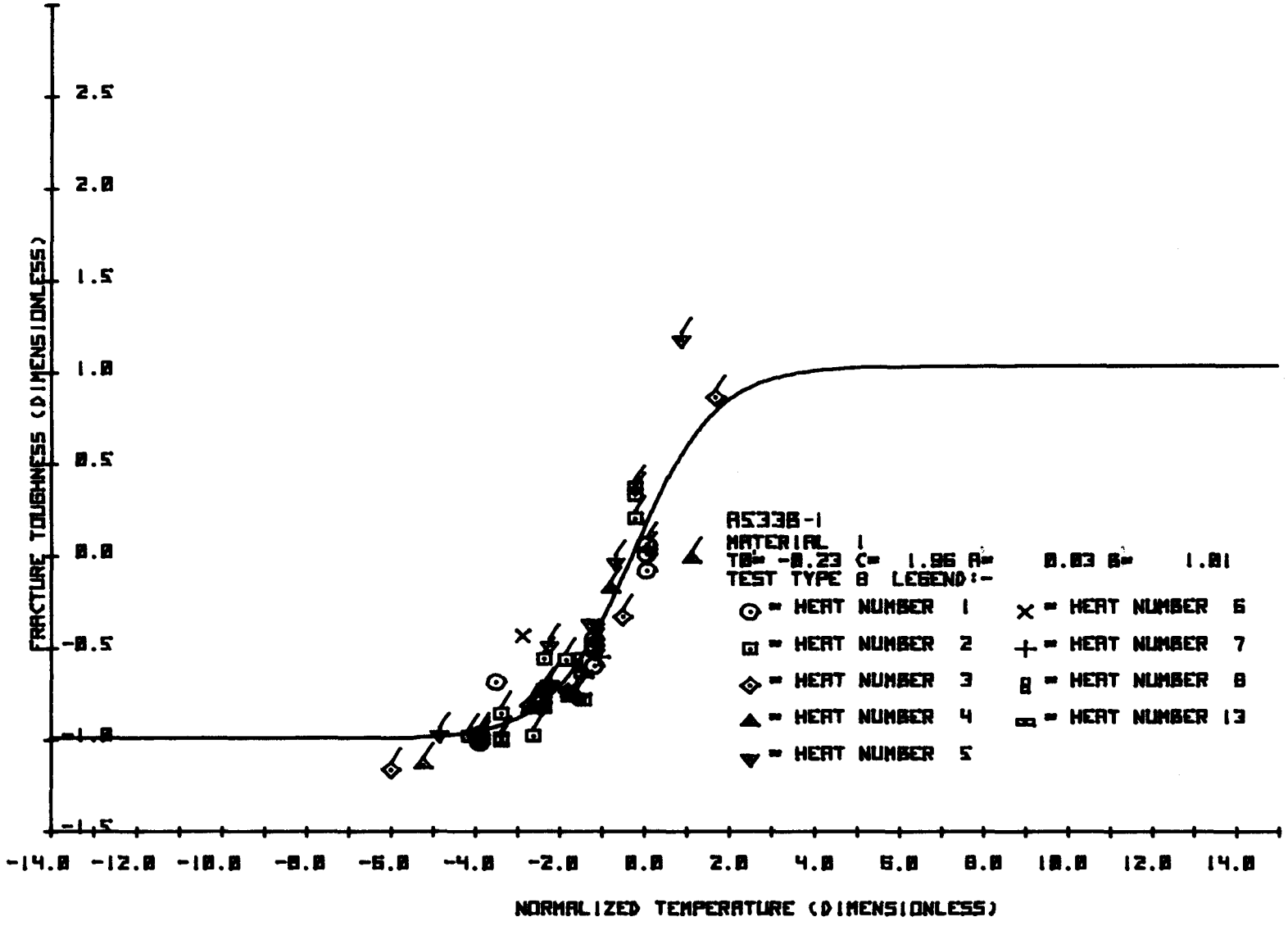

Figure 58. Normalized Fracture Toughness for Material 1, Dynamic Compact

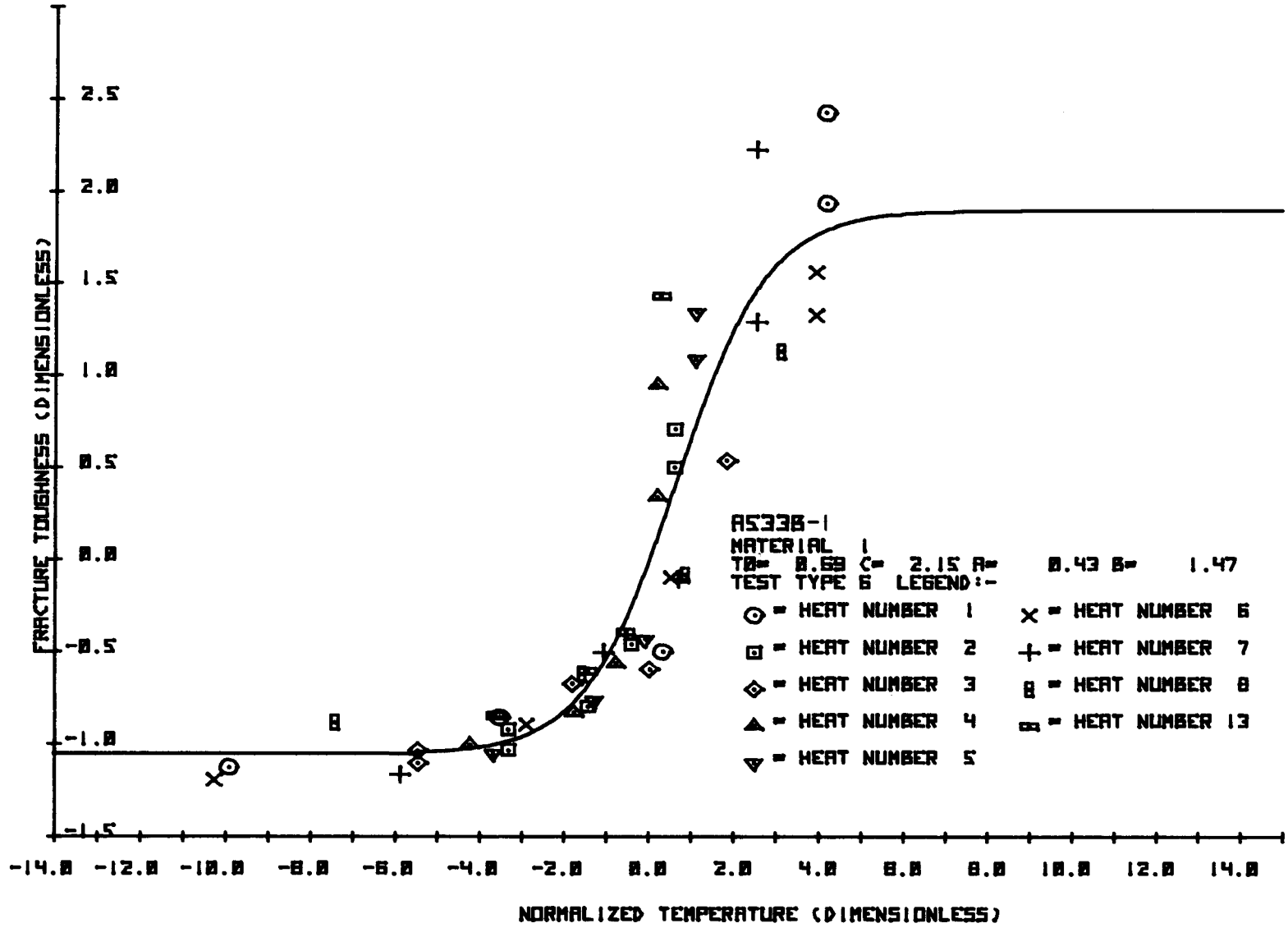

Figure 59. Normalized Fracture Toughness for Material 1, Dynamic Bend

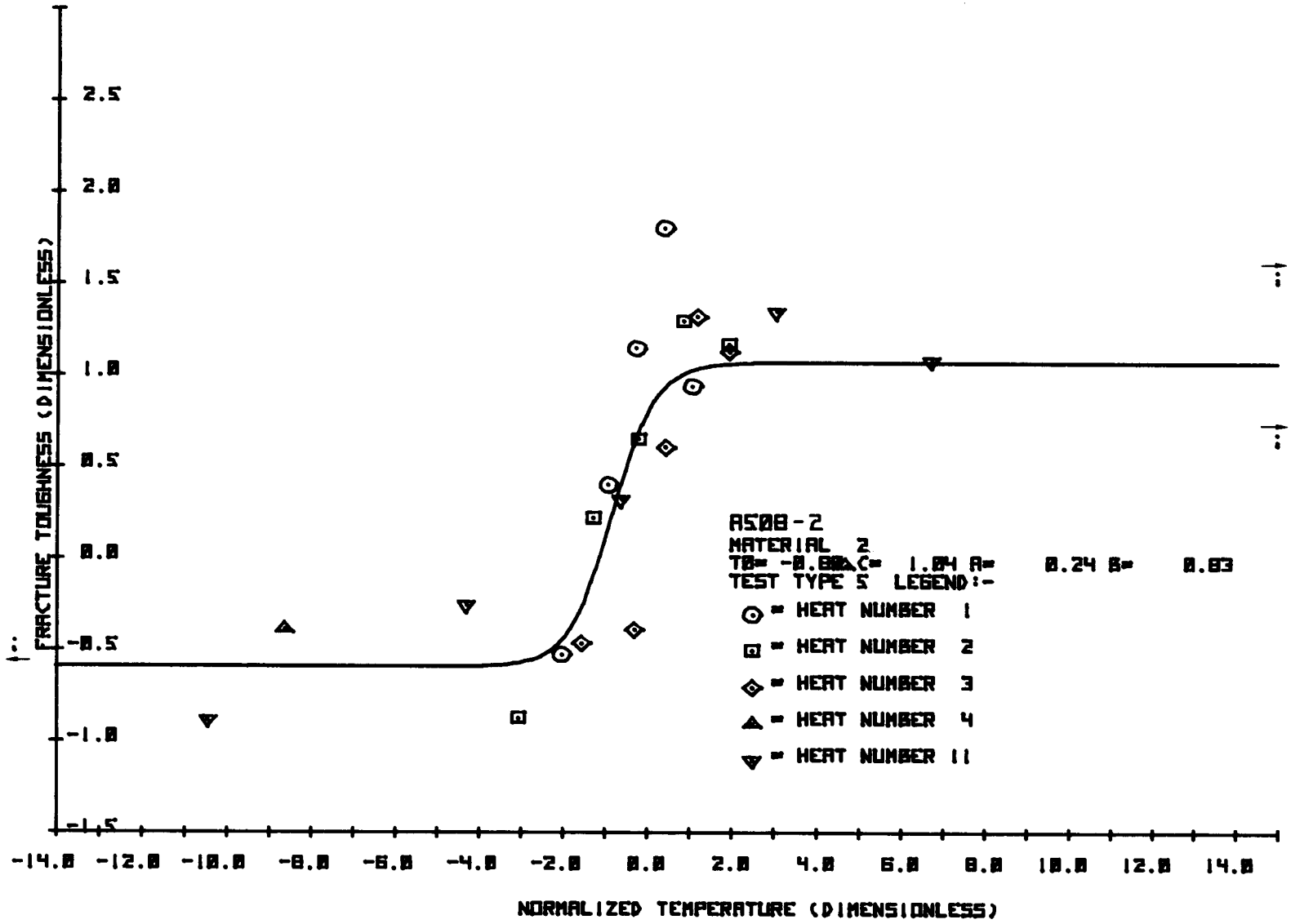

Figure 60. Normalized Fracture Toughness for Material 2, Static Compact

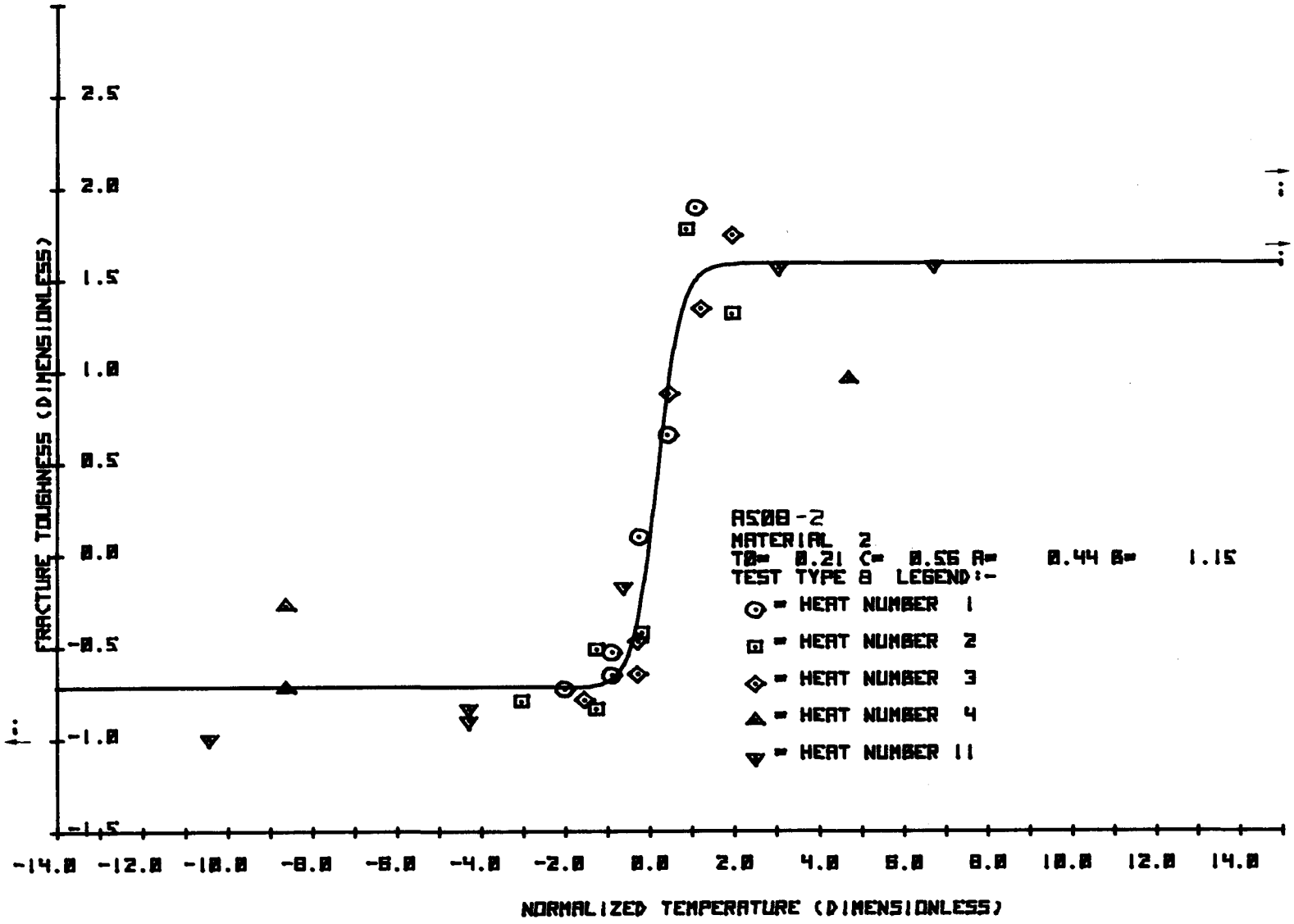

Figure 61. Normalized Fracture Toughness for Material 2, Dynamic Compact

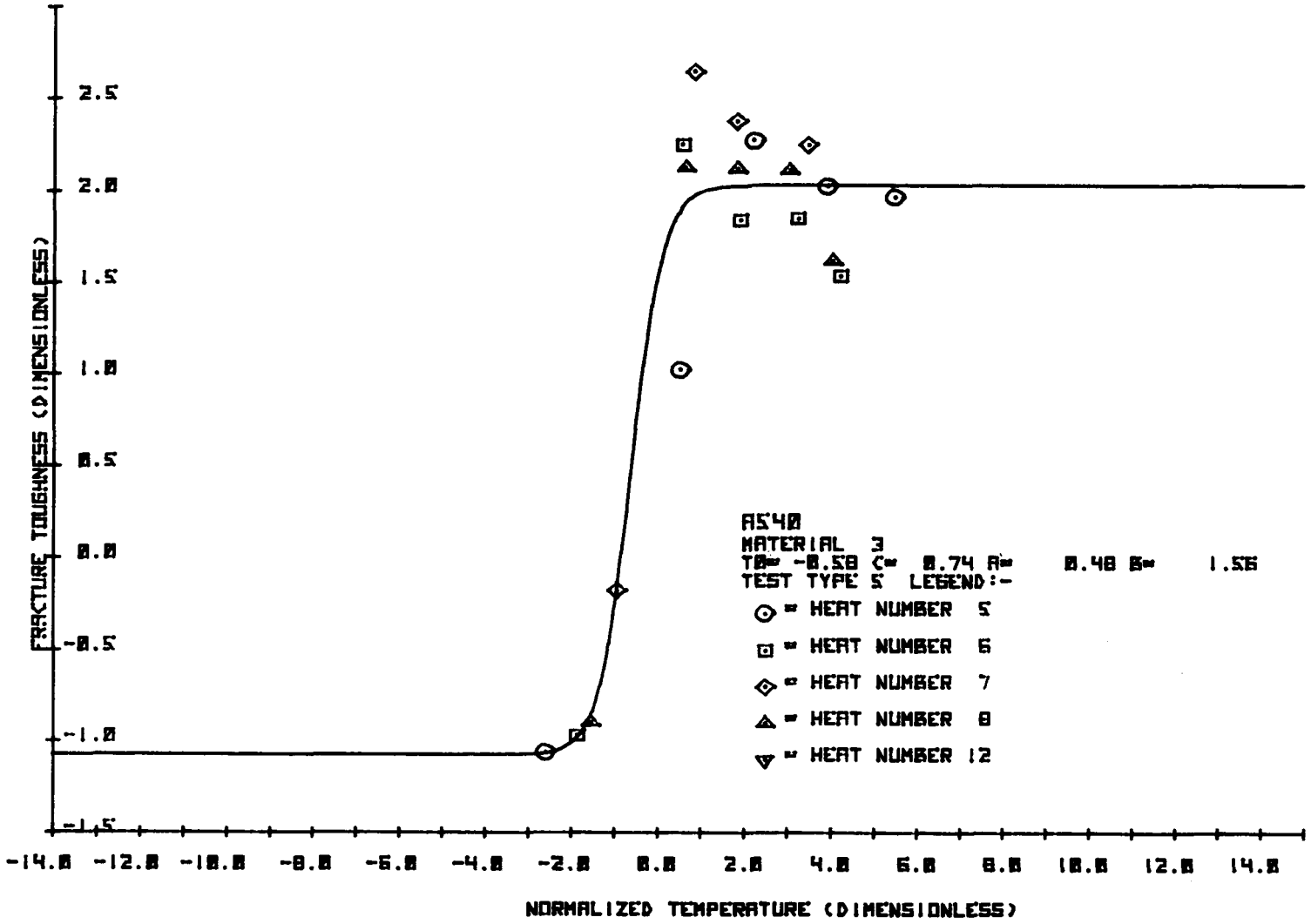

Figure 62. Normalized Fracture Toughness for Material 3, Static Compact

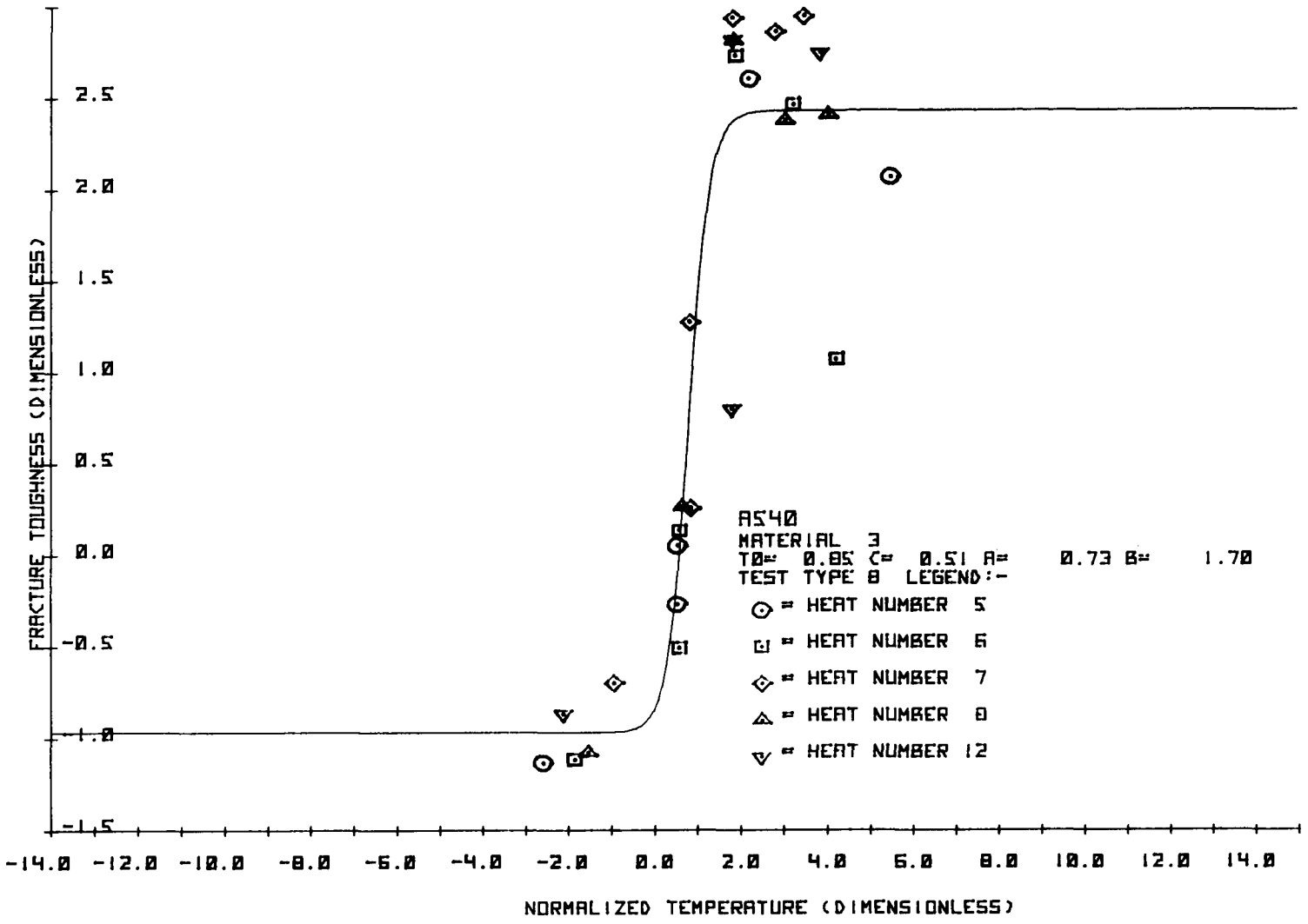

Figure 63. Normalized Fracture Toughness for Material 3, Dynamic Compact

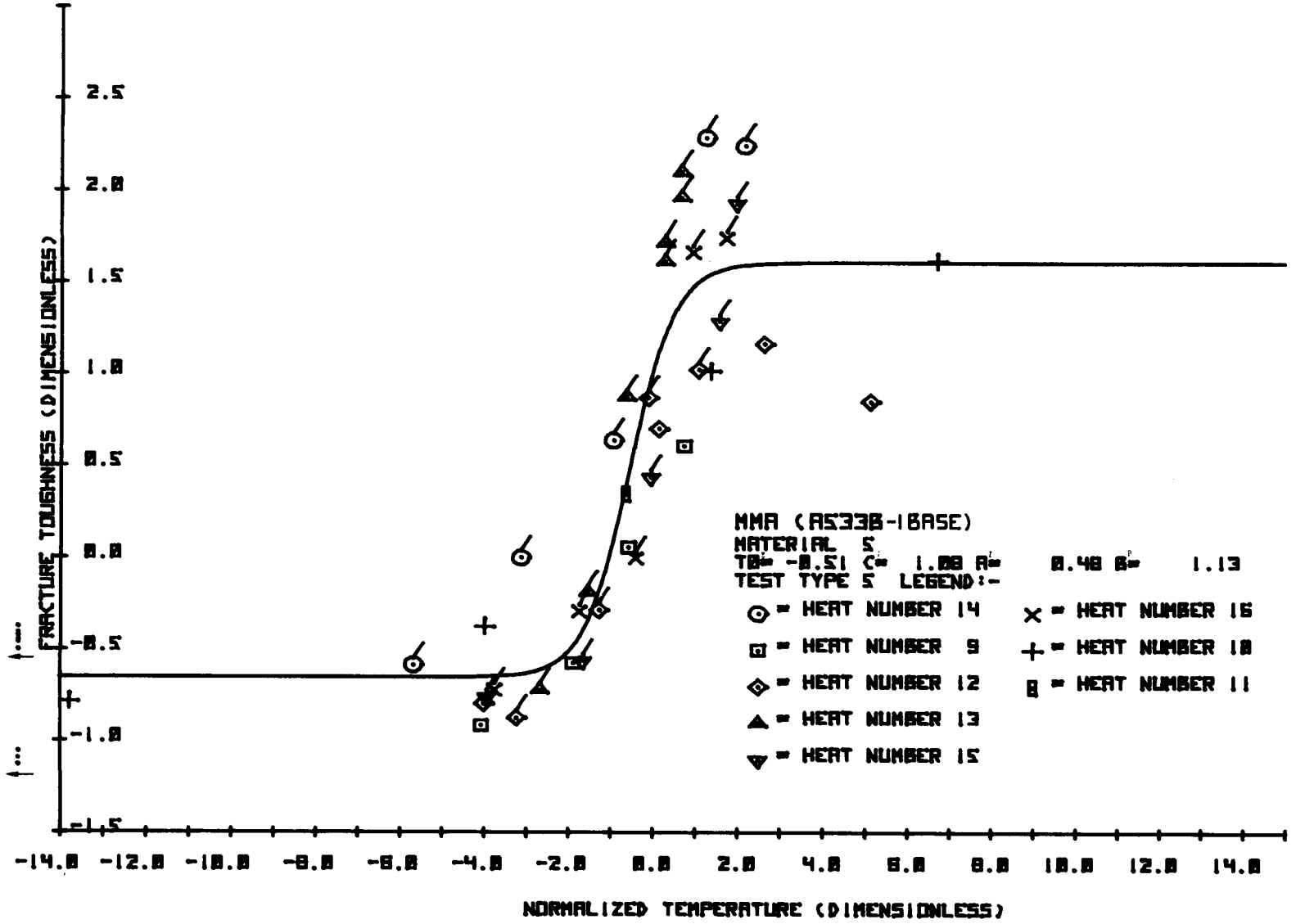

Figure 64. Normalized Fracture Toughness for Material 5, Static Compact

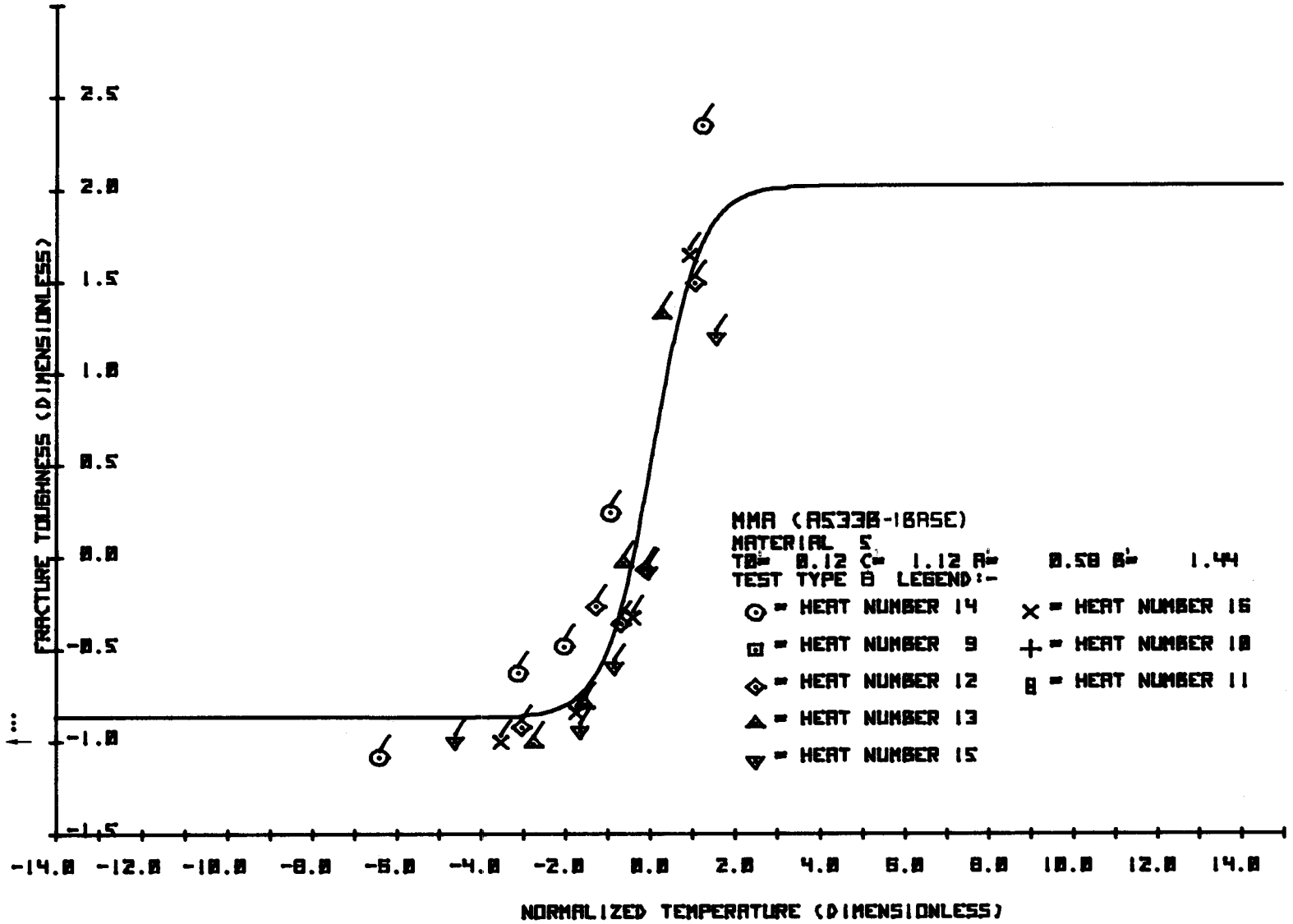

Figure 65. Normalized Fracture Toughness for Material 5, Dynamic Compact

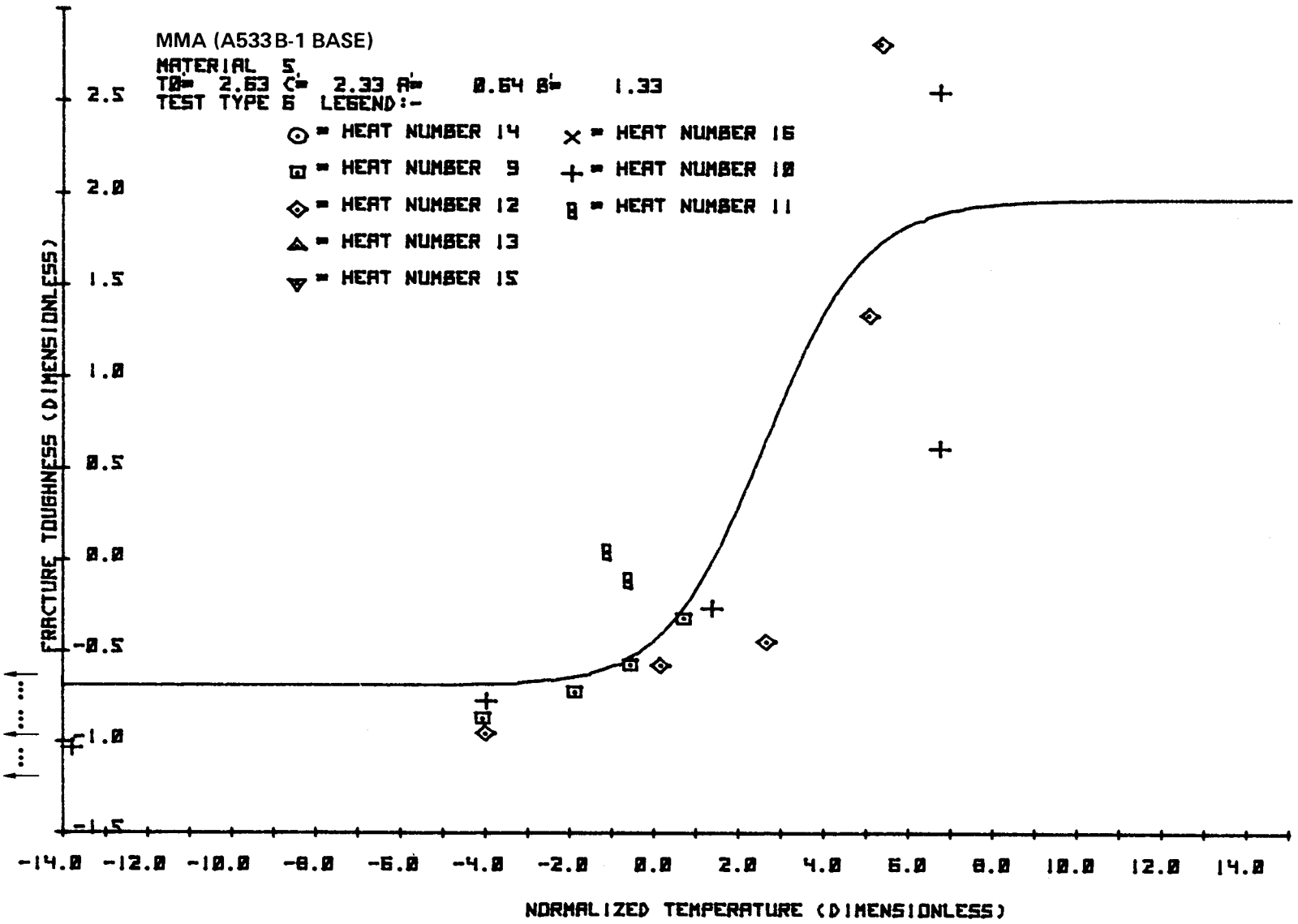

Figure 66. Normalized Fracture Toughness for Material 5, Dynamic Bend

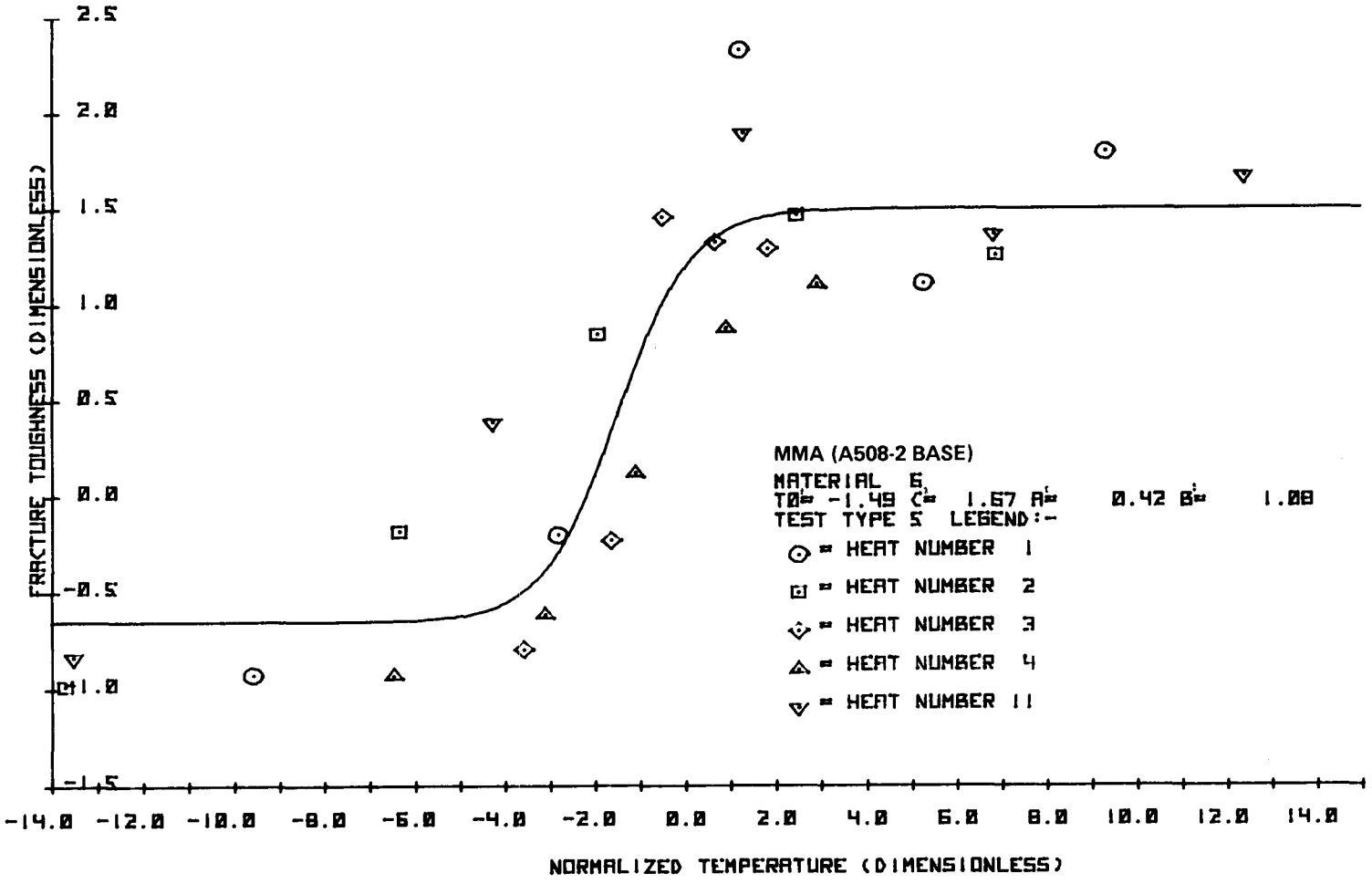

Figure 67. Normalized Fracture Toughness for Material 6, Static Compact

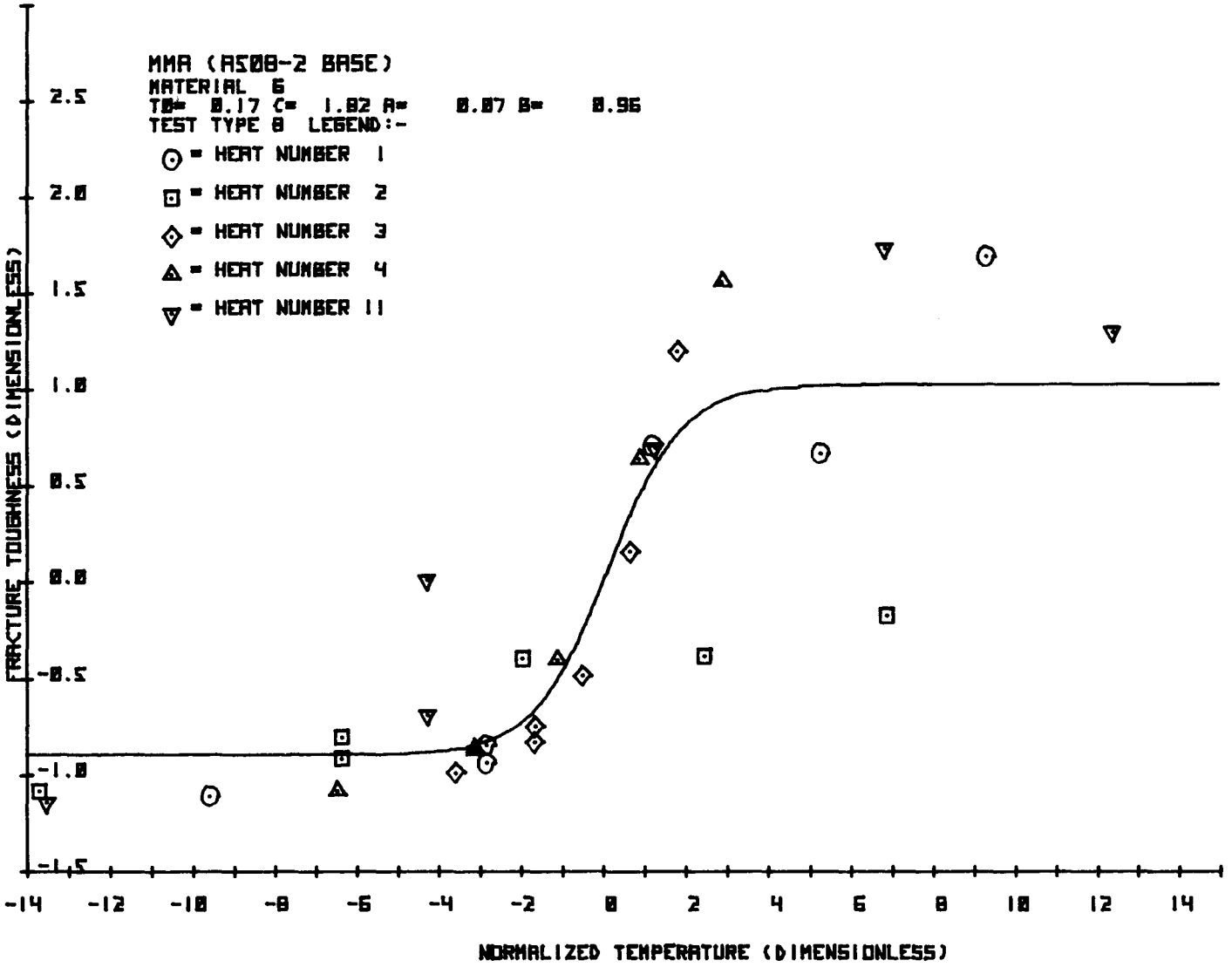

Figure 68. Normalized Fracture Toughness for Material 6, Dynamic Compact

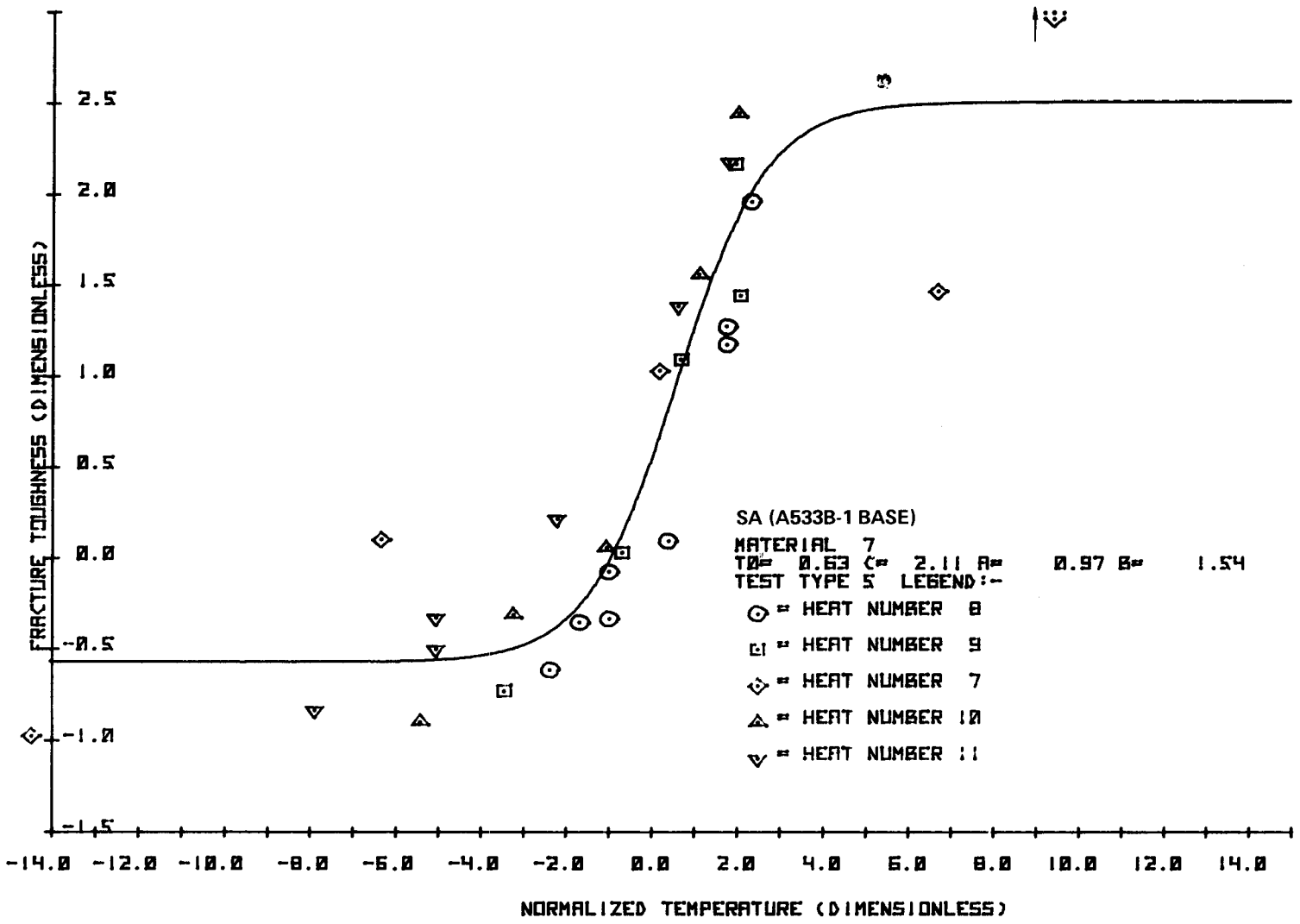

Figure 69. Normalized Fracture Toughness for Material 7, Static Compact

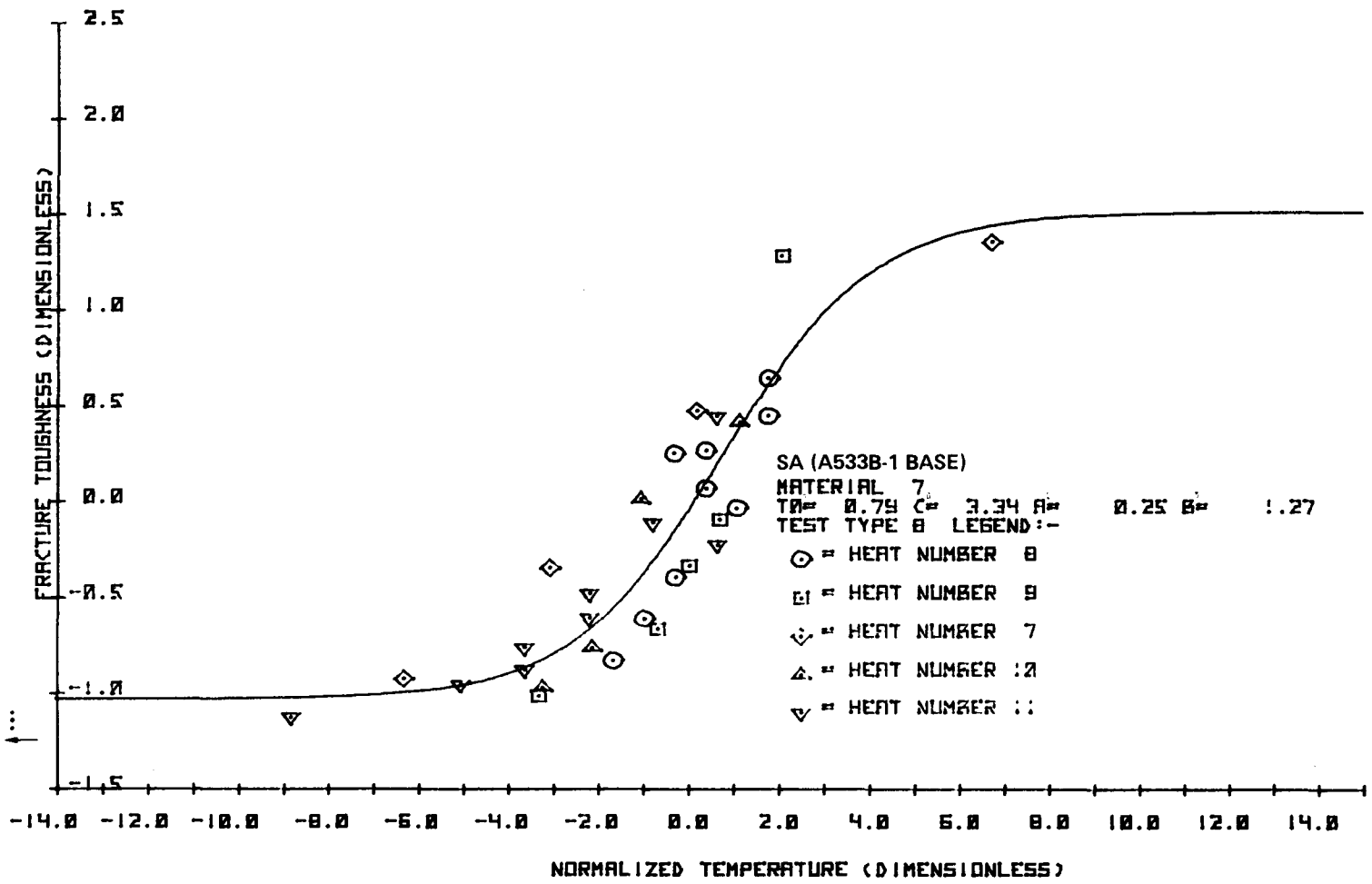

Figure 70. Normalized Fracture Toughness for Material 7, Dynamic Compact

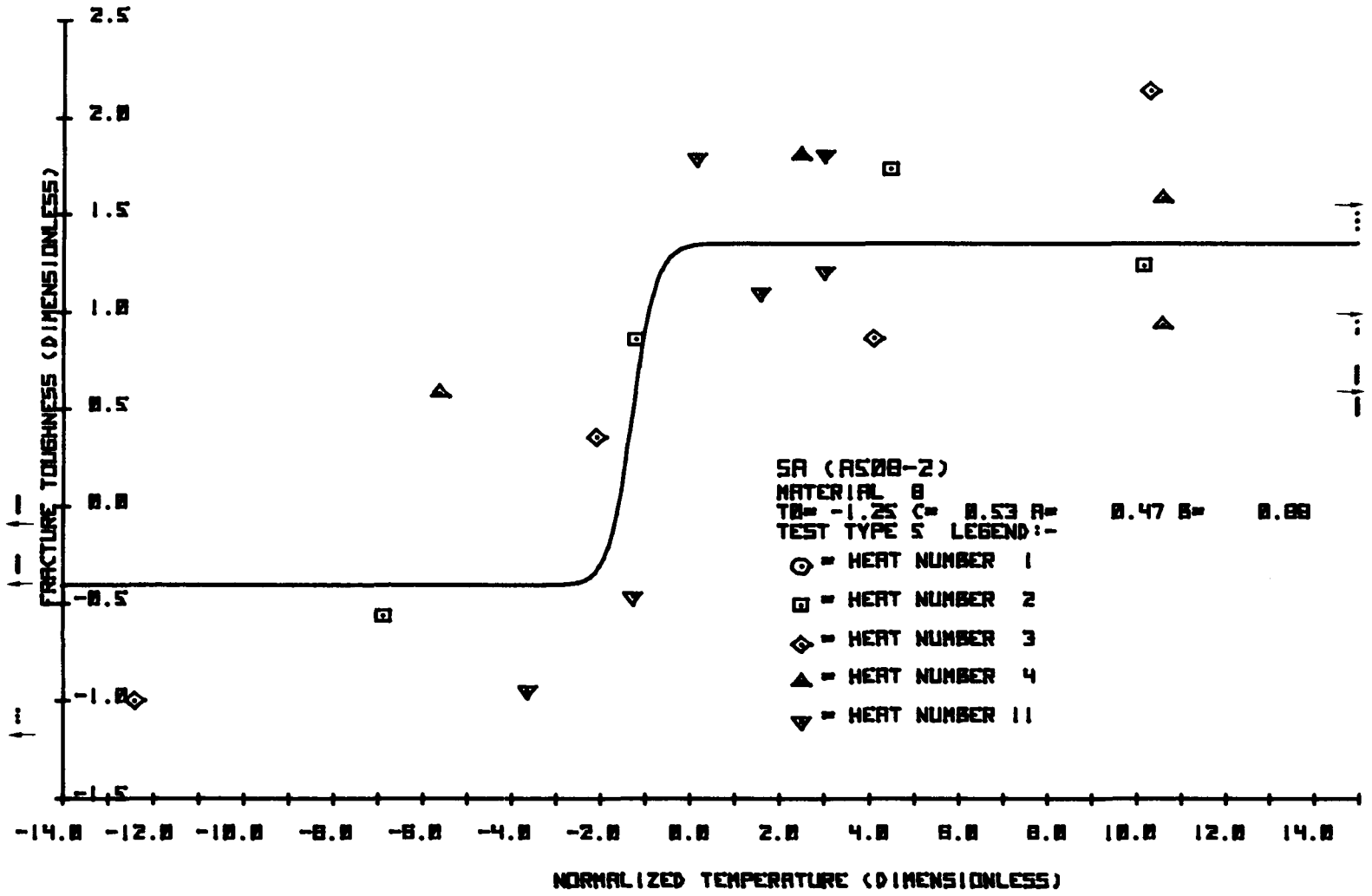

Figure 71. Normalized Fracture Toughness for Material 8, Static Compact

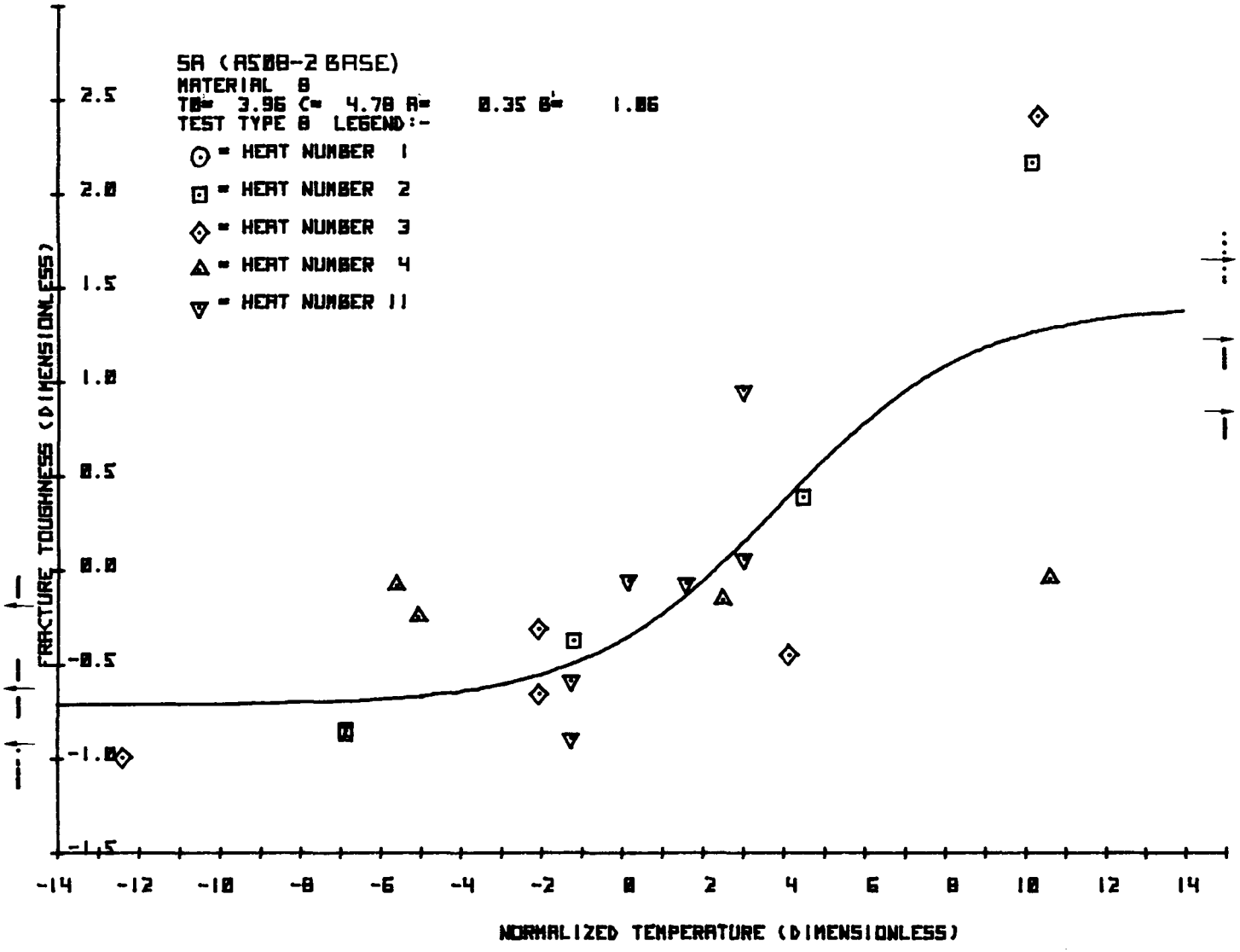

Figure 72. Normalized Fracture Toughness for Material 8, Dynamic Compact

static tests (1T and 2T compacts, test types 5 and 11, respectively) grouped, the intermediate rate dynamic (1T, 2T, 3T, and 4T compacts, test types 8, 9, 10, 7, respectively) as a second group, and impact dynamic 1T bend (test type 6) as a third group (only applicable to materials 1 and 5). The predominant test has been identified in the plot label, and the stress intensity rates corresponding to the three groups are:

Group	$\dot{K}$, ksi-in$^{1/2}$/s (MN-m$^{-3/2}$/s)
Static Compact	< 3 (3.3)
Dynamic Compact	$\sim 10^3$ (10^3)
Dynamic Bend	$\sim 10^5$ (10^5)

In most cases, the normalized curves showed quite a small amount of scatter. However, some curves such as those for material 8 showed large scatter. This could be traced to the C normalizing parameter, which for certain heats, was only about 1/10th of the C values for other heats of the same material. The use of this small C parameter shifted some fracture toughness data from the transition temperature range into the shelf regions. This difficulty is discussed in more detail in a later section.

A noteworthy feature of these analyses was the basis of the grouping, which differed in an important manner from that used for the precracked Charpy test data. For that data, the groupings were based on T_0 and C derived from the test data, so that they directly related to the material behavior. For the large specimen data, the groupings were based on the normalized temperature, so that they were based on T_0 and C for the precracked Charpy test. Thus, they do not exactly relate to the behavior of the large specimens. Furthermore, the graphs shown in Figures 57 - 72 are somewhat misleading as a guide to the computed variance. The groups were taken in a manner which grouped all the lower and upper shelf data into groups 1 and 6 respectively. The remaining groups, 2 - 5, show the detailed behavior in the property transition range between normalized temperatures of -1 to +1.

Static Tests

The normalized static 1T compact data were analyzed in the same manner as the precracked Charpy results without separating the linear elastic data. A preliminary study showed that the elastic and elastic-plastic results, when they occurred at the same temperature, formed the low toughness and high toughness sets of results, respectively. That is, the elastic data generally were below the mean, and the elastic-plastic data above it, at any particular temperature. Separation of the two sets of data thus gave skewed distributions. To simplify the analysis, therefore, all the data were treated in the same analysis. The results of the analysis are shown in Table 10 and graphically in Figure 73. All deviations were to low variance, as was the case in the precracked Charpy results.

Dynamic Tests

The data generated by test types 7, 8, 9, and 10 (dynamic compact) were analyzed in the same fashion as the static test data. The results of the analysis are summarized in Table 11 and Figure 74. The variances were of similar magnitude to those computed for the static tests, and again those values which showed large deviations were below the average.

Data generated by test type 6 (dynamic bend) were analyzed separately from the other dynamic test data because of the difference in stress intensity rate. The test results are summarized in Table 12 and Figure 75. This test was only performed by Effects Technology, Inc. (ETI), so that only materials 1 and 5 were tested, and only a few data points were available for analysis.

Table 10. Variance Analyses for the Static Fracture Toughness Tests

TABLE OF VALUES

MATERIAL	GROUP	VARIANCE	D.F.	LIMIT	SYMBOL
1	1	0.050	30	0.03	**
2	1	0.225	11	0.19	
3	1	0.068	4	0.10	
5	1	0.064	16	0.05	
6	1	0.220	7	0.24	
7	1	0.122	11	0.10	
8	1	0.344	8	0.34	
1	2	0.033	7	0.04	**
2	2	1.711	2	3.42	
5	2	0.016	2	0.03	**
6	2	0.030	2	0.06	
7	2	0.029	4	0.04	**
1	3	0.042	6	0.05	**
2	3	1.909	2	3.82	
3	3	0.001	1	0.00	**
5	3	0.175	4	0.25	
6	3	0.400	2	0.80	
7	3	0.318	2	0.64	
1	4	0.183	14	0.14	
2	4	0.599	3	0.98	
5	4	0.217	3	0.35	
6	4	0.292	1	0.83	
7	4	0.075	3	0.12	
8	4	0.472	2	0.94	
1	5	0.160	11	0.14	
5	5	0.199	3	0.32	
6	5	0.209	1	0.59	
7	5	0.191	7	0.20	
1	6	0.119	12	0.10	
2	6	0.260	7	0.28	
3	6	0.131	19	0.09	
5	6	0.287	14	0.22	
6	6	0.152	12	0.12	
7	6	0.530	3	0.87	
8	6	0.222	16	0.16	
MEAN VALUES:-					
	1	0.125	87	0.04	
	2	0.227	17	0.16	
	3	0.365	17	0.25	
	4	0.249	26	0.14	
	5	0.177	22	0.11	
	6	0.201	83	0.06	

Table 11. Variance Analyses for the Dynamic Compact Fracture Toughness Tests

TABLE OF VALUES

MATERIAL	GROUP	VARIANCE	D.F.	LIMIT	SYMBOL
1	1	0.021	23	0.01	**
2	1	0.046	14	0.03	
3	1	0.028	5	0.04	
5	1	0.038	12	0.03	
6	1	0.074	16	0.05	
7	1	0.033	9	0.03	
8	1	0.111	16	0.08	
1	2	0.019	9	0.02	
2	2	0.070	4	0.10	
3	2	0.074	4	0.10	
5	2	0.147	4	0.21	
6	2	0.013	1	0.04	
7	2	0.057	6	0.07	
8	2	0.067	1	0.19	
1	3	0.018	8	0.02	**
3	3	0.020	1	0.06	
5	3	0.152	3	0.25	
6	3	0.047	1	0.13	
7	3	0.097	11	0.08	
8	3	0.164	4	0.23	
1	4	0.055	6	0.06	
2	4	0.025	2	0.05	
3	4	0.259	2	0.52	
5	4	0.256	1	0.72	
6	4	0.034	2	0.07	
7	4	0.101	5	0.13	
8	4	0.389	2	0.78	
1	5	0.273	3	0.45	
5	5	0.015	2	0.03	
6	5	0.073	3	0.12	
2	6	0.098	10	0.09	**
3	6	0.419	14	0.32	
5	6	0.410	2	0.82	
6	6	0.653	7	0.70	
7	6	0.008	1	0.02	**
8	6	0.646	7	0.69	
MEAN VALUES:-					
	1	0.052	95	0.02	
	2	0.061	29	0.03	
	3	0.085	28	0.05	
	4	0.125	20	0.08	
	5	0.134	8	0.13	
	6	0.409	41	0.18	

Table 12. Variance Analyses for the Dynamic Bend Fracture Toughness Tests

TABLE OF VALUES

MATERIAL	GROUP	VARIANCE	D.F.	LIMIT	SYMBOL
1	1	0.01	16	0.01	**
5	1	0.09	12	0.07	
1	2	0.01	7	0.01	
5	2	0.03	2	0.06	
1	3	0.40	9	0.38	
1	4	0.31	4	0.43	
5	4	1.19	1	3.37	
1	5	0.34	3	0.55	
1	6	0.18	5	0.23	
5	6	0.83	4	1.18	
MEAN VALUES:-					
	1	0.04	28	0.02	
	2	0.02	9	0.02	
	3	0.40	9	0.38	
	4	0.48	5	0.61	
	5	0.34	3	0.55	
	6	0.47	9	0.44	

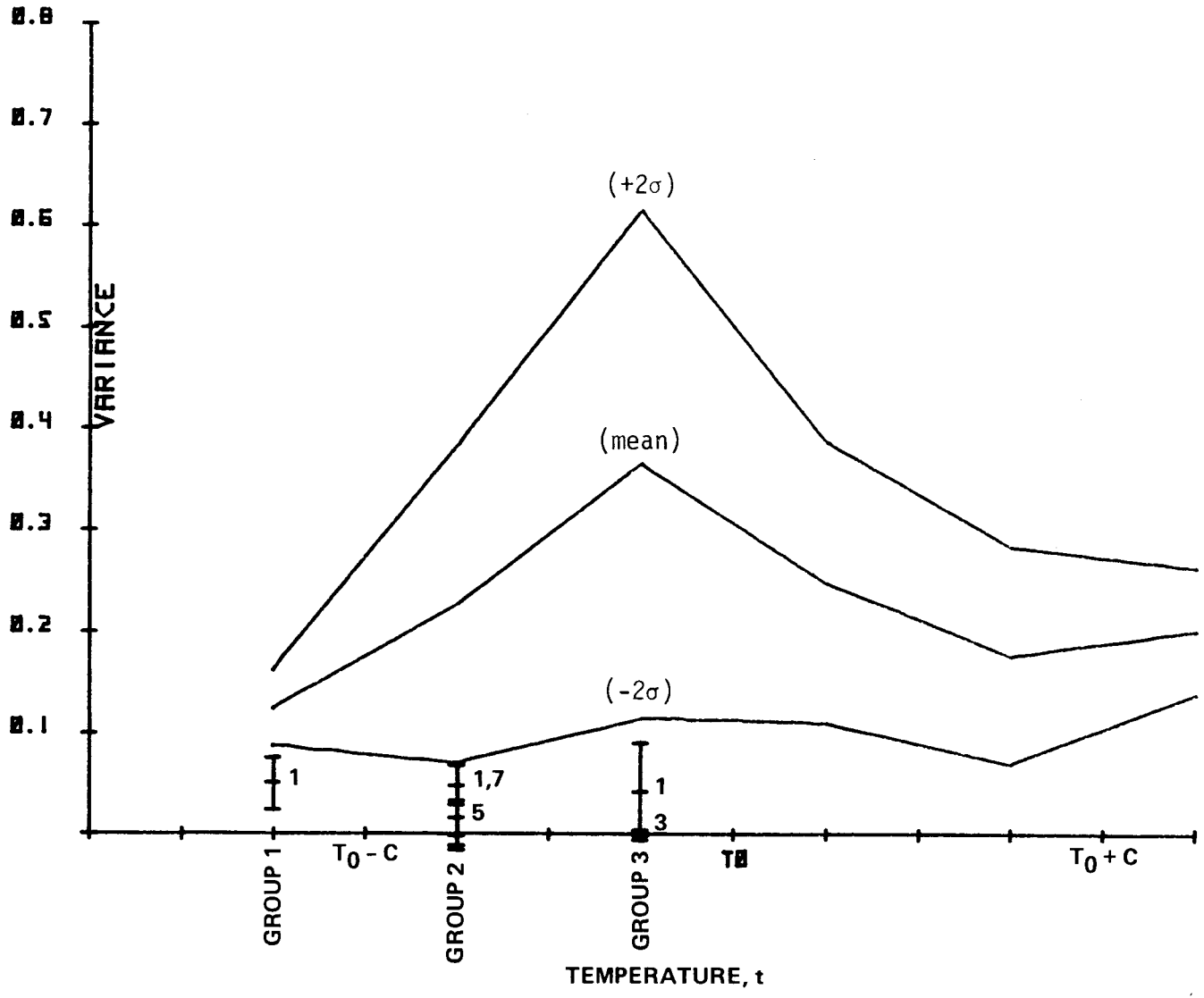

Figure 73. Combined Static Toughness Variance Estimate for All Materials

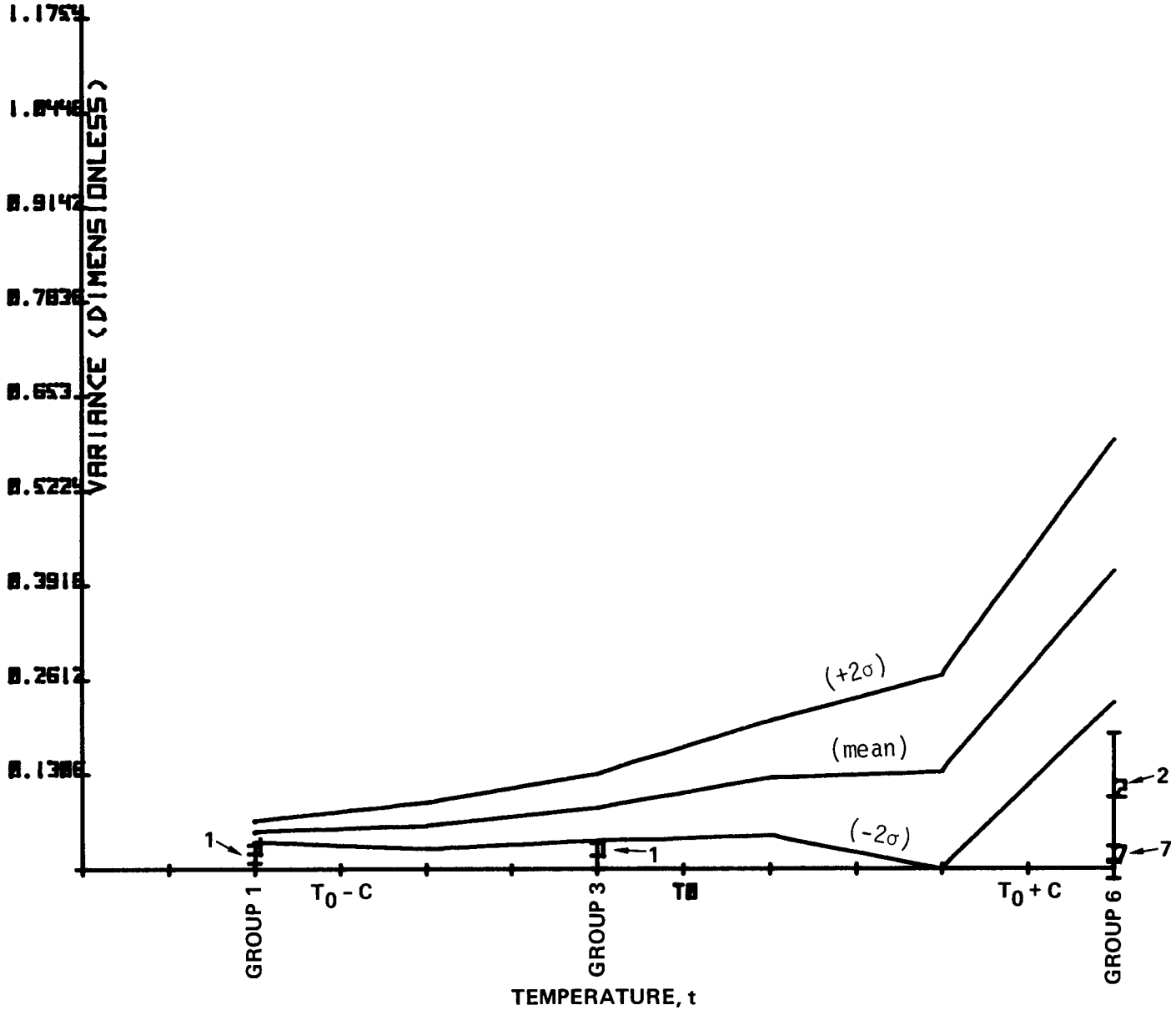

Figure 74. Combined Dynamic Compact Fracture Toughness Variance Estimate for All Materials

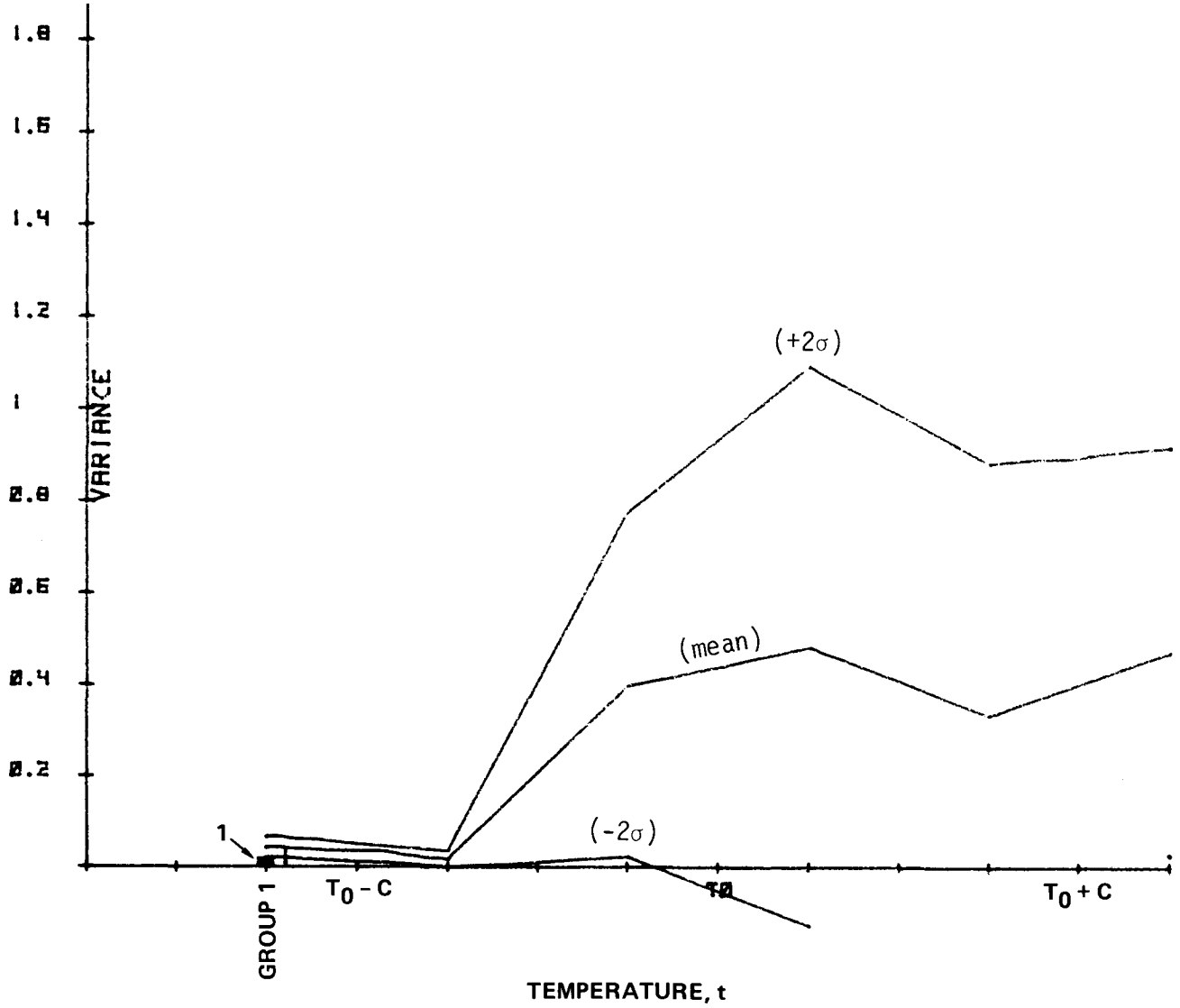

Figure 75. Combined Dynamic Bend Fracture Toughness Variance Estimate for All Materials

The Distribution of Fracture Toughness Data

The data used to compute variance in the temperature range groups were also used to determine the distribution of data about the curve. The deviation of each data value from the curve was related to the variance for the group to give a normalized deviation from the curve; that is, a deviation expressed in terms of the standard deviation. A histogram was then developed by counting the number of points lying in deviation ranges of 0.5 (standard deviation) from the curve. The moments of the distribution were also computed. The histogram generated from the point counts was then drawn with a superimposed curve developed from the Normal distribution. The curve and the histogram thus give a visual summary of the distribution data, while the computed moments allow the information to be interpreted in a quantitative fashion.

The skewness or other deviation from Normality can be tested quantitatively. The moment ratios, $\sqrt{b_1}$ and b_2 can be computed from the third and fourth moments of the distribution, and tables of these quantities have been published[46]. However, while $\sqrt{b_1}$ is an appropriate test for skewness, the statistic "a" is better than b_2 as a test for kurtosis. a is defined as:

$$a = \frac{(\text{mean deviation})}{(\text{standard deviation})} \quad . \tag{29}$$

Kurtosis is the term applied to deviations in shape from the Normal distribution; leptokurtosis means that the distribution has a higher peak and widespread tails; and platikurtosis means a humped peak and short tails. The b_2 statistic is only preferable to "a" when the data sample exceeds about 200.

The distribution of data about the tanh curve for the instrumented precracked Charpy normalized static compact and normalized dynamic compact and bend testing programs are examined in detail in Appendix E. The

instrumented precracked Charpy test results showed overall close agreement with the Normal distribution. However, group 1 (lower shelf) results were skewed towards higher toughness, while group 6 (upper shelf) were skewed towards lower toughness.

The static and dynamic compact test programs had fewer test results, but showed the same overall trends. Referring to the overall results (all materials combined, Tables E.5 and E.7), the lower shelf data were skewed high for both types of test. This result was significant at better than the 99% level. The upper shelf data for the dynamic compact test showed significant downward skew (95% level). The dynamic bend test program had even fewer test results. There was a high skew at the lower shelf, but there were too few test results to show a significant trend.

DEVELOPMENT OF REVISED K_{IR} CURVE

The development of a revised K_{IR} curve requires the results obtained from the distribution studies and an analysis of indexing procedures. The currently used RT_{NDT} concept normalizes toughness data to a certain extent, but other, more appropriate parameters may be available. In the distribution studies it was found that an ideal indexing parameter was the precracked Charpy tanh fit parameters. Before this technique was formalized, other parameters were investigated. A brief section describing these early studies will precede the final section discussing unique K_{IR} curves for the different materials.

Other Normalizing Parameters

Initially, correlations between NDTT and RT_{NDT} with T_0 and $T_0 - C$ from precracked Charpy tests were attempted. There was no consistent trend with T_0 that could be established using both precracked Charpy normalized energy and toughness. However, $T_0 - C$ from the precracked Charpy normalized energy and toughness values correlated fairly well with the Nil Ductility Transition Temperature (NDTT). Figures 76 and 77 show the $T_0 - C$ and NDTT data plotted against the expected 1:1 correlation.

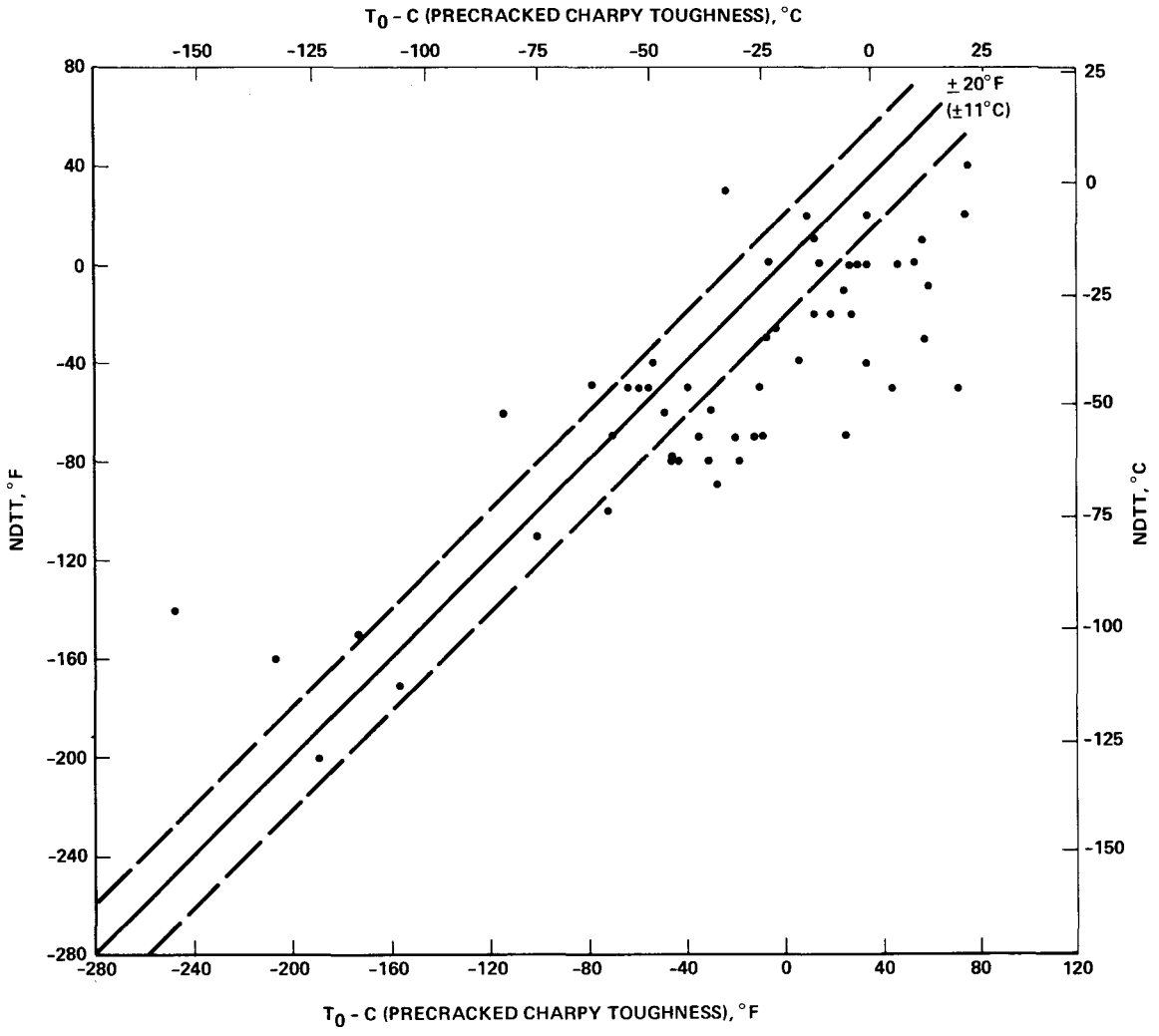

Figure 76. Comparison of NDTT with T_0 - C from Precracked Charpy Toughness Tanh Fits

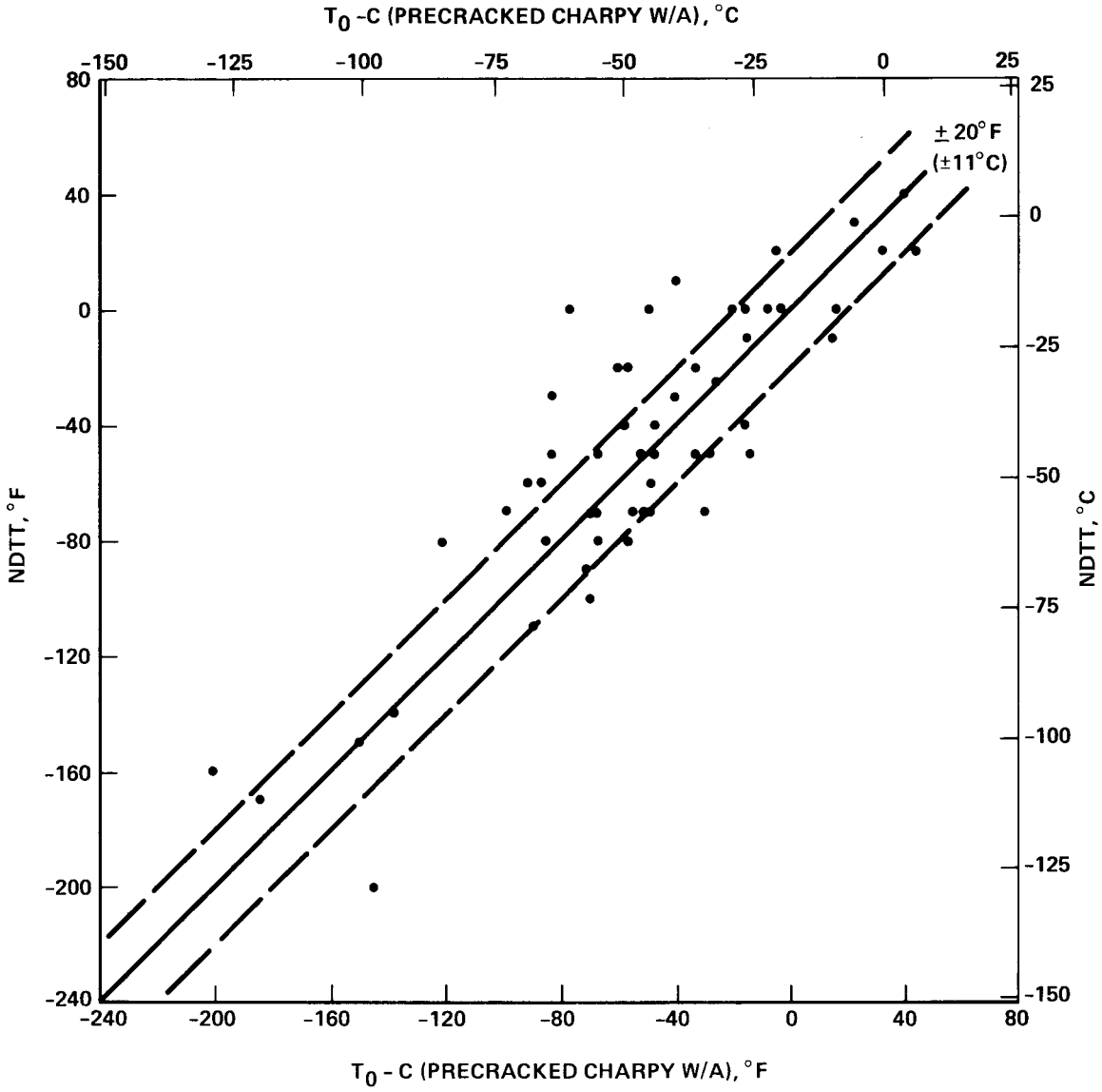

Figure 77. Comparison of NDTT with T_0 - C from Precracked Charpy Toughness Tanh Fits

There is a much better correlation using the normalized energy, as would be expected since the NDTT test is really a propagation test which should relate better with total energy (W/A, initiation plus propagation) rather than just initiation (K_{Id}). It is generally observed that the upturn (lower knee, T_0 - C) in initiation toughness occurs at a higher temperature than the upturn in the normalized energy (W/A). The data in Figure 76 are consistent with this observation since the initiation toughness transition measured by T_0 - C tends to occur above the transition measured by the NDTT (and thus W/A). Thus, using T_0 - C from the precracked Charpy toughness tanh fits would tend to give a conservative estimate of the NDTT. Figure 77 indicates that T_0 - C from the precracked Charpy W/A tanh fits provides a good estimate of the NDTT except for those points falling above the data band corresponding to the normal scatter in the NDTT test (± 20°F, 11°C). The data scatter greater than ± 20°F (11°C) tends to be skewed high. A review of the data and the tanh fits did not reveal any reasons for the deviation. However, it should be noted that two different statistical approaches are being compared for this correlation. The tanh fit to the W/A data is a mean fit result for the values of T_0 and C. The NDTT is not necessarily a mean result, but is an upper limit by the testing procedure used to obtain NDTT. Thus, the NDTT values should be skewed higher when a one-one correlation with any mean value parameter is attempted. This fact helps to explain the trend to higher NDTT values, but does not explain the overall scatter.

The correlation of T_0 - C from precracked Charpy normalized energy tanh fits with RT_{NDT} was not as good as the correlation with NDTT shown in Figure 77. This is because the points shown in Figure 77 will stay the same or be shifted to higher ordinate values depending on whether RT_{NDT} = NDTT or RT_{NDT} > NDTT (when 50 ft-lbf/35 mil [68 J/0.89 mm] criteria are not met at NDTT + 60°F [NDTT + 33°C]). However, the fact that RT_{NDT} can be greater than NDTT for some heats improves the correlation shown in Figure 76 when RT_{NDT} is used instead of NDTT. That is, some of the points in Figure 76 are shifted upwards, but the correlation is still not as good as the one between NDTT and T_0 - C (from W/A) shown in Figure 77.

An alternate approach to normalization of fracture toughness data was attempted by using a temperature-strain rate parameter based on an Arrhenius rate relationship. The relationship has the form:

$$\dot{\varepsilon} = Ae^{-H/RT} \quad , \tag{30}$$

where

$\dot{\varepsilon}$ = strain rate
A = frequency factor
H = stress activation energy term
R = universal gas constant, and
T = absolute temperature.

It has been shown that the activation energy term for yielding is a function of stress such that rearranging Equation 30:

$$H = RT \ln (A/\dot{\varepsilon}) \quad , \tag{31}$$

and therefore

$$\sigma_y \propto T \ln (A/\dot{\varepsilon}) \quad . \tag{32}$$

The value of A has been determined for body-centered-cubic steels[47] as $10^8 s^{-1}$. The value of yield stress is really composed of two terms: (1) a rate and temperature sensitive term following the relationship of Equation 31 explicitly, and (2) a frictional stress term which is insensitive to temperature and strain rate. However, the overall relationship for yield stress can be depicted using Equation 32.

Values of lower yield stress (or 0.2% offset yield) for HSST Plate 02 (A533B-1) were obtained by Steichen and Williams[48] at various temperatures and strain rates. Their data and static tensile data ($\dot{\varepsilon} = 8.3 \times 10^{-5} s^{-1}$) on the same material from the EPRI round robin[9] are shown in Figure 78 as a function of the temperature-rate parameter in Equation 32.

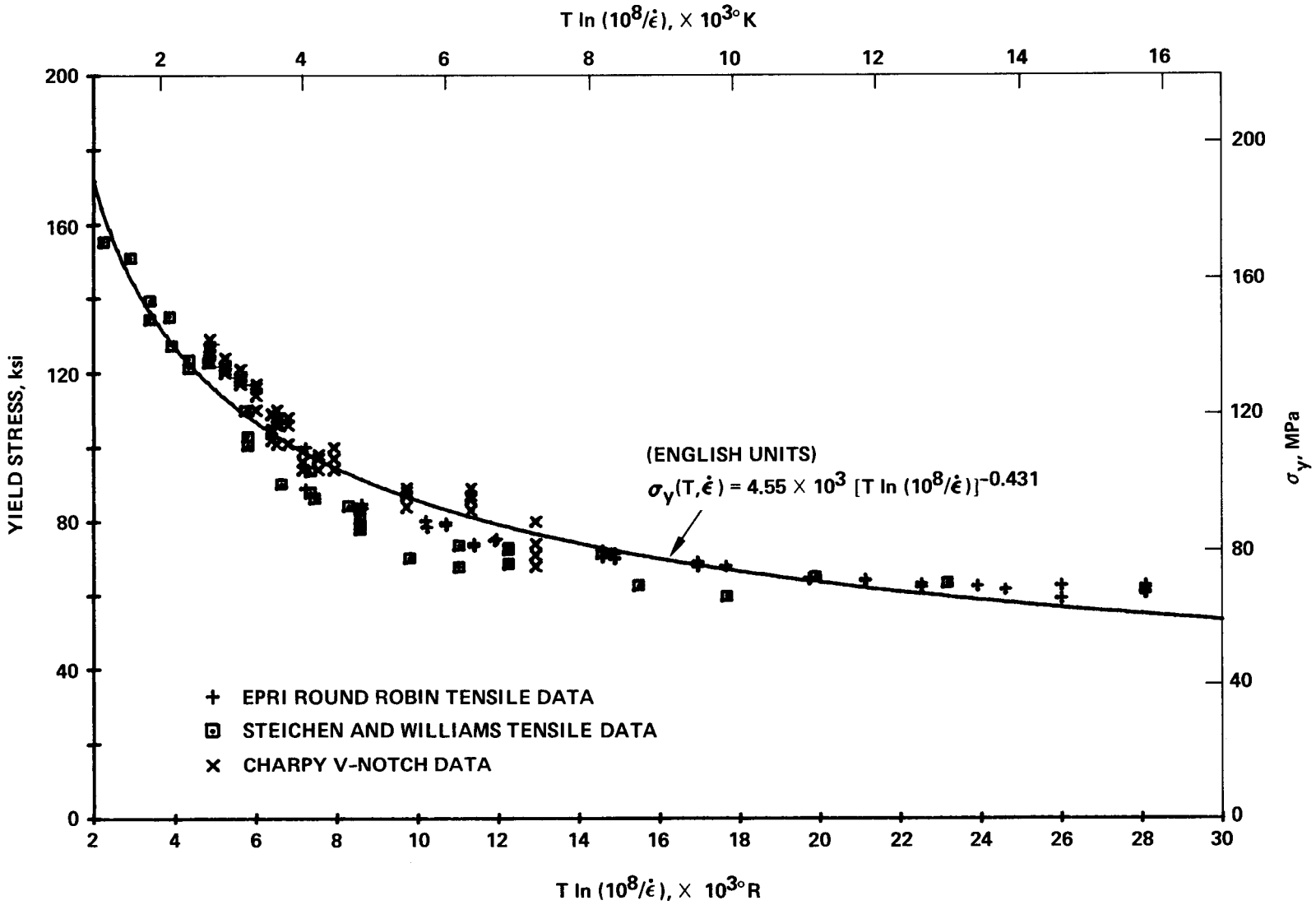

Figure 78. Yield Stress Data Normalized by the Rate-Temperature Parameter T&n $(10^8/\dot{\varepsilon})$

Included also in Figure 78 are data from instrumented Charpy V-notch tests in which the general yield load (P_{GY}) has been converted to a dynamic yield stress by using a Tresca yielding criteria and a slip line field solution[49]:

$$\sigma_y(\text{psi}) = 33.3 \left[P_{GY}\ (\text{lbf})\right] \quad . \tag{33}$$

The strain rate corresponding to the value of σ_y calculated from P_{GY} is rather ambiguous however.

Values of $\dot{\varepsilon}$ between 10^2 and $10^3 s^{-1}$ have been proposed for an impact velocity of 17 ft/s[50-53]. An elastic solution for the relationship between strain rate at the notch and mid-specimen deflection rate can be developed as follows. The compliance of a three-point bend specimen (C_s) for a span to width ratio of four is[10]

$$C_s = \frac{72}{EB}\left[g\left(\frac{a}{w}\right)\right] + \frac{20}{EB} \quad . \tag{34}$$

where E is the elastic modulus, B is the specimen thickness, and g (a/w) is a function of the specimen crack depth to width ratio. For an a/w = 0.2 for a standard Charpy V-notch specimen, Equation 34 reduces to

$$C_s = \frac{24.4}{EB} \qquad (a/w = 0.2) \quad . \tag{35}$$

Compliance is defined as displacement (d) over load (P) so that

$$P = \frac{d\ EB}{24.4} \quad . \tag{36}$$

The strain at the notch root (ε) can be defined as

$$\varepsilon = \frac{\sigma_N K_\sigma}{E} \quad , \tag{37}$$

where K_σ is the elastic stress concentration factor, and σ_N is the net section nominal bending stress,

$$\sigma_N = \frac{6Pw}{B(w-a)^2} \quad . \tag{38}$$

Combining equations 36, 37, and 38 yields:

$$\varepsilon = \left[\frac{6K_\sigma w}{24.4(w-a)^2}\right] d \quad ; \tag{39}$$

substituting dimensions and a value of $K_\sigma = 4.28$[51],

$$\varepsilon = 4.18\ [d(\text{in})] \quad . \tag{40}$$

Differentiating both sides with respect to time gives

$$\dot{\varepsilon} = 4.18\ [\dot{d}(\text{in/s})] \quad . \tag{41}$$

The deflection rate ($\dot{d}$) indicated in Equation 41 is the actual rate of loading of the specimen and not the velocity of the impacting pendulum head. Typically for mild steel at room temperature, $\dot{d} \simeq 66$ in/s for an impact velocity of 17 ft/s.* Thus, the strain rate for the Charpy V-notch sample is $\sim 275\ s^{-1}$. Figure 79 shows the same yield data as in Figure 78 at various temperatures only as a function of strain rate. Plotting the Charpy yield data at $275\ s^{-1}$ provides reasonable agreement with the other data.

Therefore, the Charpy data shown in Figure 78 are plotted using $\dot{\varepsilon} = 275\ s^{-1}$, and the overall data are in good agreement with the tensile test results. A curve of the form

---

*The machine compliance is actually greater than the specimen compliance, and the effective specimen deflection rate is less than one-half the pendulum impacting velocity.

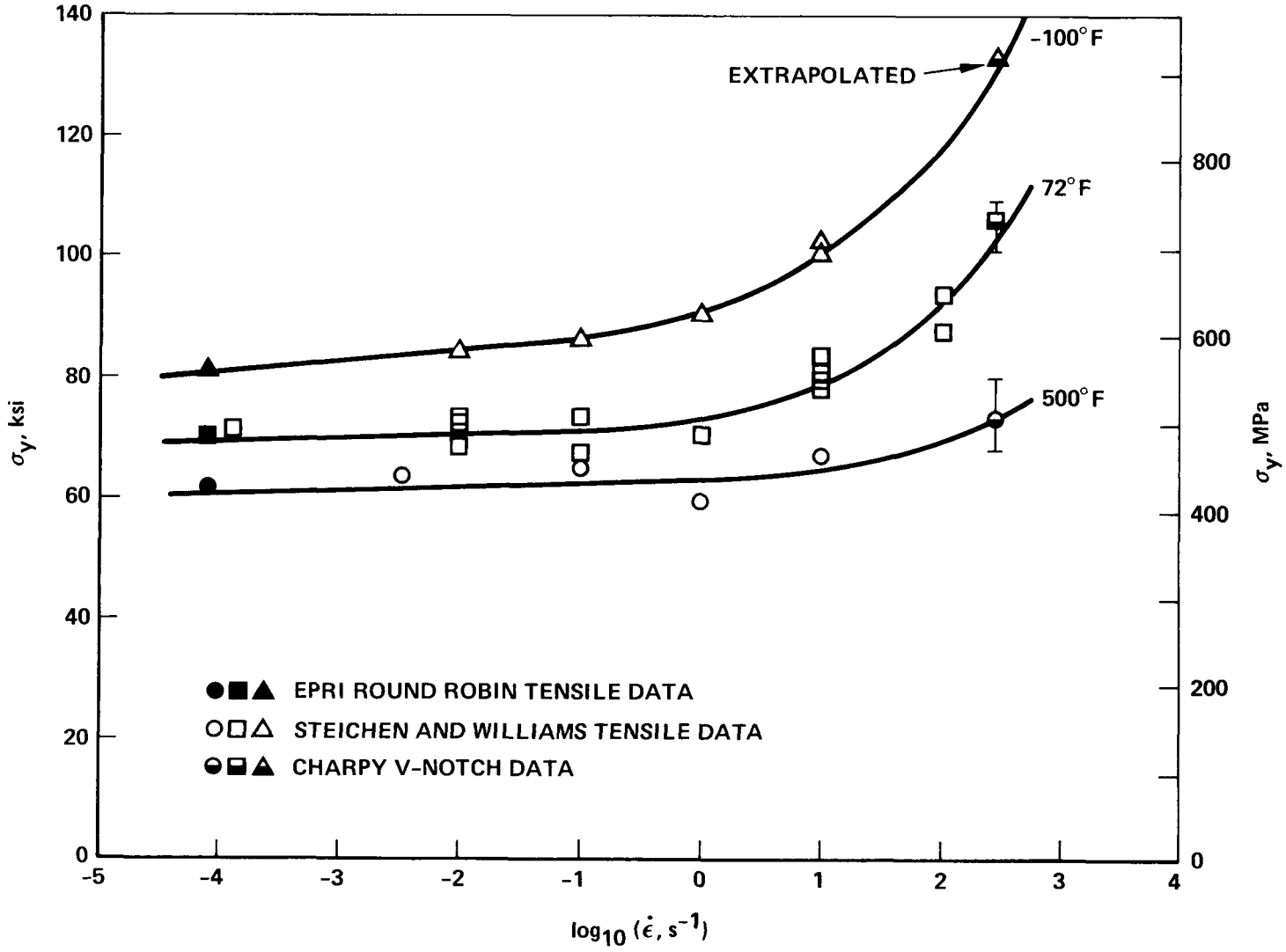

Figure 79. Yield Stress Data As a Function of Strain Rate at -100 (-73), 72 (22), and 500°F (260°C)

$$\sigma_y = C \left[T\ell n \left(\frac{10^8}{\dot{\varepsilon}} \right) \right]^{-n} \qquad (42)$$

was fitted to the data in Figure 78 by a least squares technique, and English unit values of $C = 4.55 \times 10^3$ and $n = 0.431$ were obtained. The curve fit is not perfect but will suffice for the rest of the analysis, especially since the range of interest is between 4000 and 12,000 ^{o}R (2000 to 7000^{o}K; x-axis).

Assuming that the change in fracture toughness follows the functional relationship for yield stress, the linear elastic toughness results for HSST Plate 02 from Shabbits[21] and the EPRI round robin program[9] can be equated to a strain rate and temperature. The conversion to strain rate (from a fracture toughness test) involves a calculation near the elastic-plastic interface of the plastic zone. Irwin[54] has calculated the strain rate at the elastic-plastic interface to be

$$\dot{\varepsilon} = \frac{2\sigma_{yy}}{tE} \quad , \qquad (43)$$

where σ_{yy} is the principal stress at the crack tip boundary and t is the total time of the test. However, since a triaxial stress state occurs during plane strain conditions the value of σ_{yy} is elevated to approximately 1.7 σ_y assuming no strain hardening. When strain hardening exists, as it does in A533B-1 steel ($0.1 \leq n \leq 0.2$), the elevation of σ_{yy} near the elastic-plastic boundary is closer to 3.5 σ_y[55]. Therefore, for A533B-1 steel Equation 43 can be stated as

$$\dot{\varepsilon} \simeq \frac{7\sigma_y}{tE} \quad . \qquad (44)$$

Also, the time of fracture is related to the stress intensity rate ($\dot{K}$) and stress intensity (K) by

$$t = \frac{K}{\dot{K}} \quad . \tag{45}$$

Combining Equations 44 and 45 gives an expression for $\dot{\varepsilon}$ in terms of $\dot{K}$,

$$\dot{\varepsilon} = \frac{7\sigma_y \dot{K}}{EK} \quad . \tag{46}$$

To solve for a value of $\dot{\varepsilon}$ it is necessary to also know the value of σ_y at the same test temperature and strain rate. Thus, an iterative approach is required using Equations 42 and 46.

The results for the HSST material are shown in Figure 80. If the normalization approach worked, all of the data would be superimposed onto one continuous curve. However, as shown in Figure 80 the data separates into distinct $\dot{K}$ groups. This normalization procedure does not work in this simple form. Changes in the frequency factor A or the stress concentration factor in Equations 44 and 46 would not appreciably change the trend shown in Figure 80. Note that if a K_{IR} curve could be superimposed on Figure 80, it would be an upper bound curve using this approach. Thus, this fundamental approach to normalizing (indexing) the fracture toughness data does not appear to be adequate. Therefore, the experimental data approach using the tanh fit parameters from the precracked Charpy toughness data to normalize the larger specimen data was selected.

Unique K_{IR} Curves for Specific Materials

Estimates of variance from small numbers of tests tend to be inaccurate. Hence, if the dynamic and static test types are considered separately, it is helpful to make some broad simplifying assumptions. First, the variance estimates tend to fall into three broad groups: the lower shelf, the transition range, and the upper shelf. Within these groups, there were only minor differences in variance. Consequently, since it is unrealistic to set a lower bound which fluctuates over short intervals due to variance changes, the variances were grouped within these ranges.

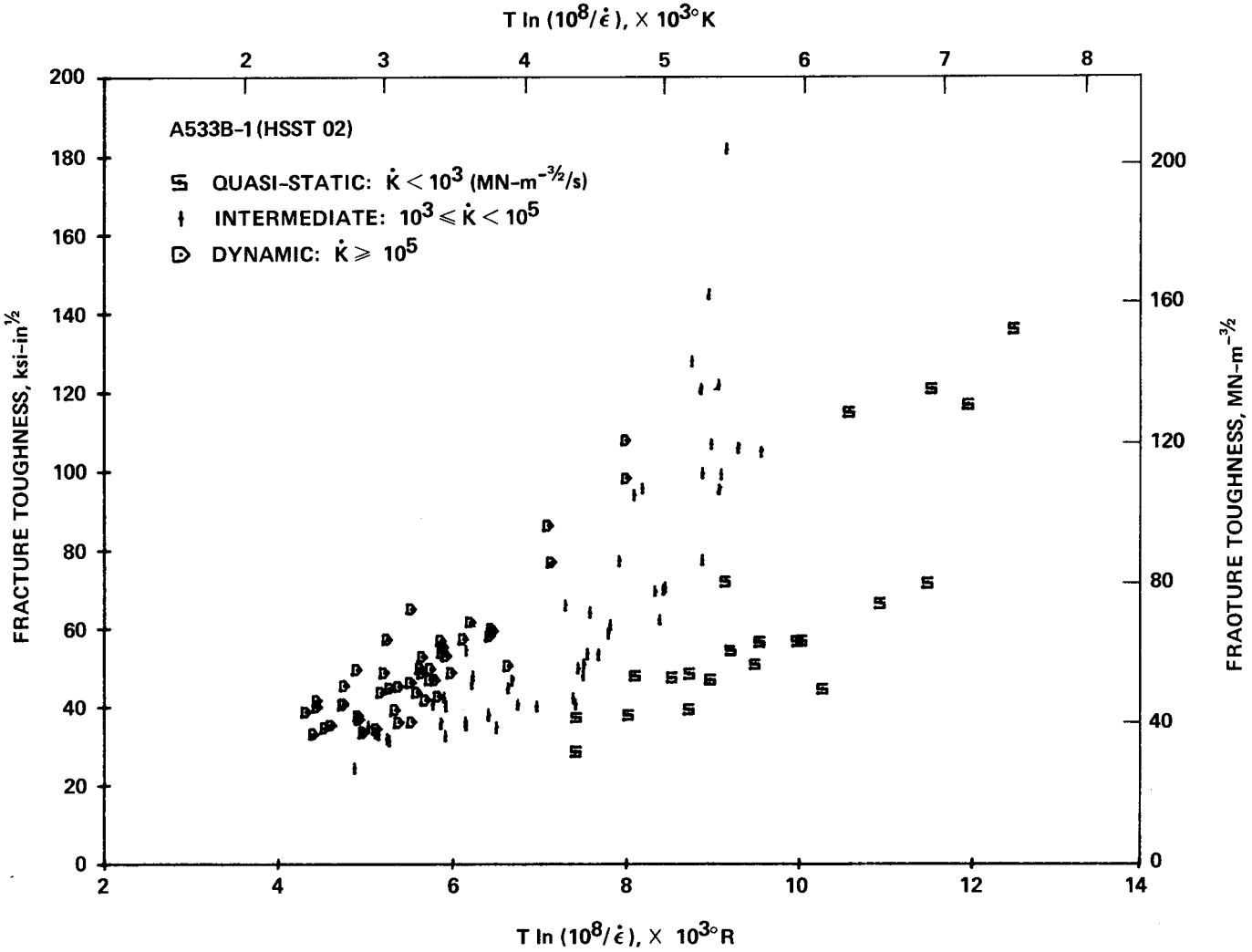

Figure 80. Linear Elastic Fracture Toughness[9,21] Normalized by the Rate-Temperature Parameter T&n $(10^8/\dot{\varepsilon})$

Specifically, groups 2 - 5 were combined into a single transition range variance for each type of test (static or dynamic). Second, although some materials tended to have lower than average variance, a grouped variance for all materials is a conservative assumption for the base materials, but it might tend to be optimistic for the weld materials.

From the distribution studies, the Normal distribution was found to be a fair representation of the spread of data about the curve over most of the range. The major problems were found at the upper shelf, where the data were skewed low. Since the reference curves cannot at this time be applied in the upper shelf range, this objection is not important. The lower shelf presents a different sort of difficulty. It is physically impossible for the data to fall below zero toughness, while limits placed using the Normal distribution could fall in any position. To overcome this objection, which manifests itself statistically in the observation that the lower shelf is skewed high, a different type of distribution was used for the lower shelf only.

The shape of a probability distribution can be characterized by the moments of the distribution. The shape of the distribution about the lower shelf, where negative fracture toughness was forbidden, was characterized as skewed on the basis of the computed moments. However, there is a class of curves developed by Pearson, which are capable of describing most probability distributions with a fair degree of accuracy. These curves have been tabulated for a wide range of moments, so that if the moments of a distribution have been computed, the complete probability distribution can be characterized by the appropriate Pearson curve[46]. Using the appropriate curve, the deviates corresponding to the required probability level for the lower bound can be read from the table.

Setting a lower bound to the reference curve presents difficult statistical and physical problems. The physical problems, being most important will be discussed first. The most straightforward

interpretation of a reference curve which will be used in the work which follows is the following:

> Suppose the fracture toughness for an unknown heat of A533B-1 steel were to be characterized using the reference curve technique. A set of instrumented precracked Charpy test results provide referencing A, B, T_0, and C values. The reference curve is entered, and a lower bound for static or dynamic fracture toughness is provided as a function of temperature. Suppose that (although the use of a reference curve assumes that no large specimen fracture toughness testing will be performed) some tests are carried out. The lower bound states that 5 tests in 100, 1 test in 200, or whatever is stated in the tolerance level, will probably lie below the curve.

By contrast, the mean fracture toughness for repeated tests will lie on or near the central line for the normalized curve. Another interpretation of the reference curve might be to predict the mean toughness of the material. This mean procedure could be performed by using modified deviates showing a lower limit on the mean predicted material toughness. Such limits would be much less severe than those for single values.

Statistical problems stem from the non-constant variance and distribution. These cause the limits to be set in a piecemeal rather than an overall fashion which is usually possible in regression studies. The difficulty is accentuated by the need for non-linear regression techniques to fit the tanh curve, preventing computation of accurate estimates for the variances and covariances of the curve coefficients (see Appendix D).

Two approaches appear to be the most feasible at this time. One approach (which will be used in the work which follows) assumes that the position of the central curve is known exactly; this statement is a fair assumption for those curves for which there are many data points such as material 1. The variance about the curve is simply estimated with the

degrees of freedom of the estimate given by the number of data points grouped for the variance estimate. If the data has a Normal distribution, the added uncertainty introduced by the estimate of variance is taken into account by the t - distribution. This distribution therefore predicts the confidence band for any specified probability level, α.

The alternative, more conservative approach assumes that the data in the sample is the sole arbiter of the position of the mean of the curve. The position of this mean center line then has an uncertainty which is proportional to $\sigma/\sqrt{n}$, where n is the number of test results lying within the sample. Because of this added uncertainty, the position of the lower bound is based upon the following concepts:

1. What is the certainty required that a specified fraction of future tests will lie above the lower bound?
2. What is the fraction of tests to lie above the bound?

This added complication becomes more important as the number of test results falls, and the scatter becomes greater, as is the case for the weld metal curves.

At the lower shelf, the development of a lower bound using the Pearson curve presents fewer options. When the variance and the moments of the distribution of the data are not known exactly, theoretical treatments which define the lower bound are not available. Solutions could be developed using, for example, stochastic models for the system of data, but such limits would be hard to defend, and would require a small research program in themselves. For the case in which there is a large sample size, as for the A533B-1 material, the Pearson deviates are quite accurate. However, when the sample size is small, as for the other materials (especially the weldments), this assumption is less accurate. We have countered this small sample size in part by using the grouped data for all materials. This assumption introduces conservatism in the lower bound for the well characterized materials, while there is additional uncertainty concerning the non-base metal material.

Bounds set by the t-distribution and by the Pearson curve are quite different. Consequently, there must be some transition between the two if an abrupt change is to be avoided. In the lower bounds presented here, the t-distribution bound was assumed not to pass below the highest level of the Pearson distribution-based bound.

The results are presented in Figures 81-96. The coefficients of the central curve (labeled A', B', T_0', and C', and not to be confused with the normalizing parameters taken from the precracked Charpy curves) define the mean line, f_m, as a function of normalized temperature t;

$$f_m = A' + B' \tanh \left[\frac{t - T_0'}{C'} \right] \quad , \tag{47}$$

where A', B', T_0', and C' designate the normalized curve tanh coefficients. The lower bound is the deviate D below the line f_m (95 and 97.5 confidence bounds).

Discussion of Lower Bound Results

The lower bound curves shown in Figures 81-96 represent the culmination of a set of analyses, beginning with the tanh curve analysis of the precracked Charpy test. At the time the precracked Charpy tests were performed, there had been no anticipation of the eventual role of the tanh coefficients as normalizing parameters. It transpires that some of the experimental techniques and the choice of specific test temperatures used in the performance of those tests were the cause of much of the variability of the normalized curves. It appears that the major source of error in the curves is in the C coefficient of the tanh fit to the precracked Charpy data which should correct for differences in the rate of property transition between the shelves. For some of the materials, there were unreasonably large variations in the C values which resulted in systematically large differences in the slopes of the transition of the normalized data. The cause of the problem is not difficult to find. Referring to Table 9, which shows the instrumented precracked Charpy test results in summary, groups 1 and 6, the lower and upper shelf groups, con-

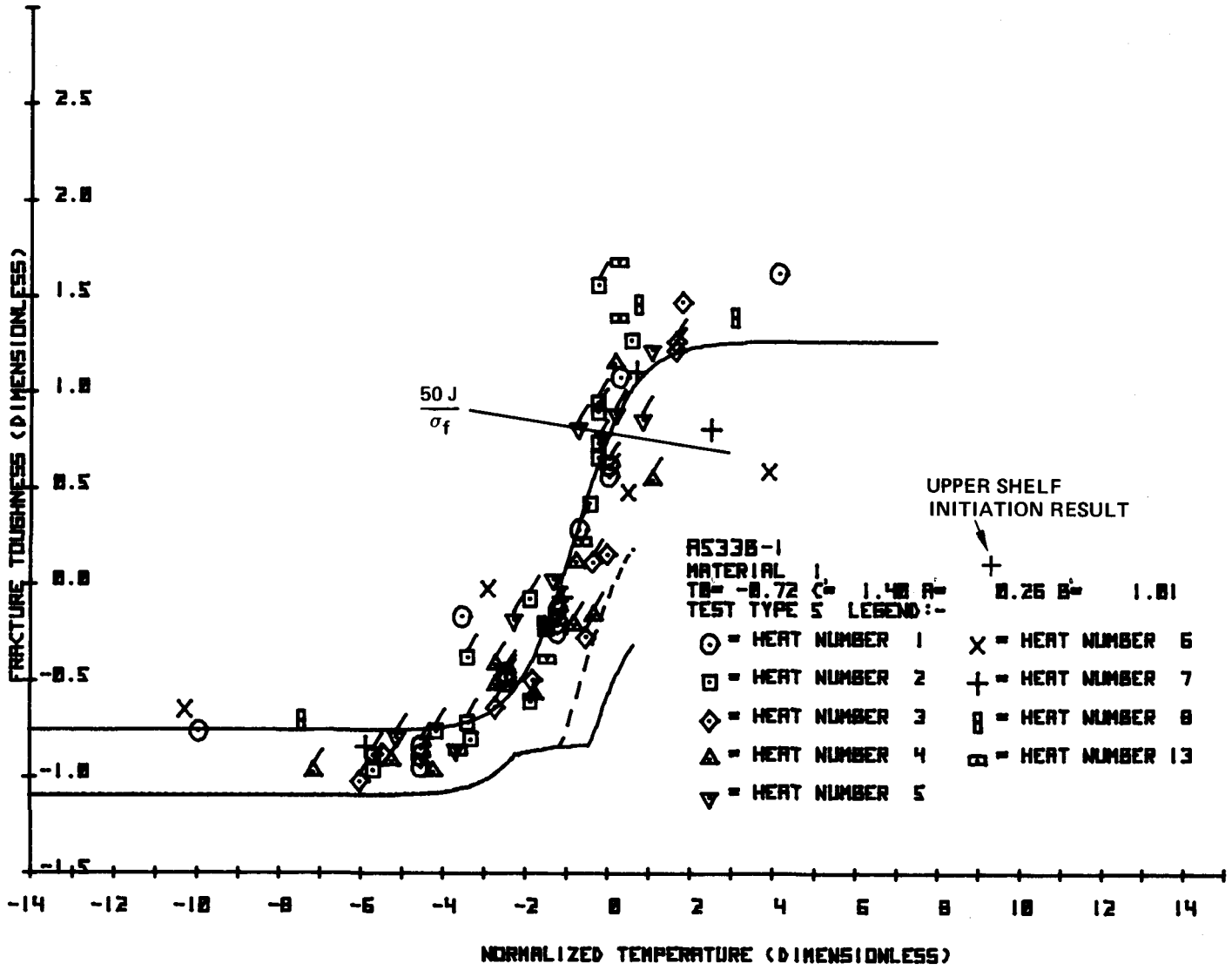

Figure 81. Lower Bound Curve for Material 1, Static Compact

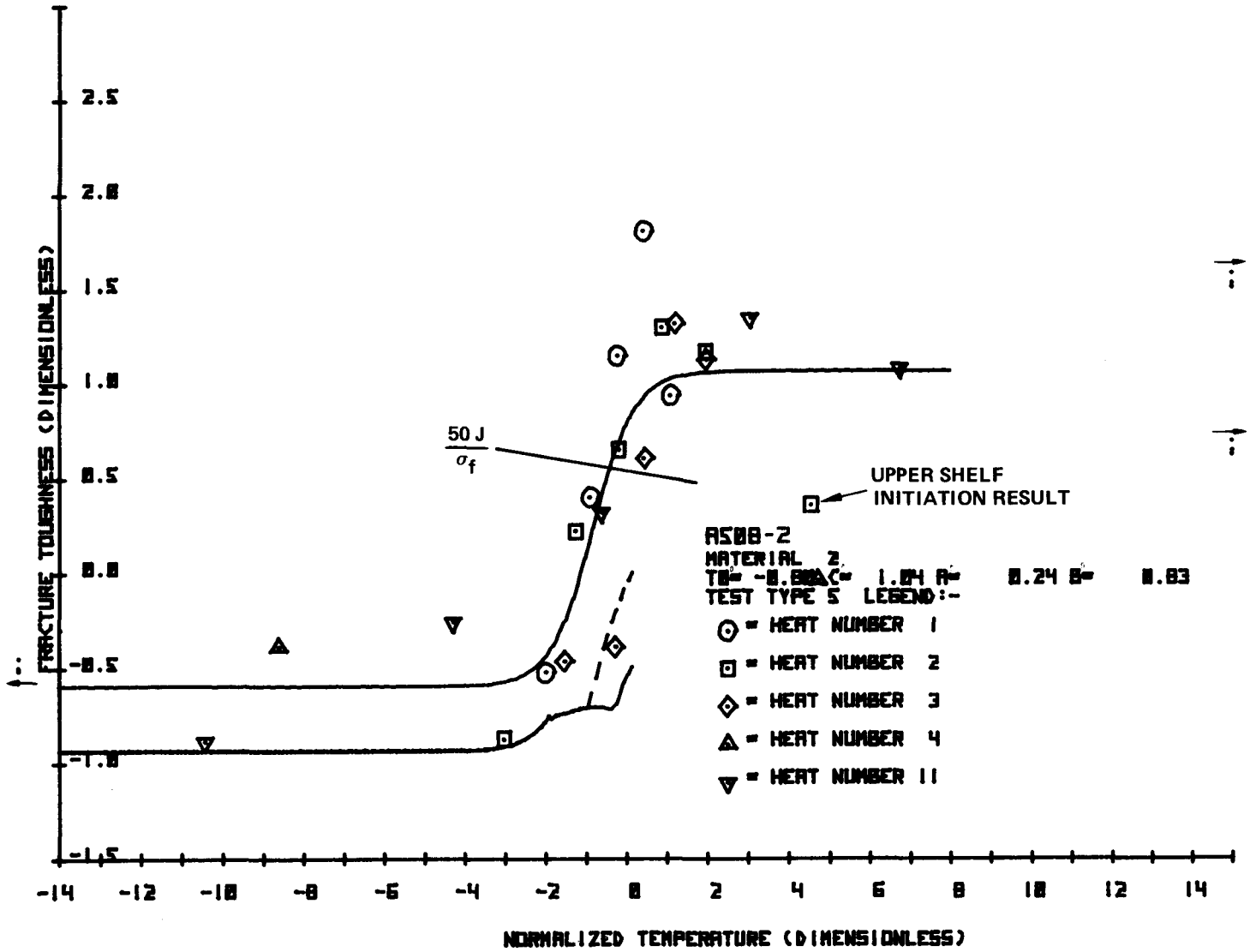

Figure 82. Lower Bound Curve for Material 2, Static Compact

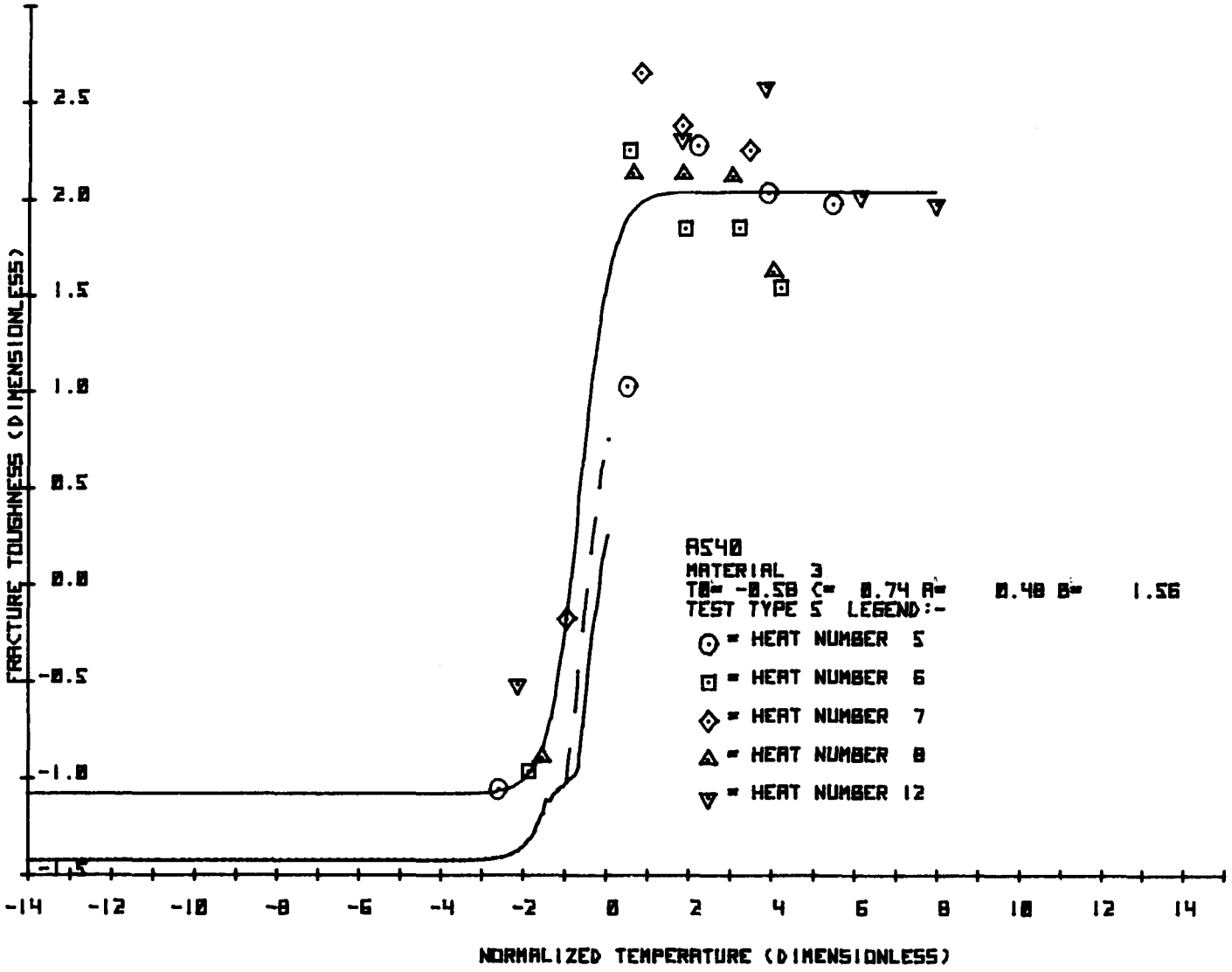

Figure 83. Lower Bound Curve for Material 3, Static Compact

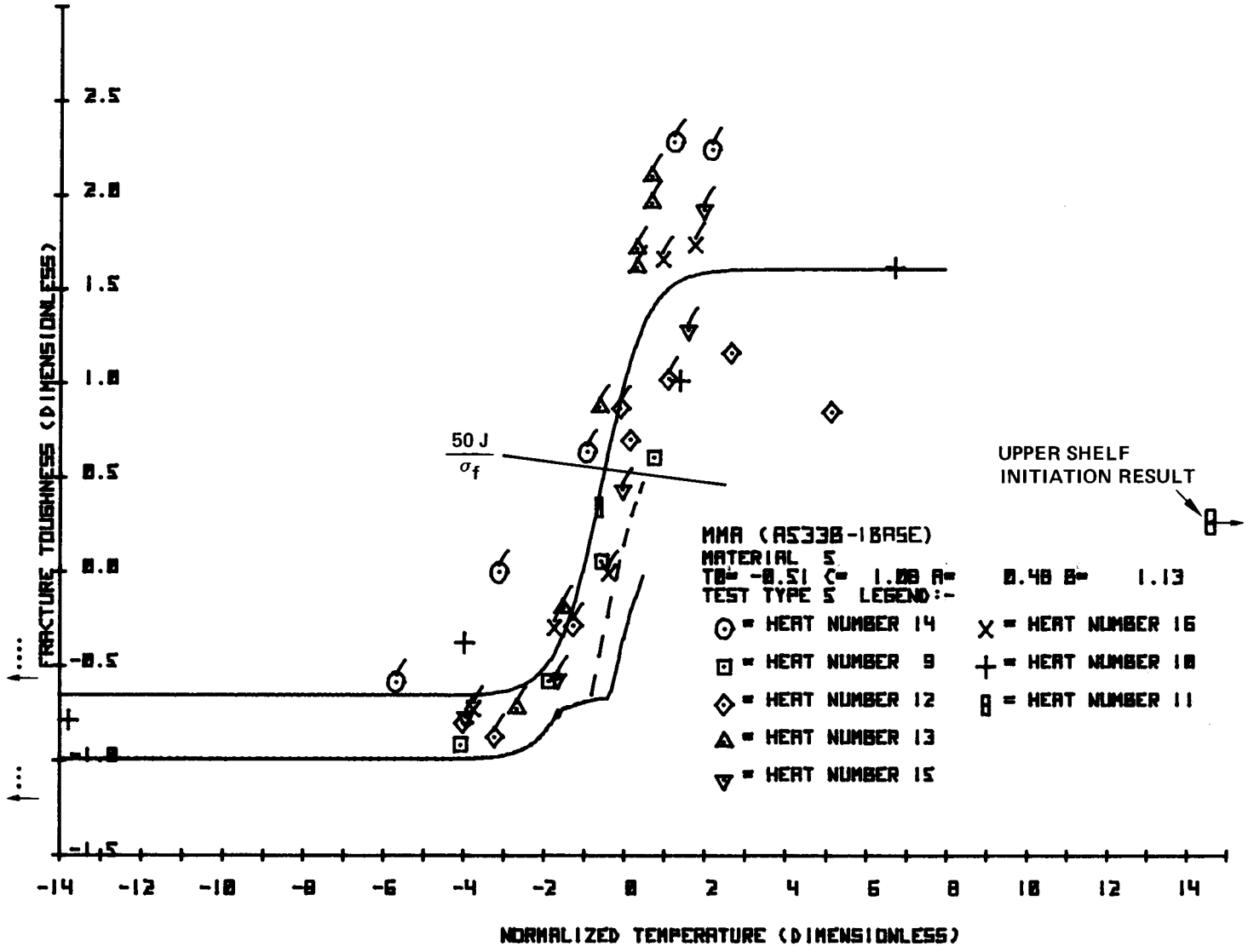

Figure 84. Lower Bound Curve for Material 5, Static Compact

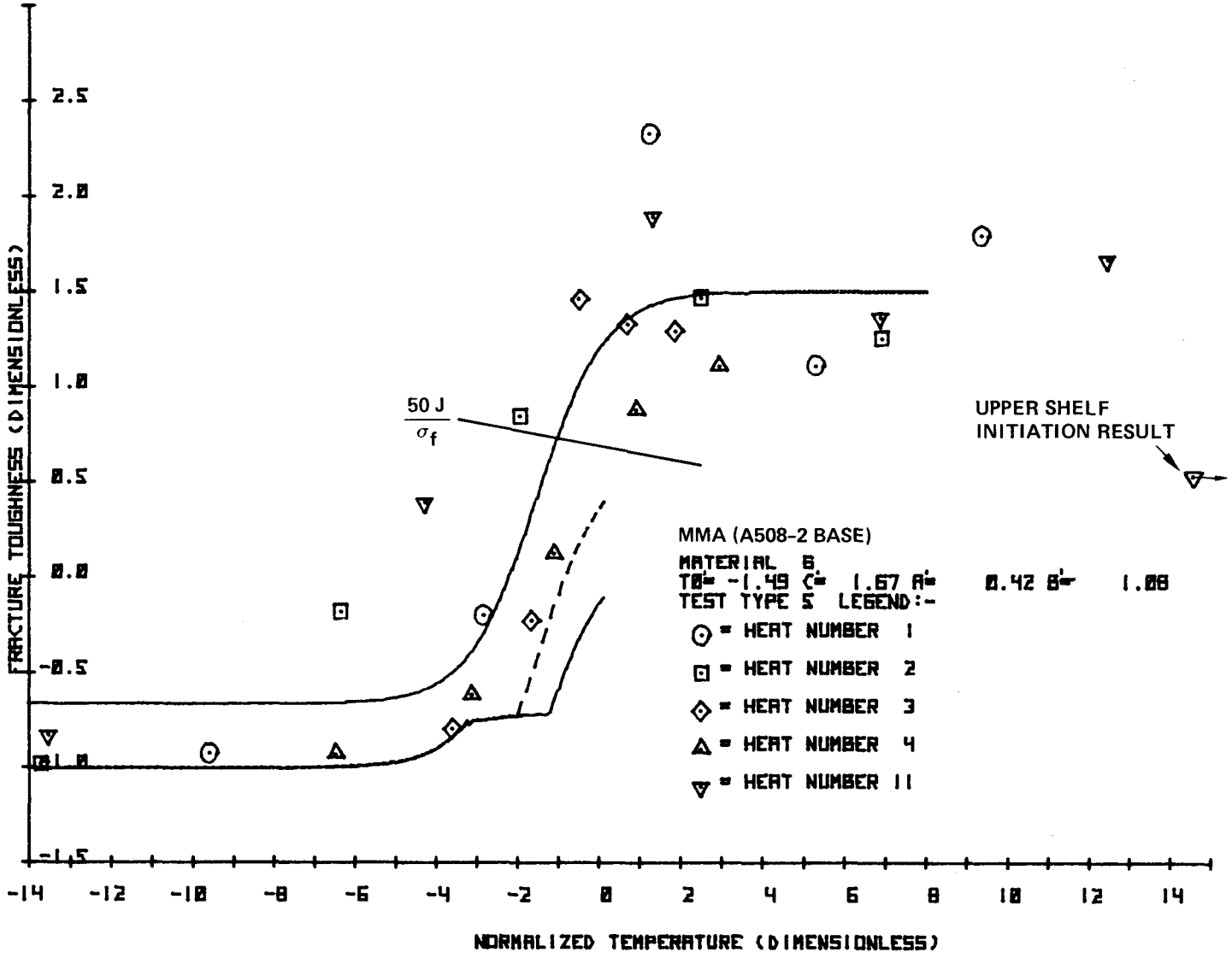

Figure 85. Lower Bound Curve for Material 6, Static Compact

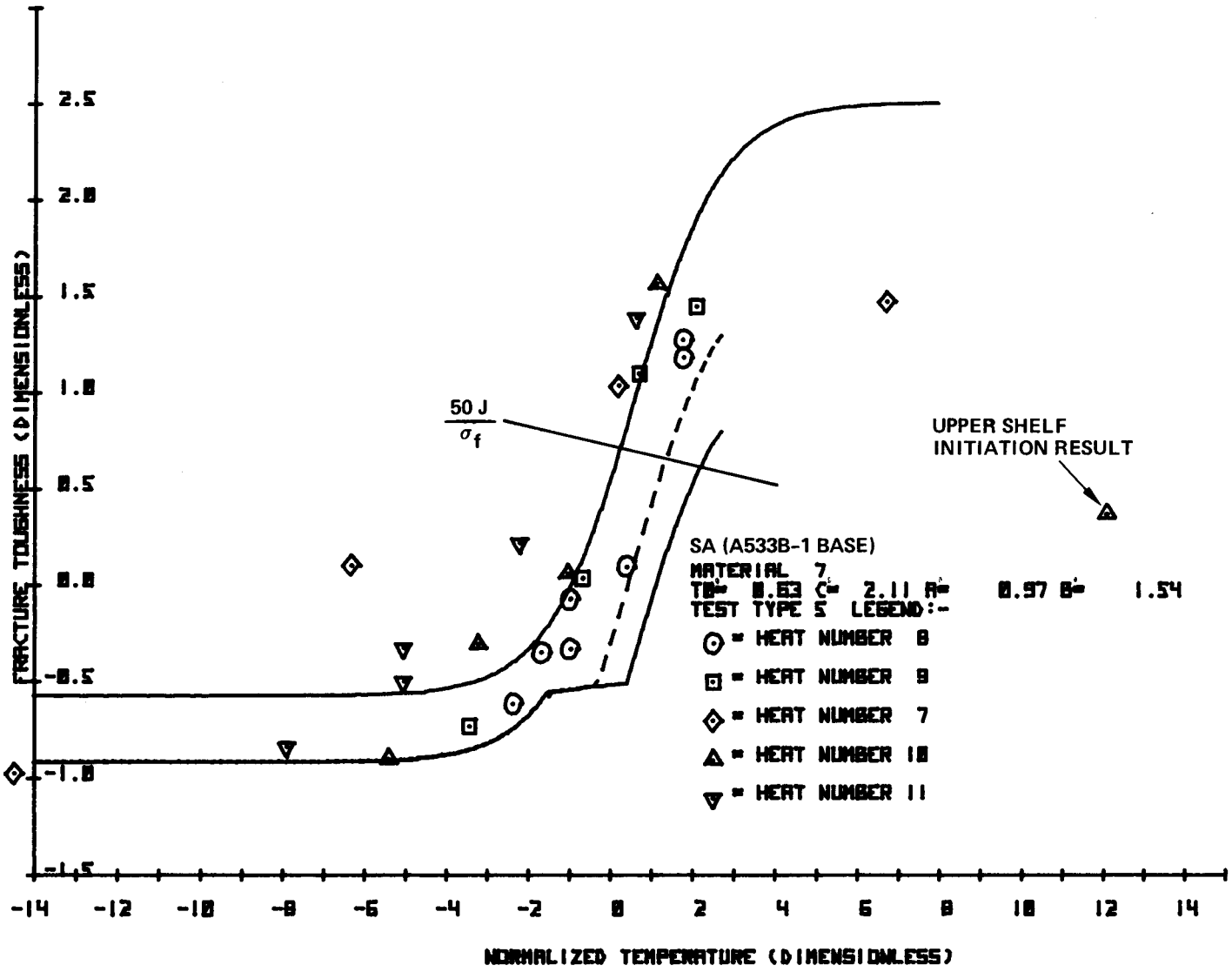

Figure 86. Lower Bound Curve for Material 7, Static Compact

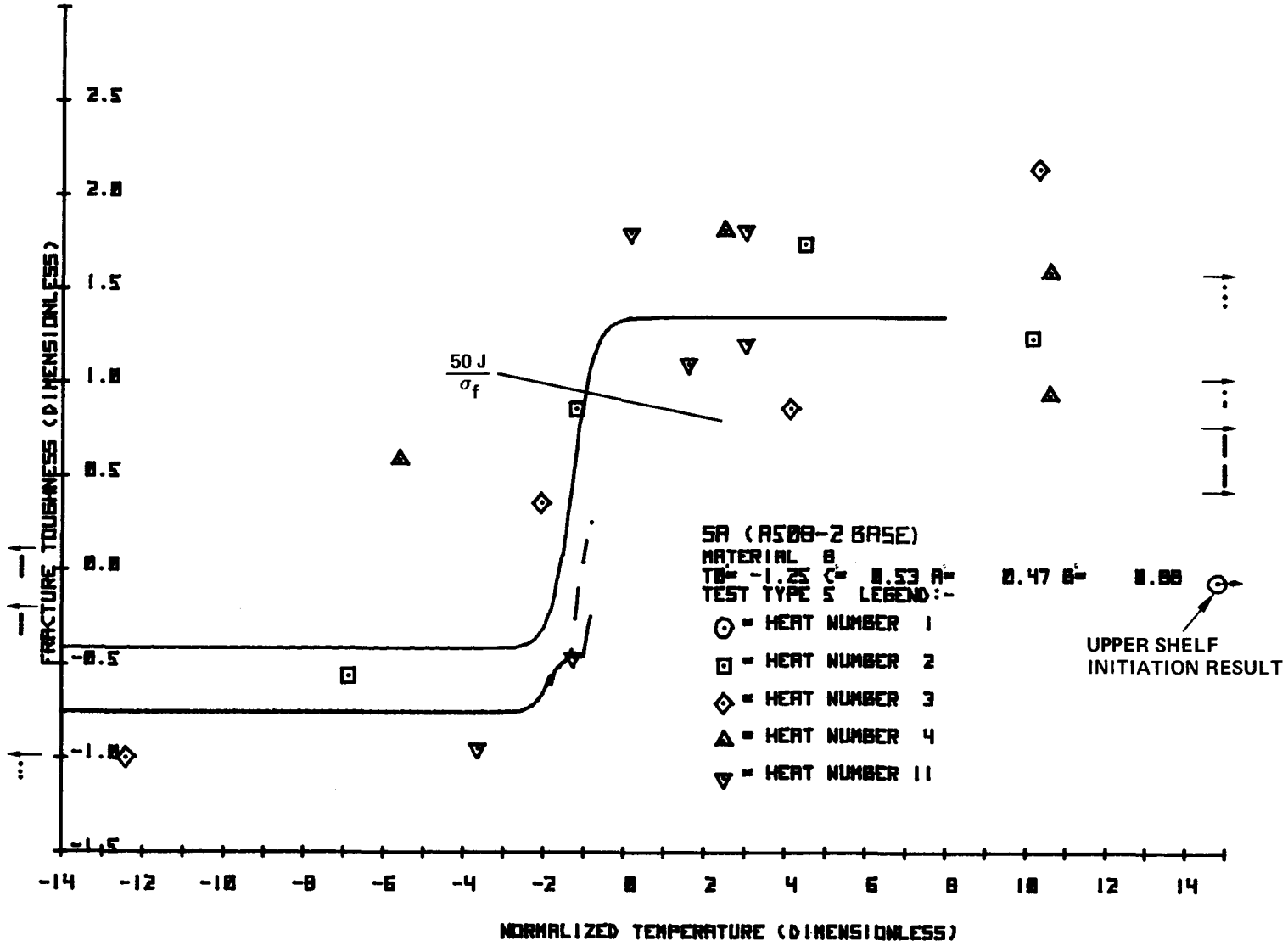

Figure 87. Lower Bound Curve for Material 8, Static Compact

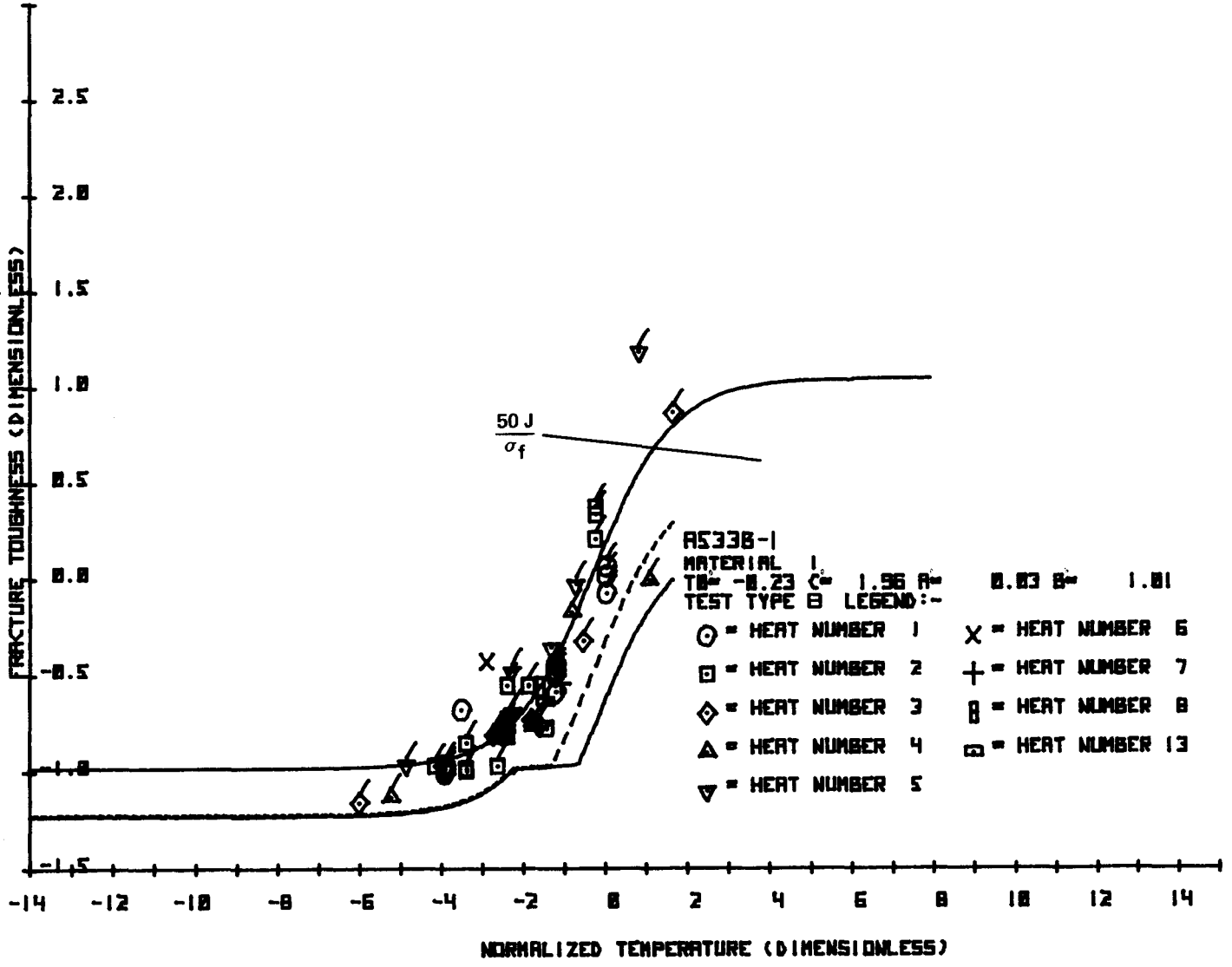

Figure 88. Lower Bound Curve for Material 1, Dynamic Compact

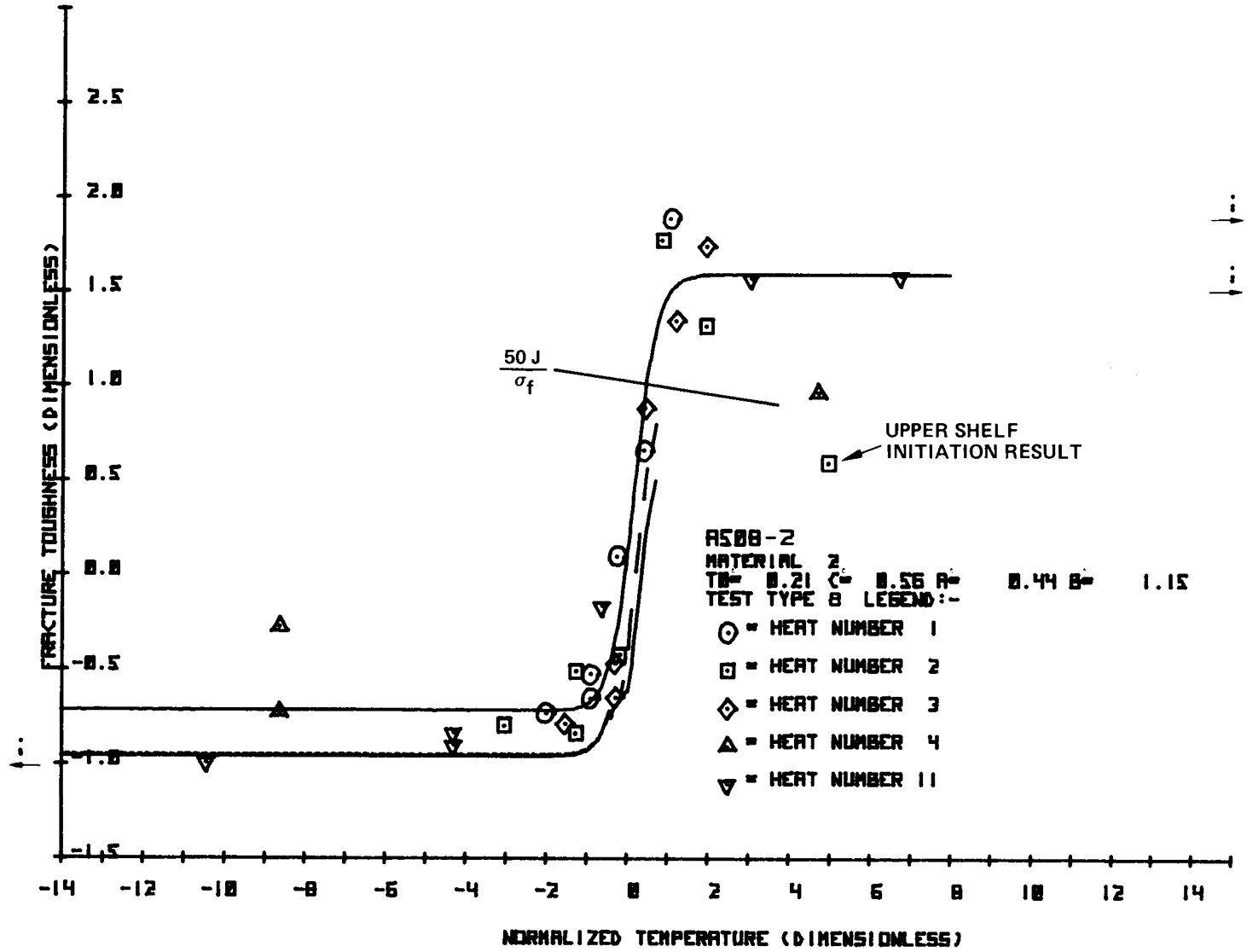

Figure 89. Lower Bound Curve for Material 2, Dynamic Compact

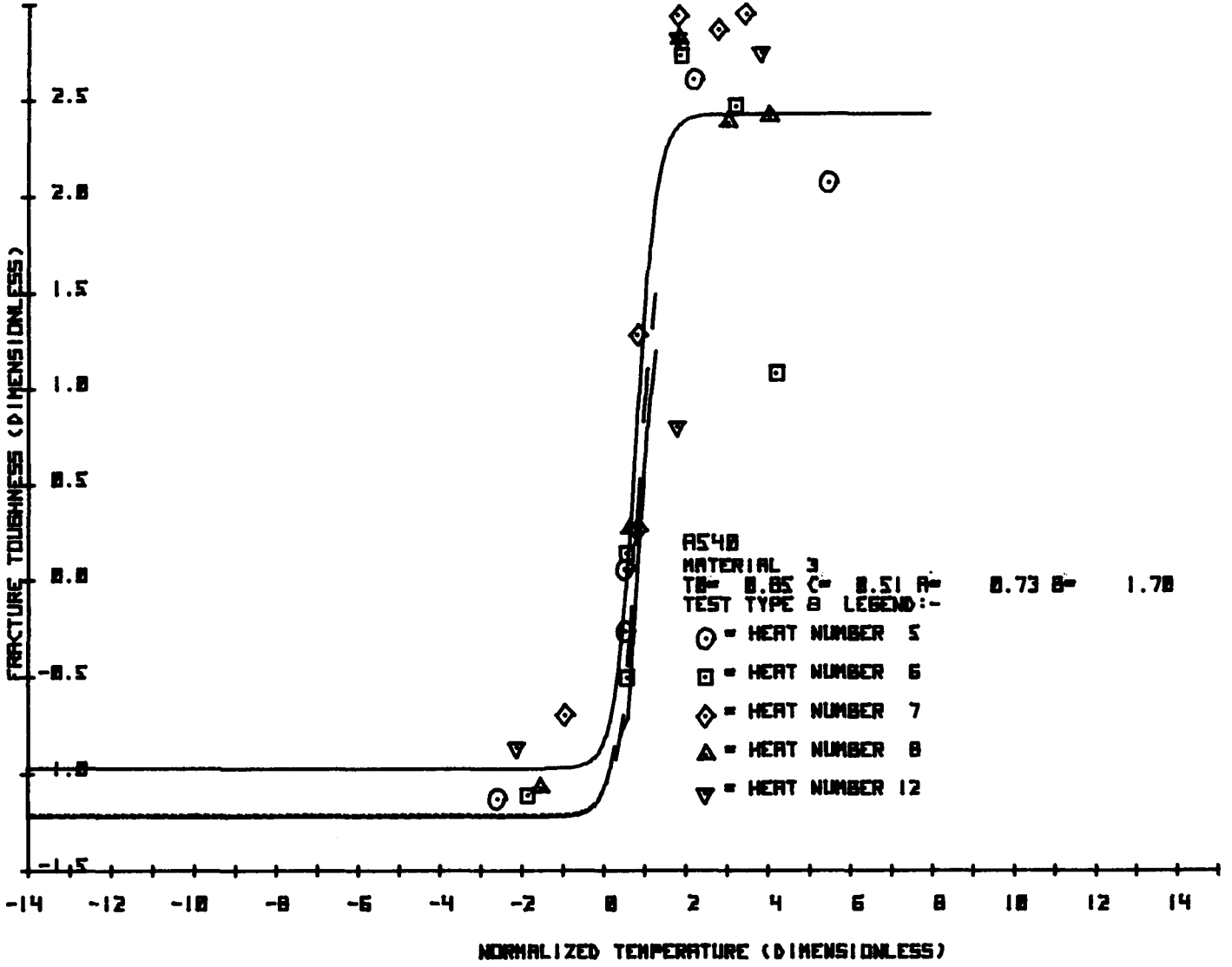

Figure 90. Lower Bound Curve for Material 3, Dynamic Compact

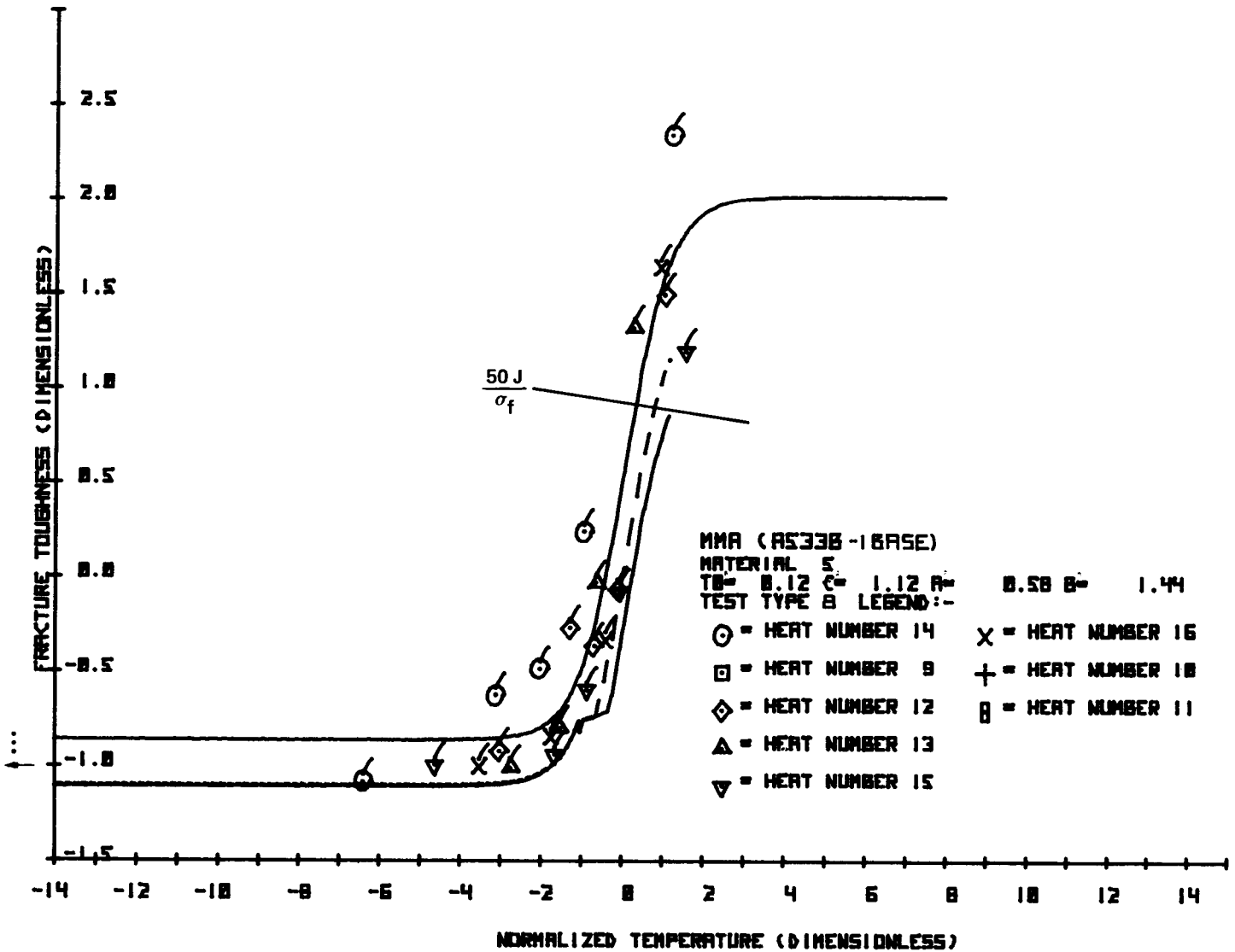

Figure 91. Lower Bound Curve for Material 5, Dynamic Compact

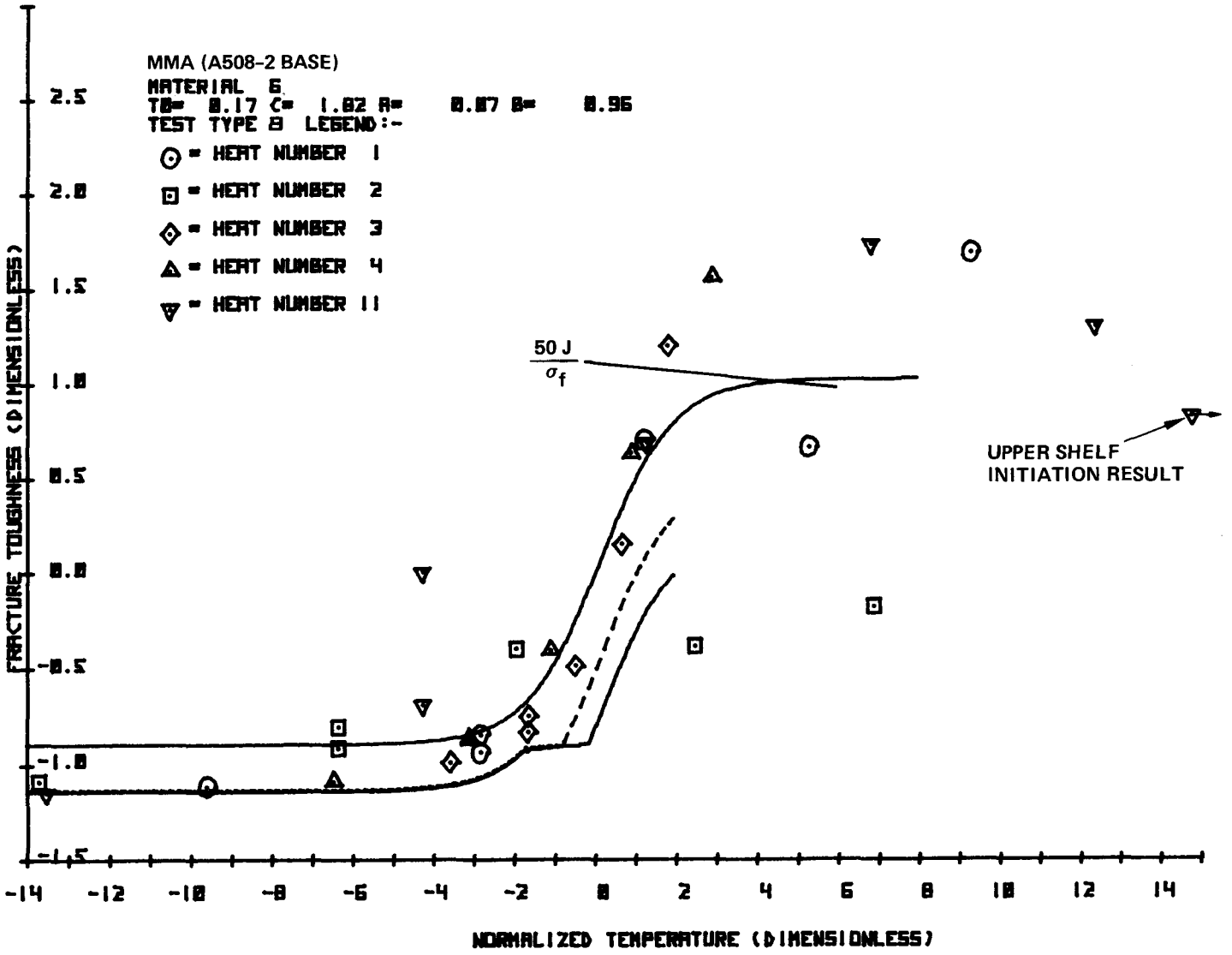

Figure 92. Lower Bound Curve for Material 6, Dynamic Compact

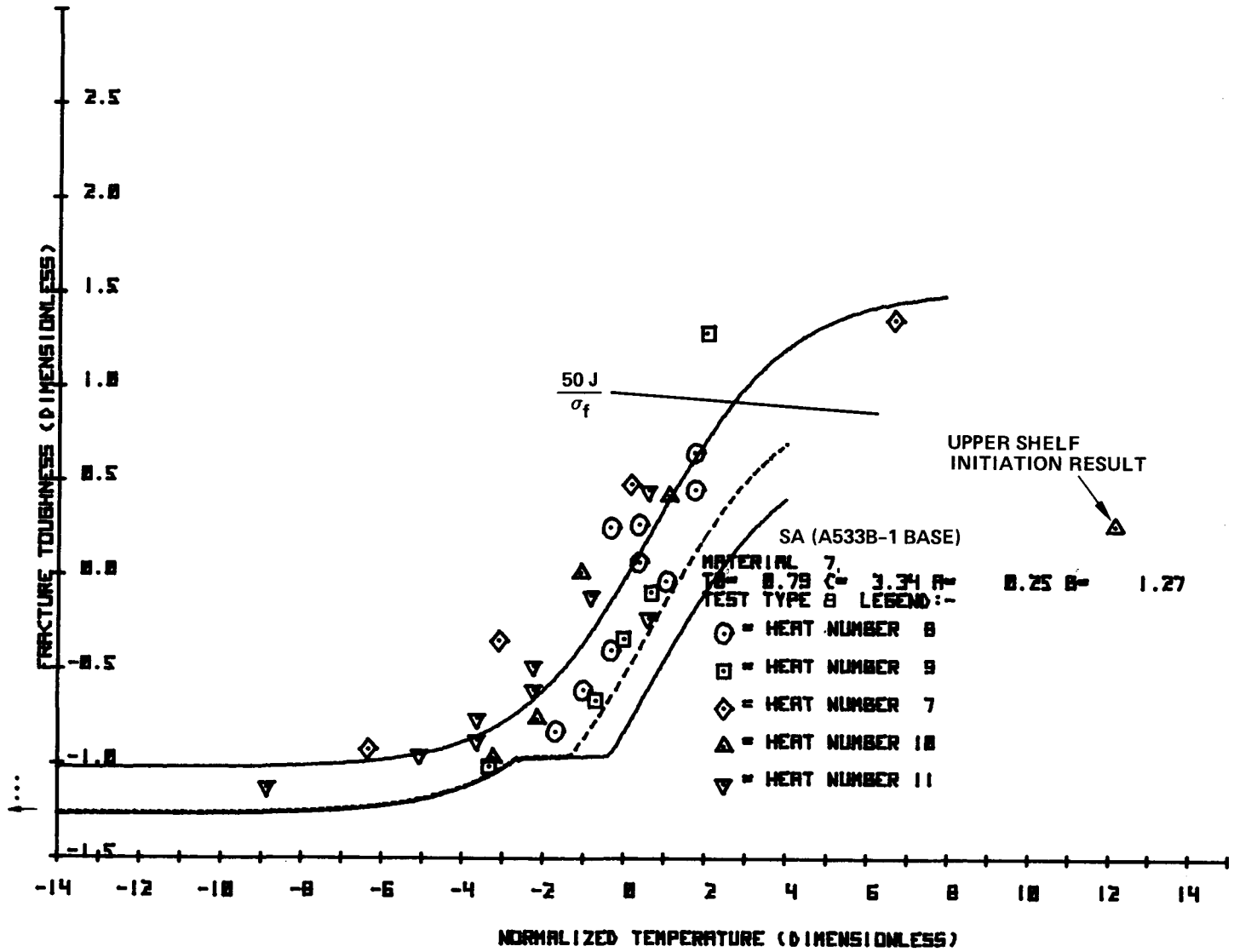

Figure 93. Lower Bound Curve for Material 7, Dynamic Compact

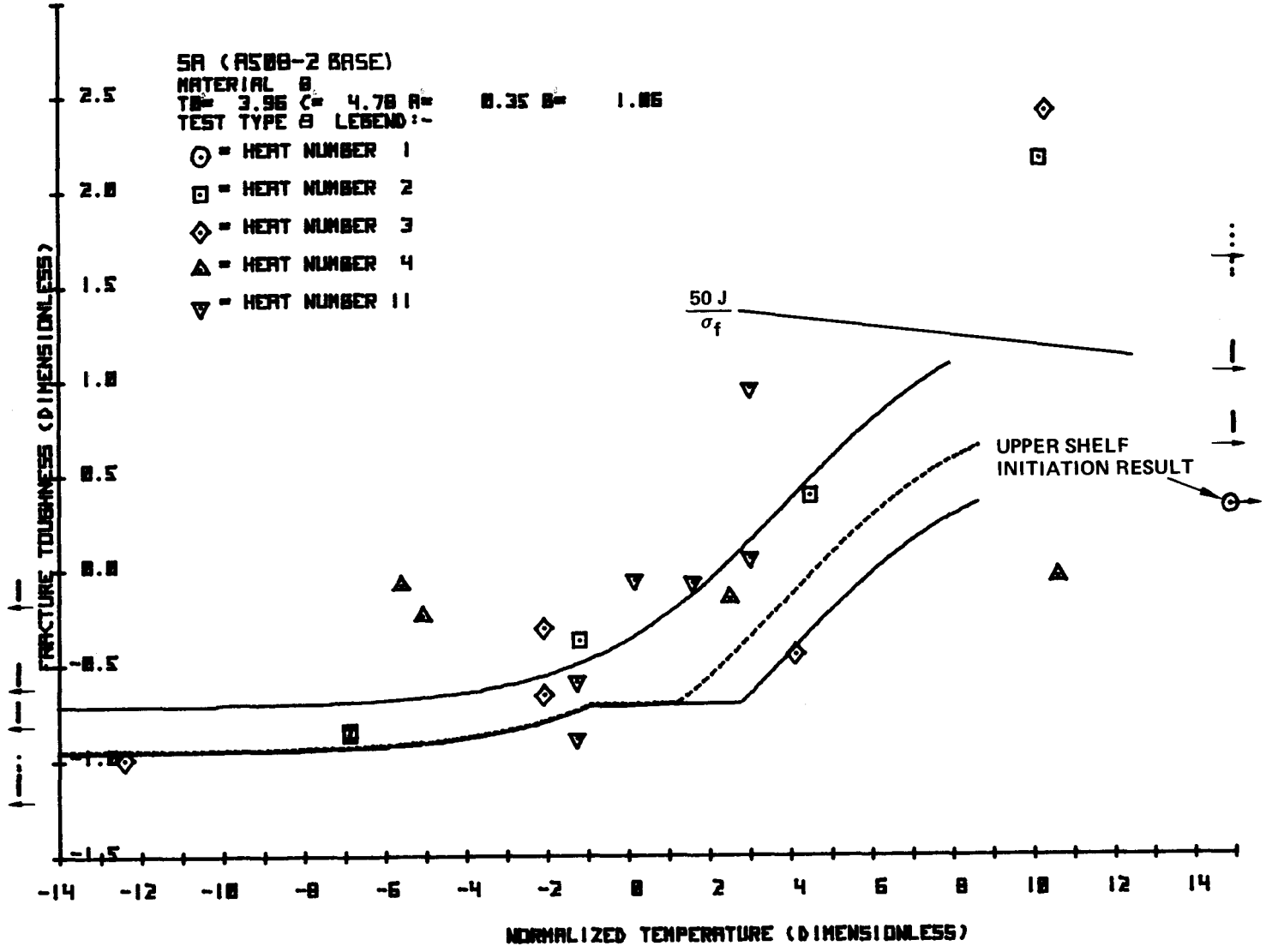

Figure 94. Lower Bound Curve for Material 8, Dynamic Compact

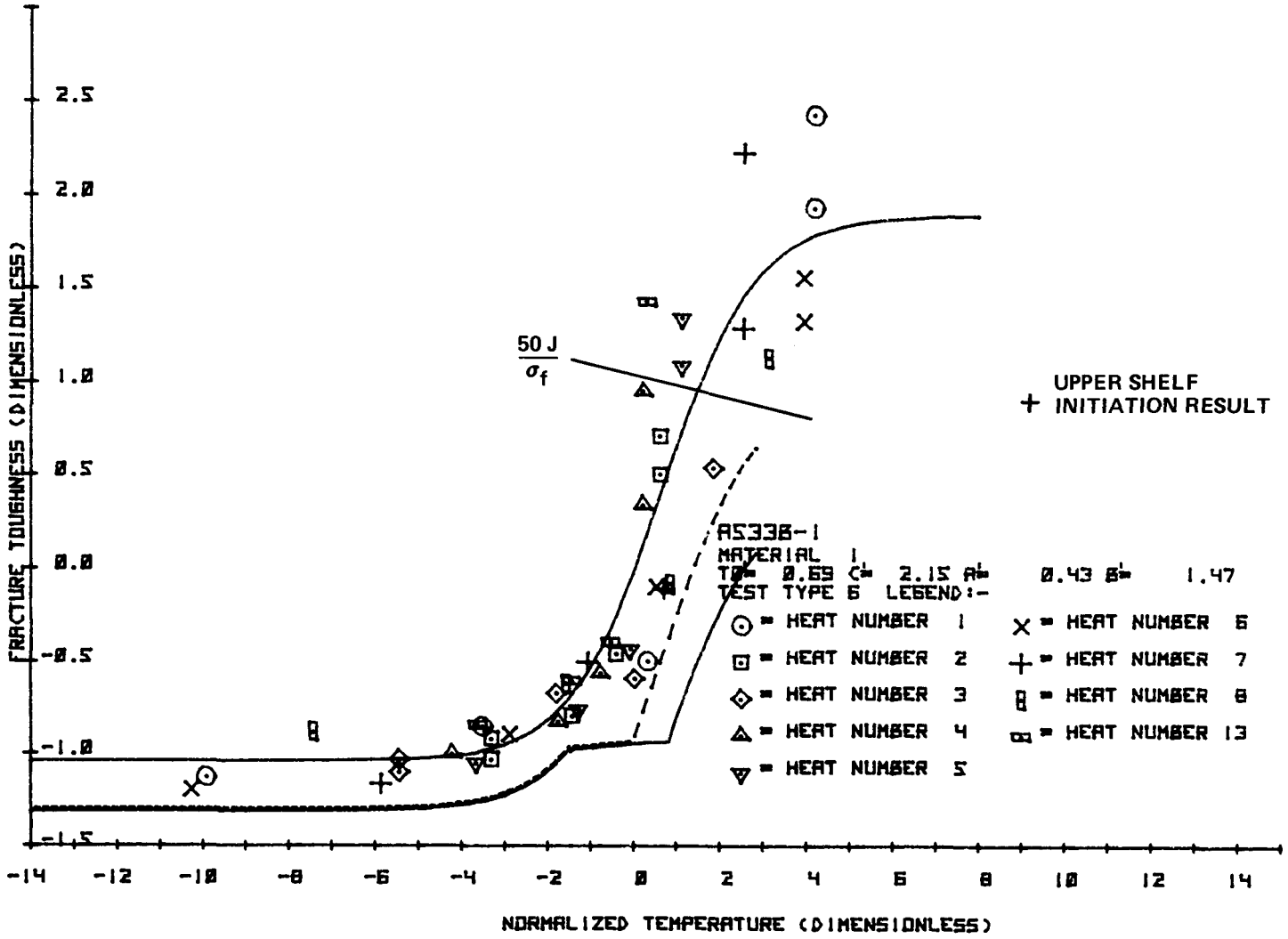

Figure 95. Lower Bound Curve for Material 1, Dynamic Bend

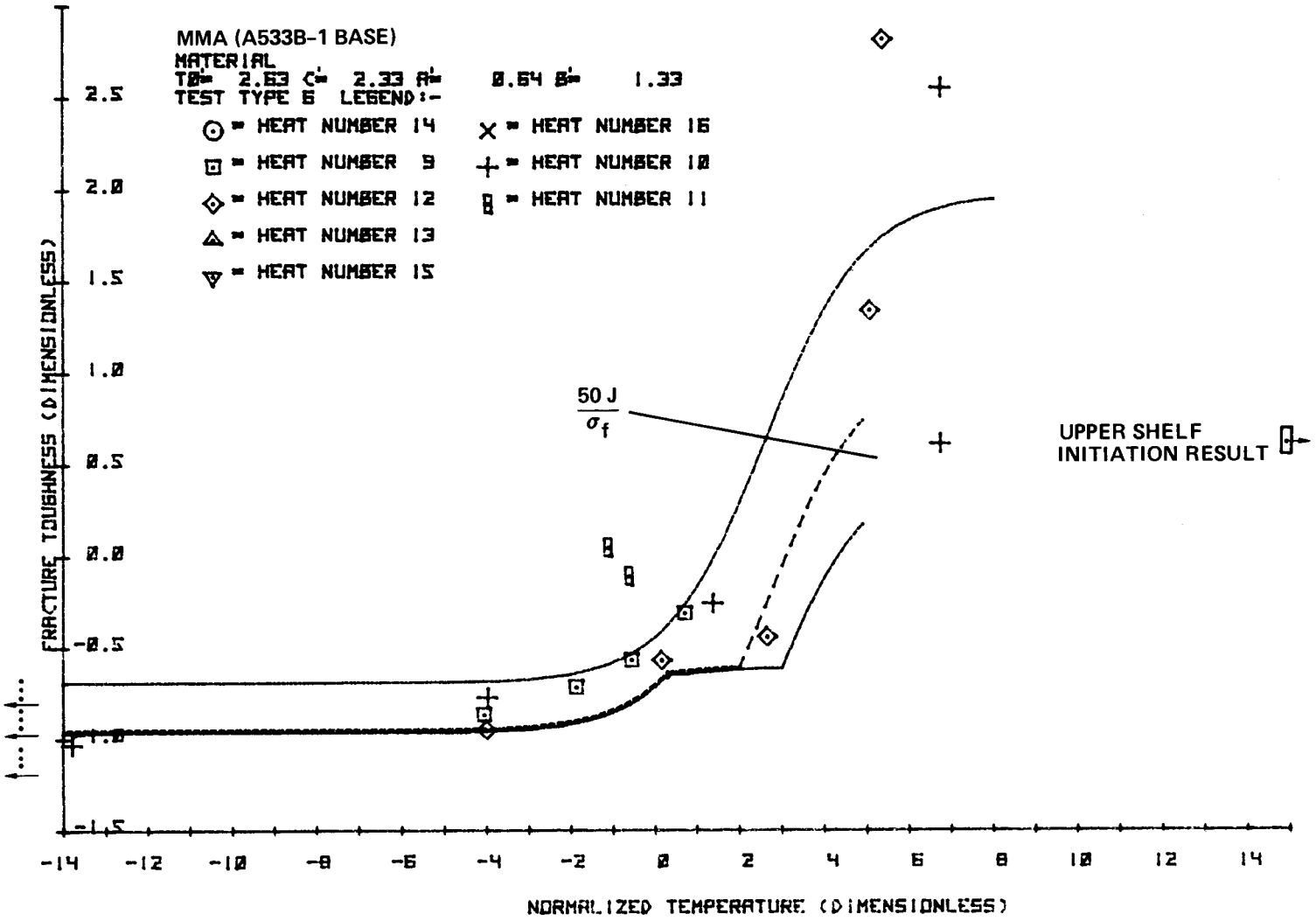

Figure 96. Lower Bound Curve for Material 5, Dynamic Bend

tained over 80% of all the data points. These groups have the minimum influence on the determination of the C values; thus, the values of C were set by less than 20% of the data. The situation varied from laboratory to laboratory, with material types 6 and 8 (B&W) being the worst. For reference to the curves, the minimum accuracy of the coefficients must be stated if the lower bounds are to be accurate. It is because of problems of this type, that no fine tuning of the bounds for weld material has been performed. The upper shelf initiation fracture toughness results obtained at $350^{o}F$ are also shown in Figures 81-84 and 86-96, together with the cutoff for valid elastic-plastic results ($50\ J/\sigma_f$). This cutoff corresponds very well to the change in fracture mode for the large samples of base metal (A533B-1 and A508-2) as discussed in earlier sections. Since the data in Figures 81-96 are normalized and dimensionless, it may be constructive to perform a sample calculation demonstrating how the normalized curve can be entered. In the discussion to follow, actual heat data will be constructed to further describe the methodology.

The heat-to-heat variation was removed by normalizing both the fracture toughness and temperature data by:

$$f = \frac{F - A}{B} \quad , \tag{48}$$

where f is the normalized fracture toughness, F is the measured fracture toughness and A and B are the tanh curve fit parameters for the precracked Charpy data for the particular material of interest; and

$$t = \frac{T - T_0}{C} \quad , \tag{49}$$

where t is the normalized temperature, T is the test temperature, and T_0 and C are the precracked Charpy tanh values. Thus, t is a measure of the number of C units that the temperature differed from the central transition temperature, and f is a measure of the number of B units that the toughness deviated from the toughness midway between the shelves. To index the curve in Figure 91 for heat CJ (for example), we need the precracked Charpy tanh fit parameters. From Reference 7 the parameters are (in English units):

$$A = 161.53 \text{ ksi-in}^{1/2},$$
$$B = 110.49 \text{ ksi-in}^{1/2},$$
$$T_o = 18.65^{\circ}\text{F}, \text{ and}$$
$$C = 27.50^{\circ}\text{F}.$$

For the case of the static 1T compact result (197 ksi-in$^{1/2}$; 216 MN-m$^{-3/2}$) at 350°F (171°C), the values of f and t would be:

$$f = 0.32, \text{ and}$$
$$t = 12.05.$$

The point shown in Figure 91 corresponds to these values.

The initiation toughness results shown in the figures reflect a crucial problem related to the K_{IR}-type curve. The upper limit of approximately 200 ksi-in$^{1/2}$ (220 MN-m$^{-3/2}$) for the top of the current K_{IR} curve may be too high in several cases. In addition, a lower bound in the upper shelf should probably be set by a static initiation toughness test. Such a lower bound would occur naturally for reference curves of the type developed in this program.

To compare the new statistically based reference curve with the existing K_{IR} concept, several specific heat curves have been constructed. Figures 97 and 98 show the Round Robin HSST Plate 02 results[9] referenced with the new approach, with statistical limits compared to the K_{IR}-code curve[45]. Figures 99 and 100 show the results for heat BBB (A508-2), and the results for heat CJ (submerged arc weld in A533B-1) are shown in Figures 101 and 102. The original K_{IR} curve appears to be conservative in most cases except at low temperatures.

Discussion of the New Reference Curve Procedure

The current K_{IR} design curve may be improved in the following ways:

1. Presently heats are referenced to the curves only on the basis

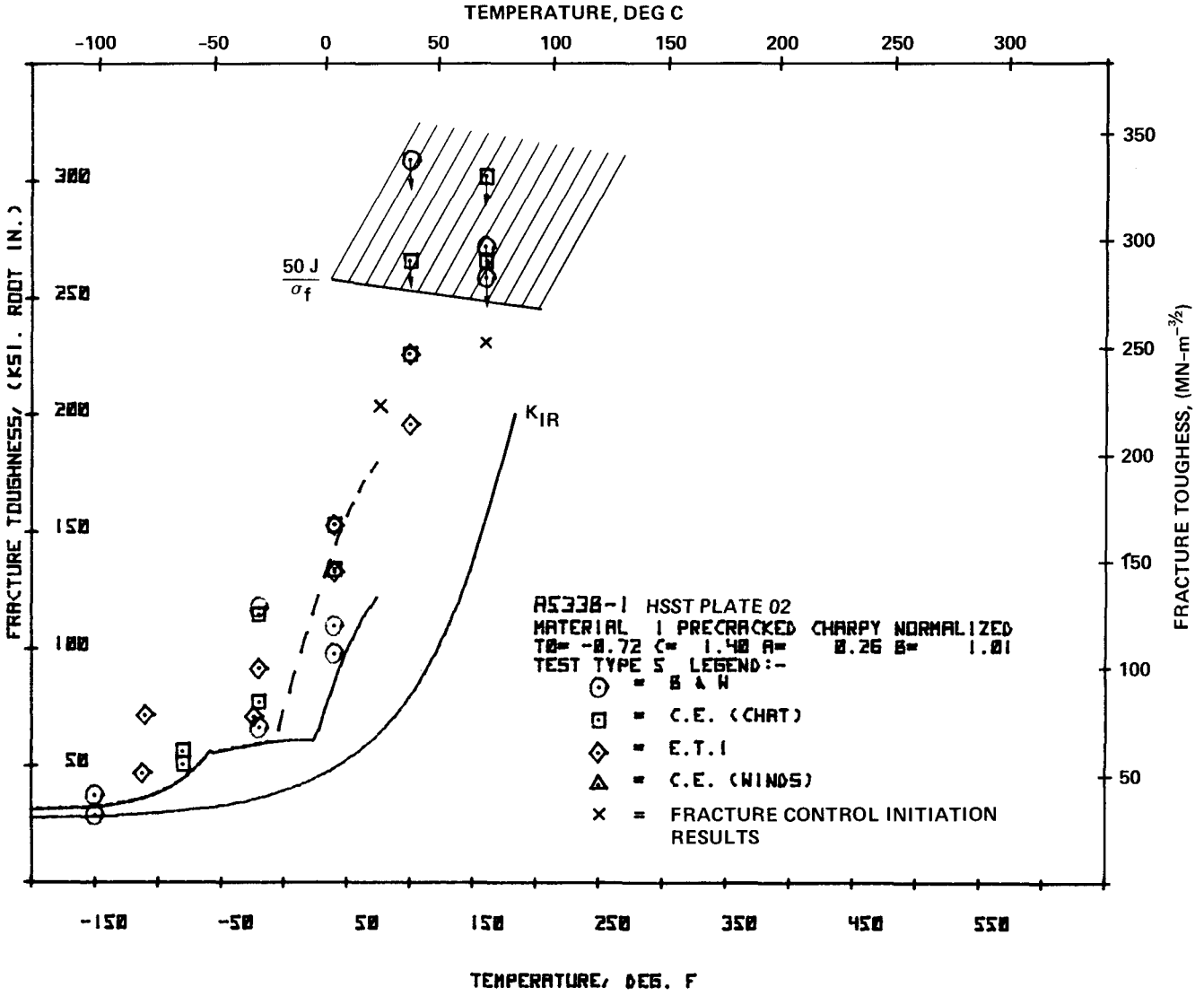

Figure 97. Use of Normalizing Procedure and Lower Bound Curve for Static Compact HSST Plate 02 Data[9]

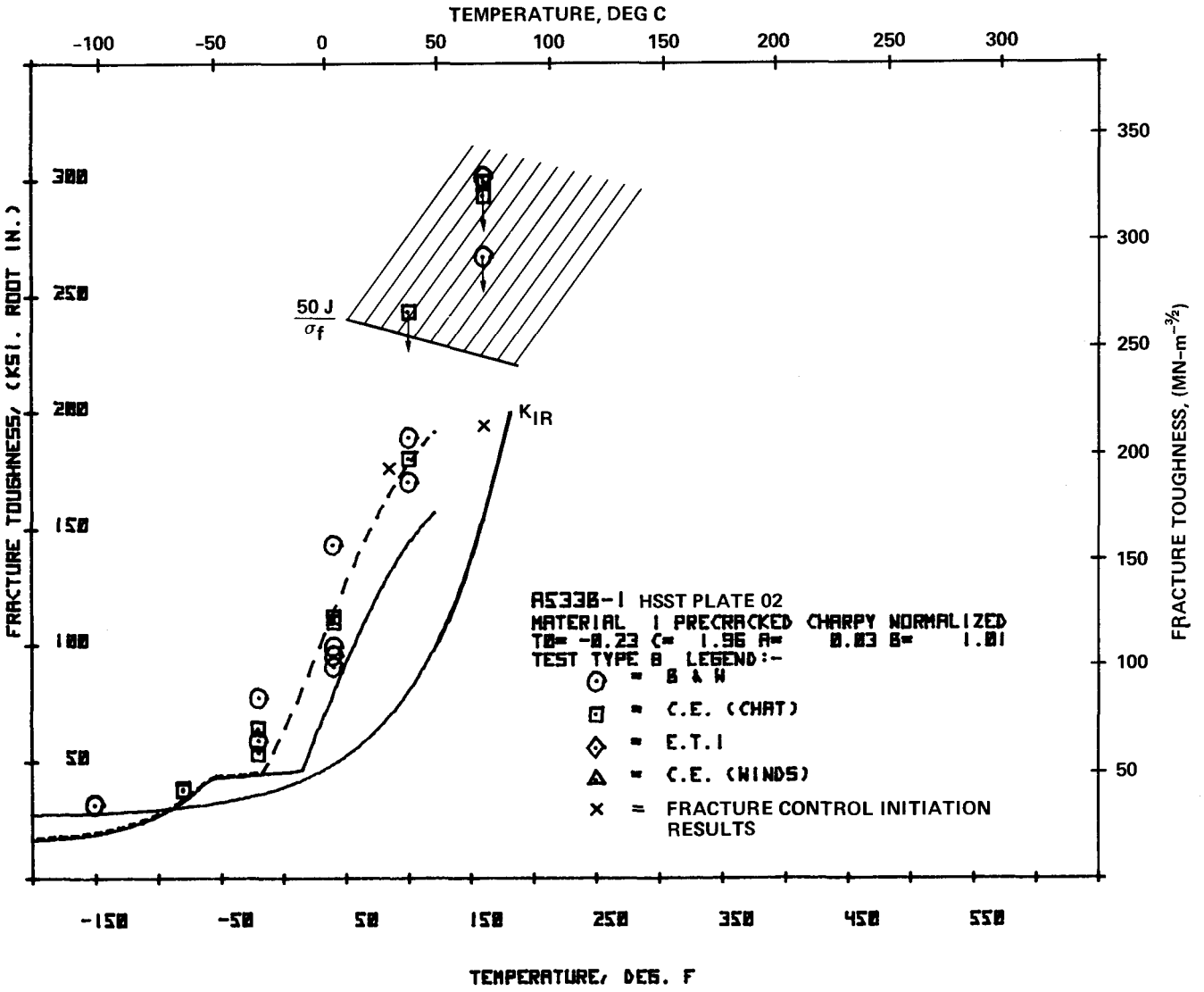

Figure 98. Use of Normalizing Procedure and Lower Bound Curve for Dynamic Compact HSST Plate 02 Data[9]

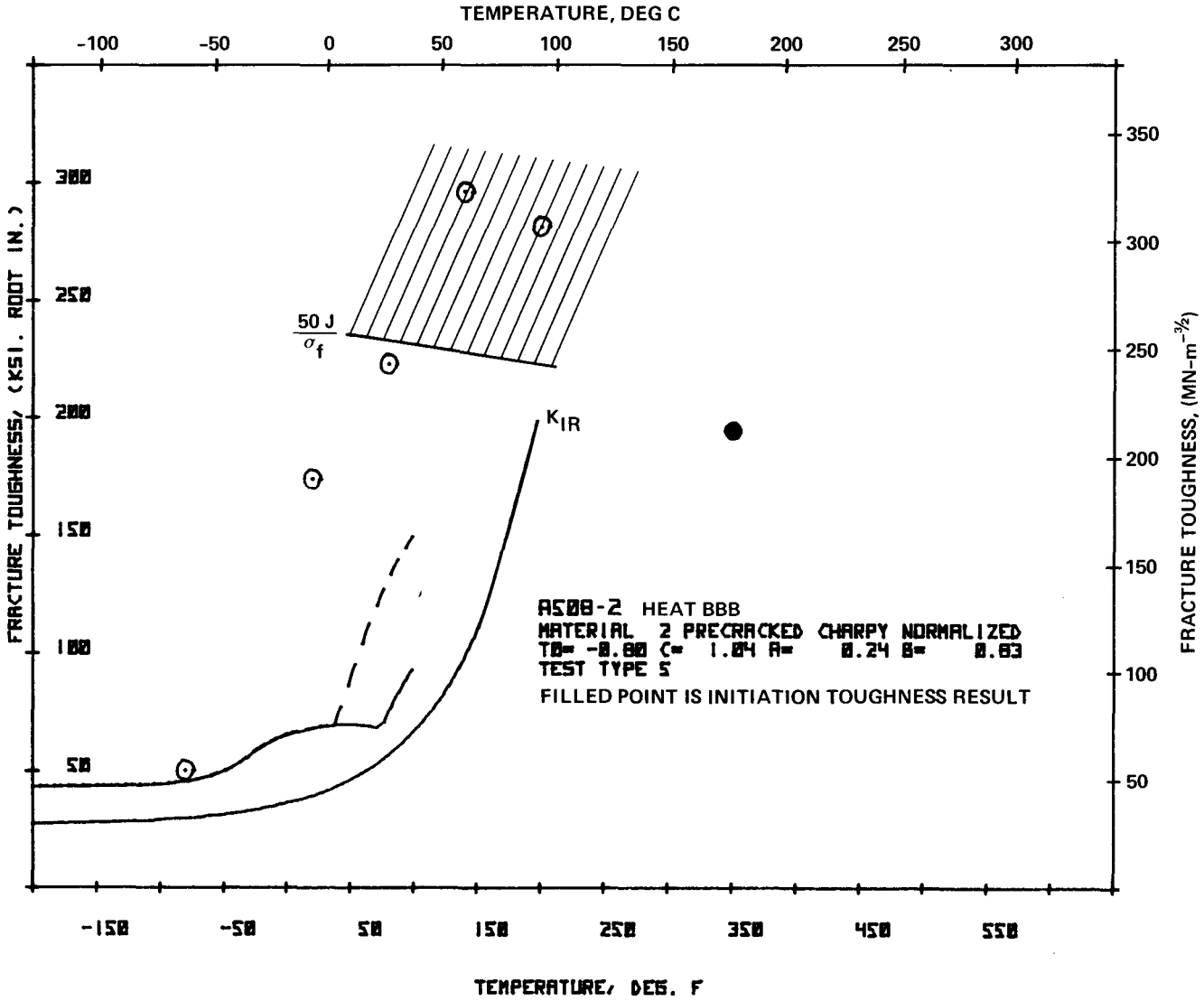

Figure 99. Comparison of the K_{IR} Curve with a Statistically Based Lower Bound Curve Based on Static Compact Data for Heat BBB

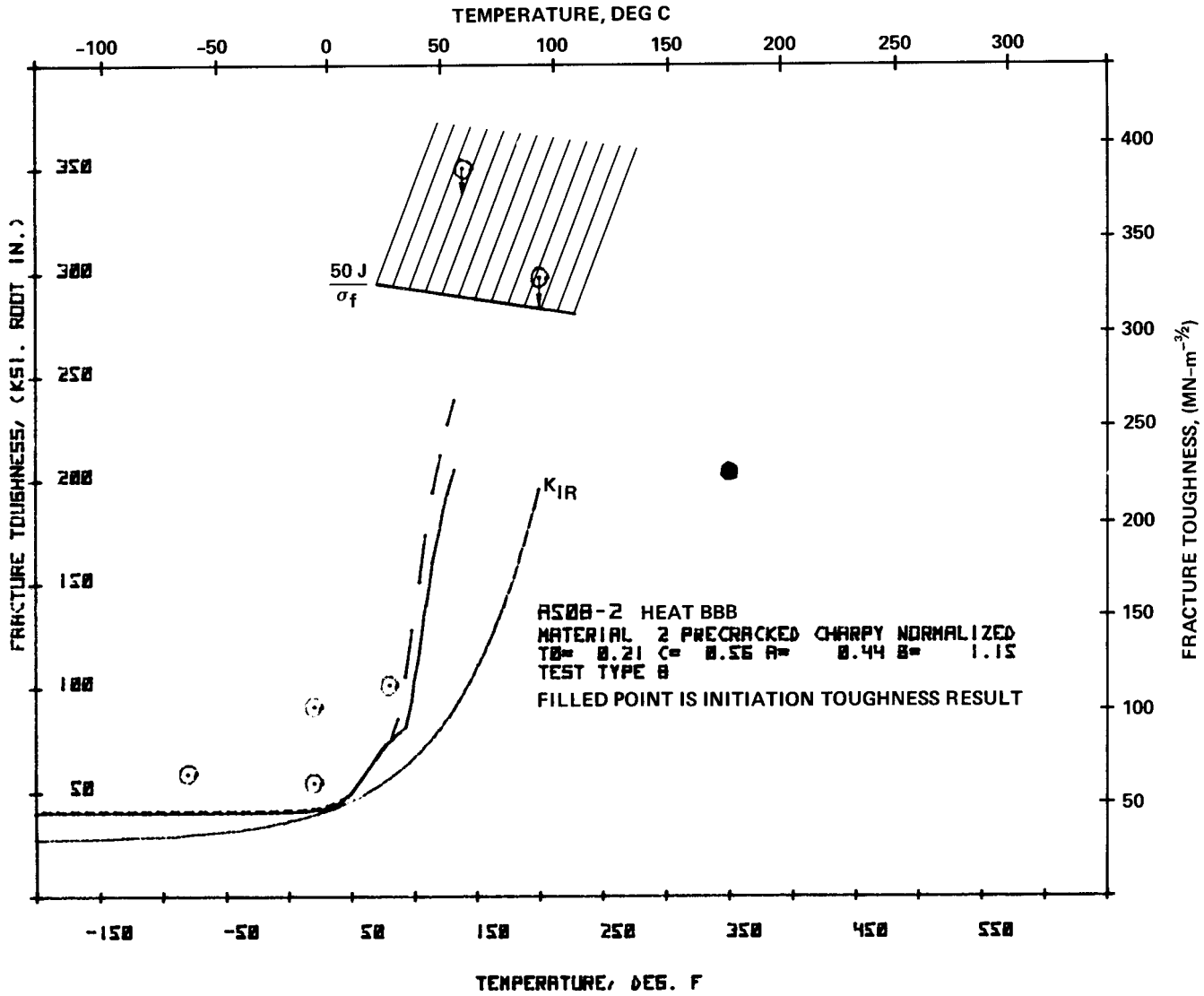

Figure 100. Comparison of the K_{IR} Curve with a Statistically Based Lower Bound Curve Based on Dynamic Compact Data for Heat BBB

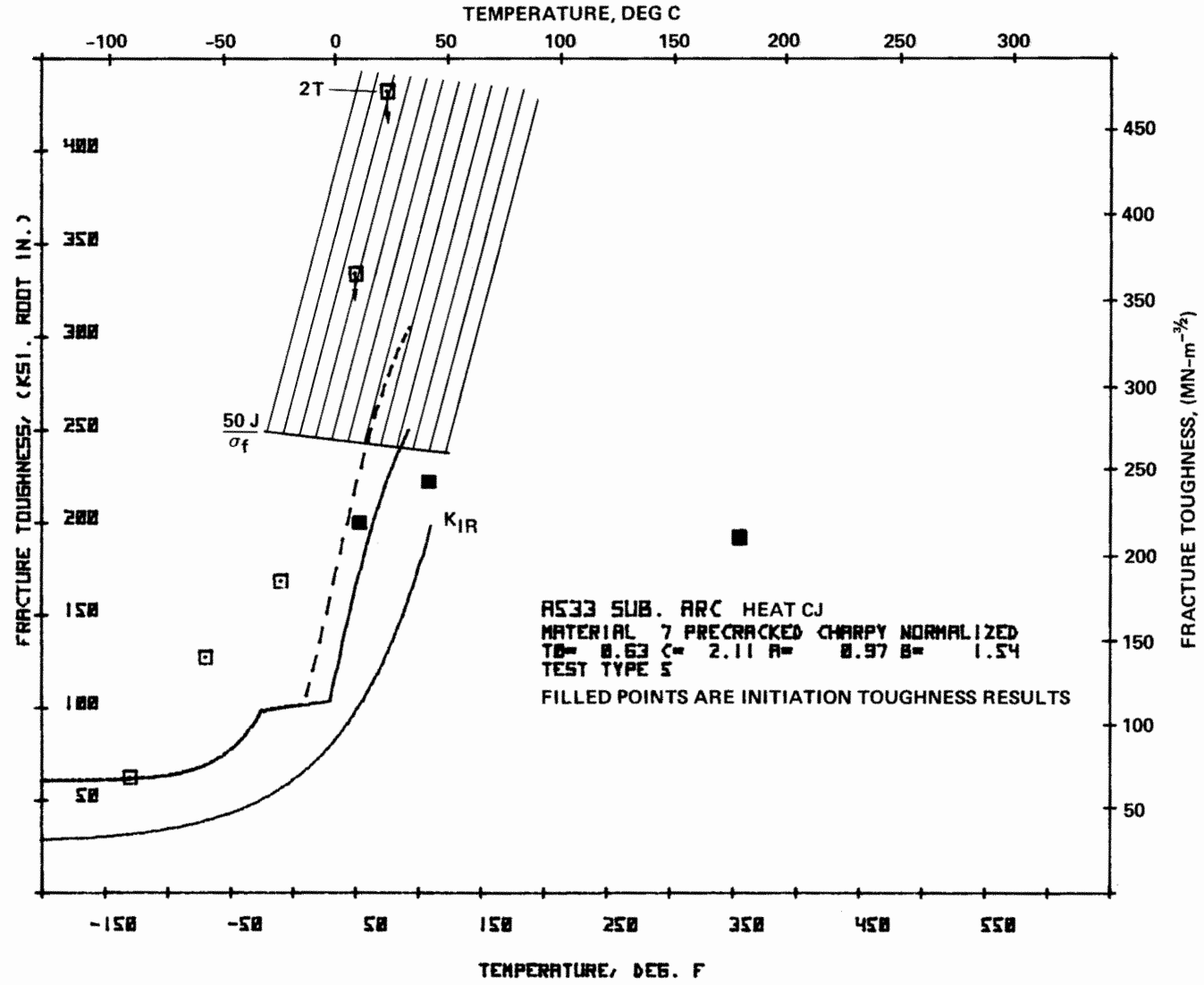

Figure 101. Comparison of the K_{IR} Curve with a Statistically Based Lower Bound Curve Based on Static Compact Data for Heat CJ

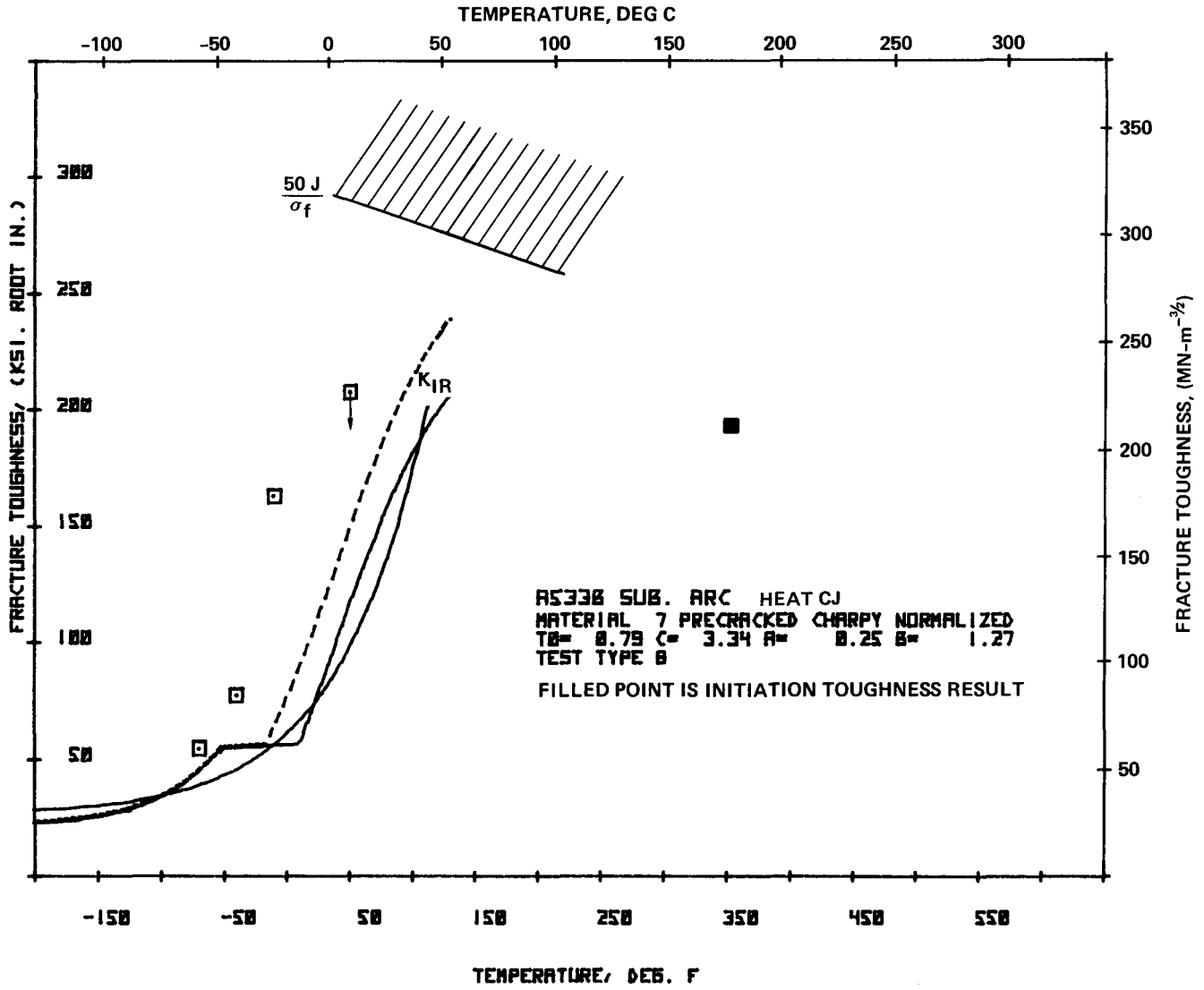

Figure 102. Comparison of the K_{IR} Curve with a Statistically Based Lower Bound Curve Based on Dynamic Compact Data for Heat CJ

of their RT_{NDT} temperature. In fact, heat-to-heat differences include four major features:

a. The position of the lower shelf,

b. The position of the upper shelf,

c. The temperature at which the property transition occurs, and

d. The range of temperature over which it occurs.

These four features should be accomodated in any new procedure.

2. The K_{IR} design curve is a lower bound curve without a defined statistical meaning. It was based on both arrest and large specimen initiation fracture toughness measurements, two measures of toughness which are not necessarily equal for any particular material. Consequently, when the K_{IR} curve is used to predict large specimen fracture toughness, it is extremely conservative above the lower shelf region, but optimistic at the lower shelf. Separate curves for static, dynamic, and arrest toughness should be developed to give the designer the option to choose the parameter which best describes operating and accident conditions.

3. The K_{IR} curve was based upon only a few heats of material. The current program in a large measure removes these shortcomings. The individual heats of material were characterized by two measures of position, and two of range, i.e.,

a. Toughness position - the fracture toughness midway between the two shelves (A);

b. Toughness range - the range of toughness (B), such that the shelves are at A ± B;

c. Transition temperature - the temperature at the midpoint of the property transition (T_0); and

d. Transition range - a measure of the range of temperature over which the property transition takes place (C).

The fracture toughness of individual heats was conveniently measured using the instrumented precracked Charpy test. A non-linear regression procedure was then used to determine A, B, T_0, and C by fitting the expression:

$$\text{Fracture toughness} = A + B \tanh\left[\frac{T - T_O}{C}\right] \quad . \qquad (28)$$

The instrumented precracked Charpy test specimen is too small to develop an accurate measure of fracture toughness over a broad temperature range, although it is a good measure of heat-to-heat variation. Overall reference curves were developed using large specimen static and dynamic fracture toughness tests from 50 heats of eight materials. Heat-to-heat variation was removed by normalizing both the fracture toughness and temperature data as follows:

$$f = \frac{F - A}{B} \quad , \text{ and } \quad t = \frac{T - T_O}{C} \quad . \qquad (48,49)$$

The f and t values were then used to generate normalized fracture toughness curves for both static and dynamic tests for each material. The variance and distribution of the results about a central tanh curve

$$f_m = A' + B' \tanh \frac{t - T'_O}{C'} \quad , \qquad (47)$$

allowed lower bounds of pre-determined statistical significance to be drawn. The bounds can be referenced to any heat for which a suitable set of instrumented precracked Charpy tests have been performed.

The results we have presented reveal strengths and weaknesses in the approach. The main strengths of the approach are:

a. The new reference curve is substantially less penalizing than the K_{IR} curve.

b. If the referencing tecnhique is performed properly, the curve is relatively well understood statistically.

c. The technique allows a more informed application of results, since it treats tests which should give different results on different curves instead of grouping them on a single curve. Thus, the choice is left open for the designer who can choose static, dynamic, or worst case limits.

d. The need for a properly defined upper shelf bound has been

anticipated.

The weaknesses lie in the following:

a. The referencing procedure (instrumented precracked Charpy) must employ much tighter control than was exercised in this program.

b. A four parameter referencing scheme is more complicated than the RT_{NDT} concept. An educational effort will be needed before it can be widely used.

c. Although the statistics are qualitatively better than those for K_{IR}, considerable improvement is still needed. This is especially the case for weld material.

CONCLUSIONS

The following conclusions were reached as a result of the performance of the program:

EPRI PROCEDURES AND ACCEPTANCE CRITERIA

1. The most concise manner in which to specify the requirements for obtaining reliable load-time data from an instrumented impact test is:

$$t \geq 3\tau \qquad \text{(Inertial Loading)}$$

$$t \geq 1.1\ T_R \qquad \text{(Limited Response)}$$

If it is not possible to meed the inertial loading criterion above, it may still be possible to obtain meaningful data by electronically filtering the signal in a controlled manner.

2. Instrumented impact tests produce load-time data which require a correction of the initiation energy to account for machine compliance. The calculational procedure for elastic-plastic (post general yield) tests used in the EPRI procedures

$$E_I = W_M - \frac{P_M^2 C_M}{2} \quad ;$$

$$C_M = \frac{\bar{V}t_{GY}}{P_{GY}} - C_s$$

was experimentally verified by comparing load-time and load-displacement data from compact specimen tests.

3. The EPRI procedures state that an instrumented impact test result is elastic as long as fracture occurs before general yielding ($P_M < P_{GY}$). This corresponds to an upper limit in the elastic toughness of

$$K_{Id} = 0.504\ \sigma_{yd} \qquad \text{(Precracked Charpy, a/w = 0.5)}$$

$$K_{Id} = 1.135\ \sigma_{yd} \qquad \text{(1-in. Bend)}$$

The use of this criterion to define linear elastic fracture behavior was supported by the fracture toughness - specimen strength ratio correlations.

4. A review of recent analyses of the mechanics of instrumented impact testing indicates that the use of a static analysis to calculate dynamic fracture toughness is reasonable when the EPRI test procedures are followed (1 above).

5. The original EPRI acceptance criteria were limited to linear elastic fracture toughness requirements. The criteria have been expanded to include elastic-plastic criteria (Table 1), with the two most important additions being

1. The mode of fracture initiation should be noted
2. a, b, B, $\geq \frac{50\ J}{\sigma_f}$.

FRACTURE MODE AND INITIATION STUDIES

1. For A533B-1 steel, the fracture mode transition (cleavage to ductile initiation) corresponds to the $\frac{50\ J}{\sigma_f}$ limit for 1T compact specimens, whereas the fracture mode transition occurs closer to the $\frac{25\ J}{\sigma_f}$ limit for precracked Charpy specimens.

2. For A533B-1 steel specimens (of a given thickness and stress intensity rate) which exhibited cleavage initiation, the elastic-plastic toughness values were always greater than the linear elastic values.

3. For fibrous initiation in A533B-1 steel, the $\frac{50\ J}{\sigma_f}$ specimen size criterion does not appear to apply. Small specimen results violating this criterion agree quite favorably with "valid" data.

4. There appears to be only a slight positive effect of doubling the ligament depth and span on the precracked Charpy sample to increase elastic constraint.

5. Decreasing the specimen thickness and increasing the specimen loading rate cause an increase in the slope of the R-curve.

6. The single-specimen electric-potential technique for detecting fibrous crack initiation did not provide an unambiguous indication of initiation in A533B-1 steel, although an offset potential approach may have promise.

UPPER SHELF FRACTURE TOUGHNESS STUDIES

1. For all eight heats studied, the initiation fracture toughness based on R-curves (K_{Jc}) was less than the previously reported upper shelf toughness based on instrumented precracked Charpy equivalent energy values (K_d^*).

2. For most of the materials studied, the dynamic initiation toughness exceeded the static initiation toughness by approximately 35 ksi-in$^{1/2}$ (39 MN-m$^{-3/2}$).

3. Users of the EPRI fracture toughness data bank (RP 232) should take into account the nonconservative nature of the upper shelf equivalent energy values, along with the $\frac{50\ J}{\sigma_f}$ validity limit for elastic-plastic data.

4. The Barsom, Rolfe, and Novak upper shelf correlation

$$\left(\frac{K_{Ic}}{\sigma_y}\right)^2 = 5\left[\frac{C_V}{\sigma_y} - 0.05\right]$$

can be used to approximate the upper shelf initiation fracture toughness (K_{Jc}) for the eight heats studied. The use of the correlation for predicting static K_{Jc} values appears nonconservative in many cases.

4. The correlation between fracture toughness and specimen strength ratio can be used to predict thick section behavior from small specimens.

VARIANCE AND DISTRIBUTION OF FRACTURE TOUGHNESS DATA

1. The distribution of fracture toughness data about a fitted tanh curve is qualitatively the same for both instrumented precracked Charpy test data, and normalized large specimen fracture toughness data. The

lower shelf results have a lower variance than either the transition range results or the upper shelf results. Lower shelf data is skewed high, transition data is close to the Normal distribution, while upper shelf data is skewed low.

2. Normalization of fracture toughness test results using instrumented precracked Charpy test data works well if the test temperatures for the precracked Charpy tests have been well selected. Heat-to-heat variation was removed by normalizing both fracture toughness and temperature:

$$f = \frac{F - A}{B}$$

$$t = \frac{T - T_0}{C}$$

where f and t are the normalized parameters and A, B, T_0 and C are the precracked Charpy tanh fit parameters. The full, four parameter normalization procedures do not work well if there were too few points in the property transition range. In such a case, the value of C is subject to large uncertainty and the normalization process is inappropriate.

3. The non-linear regression procedures used in this program show variance and covariance estimates for the A and B coefficients, and upper limit estimates for the T_0 and C coefficients. These data could be used as quality control criteria; curves should not be used to enter the reference curves if the variance and covariance estimates exceed some stated value.

LOWER BOUND TOUGHNESS CURVES

1. When the instrumented precracked Charpy test temperatures have been well selected, a reference curve can be used to show a statistically-based lower bound (L.B.) fracture toughness for either static or dynamic test methods; i.e.,

$$\text{L.B.} = A' + B' \tanh\left[\frac{T - T_0'}{C'}\right] - D$$

where A', B', T_0' and C' are the normalized data tanh fit parameters and D is the statistical deviate below the mean line.

2. The referencing procedures highlighted the fact that the onset of the upper shelf restricts the size of maximum toughness which can be referenced. The lower bound is a deviation below the mean curve in the toughness direction. This lower bound cannot be continued beyond the level of the transition into the upper shelf. For many materials, this occurs at a low toughness.

REFERENCES

1. Server, W.L., W. Oldfield, and R.A. Wullaert, "Experimental and Statistical Requirements for Developing a Well-Defined K_{IR} Curve," FCC 76-6, Quarterly Progress Report No. 1 to the Electric Power Research Institute, March 1976.

2. Server, W.L. and R.A. Wullaert, "Experimental and Statistical Requirements for Developing a Well-Defined K_{IR} Curve," FCC 76-9, Quarterly Progress Report No. 2 to the Electric Power Research Institute, June 1976.

3. Stahlkopf, K.E., R.E. Smith, W.L. Server, and R.A. Wullaert, "Preliminary Results on a Program for Developing Fracture Toughness Data on Ferritic Nuclear Pressure Vessel Steels," presented at the 9th National Symposium on Fracture Mechanics, Pittsburgh, PA, August 1975 (to be published in Cracks and Fracture, ASTM STP 601).

4. Server, W.L., J.W. Sheckherd, and R.A. Wullaert, "Fracture Toughness Data for Ferritic Nuclear Pressure Vessel Materials; Task B - Laboratory Testing, Final Report," EPRI NP - 119, April 1976.

5. Marston, T.U., M.P. Borden, J.H. Fox, and L.D. Reardon, "Fracture Toughness of Ferritic Materials in Light Water Nuclear Reactor Vessels, Final Report," EPRI 232-2, December 1975.

6. Van Der Sluys, W.A., R.R. Seeley, and J.E. Schwabe, "Determining Fracture Properties of Reactor Vessel and Forging Materials, Weldments, and Bolting Materials, Final Report," EPRI NP - 122, July 1976.

7. Wullaert, R.A., W. Oldfield, and W.L. Server, "Fracture Toughness Data for Ferritic Nuclear Pressure Vessel Materials; Task A - Program Office, Final Report," EPRI NP - 121, April 1976.

8. Wullaert, R.A., J.W. Sheckherd, W.L. Server, and W. Oldfield, "HTGR Fracture Toughness Program, Final Report," EPRI NP - 120, April 1976.

9. Oldfield, W., R.A. Wullaert, W.L. Server, and T.R. Wilshaw, "Fracture Toughness Data for Ferritic Nuclear Pressure Vessel Materials; Task A - Program Office, Control Material Round Robin Program," Effects Technology, Inc. Report TR 75-34R, July 1975.

10. Ireland, D.R., W.L. Server, and R.A. Wullaert, "Procedures for Testing and Data Analysis," Effects Technology, Inc. Report TR 75-43, October 1975 (originally printed as a working document, Effects Technology Report TR 74-32, May 1974).

11. Wullaert, R.A., W. Oldfield, W.L. Server, and T.R. Wilshaw, "Statistical Analysis of Interlaboratory Dynamic Fracture Toughness Data," presented at the Dynamic Fracture Toughness Conference, London, July 1976 (to be published as Conference Proceedings by the Welding Institute).

12. Oldfield, W., "Curve Fitting Impact Test Data: A Statistical Procedure," ASTM Standardization News, Vol. 3, No. 11, November 1975.

13. Stahlkopf, K.E., W.L. Server, R.E. Smith, R.A. Wullaert, "A Methodology for Evaluating the Variability in Fracture Properties of Ferritic Nuclear Pressure Vessel Steels," to be presented at the Winter Annual ASME Meeting, New York, December 1976 (and to be published in Journal of Pressure Vessel Technology).

14. Server, W.L., R.A. Wullaert, and J.W. Sheckherd, "Verification of the EPRI Dynamic Fracture Toughness Testing Procedures," Effects Technology Report TR 75-42, October 1975.

15. Server, W.L., R.A. Wullaert, and J.W. Sheckherd, "Evaluation of Current Procedures for Dynamic Fracture Toughness Testing," presented at the 10th National Symposium on Fracture Mechanics, Philadelphia, PA, August 1976 (to be published in an ASTM STP).

16. Preliminary Testing Guidelines from ASTM Task Groups E24.01.09 and E24.01.10, "Guidelines for J_{Ic} Tests" and "Guidelines for Measurement of Toughness K_{Mb} and K_{Bb}."

17. Griffis, C.A., "Elastic-Plastic Fracture Toughness: A Comparison of J-Integral and Crack Opening Displacement Characterizations," Transactions of the ASME, Journal of Pressure Vessel Technology, 75-PVP-38.

18. Williams, J.A., presentation of preliminary data at the Fourth Water Reactor Safety Research Information Meeting, Gaithersberg, MD, September 1976.

19. Rice, J.R., P.C. Paris, and J.G. Merkle, "Some Further Results of J-Integral Analysis and Estimates," Progress in Flaw Growth and Fracture Toughness Testing, ASTM STP 536, ASTM, 1973.

20. Server, W.L., unpublished work.

21. Shabbits, W.O., "Dynamic Fracture Toughness Properties of Heavy Section A533 Grade B Class 1 Steel Plate," HSST Program 5th Annual Information Meeting, March 1971.

22. Clark, G.A., et al, "Single Specimen Tests for J_{Ic} Determination," Mechanics of Crack Growth, ASTM STP 590, 1976, pp. 27 - 42.

23. Underwood, J.H., et al, "End-On Ultrasonic Crack Measurements in Steel Fracture Toughness Specimen and Thick-Wall Cylinders," The Section and Measurement of Cracks, The Welding Institute, Cambridge, England, 1976, pp. 31 - 39.

24. Hickerson, J., "Use of the Resonant Frequency Technique in J_{Ic} Testing," presented at the ASTM E24 committee meeting, Lake Buena Vista, Florida, March 1976.

25. Marston, T., presentation at the EPRI Fracture Toughness Program Information Meeting, Palo Alto, CA, March 1975.

26. Chipperfield, C.G., "The Toughness of Cold Worked 316 Stainless Steel at 20°C," TRG Report 2718 (R), September 1975.

27. Marandet, B., and G. Sanz, "Characterization of the Fracture Toughness of Steels by the Measurement with a Single Specimen of J_{Ic} and the Parameter K_{Bb}," presented at the Tenth National Fracture Mechanics Symposium, Philadelphia, PA, August 1976.

28. Bachmann, V., and D. Munz, "Unusual Potential Drop During the Application of the Electrical Potential Method in a Fracture Mechanics Test," Journal of Testing and Evaluation, Vol. 4, No. 4, July 1976, pp. 252 - 260.

29. Ritchie, R.O., private communication.

30. Loss, F.J., editor, "Structural Integrity of Water Reactor Pressure Boundary Components," NRL Report 8006, NRL NUREG 1, August 1976.

31. Loss, F.J., private communication.

32. Borden, M.P., preliminary data summary of Combustion Engineering data generated for EPRI program RP 232 - 4.

33. Sumpter, J.D.G. and C.E. Turner, "A Method for Laboratory Determination of J_c," presented at the Ninth Fracture Mechanics Symposium, Pittsburgh, PA. 1975.

34. Merkle, J.G. and H.T. Corten, " A J-Integral Analysis for the Compact Specimen, Considering Axial Forces as Well as Bending Effects," ASME Paper 74-PVP-33, March 1975.

35. Rice, J.R., P.C. Paris, and J.G. Merkle, "Some Further Results of J-Integral Analysis and Estimates," Progress in Flaw Growth and Fracture Toughness Testing, ASTM STP 536, 1973, pp. 231 - 245.

36. Keller, H.P. and D. Munz, "Effect of Specimen Size on J-Integral and Stress Intensity Factor at the Onset of Crack Extension," presented at the Tenth National Symposium on Fracture Mechanics, Philadelphia, PA, August 1976.

37. Robinson, J.N., "An Experimental Investigation of the Effect of Specimen Type on the Crack Tip Opening Displacement and J-Integral Fracture Criteria," to be published in the International Journal of Fracture.

38. Davies, O.L. and P.L. Goldsmith, editors, Statistical Methods in Research and Production, Hafner, 1972, p. 195.

39. Wullaert, R.A., D.R. Ireland, and A.S. Tetelman, "The Use of the Precracked Charpy Specimen in Fracture Toughness Testing," Fracture Prevention and Control, American Society for Metals, 1974.

40. Barsom, J.M., and S.T. Rolfe, "Correlations Between K_{Ic} and Charpy V-Notch Test Results in the Transition Temperature Range," Impact Testing of Metals, ASTM STP 466, American Society for Testing and Materials, 1970.

41. Corten, J.T., and R.H. Sailors, "Relationship Between Material Fracture Toughness Using Fracture Mechanics and Transition Temperature Tests," T&A.M. Report No. 346, University of Illinois, August, 1971.

42. Hawthorne, J.R., Radiation Effects Information Generated on the ASTM Reference Correlation Monitor Steels, ASTM Data Series Publication DS 54, American Society for Testing and Materials, 1974.

43. Yukawa, S., "Correlation of Specimen Strength Ratios with K_{Ic}," presented at the NRC/CSNI International Meeting on Elastic-Plastic Fracture Mechanics, San Francisco, Calif., June 1976.

44. Succop, G., and W.F. Brown, Jr., "Estimation of K_{Ic} from Slow-Bend Precracked Charpy Specimen Strength Ratios," NASA TMX-71834, presented at the Developments and Fracture Mechanics Test Method Standardization Symposium, St. Louis, MO, February 1976.

45. ASME Boiler and Pressure Vessel Code, Section III, "Nuclear Power Plant Components, Summer 1972 Addenda, June 1972.

46. Pearson, E.S. and H.O. Hartley, Editors, Biometrika Tables for Statisticians, Vol. 1, Third Edition, Cambridge University Press, 1970

47. Bennett, P.E. and G.M. Sinclair, "Parameter Representation of Low-Temperature Yield Behavior of Body-Centered-Cubic Transition Metals," Journal of Basic Engineering, June 1966.

48. Steichen, J.M. and J.A. Williams, "High Strain Rate Tensile Properties of Irradiated ASTM A533 Grade B Class 1 Pressure Vessel Steel," HSST Technical Report No. 32, July 1973.

49. Green, A.P. and B.B. Hundy, "Initial Plastic Yielding in Notch Bend Tests," Journal of Mechanics and Physics of Solids, Vol. 4, 1956.

50. Lequear, H.A. and J.D. Lubahn, Welding Journal, Vol. 33, 1954.

51. Rau, C.A., Jr., "The Effect of Drilled Holes on Notch Toughness," Ph.D. Thesis, Stanford University, April 1967.

52. Wullaert, R.A., "The Effect of Nickel on the Microstructure and Mechanical Properties of Ferritic Steels," Ph.D. Thesis, Stanford University, June 1969.

53. Wilshaw, T.R., "Deformation and Fracture of Mild Steel Charpy Specimens," Journal of the Iron and Steel Institute, Vol. 204, September 1966.

54. Irwin, G.R., "Crack Toughness Testing of Strain-Rate Sensitive Materials," Journal of Engineering for Power, Transactions of ASME, Series A, Vol. 86, 1964.

55. Rice, J.R. and G.F. Rosengren, "Plain Strain Deformation Near a Crack Tip in a Power-Law Hardening Material," Journal of the Mechanics and Physics of Solids, Vol. 16, No. 1, January 1968.

APPENDIX A

REVIEW OF THE MECHANICS OF INSTRUMENTED IMPACT TESTING

T.R. WILSHAW

Consultant, Hillocks Farm
Billington, England

Introduction

The instrumented version of the precracked Charpy test in which the applied impact force is measured from the tup has many obvious practical advantages; at the same time, however, a lack of understanding of the mechanics of the test have been responsible for the relatively slow acceptance of the test and perpetuated a continuing debate as to the limitations of the test and the validity of the test data. More specifically, the antagonists have objected to the use of quasi-static assumptions which are necessary to calculate the fracture toughness from the measured applied forces. Furthermore, how is the applied force simply related to the bending moment experienced by the specimen and how important are the inertia effects? Indeed, should we continue to instrument the tup, which is certainly a practical approach, or should each specimen be instrumented directly? In view of the uncertainties in estimating the fracture load, an alternative suggestion has been made to measure the time of fracture which has more physical significance but is fraught with experimental difficulties.

Despite these very real problems, the protagonists have to a large extent avoided many of the complications by treating the impact tests as extensions of static bend tests by simply reducing the impact velocity to obtain load-time records which have the essential form as those obtained from static bend tests. Even so, stress intensity rates of the order of 10^5 ksi-in$^{\frac{1}{2}}$/sec (10^5 MN-m$^{-3/2}$/s) may be readily achieved to enable the acquirement of fracture data so essential to our understanding of the mechanical behavior of structural steels and many other materials under high rates of loading.

Specific testing procedures have been proposed as part of the EPRI program largely on the basis of many years of practical experience and a considerable amount of data. While these procedures appear to provide a reasonable working basis at the present time, they are necessarily empirical and as such cannot satisfy the objections raised by the declining number of antagonists. Theoretical developments in our understanding of the mechanics of the fracture of cracked beams in bending have not been forthcoming until recently. The problem has simply been too complicated for

materials scientists, but recently the importance of the problem has attracted the attention of applied mechanicians, who have made significant progress of direct relevance to the acceptance of the current EPRI procedures.

In what follows we shall be largely concerned with small scale tests i.e., using specimens of essentially Charpy dimensions. Large scale test pieces have associated problems which are being addressed by the NRL/EPRI program and shall become apparent in the course of the general discussion. We shall proceed to review the important results of the recent theoretical developments which also illustrate the range of techniques which have been employed in the study of the impact mechanics of dynamically loaded cracked bodies.

Recent Theoretical Developments

Finite element and finite difference methods of dynamic stress analysis are now being widely used for problems of this nature; both numerical techniques lead to the same final result and the particular choice of method appears to be governed largely by economic factors. Anderson, et al[1a] analyzed a precracked Charpy system by taking the load-time impulse on the specimen represented by a half oscillation (Figure A.1) as his initial boundary condition*. The dynamic stress intensity factor may be computed from these load input conditions and is shown in Figure A.2. The initial decrease in the stress intensity factor is caused by the reflected stress wave; the general trend, however, is a monotonic increase in K_I with time in marked contrast to the sinusoidally varying load input. The maximum in K_I is attained while no load is being applied to the specimen. This classical example of the effect of inertia is central to the interpretation of load-time traces and we shall discuss this aspect at length in the next section.

---

*Note that this would not satisfy the validity criterion according to the EPRI procedures, but is a highly significant example in the case of large scale tests.

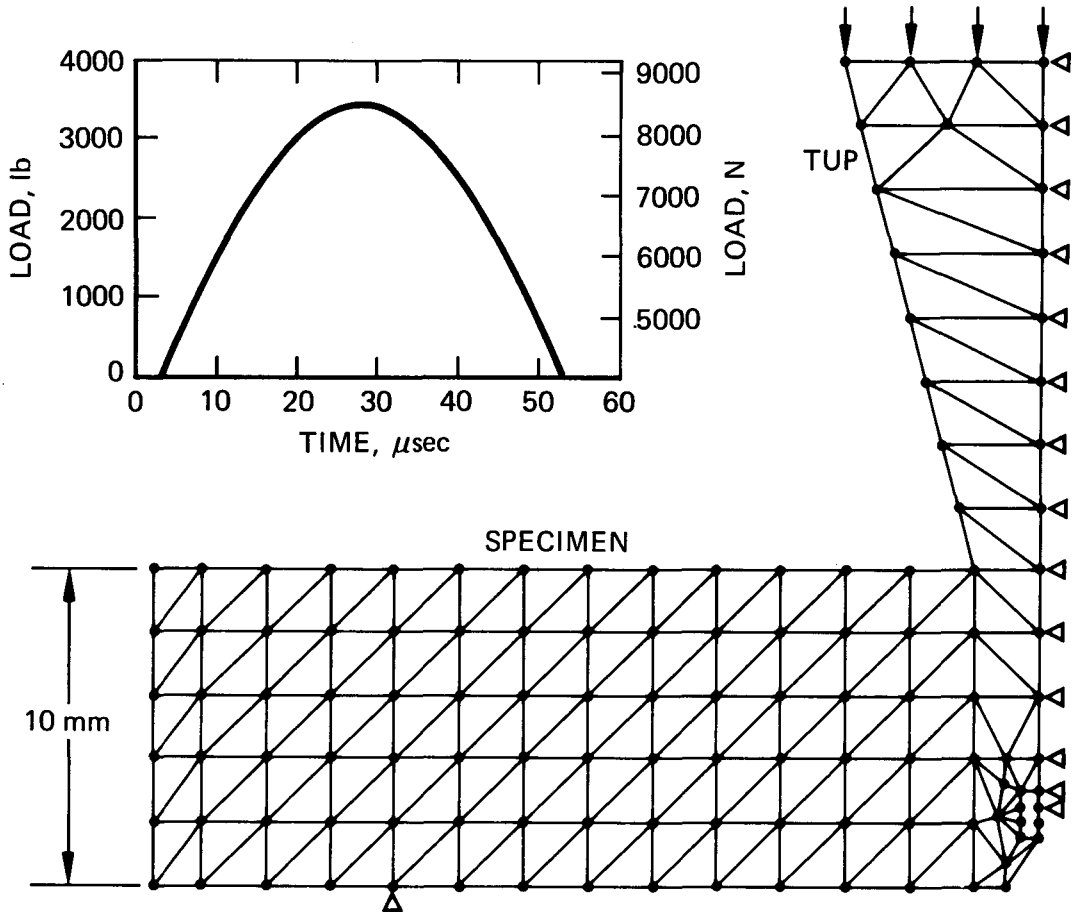

Figure A.1. Model of a Precracked Charpy Specimen Including the Prescribed Load-Time Curve(1a).

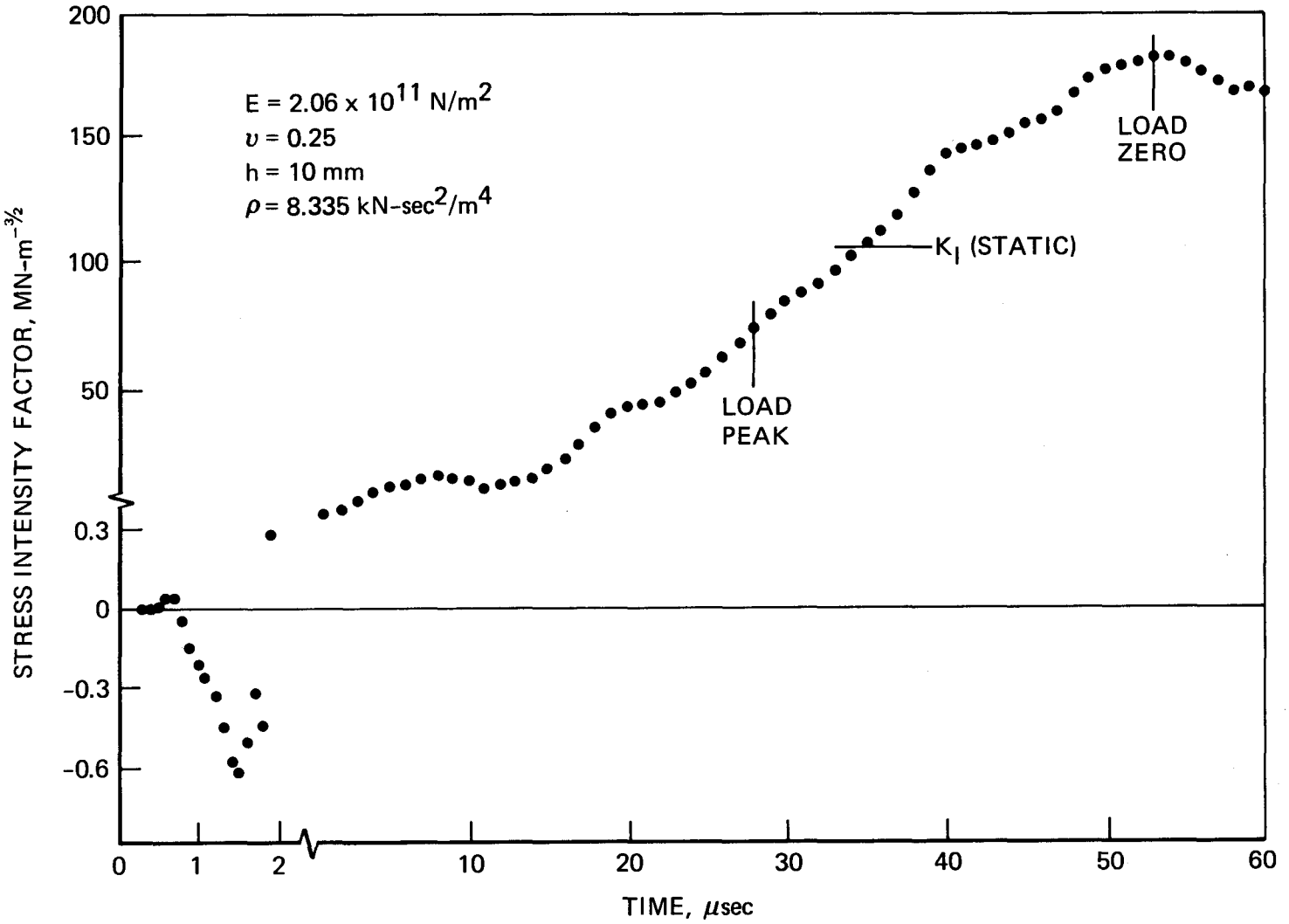

Figure A.2. Opening-Mode Stress-Intensity Factor as a Function of Time in the Model of the Charpy Impact Test[1a].

Ayres[2a] adopted an alternative set of boundary conditions by specifying the displacement-time characteristics of the loading point (e.g., constant velocity). Using finite element analysis he proceeded to compute the form of the load-time response which turned out to be in reasonable agreement with experimental curves as shown in Figure A.3. Furthermore, he computed the corresponding J-integral which is presented in Figure A.4, and we may note the comparative smooth form of this latter curve compared with the relatively large load oscillation shown in Figure A.3. We shall return to this point again later when discussing the work of Turner, et al[3a].

The earliest analytical attempt to calculate the hammer load-time characteristic of a prismatic bar subjected to impact bending was made by Nash[4a] in the late sixties at NRL. Starting from first principles he predicted the form of the load-time curve for the large scale dynamic tear test. The calculated bending moments indicated a monotonic increase with time despite the large oscillations in the hammer force which drives the specimen.

Following this successful but necessarily complex analysis, Griffis[5a] also at NRL, and Turner, et al[6a] of Imperial College, London, independently adopted a considerably simplified approach using beam and spring models, see Figure A.5. These models have the virtue of simplicity without, it turns out, sacrificing too much physical reality. We shall describe the results of the Turner model in greater detail in the next section. Analytical methods are used to predict forces and bending moments and the stress intensity factors are then calculated from the bending moments. In contrast, the numerical methods are capable of calculating K_I directly from the computed values of stress in the region of the crack tip. In addition, the latter method predicts the behavior of the specimen during the stress wave transit period and is generally a more powerful tool. However, the analytical approaches - particularly in simplified form provide a valuable means of identifying the role of the important variables, e.g. geometrical parameters, velocity, without resorting to lengthy and costly computation.

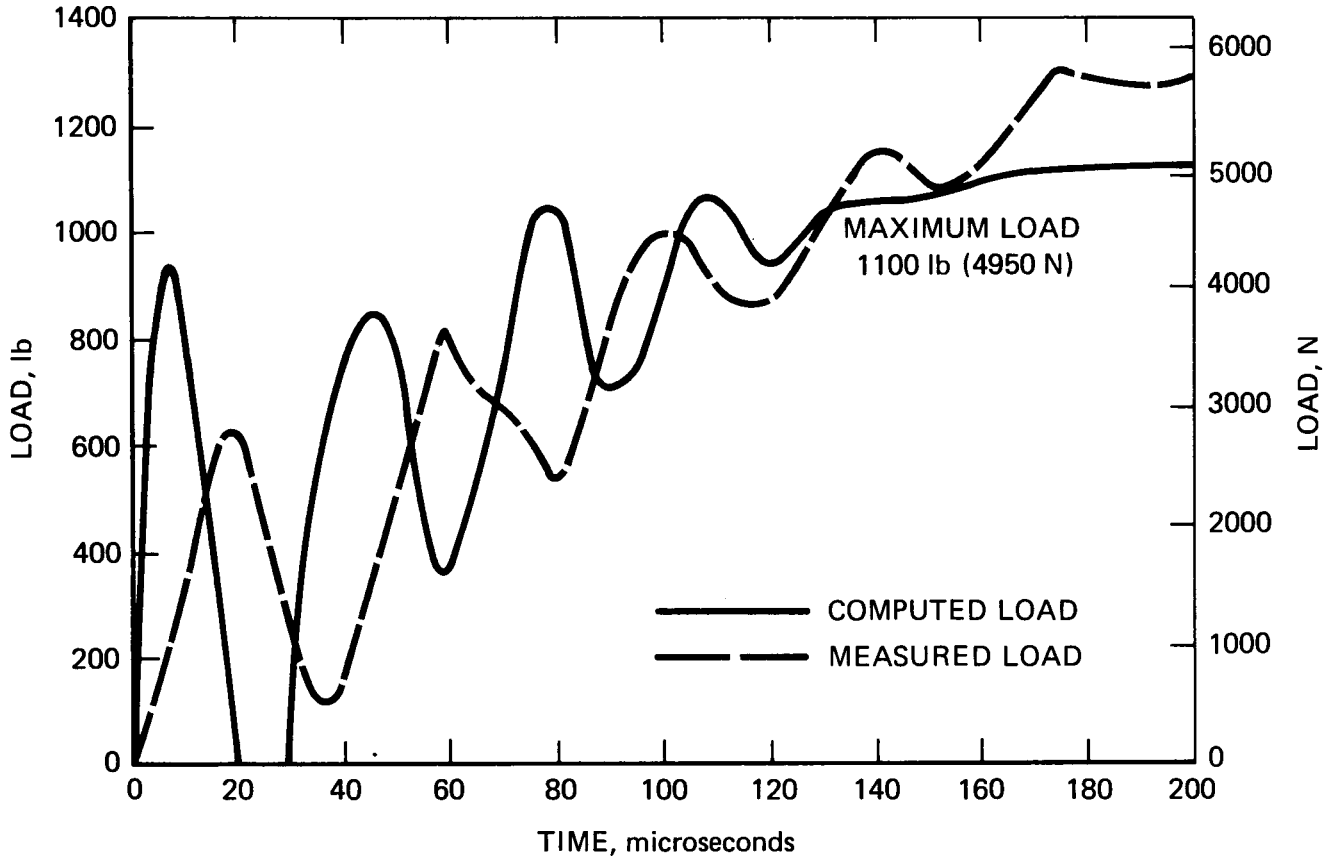

Figure A.3. Load Time Curve Computed from Elastic Plastic Dynamic Analysis with Constant Velocity of Loaded Point[2a].

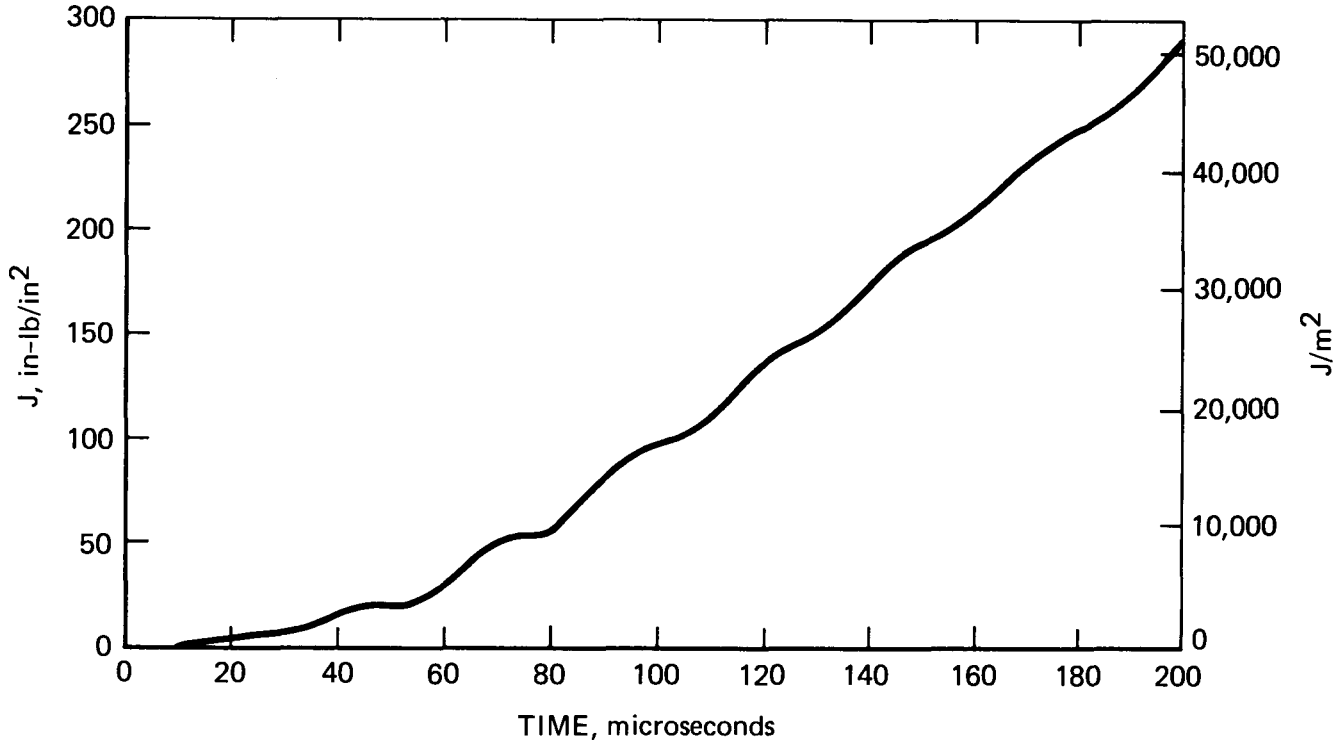

Figure A.4. J Integral vs. Time Computed from Elastic Plastic Dynamic Analysis with Constant Velocity Input[2a].

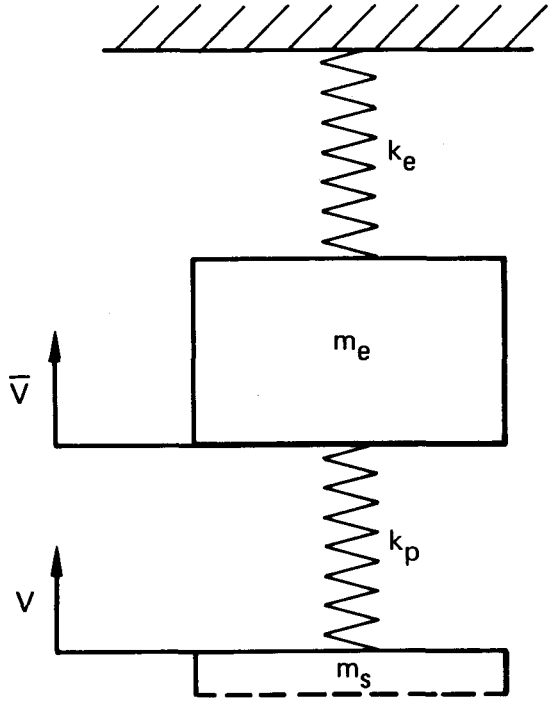

Figure A.5. Equivalent Model of Impact System: m_e = Effective Mass of Testpiece for Linear Motion; m_s = Mass of Striker $m_s > m_e$; k_e = Effective Stiffness of Testpiece and Abutments; k_p = Contact Stiffness of Striker on Beam(6a)

Also in the mid-sixties, Priest, et al[7a], working at British Steel Corporation began to experimentally measure the dynamic bending moment directly using resistance strain gages attached to the specimen. By placing gages across the throat of the notch (crack) they showed that the dynamic bending moment continued to increase with very small perturbations compared with the relatively larger oscillations in the tup force-time records. The subsequent theoretical predictions already described are supported by the experimental measurements.

More recently Kobayashi[8a] has applied the full field method of dynamic photo-elasticity to analyze the behavior of impact bend tests. So far he has only reported on the results of one geometry at one velocity so that it is not possible to draw general conclusions. However, this is a powerful technique since it provides measurements of K_I rather than bending moments, and is likely to be of considerable value in the case of short-time fracture behavior as experienced with high impact velocities and/or with large specimens.

To summarize at this stage; it is apparent that the necessary theoretical and experimental tests are now available for a determination of the load-time curve, the dynamic bending moments, and the dynamic stress intensity factor. Although it could be very instructive to carry out a few complimentary methods on the same set of impact conditions, there is now sufficient data and evidence available to facilitate an assessment of the potential of impact fracture tests and the validity of the current EPRI procedures. We shall examine these aspects more fully in the following section.

The Interpretation of Impact Bend Fracture Data

We shall begin by making some general comments on the general features pertaining to the mechanical response of impact bend tests in relation to the load (force)-time response measured from the impacting hammer (tup). It is generally accepted that the inertia effects which are associated with dynamic loading complicate and distort the load-time response so that it is no longer a direct analogue of the dynamic bending moment. Current practice is to reduce any inertial effects by increasing the time to fracture

so that the force measured on the hammer is an acceptable measure of the bending moment experienced by the specimen. While this is a practical proposition in the case of Charpy size specimens it becomes increasingly untenable as the specimen size is increased.

Upon initial impact the hammer sets up a compressive stress wave which extends into the specimen and rapidly attenuates; the wave propagation back into the tup is recorded as a short pressure pulse in the beginning of the load-time record. The magnitude of the pulse is directly proportional to the impact velocity and to a lesser extent on the acoustic impedence mismatch between the hammer and the specimen. The pulse height is independent of the specimen size and geometry and thus assumes less significance in the case of larger specimens because of the increased load scales. By the time the compressive wave has traversed the thickness of the specimen the whole body of the specimen begins to oscillate at close to its natural frequency. The flexural motion of the simply supported beam causes partial* unloading of the hammer followed by a cycle of rapid loading as the specimen flexes back into the tup. This behavior is directly reflected in the load-time response. Eventually the amplitude of the specimen oscillations become damped by plastic deformation and other energy absorbing processes, so that as general yield is approached the load-time response becomes smoother. The question then arises; how can valid fracture measurements be made while the load-time response is behaving in such an apparently complex manner?

Effect of Initial Stress Waves

The initial elastic stress pulse is an inevitable consequence of impact loading. Attempts to reduce or eliminate this phenomenon are largely futile since any reduction is always at the expense of the stress intensity rate. The initial stress pulse puts the crack into compression

---

*In the case of deeply cracked specimens, the specimen may actually lose contact with the hammer causing total unloading.

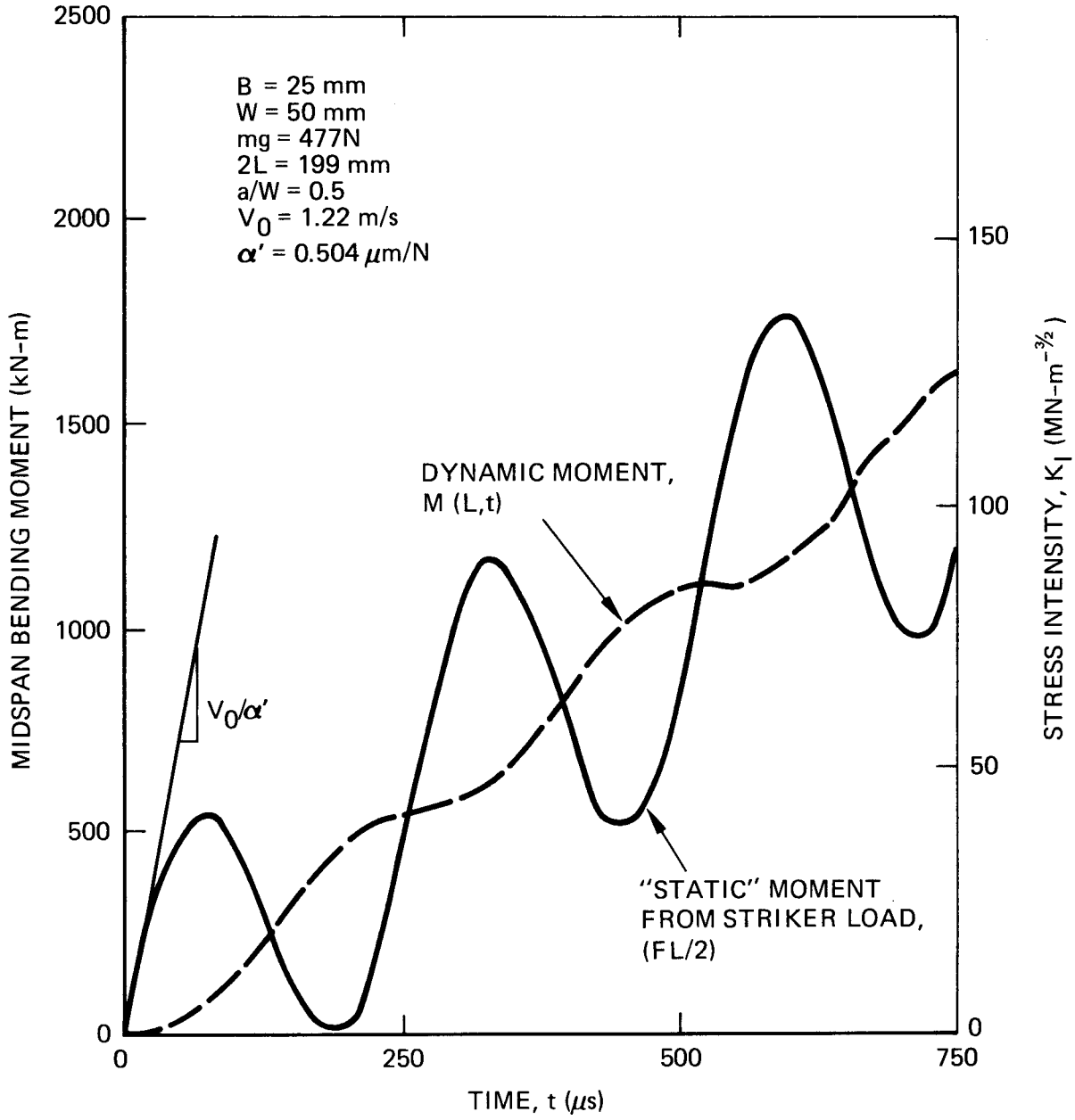

Figure A.6. "Static" and Dynamic Midspan Bending Moment as Computed According to Beam-Spring Model[5a].

and furthermore as a result of rapid attenuation cannot cause any significant crack extension or damage during the preliminary state of loading. Thus apart from complicating the load-time trace the initial stress pulse has no deleterious effects on the overall outcome of the test.

Effect of Specimen Oscillations

The flexural motion of the specimen results in a dynamic bending moment distribution which is considerably different from the corresponding static case, as shown in Figure A.6. Despite these differences it turns out that the stress intensity coefficient is not significantly modified as shown by Turner, et al[3a] using a finite element analysis and illustrated in Figure A.7. Thus, it is perfectly valid to use the static relationships between the central bending moment and stress intensity factor.

Since the central bending moment is not generally measured directly, how may we estimate it from the hammer force?

Relationship Between Tup Signal and Central Bending Moment

In contrast to the complex analysis of Nash, Turner chose to analyze the problem by representing the dynamic loading system by masses coupled by elastic springs as shown in Figure A.5. The equation of motion for the forced vibration of the beam driven under a constant striker velocity may be derived from a consideration of force equilibrium. The solution to this equation of motion leads directly to a prediction of the time dependence of the force on the specimen which has a linear term and damped sinusoidally varying term; together they comprise the characteristic load-time curve typical of Figure A.8.

This time varying force on the beam may then be used to predict the central bending moment using the forced vibration beam theory developed originally by Timoshenko[9a] and shown in Figure A.9. The significant result is that the ripples in the time varying central bending moment are considerably smaller than those in the time varying force which produced

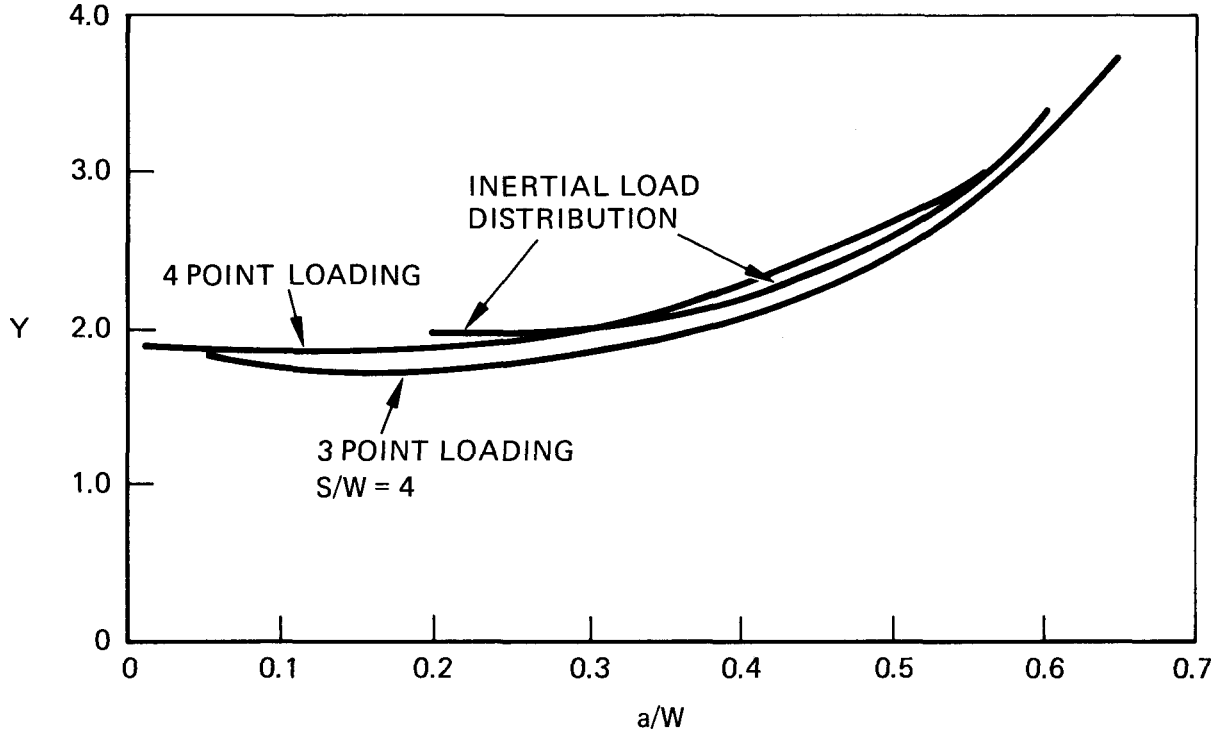

Figure A.7. Stress Intensity Coefficient for Static and Inertia Loaded Beam[3a].

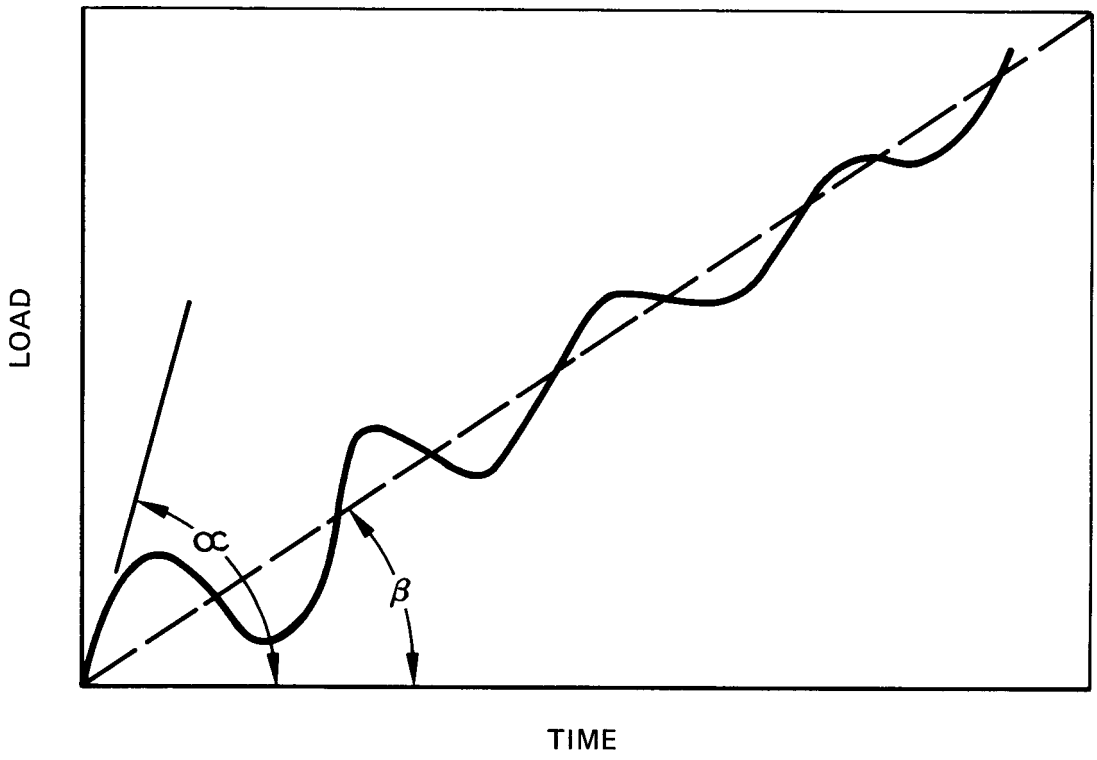

Figure A.8. Pendulum Load-Time Record Showing Actual Dynamic Stiffness, α, and Effective Stiffness, β.

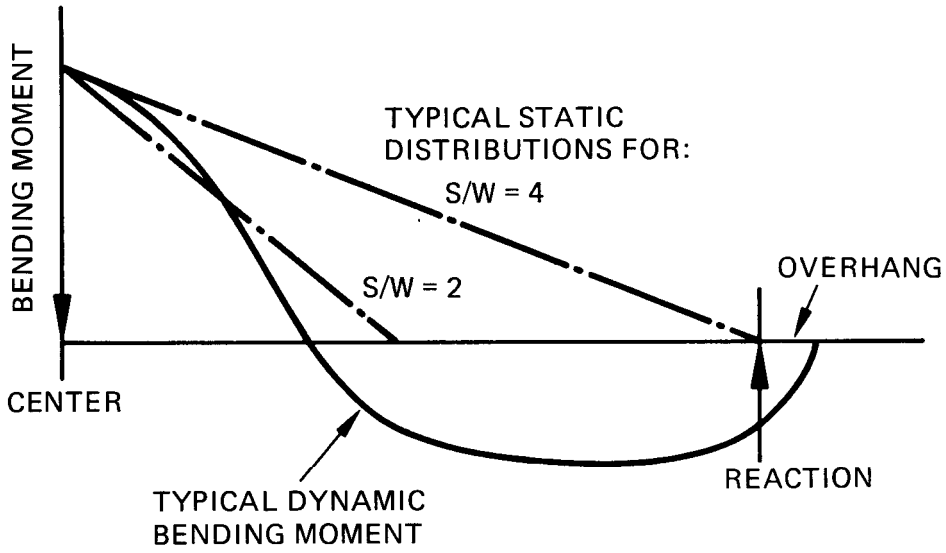

Figure A.9. Typical Bending Moment Diagram for Impact Loading of Simply Supported Beam(9a)

them. For example, in the case of the precracked Charpy specimen with crack depth ratios a/w in the range 0.2 - 0.3, the ripples are only about ten percent at the first oscillation* and thereafter continue to decrease and eventually damp out with subsequent oscillations. After approximately two full oscillations the central bending moment is essentially linear with time. These results are in general agreement with the experimental data of Priest and the theoretical analyses of Ayers and Griffis.

We may now reasonably assume on the basis of the available evidence, and contrary to initial intuitive suppositions, that the impacted Charpy specimen is suprisingly well behaved: the stress intensity factor is directly related to the central bending moment according to static analyses. Furthermore, after the first two oscillations the stress intensity factor varies approximately linearly with time. Herein lies the justification for determining the dynamic fracture toughness from instrumented impact tests, for although inertia effects may profoundly influence the form of the load-time curve they do not as it turns out have a corresponding effect on the time dependence of the stress intensity factor.

Because of the inertia effects, there is no simple relationship between the force on the tup and the central bending moment (and hence the stress intensity factor). Since it is impractical to instrument each specimen we must find a suitable method of interpreting the load-time curve obtained from the tup.

One approach is to estimate the mean load line through the load oscillations and then to determine the time to fracture by some independent form of instrumentation on the specimen. In the case of small specimens this is highly inconvenient and may be unreliable. Measurements of the onset of crack extension are subject to experimental difficulties, but in the case of larger specimens, there may be no alternative.

---

*Note that stress wave phenomena are reflected in this analysis so that the first load peak is considerably reduced.

The only remaining method appears to be to estimate the bending moment directly from the load at fracture, provided that at least three load oscillations have occurred. Attempts to electronically curve fit the oscillations by filtering seem reasonable provided that the attendant attenuation is not excessive. The acceptable level of attenuation and frequency response is specified as part of the EPRI procedures. There will always be an uncertainty of +0 - ½ oscillations in any estimate of the time to fracture. Thus <u>at worst</u> the error in estimating the fracture load following three oscillations will be a ten percent overestimate; generally the error will be considerably less than this amount. Experimental data[10a,11a] have shown this amount to be generally lower than ten percent as shown in Figure A.10. The current procedure of calculating the fracture toughness from the measured fracture load seems satisfactory.

Therefore in summary, recent analyses of the mechanics of impact fracture testing of small precracked bars in bending generally support the empirically based EPRI procedures. Essentially these procedures ensure that the inertia effects are not excessive and that the load-time curve is a reasonable analogue of the central bending moment and, hence, the stress intensity factor. Even under the most severe <u>permissible</u> conditions where the inertial effects are greatest, the errors in fracture toughness values are never greater than ten percent.

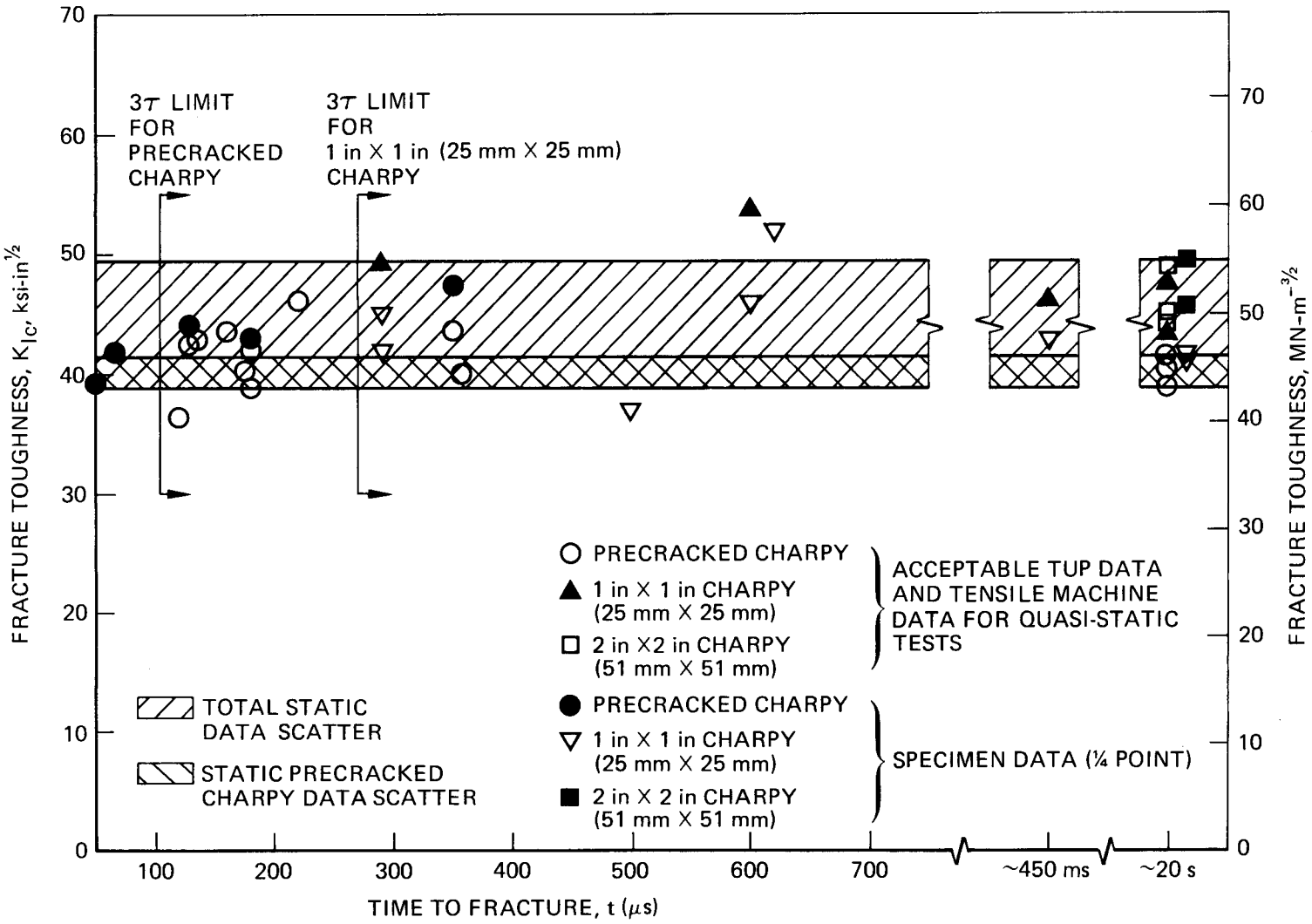

Figure A.10. Acceptable Toughness Results for 4340 Steel as a Function of Time to Fracture(11a)

REFERENCES

1a. Anderson, J.M., Aberson, J.A., King, W.W., "Finite Element Analysis of Cracked Structures Subjected to Shock Loads," Computational Fracture Mechanics, ASME, June 1975.

2a. Ayers, D.J., "Dynamic Plastic Analysis of Ductile Fracture in Charpy Specimens," ASME Symposium on Finite Element Methods in Mechanics, June 1975, Troy, N.Y.

3a. Turner, C.E., "Dynamic Fracture Toughness Testing by Instrumented Impact Testing," ISPRA Advanced Seminar on Fracture Mechanics, October 1975.

4a. Nash, G.E., "An Analysis of the Forces and Bending Moments Generated During the NRL Dynamic Tear Test," NRL Report 6864, January 1969.

5a. Griffis, C.A., "Further Analytical and Experimental Study of Inertial Loading in Notched Beam Impact Tests," in NRL Memorandum Report 3289, May 1976, P. 16.

6a. Glover, A.P., Johnson, F.A., Radon, J.C., and Turner, C.E., "Dynamic Fracture Toughness Measurement by Instrumented Impact Bend Testing and Compact K Testing," Conference on Dynamic Toughness, Welding Institute/ ASM, July 1976.

7a. Venzi, S., Priest, A.H., and May, J.J., "Influence of Inertia Load in Instrumented Impact Tests," Impact Testing of Metals, ASTM STP 466, March 1970.

8a. Kobayashi, A.S., "Dynamic Photoelastic Analysis of Three Dynamic Fracture Specimens," Conference on Dynamic Toughness, Welding Institute/ASM, July 1976.

9a. Timoshenko, S., Vibrations Problems in Engineering, 2nd Ed., New York, Van Nostrand, 1937.

10a. Server, W.L., R.A. Wullaert, and J.W. Sheckherd, "Verification of the EPRI Dynamic Fracture Toughness Testing Procedures," Effects Technology Report TR 75-42, October 1975.

11a. Server, W.L., R.A. Wullaert, and J.W. Sheckherd, "Evaluation of Current Procedures for Dynamic Fracture Toughness Testing," presented at the Tenth National Symposium on Fracture Mechanics, Philadelphia, PA, August, 1976 (to be published in an ASTM STP).

APPENDIX B

REVIEW OF EPRI PROCEDURES FOR INSTRUMENTED IMPACT TESTING

The instrumented impact testing procedures initially developed for the EPRI program[1b] centered around the use of the parameter Θ, which reflects the apparent specimen oscillatory nature and is dependent upon the material and support span (S). The parameter was defined as

$$\Theta = 20S \quad , \tag{B-1}$$

where the empirical parameter 20 μs/in (787 μs/m) was derived for standard Charpy V-notch (a/w = 0.2) and 1-in. (25 mm) bend geometries. The criteria related to Θ for impact testing were

$$t \geq 1.5\ T_R \tag{B-2}$$

and

$$T_R \geq 2\Theta \quad , \tag{B-3}$$

where t is either the time to fracture for a linear elastic fracture or the time to general yield for a post-general yield fracture; T_R is the 0.915 dB response time of the total instrumentation system (defined later in Equation B-7).

These criteria were used throughout the EPRI testing program and were later experimentally examined in detail[2b]. The experimental verification revealed that the procedures were adequate, and a new format for presenting the procedures was developed. The instrumented impact procedures have again been examined, and the following discussion represents the most current specification for ensuring reliable test results.

The EPRI impact testing procedures rely heavily on existing ASTM methods as they pertain to instrumented impact testing. The measurement criteria related to sample geometry and dimensions, crack length and shape, fatigue precracking, and testing jig requirements are maintained as much as possible.

The load signal measured from an instrumented tup during an impact

$$\tau = 3.36 \frac{W}{C_0} (EBC_S)^{1/2} \qquad \text{FOR L/W = 4}$$

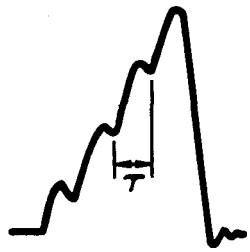

W ≡ SPECIMEN WIDTH
B ≡ SPECIMEN THICKNESS
L ≡ SUPPORT SPAN (THREE-POINT BEND)
C_0 ≡ SOUND SPEED IN THE SPECIMEN
C_S ≡ SPECIMEN COMPLIANCE
E ≡ YOUNG'S MODULUS OF THE SPECIMEN

Figure B.1. Apparent Specimen Oscillation Period τ For a Three-Point Bend Test

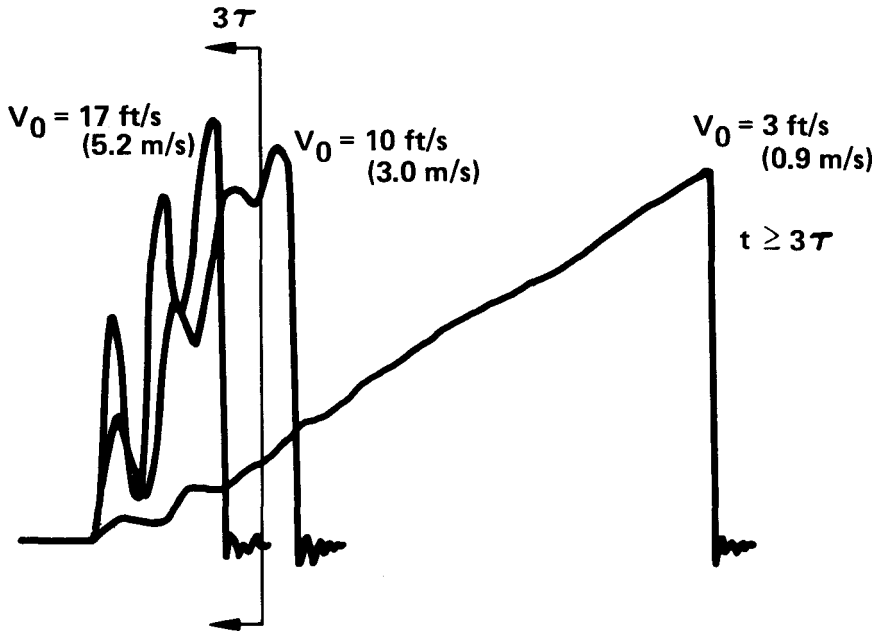

Figure B.2. Time to Fracture Criterion for an Acceptable Test Result

test oscillates about the actual load required to deform the sample. Therefore, the signal analysis procedure employed should minimize the deviation of the apparent load from the actual specimen deformation load. A simplistic view of the impact event allows three major areas for test specification to be identified: inertial loading, limited frequency response, and electronic curve-fitting.

The impact of an unsupported specimen will create inertial oscillations in the contact load between tup and specimen, and a time approximately equal to 2τ is required for the load to be dissipated. τ is related to the period of the apparent specimen oscillations (see Figure B.1; τ is similar to Θ in Equation B-3) and can be predicted for a span to width ratio of 4 by

$$\tau = 3.36 \frac{W}{C_o} (EBC_s)^{\frac{1}{2}} \quad , \qquad \text{(B-4)}$$

where,

W = beam width
B = beam thickness
C_s = specimen compliance
E = Young's modulus, and
C_o = speed of sound in the specimen.

The value of 3.36 in Equation B-4 is an empirical fit to data generated using aluminum, beryllium, and steel samples with varying spans and a/w ratios. Theoretically, for a free standing wave it can be shown that Equation B-4 is valid when the factor is 4/n, where n is the mode of oscillation. Since the oscillation pattern during impact appears to be a combination of mode 1 and mode 3 with mode 1 dominating, the empirical factor of 3.36 seems quite reasonable.

The appearance of the tup signal during the time 2τ is nearly the same as that for an unsupported specimen. When any time t is less than 2τ, it is not possible to use the tup signal to measure the specimen load (and therefore determine fracture toughnesss) due to inertial effects. This

$$T_R = \frac{0.35}{f_{10}}$$

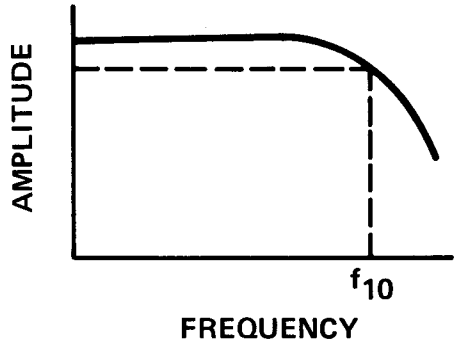

f_{10} = FREQUENCY CORRESPONDING TO A TEN PERCENT ATTENUATION (0.915 dB) IN AMPLITUDE OF A SINE WAVE SIGNAL

Figure B.3. Definition of the Response Time for a Sinusoidal-Type Wave Form

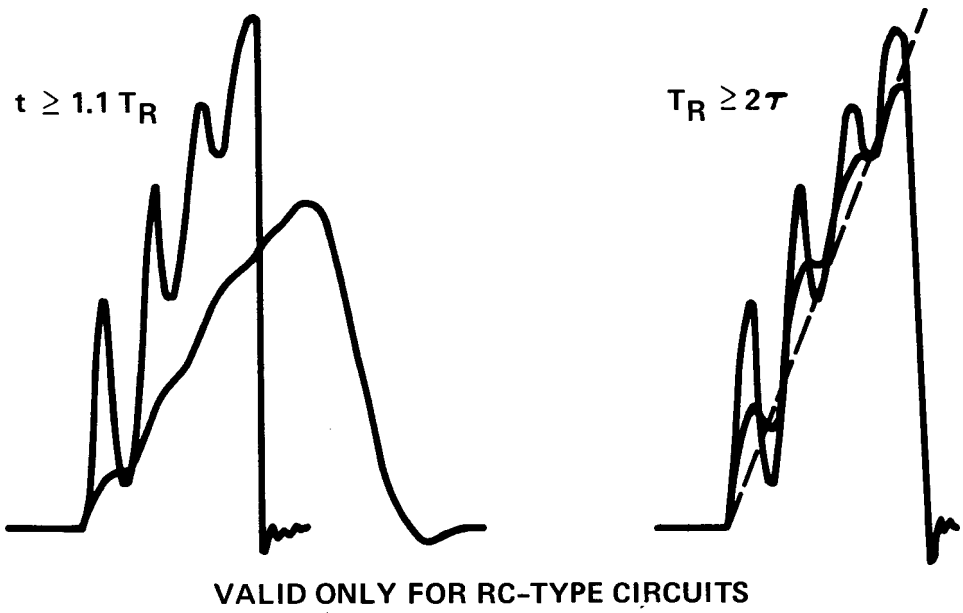

Figure B.4. Effects of Electronically Overfiltering and Curve-Fitting

inertial effect is shown schematically in Figure B.2. A tentative specification for reliable load or time evaluation is

$$t \geq 3\tau \quad , \qquad \text{(B-5)}$$

The constant 3 in Equation B-5 may be as low as 2.3 - 2.5 without adversely affecting the test results if the curve-fitting technique described below is followed, but a value of 3 was conservatively chosen. The original EPRI procedures corresponded to the 2.3 - 2.5 factor mentioned above.

The potential problem of limited frequency response of the transducer amplifier is avoided by specifying

$$t \geq 1.1\ T_R \quad , \qquad \text{(B-6)}$$

where T_R is defined as the 0.915 dB response time of the instrumentation, i.e.,

$$T_R = \frac{0.35}{f_{.915dB}} \quad , \qquad \text{(B-7)}$$

where $f_{.915\ dB}$ is the frequency at 0.915 dB (10 percent) attenuation (see Figure B.3). The specification in Equation B-6 results in approximately 4 percent amplitude attenuation of a sine wave signal at a rise time equal to 3τ if $T_R \simeq 2\tau$. This upper limit attenuation level does not appear to affect the maximum load response for instrumented impact tests. It is important to note that the electronic attenuation must be indicative of an RC circuit.

The curve-fitting of the oscillations is achieved by specifying a minimum T_R such that the amplitude of the oscillations is reduced to make a minimal disparity between tup contact load and the effective specimen midspan load. For the bend test, it has been empirically found that

$$T_R \geq 2\tau \qquad \text{(B-8)}$$

is adequate for the electronic curve-fitting (similar to Equation B-3). However, it has been shown that the constant 2 may be reduced to 1.4 (which

corresponds to an equivalent 0.445 dB [5 percent] attenuation) without affecting the results[2b]. Another alternative to Equation B-8 is to curve-fit lower T_R data by computer techniques. Also, it has been shown that filtering below a level of 1.4τ when the requirements of Equation B-5 are met causes less than a five percent increase in the load measured[2b].

The most concise manner to state these requirements related to limited frequency response and curve-fitting is:

$$1.4\tau \leq T_R \leq 0.9\ t \quad . \tag{B-9}$$

Equation B-9 requires that the signal is not over filtered (Equation B-6) but that the filtering is sufficient to electronically curve-fit the signal oscillations (Equation B-8). Figure B.4 schematically shows the effects of Equation B-9. As alluded to previously, the use of Equation B-8 is overly restrictive, and future specifications need only specify the requirements of Equations B-5 and B-6. The original EPRI procedures required the 2θ (Equation B-3) criterion or the equivalent[3b] since the fracture time criteria in Equation B-2 corresponds to approximately 2.3τ (as τ is now defined). It should be noted that often the requirements of Equation B-5 cannot be met, but the original 2.3τ criterion can be met; if filtering were utilized the 2.3τ data would still be acceptable.

The requirements for obtaining acceptable load-time records (in particular, Equation B-5) result in the need to control the impact velocity (V_0). In controlling the impact velocity, a corresponding control of the total available energy (E_0) is inherent. The reduction in tup velocity during the impact loading of the specimen should, therefore, be minimized. A conservative requirement is

$$E_0 \geq 3\ W_M \quad , \tag{B-10}$$

where W_M is the energy dissipated to maximum load. This requirement insures that the tup velocity is not reduced by more than 20 percent during the initiation fracture event (assumed to be maximum load). The require-

ment of Equation 11 is shown schematically in Figure B.5. A total fracture energy criterion is important if normalized total energy values are desired. It is then important that the sample be completely fractured, in addition to the requirement of Equation B-10, i.e.,

$$E_O > \Delta E_O \quad , \qquad \text{(B-11)}$$

where ΔE_O is the energy consumed in completely fracturing the sample. A complete review of the new procedures compared to the original EPRI procedures is shown in Table B.1.

Another procedural update is reflected in the impact test compliance technique for elastic-plastic (post-general yield) data analysis. The compliance technique is required since the real specimen deformation energy to maximum load (or initiation load) is required to calculate the equivalent energy or J-integral estimate of fracture toughness. The EPRI procedures indicate the true value of initiation energy (maximum load) to be

$$E_I = W_M - \frac{P_M^2 C_M}{2} \quad , \qquad \text{(B-12)}$$

where E_I is the true specimen energy, W_M is the energy corresponding to the trace record, P_M is the maximum load, and C_M is the "extraneous compliance" which includes plastic terms expressed as elastic equivalents, i.e.,

$$C_M = \frac{\bar{V} t_{GY}}{P_{GY}} - C_s \quad , \qquad \text{(B-13)}$$

where $\bar{V}$ is the average impact velocity to maximum load,

t_{GY} is the time to general yield,

P_{GY} is the general yield load, and

C_s is the known elastic specimen compliance.

Assuming the compliance C_M to be linear as indicated in Equation B-12, and ignoring the small amount of inertial energy, E_I can be expressed as

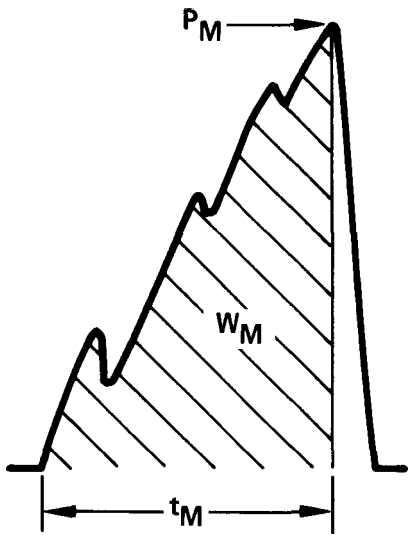

REDUCTION IN TUP VELOCITY SHOULD BE LESS THAN 20 PERCENT:

$E_0 \geq 3 W_M$

$E_0 \equiv$ TOTAL AVAILABLE ENERGY ($\frac{1}{2} M V_0^2$)

Figure B.5. Energy Criterion for Acceptable Impact Test Data

Table B.1. Comparison of Latest Test Requirements with Original EPRI Requirements

	CURRENT REQUIREMENTS	ORIGINAL EPRI REQUIREMENTS
INERTIAL EFFECTS	$t \geqslant 3\tau$	$t \geqslant 2.3\tau$
LIMITED FREQUENCY RESPONSE	$t \geqslant 1.1\, T_R$	$t \geqslant 1.5\, T_R$
ELECTRONIC CURVE FITTING	ONLY REQUIRED IF $2.3\tau \leqslant t < 3\tau$; $T_R \geqslant 1.4\tau$	$T_R \geqslant 2\tau$

$$E_I = \frac{P_{GY}^2 C_s}{2} + W_M - \frac{P_{GY} t_{GY} \bar{V}}{2} + \frac{(P_M^2 - P_{GY}^2) C_M}{2} \quad . \qquad \text{(B-14)}$$

Since the plastic compliance contributions occur early in the impact event (probably well before general yield), including them in the value of C_M as indicated in Equation B-14 is conservative. If the elastic machine compliance (C_e) is used instead of C_M, Equation B-14 becomes

$$E_I = \frac{P_{GY}^2 C_s}{2} + W_M - \frac{P_{GY} t_{GY} \bar{V}}{2} + \frac{(P_M^2 - P_{GY}^2) C_e}{2} \quad . \qquad \text{(B-15)}$$

The value of C_e is similar for all calibrated Charpy impact machines and is approximately 2×10^{-6} in/lb (3.75×10^{-8} m/N)[4b].

The difference in toughness values from using C_e rather than C_M typically results in a higher value of fracture toughness of about 9 ksi-in$^{\frac{1}{2}}$ (10 MN-m$^{-3/2}$) in the upper shelf region. However, the use of Equation B-12 (and, therefore Equation B-14) is therefore slightly conservative. Also, since the inertia area is ignored the E_I value may be slightly high; however, this inertia area is much smaller than the compliance change contribution.

REFERENCES

1b. Ireland, D.R., W.L. Server, and R.A. Wullaert, "Procedures for Testing and Data Analysis," Effects Technology Report TR 75-43, October 1975.

2b. Server, W.L., R.A. Wullaert, and J.W. Sheckherd, "Verification of the EPRI Dynamic Fracture Toughness Testing Procedures," Effects Technology Report TR 75-42, October 1975.

3b. Marston, T.U., M.P. Borden, J.H. Fox, and L.D. Reardon, "Fracture Toughness of Ferritic Materials in Light Water Nuclear Reactor Vessels, Final Report," EPRI 232-2, December 1975.

4b. Server, W.L., and D.R. Ireland, "Nonstandard Test Techniques Utilizing the Instrumented Charpy and Izod Tests," Instrumented Impact Testing, ASTM STP 563, ASTM, 1974, pp. 74 - 91.

APPENDIX C

TABULATED RESULTS FOR J INITIATION TESTS ON HSST PLATE 02 AND ARCHIVE MATERIALS FROM EPRI RP 232 PROGRAM

Table C.1. Precracked Charpy Results - HSST Plate 02

Temperature ^{o}F (^{o}C)	$\dot{K}$ ksi-in$^{1/2}$/s (MN-m$^{-3/2}$/s)	J in-lb/in^2 (kJ/m^2)	Δa in (mm)
-20 (-29)	<3 (3.3)	711 (125)	0.002* (0.05)
		765 (134)	0.003* (0.08)
40 (4)	<3 (3.3)	139 (24.3)	~0
		265 (46.4)	~0
		381 (66.7)	0.001 (0.03)
		502 (87.9)	0.002 (0.05)
		676 (118)	0.002 (0.05)
		1117 (196)	0.006 (0.15)
		954 (167)	0.066† (1.68)
		1474 (258)	0.082† (2.08)
40 (4)	~10^4 (10^4)	1089 (191)	0.003 (0.08)
		1707^P-755^C (299-132)	0.045† (1.14)
		1507^P-1215^C (264-213)	0.055† (1.40)
		2007^P-979^C (351-171)	0.065† (1.65)
75-80 (24-27)	<3 (3.3)	1450 (254)	0.008 (0.20)
		1705 (299)	0.009 (0.23)
		1797 (315)	0.010 (0.25)
		1849 (324)	0.013 (0.33)
		2249^P (394)	0.020 (0.51)
		2370^P (415)	0.020 (0.51)
		2414^P (423)	0.021 (0.53)
		2884^P (505)	0.031 (0.79)
75-80 (24-27)	~10^4 (10^4)	1258 (220)	0.004 (0.10)
		1638 (287)	0.008 (0.20)
		2005 (351)	0.010 (0.25)
		2697^P (472)	0.017 (0.43)
		2864^P (502)	0.021 (0.53)
		2987^P (523)	0.025 (0.64)
		3628^P (635)	0.037 (0.94)

Table C.1. Continued

Temperature °F (°C)	$\dot{K}$ ksi-in$^{1/2}$/s (MN-m$^{-3/2}$/s)	J in-lb/in^2 (kJ/m^2)		Δa in (mm)	
75 (24)	~10^5 (10^5)	404	(70.8)	0.003	(0.08)
		707P	(124)	0.004*	(0.10)
		942P	(165)	0.005*	(0.13)
		852	(149)	0.005*	(0.13)
160 (71)	<3 (3.3)	1087	(190)	0.006	(0.15)
		1813	(318)	0.011	(0.28)
		2353P	(412)	0.018	(0.46)
		2804P	(491)	0.020	(0.51)
		3550P	(622)	0.029	(0.74)
		3856P	(675)	0.039	(0.99)
160 (71)	~10^4 (10^4)	260	(45.5)	<0.001	(0.03)
		685	(120)	0.001	(0.03)
		1523	(267)	0.007	(0.18)
		1891	(331)	0.010	(0.25)
		3063	(536)	0.017	(0.43)
		3812	(668)	0.023	(0.58)
		4560P	(799)	0.036	(0.91)
160 (71)	~10^5 (10^5)	1303	(228)	0.004	(0.10)
		1642	(288)	0.011	(0.28)
		1922	(337)	0.012	(0.30)
		2627	(460)	0.023	(0.58)
		3457P	(605)	0.034	(0.86)

*Fibrous crack extension prior to cleavage instability measured from broken sample without heat-tinting

†Cleavage instability extension measured by heat-tinting (includes any fibrous growth that may or may not have occurred)

PBeyond maximum load displacement

CValue corresponding to cleavage instability at maximum load

Table C.2. Results for 0.394T Bend Samples - HSST Plate 02

Temperature ^{o}F (^{o}C)	$\dot{K}$ ksi-in$^{1/2}$/s (MN-m$^{-3/2}$/s)	K_{Id} - linear elastic ksi-in$^{1/2}$ (MN-m$^{-3/2}$)
-20 (-29)	~10^5 (10^5)	40.9 (45.0) 37.4 (41.1) 36.6 (40.3) 38.3 (42.1) average

Temperature ^{o}F (^{o}C)	$\dot{K}$ ksi-in$^{1/2}$/s (MN-m$^{-3/2}$/s)	J in-lb/in^2 (kJ/m^2)	Δa in (mm)
78 (26)	<3 (3.3)	358 (62.7)	0.001 (0.03)
		1030 (180)	0.004 (0.10)
		1769 (310)	0.011 (0.28)
		2245 (393)	0.016 (0.41)
		2794^{P}(489)	0.028 (0.71)
		4096^{P}(717)	0.052 (1.32)
		3535^{P}(619)	0.055 (1.40)
75 (24)	~10^5 (10^5)	385 (67.4)	0.002*(0.05)
		652 (114)	0.003*(0.08)
		1206 (211)	0.005*(0.13)
160 (71)	~10^5 (10^5)	673 (118)	0.003 (0.08)
		1278 (224)	0.009 (0.23)
		2052 (359)	0.022 (0.56)
		2428 (425)	0.032 (0.81)
		4265^{P}(747)	0.057 (1.45)

^{P} Beyond maximum load displacement

* Fibrous crack extension prior to cleavage instability measured from broken sample without heat-tinting

Table C.3. Results for 1T Bend Samples - HSST Plate 02

Temperature ^{o}F (^{o}C)	$\dot{K}$ ksi-in$^{\frac{1}{2}}$/s (MN-m$^{-3/2}$/s)	J in-lb/in^2 (kJ/m^2)	Δa in (mm)
72 (22)	~10^5 (10^5)	1214 (213)	0.006* (0.15)
		2303 (403)	0.030 (0.76)
		3057 (535)	0.044 (1.12)
		4100 (718)	0.086 (2.18)
160 (71)	~10^5 (10^5)	4781 (837)	0.090 (2.29)
		9066^{p} (1580)	0.141 (3.58)
		7371^{p} (1291)	0.179 (4.55)

* Fibrous crack extension prior to cleavage instability measured from broken sample without heat-tinting

^{p} Beyond maximum load displacement

Table C.4. Results for 1T Compact Samples - HSST Plate 02

Temperature °F (°C)	$\dot{K}$ ksi-in$^{1/2}$/s (MN-m$^{-3/2}$/s)	J in-lb/in^2 (kJ/m^2)	Δa in (mm)
75-80 (24-27)	<3 (3.3)	1062 (186)	0.007* (0.18)
		1009 (177)	0.008 (0.20)
		1406 (246)	0.013 (0.33)
		1541 (270)	0.022 (0.56)
		1708 (299)	0.035* (0.89)
		1870^p (327)	0.048 (1.22)
		2661^p (466)	0.052* (1.32)
		3697^p (647)	0.078 (1.98)
80-85 (27-29)	~10^3 (10^3)	1114 (195)	0.008* (0.20)
		1060 (186)	0.015* (0.38)
		1531 (268)	0.016 (0.41)
160 (71)	<3 (3.3)	1220 (214)	0.005 (0.13)
		1670 (292)	0.011 (0.28)
		1955 (342)	0.023 (0.58)
		2718 (476)	0.062 (1.57)
		3783^p (663)	0.078 (1.98)
160 (71)	~10^3 (10^3)	1334 (234)	0.009 (0.23)
		1632 (286)	0.021 (0.53)
		2374^p (416)	0.031 (0.79)
		2615^p (458)	0.048 (1.22)
		4409^p (772)	0.088 (2.24)

*Fibrous crack extension prior to cleavage instability measured from broken sample without heat-tinting

^{p}Beyond maximum load displacement

Table C.5. R-Curve Results for Eight Heats Tested at 350°F (177°C)

HEAT	MATERIAL	TEST TYPE	J in-lb/in^2 (kJ/m^2)	Δa in (mm)
EG	A533B-1	Static 1T Compact	672 (118)	0.004 (0.10)
			902 (158)	0.024 (0.61)
			1557 (273)	0.063 (1.60)
			2383^P(417)	0.078 (1.98)
		Dynamic 1T Bend	1972 (345)	0.015 (0.38)
			2718 (476)	0.038 (0.97)
			4260 (746)	0.070 (1.78)
			6027^P(1056)	0.145 (3.68)
BBB	A508-2	Static 1T Compact	1098 (192)	0.010 (0.25)
			1710 (299)	0.024 (0.61)
			2409 (422)	0.047 (1.19)
			3591^P(629)	0.091 (2.31)
		Dynamic 1T Compact	1679 (294)	0.017 (0.43)
			2316 (406)	0.028 (0.71)
			3136 (549)	0.051 (1.30)
			3914^P(685)	0.083 (2.11)
EN	A302B	Static 1T Compact	392 (68.7)	0.010 (0.25)
			618^P(108)	0.062 (1.57)
			865^P(151)	0.161 (4.09)
			1052^P(184)	0.189 (4.80)
		Dynamic 1T Bend	2194 (384)	0.134 (3.40)
			2392^P(419)	0.156 (3.96)
			3929^P(688)	0.274 (6.96)
			5121^P(897)	0.414 (10.52)
NA	A302B	Static 1T Compact	405 (70.9)	0.027 (0.69)
			776^P(136)	0.078 (1.98)
			1016^P(178)	0.195 (4.95)
			1275^P(223)	0.221 (5.61)
		Dynamic 1T Bend	2391 (419)	0.120 (3.05)
			2305^P(404)	0.212 (5.38)
			3922^P(687)	0.292 (7.42)
			5554^P(973)	0.433 (11.00)
EK	MMA Weld Metal (A533B-1 Base)	Static 1T Compact	979 (171)	0.012 (0.30)
			1429 (250)	0.027 (0.69)
			1852*(324)	0.032 (0.81)
			2625^P(460)	0.082 (2.08)

Table C.5. Continued

HEAT	MATERIAL	TEST TYPE	J in-lb/in^2 (kJ/m^2)	Δa in (mm)
EK	MMA Weld Metal (A533B-1 Base)	Dynamic 1T Bend	2099 (368)	0.021 (0.53)
			2589 (453)	0.023 (0.58)
			4626 (810)	0.058 (1.47)
			6271 (1098)	0.059 (1.50)
			5793^{P}(1015)	0.118 (3.00)
BKM	MMA Weld Metal (A508-2 Base)	Static 1T Compact	1078 (189)	0.010 (0.25)
			1878 (329)	0.027 (0.69)
			2739 (480)	0.036 (0.91)
			4310^{P}(755)	0.093 (2.36)
		Dynamic 1T Compact	1770 (310)	0.021 (0.53)
			2248 (394)	0.028 (0.71)
			3354^{PT}(587)	0.062 (1.57)
			4108 (719)	0.078 (1.98)
CJ	SA Weld Metal (A533B-1 Base)	Static 1T Compact	1248 (219)	0.009 (0.23)
			1788 (313)	0.026 (0.66)
			1859 (326)	0.027 (0.69)
			2352^{P}(412)	0.048 (1.22)
		Dynamic 1T Compact	806 (141)	0.005 (0.13)
			1607 (281)	0.020 (0.51)
			2096^{P}(367)	0.028 (0.71)
			3235P(567)	0.058 (1.47)
BAS	SA Weld Metal (A508-2 Base)	Static 1T Compact	602 (105)	0.008 (0.20)
			718 (126)	0.013 (0.33)
			1186 (208)	0.039 (0.99)
			1732^{P}(303)	0.066 (1.68)
			2098^{P}(367)	0.093 (2.36)
		Dynamic 1T Compact	676 (118)	0.007 (0.18)
			1233 (216)	0.020 (0.51)
			1794^{P}(314)	0.047 (1.19)
			2577P(451)	0.086 (2.18)

^{P} Beyond maximum load deflection

* Based on load-ram displacement curve corrected for machine compliance

^{T} Thickness was 0.882 in (22.4 mm)

APPENDIX D

NON-LINEAR REGRESSION

Introduction

The tanh equation;

$$Y = A + B \tanh \left[\frac{T - T_0}{C}\right] \qquad \text{(D-1)}$$

requires the use of iterative procedures when it is fitted to data using "least squares" techniques. Such procedures seek an optimum set of A, B, T_0, and C which minimizes the sum of squares of the deviations of the dependent variable, Y, about the fitted curve.

The problem has been described in some detail[1d] and an iterative procedure based on the method of steepest descent has been used with some success to analyze most of the test data developed in the EPRI program. However, it has become necessary to determine additional statistics in the curve fitting process which are not conveniently found by the secant procedure, so that further program development has been found to be necessary.

Numerical Procedures

The optimization task as been discussed in Reference 1d. Figures 1 and 2 of that reference (shown as Figures D.1 and D.2 here) show the task of optimizing the equation for a single variable, T_0. The procedure describes there selected two values of T_0, computed the gradient in variance at each position, and hence estimated the position of minimum variance using the secant method (D.2). This method had the advantage of being robust, and readily compatible with other procedures which could be used should the secant method diverge.

There are alternative schemes which are more efficient than this method. One alternative is to replace the method of steepest descent using the secant method by the Newton-Raphson techniques, in which the gradients are computed directly from the differential of Equation D.1. A particularly attractive approach is described in the literature[2d] and

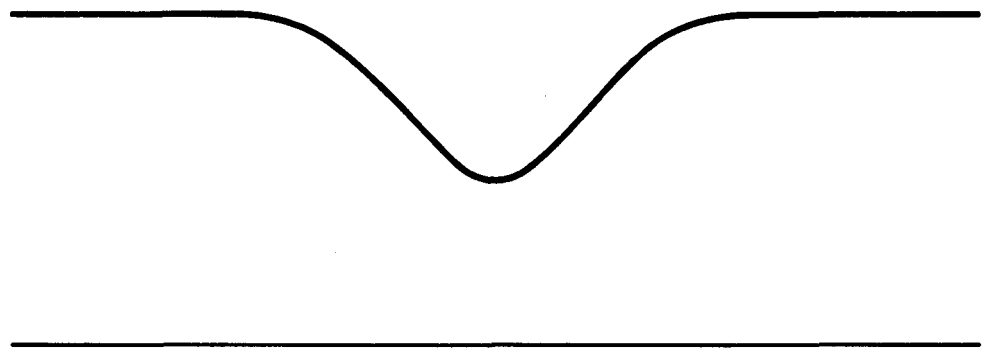

Figure D.1. (Schematic) Change in Variance with T_0

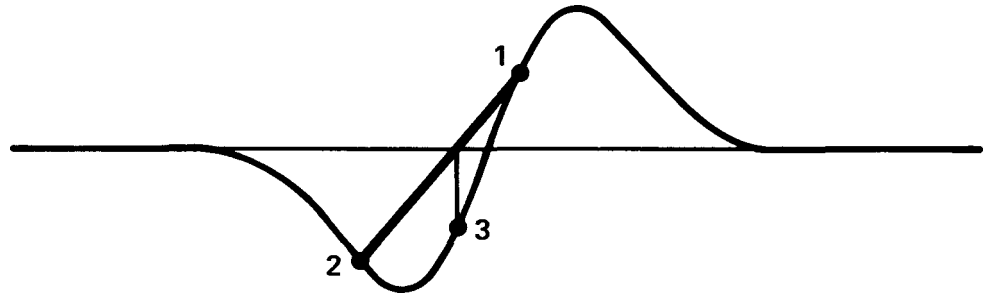

Figure D.2. (Schematic) Change in the Differential, dV/dT_0, with T_0

embodies a combination of the Newton-Raphson method with standard regression techniques. The non-linear equation (Equation D.1), is expressed in a linear form by means of a Taylor series expansion.

$$y = B \tanh x - \frac{B\ \delta T_0}{C}\ \text{sech}^2\ x - \frac{B}{C}\ \delta C\ (x\ \text{sech}^2\ x) \quad , \qquad \text{(D-2)}$$

where $y = Y - \overline{Y}$ ($\overline{Y}$ is the mean value of Y), and $x = (T - T_0)/C$. This equation can be fitted to the test data using standard regression methods, which develop the quantities B, $B\ \delta\ T_0/C$, and $B\ \delta C/C$ as the coefficients of a regression of dependent variable y on independent variables tanh x, sech^2 x, and x sech^2 x. The original estimates of T_0 and C are then changed by the quantities δT_0 and δC, and the regression analysis repeated. After several repetitions of the process, T_0 and C can be found to any predetermined accuracy.

A great advantage of the approach is that standard regression procedures compute the standard errors of the coefficients directly from the inverse of the information matrix. Hence, the quantities V(B), $V(B\ \delta T_0/C)$, and $V(B\ \delta C/C)$ (V means variance) are generated by this process. Reference 3d uses these as upper limits to the variance of B, T_0, and C respectively. However, analysis of variance techniques might allow better estimates of the values for T_0 and C.

Discussion

The techniques described here have been found to work well. Further development of the procedures using, for example, the Marquardt Compromise[4d], has not been found useful in this work.

Curve fitting has shown that there are preferred arrangements of the test data which minimize the uncertainty in the estimates of the coefficients. Such arrangements might well be specified in any codes which might use the coefficients for a normalizing scheme.

Work described in the main body of this report has shown that the variance of the test data is not uniform over the temperature range of

the tests. Consequently, a weighting scheme could be used with some advantage. One simple scheme would merely give linear elastic measurements greater weight than those generated in the elastic-plastic regime.

Summary

Non-linear equations such as the tanh equation:

$$Y = A + B \tanh \left[\frac{T - T_O}{C}\right] \qquad \text{(D-1)}$$

used to describe data which exhibits a property transition between two shelves, cannot be fitted to test data directly but require the use of iterative procedures. A scheme has been described elsewhere[1d], but it suffered from the disadvantage that the accuracy of the coefficients A, B, T_O, and C could not be computed conveniently. An alternative approach has been developed which computes upper limits to the accuracy of the coefficients. The use of weighted data is recommended.

REFERENCES

1d. Oldfield, W., "Curve Fitting Impact Test Data; A Statistical Procedure," ASTM Standardization News, Vol. 3, No. 11, November 1975.

2d. Conté, S.D., Elementary Numerical Analysis, McGraw-Hill, 1965.

3d. Williams, E.J., Regression Analysis, Wiley.

4d. Draper, N.R. and Smith, H. Applied Regression Analysis, Wiley, 1966.

APPENDIX E

DISTRIBUTION OF FRACTURE TOUGHNESS DATA

Precracked Charpy Test

Histograms for the overall distribution of data in each group are presented in Figures E.1 - E.6. The data for all groups are combined in Figure E.7. The statistics are summarized in Table E.1. Those data lying outside the ± 2.5 σ range are not included, but are summarized in Table E.2. The a and $\sqrt{b_1}$ statistics are tabulated from Reference 1e in Table E.3.

In a preliminary study, the K_{Id} data were separated from the elastic-plastic data. The K_{Id} data were found to form tbe low-toughness end of the distribution, such that the K_{Id} data were skewed low and the elastic-plastic data were skewed high. This separation was therefore eliminated in the work described here.

The distribution of the data can be assessed by comparing the results in Table E.1 with the published statistics in Table E.3. Consider first the overall data (Figures E.1 - E.6). From the "a" statistic, groups 1 and 6 are highly significant leptokurtosic (extended tails). On the other hand, group 2 is significantly platikurtosic. Group 1 showed highly significant skew high, while group 6 showed highly significant skew low. None of the other groups showed significant skewness.

The results for the individual materials tended to agree with the overall analysis. Materials 1, 5, 8, and 9 showed highly significant leptokurtosis in group 1. Similarly, materials 1, 6, 8, and 9 showed leptokurtosis in group 6 at varying significance levels. Material 5, group 2 was highly significant platikurtosic, while material 3, group 5 was platikurtosic at the 90% significance level. Materials 1, 7, 8, and 9 showed high skew in group 1, while materials 5, 6, and 9 showed low skew in group 6. The only anomalous result was for material 1 group 6 which showed highly significant high skew, in contrast to the same material in the round robin where this group was skewed low. It is hard to resist the feeling that this skewness is largely a result of testing as opposed to material variability.

Table E.1. Precracked Charpy Toughness Distribution Statistics

MATERIAL 1

GP	A VALUE	ROOT B1	B2	#
1	0.7230	1.3123	5.5126	93
2	0.7587	0.8989	3.8544	15
3	0.8525	-0.0042	1.9038	11
4	0.7900	-0.4979	2.3980	15
5	0.8208	-0.8370	2.6170	16
6	0.7287	0.4228	4.7194	107

MATERIAL 2

GP	A VALUE	ROOT B1	B2	#
1	0.8152	-0.6269	2.4697	22
2	0.8917	0.6866	1.8984	8
3	0.6924	1.2486	3.1273	5
4	0.8504	-1.2671	1.6700	4
5	0.6194	1.7243	2.9815	3
6	0.8370	-0.0725	2.7682	34

MATERIAL 3

GP	A VALUE	ROOT B1	B2	#
1	0.8638	0.7165	2.0407	14
2	0.8564	0.5980	1.8198	8
3	0.8112	-1.1566	2.0325	8
4	0.7747	-0.3508	2.2322	8
5	0.9013	0.5842	1.6706	11
6	0.7837	0.0097	2.6714	26

MATERIAL 4

GP	A VALUE	ROOT B1	B2	#
1	0.8777	-1.3581	2.0054	3
2	0.7726	1.3928	1.9624	2
4	1.0000	-1.0000	1.0000	1
5	0.9918	0.3784	1.0640	2
6	0.7896	-0.8558	3.0533	9

MATERIAL 5

GP	A VALUE	ROOT B1	B2	#
1	0.7166	-0.2126	3.7580	54
2	0.9487	-0.9223	1.3697	11
3	0.7814	1.2665	2.6244	9
4	0.8169	-0.6684	2.6149	9
5	0.5085	-2.5268	7.0217	8
6	0.7842	-0.5162	2.8922	80

Table E.1. (continued)

MATERIAL 6

GP	A VALUE	ROOT B1	B2	#
1	0.8190	0.1878	2.3071	34
2	1.0000	-1.0000	1.0000	1
3	0.9978	-0.4639	1.0183	3
4	0.7267	1.4125	1.9968	2
5	0.7928	-1.3049	2.6616	4
6	0.7526	-0.8067	3.6980	38

MATERIAL 7

GP	A VALUE	ROOT B1	B2	#
1	0.8575	0.7876	2.0928	33
2	0.7394	1.5122	4.0056	7
3	1.0000	-1.0000	1.0000	1
4	0.7846	0.9224	2.6629	6
5	0.8423	-0.4605	2.0427	6
6	0.6721	-0.1973	5.4500	46

MATERIAL 8

GP	A VALUE	ROOT B1	B2	#
1	0.5989	2.2136	9.1271	32
2	1.0000	-1.0000	1.0000	1
4	0.9999	-0.0376	1.0006	2
5	1.0000	1.0000	1.0000	1
6	0.7613	-0.3464	3.3029	47

MATERIAL 9

GP	A VALUE	ROOT B1	B2	#
1	0.6498	2.1574	8.0030	61
2	0.9034	0.5861	1.5644	8
3	0.8285	-0.7431	2.2648	16
4	0.8402	-1.3989	2.1560	3
5	0.9155	0.1697	1.3648	6
6	0.7164	-1.9512	8.5367	71

OVERALL

GP	A VALUE	ROOT B1	B2	
1	0.7328	0.9755	5.0066	346
2	0.8483	0.4865	2.4444	61
3	0.8229	-0.1121	2.2028	53
4	0.8097	-0.3654	2.2696	50
5	0.8013	-0.4775	2.7997	57
6	0.7485	-0.4378	4.5414	458

Table E.2. Precracked Charpy Outlying Values

GROUP	MATERIAL	DEVIATION (σ)
1	1	3.38
	1	2.76
	1	3.18
	1	3.24
	5	-2.94
	8	2.80
	8	3.84
	9	3.99
	9	3.52
2, 3, 4, 5	none	
6	1	3.52
	1	3.19
	6	-2.87
	7	-3.34
	9	-4.76

Table E.3. Published Statistical Tables for Quantitatively Testing for Normality[1e]

A. *Percentage points of the distribution of* $a = (\textit{mean deviation})/(\textit{standard deviation})$

Size of sample n	$n-1$	Percentage points						Mean	Standard deviation
		Upper 1%	Upper 5%	Upper 10%	Lower 10%	Lower 5%	Lower 1%		
11	10	·9359	·9073	·8899	·7409	·7153	·6675	·81805	·05784
16	15	·9137	·8884	·8733	·7452	·7236	·6829	·81128	·04976
21	20	·9001	·8768	·8631	·7495	·7304	·6950	·80792	·04419
26	25	·8901	·8686	·8570	·7530	·7360	·7040	·80590	·04011
31	30	·8827	·8625	·8511	·7559	·7404	·7110	·80456	·03697
36	35	·8769	·8578	·8468	·7583	·7440	·7167	·80360	·03447
41	40	·8722	·8540	·8436	·7604	·7470	·7216	·80289	·03241
46	45	·8682	·8508	·8409	·7621	·7496	·7256	·80233	·03068
51	50	·8648	·8481	·8385	·7636	·7518	·7291	·80188	·02919
61	60	·8592	·8434	·8349	·7662	·7554	·7347	·80122	·02678
71	70	·8549	·8403	·8321	·7683	·7583	·7393	·80074	·02487
81	80	·8515	·8376	·8298	·7700	·7607	·7430	·80038	·02332
91	90	·8484	·8353	·8279	·7714	·7626	·7460	·80010	·02203
101	100	·8460	·8344	·8264	·7726	·7644	·7487	·79988	·02094
201	200	·8322	·8229	·8178	·7796	·7738	·7629	·79888	·01491
301	300	·8260	·8183	·8140	·7828	·7781	·7693	·79855	·01220
401	400	·8223	·8155	·8118	·7847	·7807	·7731	·79838	·01058
501	500	·8198	·8136	·8103	·7861	·7825	·7757	·79828	·00947
601	600	·8179	·8123	·8092	·7873	·7838	·7776	·79822	·00865
701	700	·8164	·8112	·8084	·7878	·7848	·7791	·79817	·00801
801	800	·8152	·8103	·8077	·7885	·7857	·7803	·79813	·00749
901	900	·8142	·8096	·8071	·7890	·7864	·7814	·79811	·00707
1001	1000	·8134	·8090	·8066	·7894	·7869	·7822	·79808	·00670

B. *Percentage points of the distribution of* $\sqrt{b_1} = m_3/m_2^{\frac{3}{2}}$

Size of sample n	Percentage points		Standard deviation	Size of sample n	Percentage points		Standard deviation	Size of sample n	Percentage points		Standard deviation
	5%	1%			5%	1%			5%	1%	
25	·711	1·061	·4354	200	·280	·403	·1706	1000	·127	·180	·0772
30	·662	·986	·4052	250	·251	·360	·1531	1200	·116	·165	·0705
35	·621	·923	·3804	300	·230	·329	·1400	1400	·107	·152	·0653
40	·587	·870	·3596	350	·213	·305	·1298	1600	·100	·142	·0611
45	·558	·825	·3418	400	·200	·285	·1216	1800	·095	·134	·0576
50	·534	·787	·3264	450	·188	·269	·1147	2000	·090	·127	·0547
				500	·179	·255	·1089				
60	·492	·723	·3009	550	·171	·243	·1039	2500	·080	·114	·0489
70	·459	·673	·2806	600	·163	·233	·0995	3000	·073	·104	·0447
80	·432	·631	·2638	650	·157	·224	·0956	3500	·068	·096	·0414
90	·409	·596	·2498	700	·151	·215	·0922	4000	·064	·090	·0387
100	·389	·567	·2377	750	·146	·208	·0891	4500	·060	·085	·0365
				800	·142	·202	·0863	5000	·057	·081	·0346
125	·350	·508	·2139	850	·138	·196	·0837				
150	·321	·464	·1961	900	·134	·190	·0814				
175	·298	·430	·1820	950	·130	·185	·0792				
200	·280	·403	·1706	1000	·127	·180	·0772				

N.B. As the sampling distribution of $\sqrt{b_1}$ is symmetrical about zero, the same values, with negative sign, correspond to the lower limits.

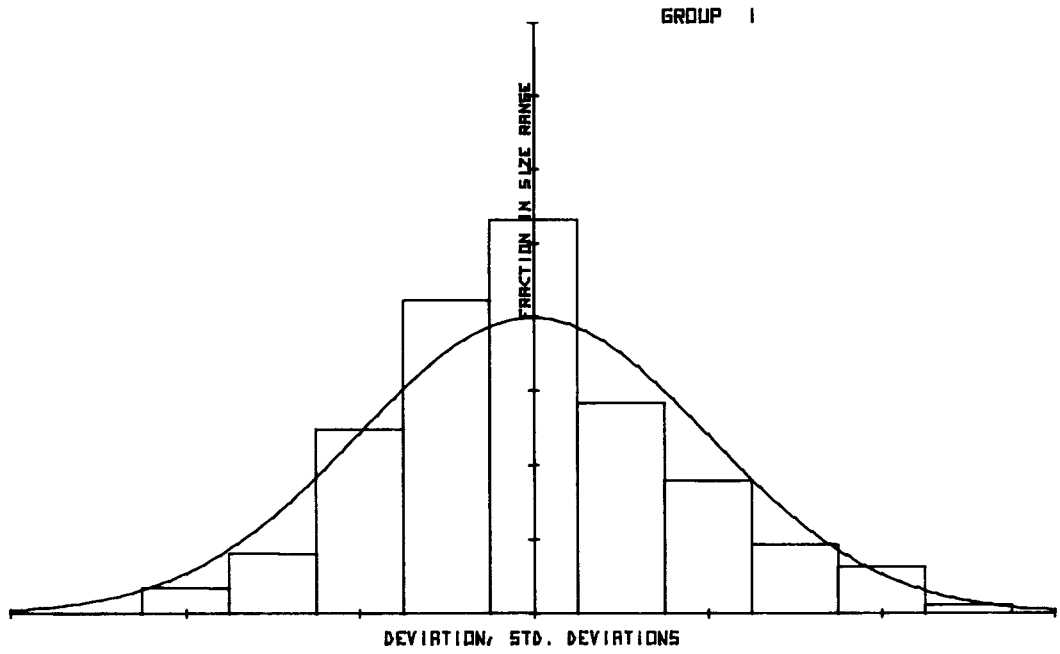

Figure E.1. Precracked Charpy Histogram Distribution for Temperature Group 1

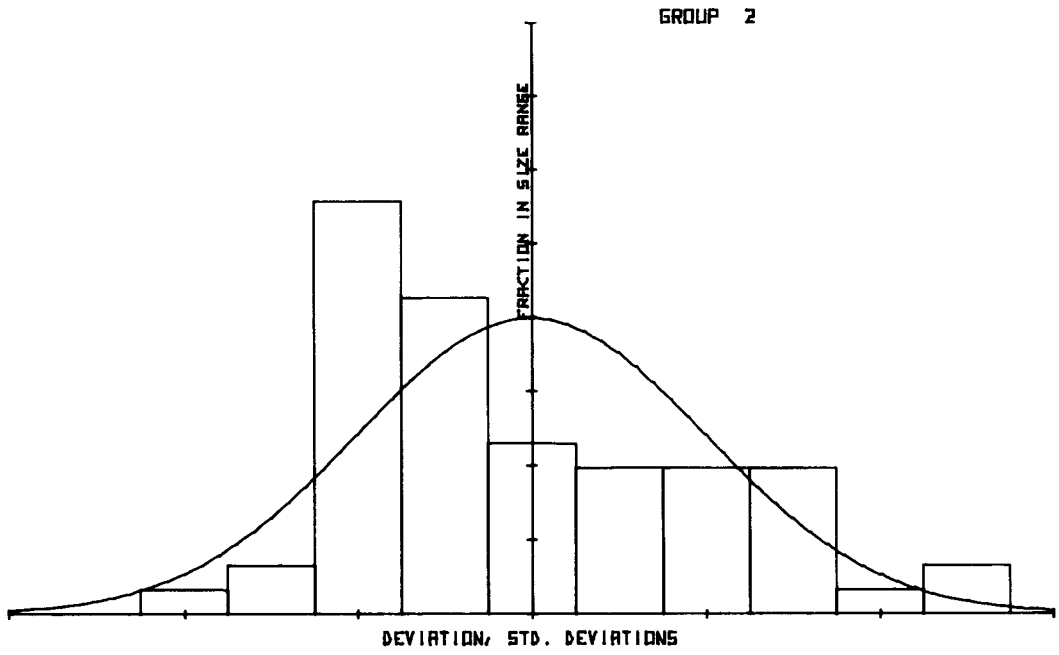

Figure E.2. Precracked Charpy Histogram Distribution for Temperature Group 2

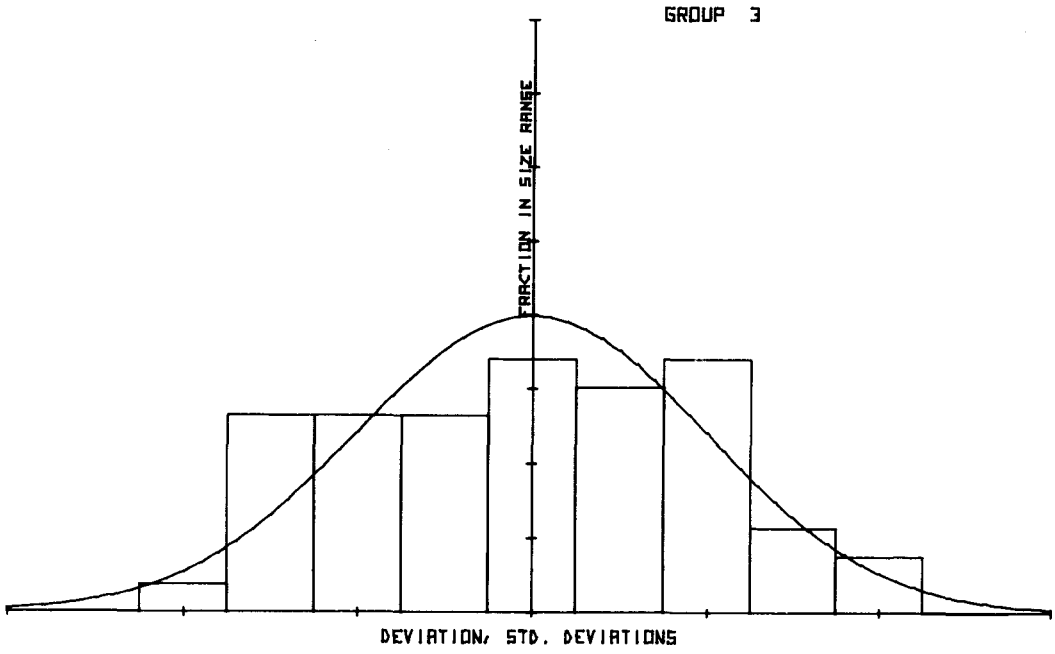

Figure E.3. Precracked Charpy Histogram Distribution for Temperature Group 3

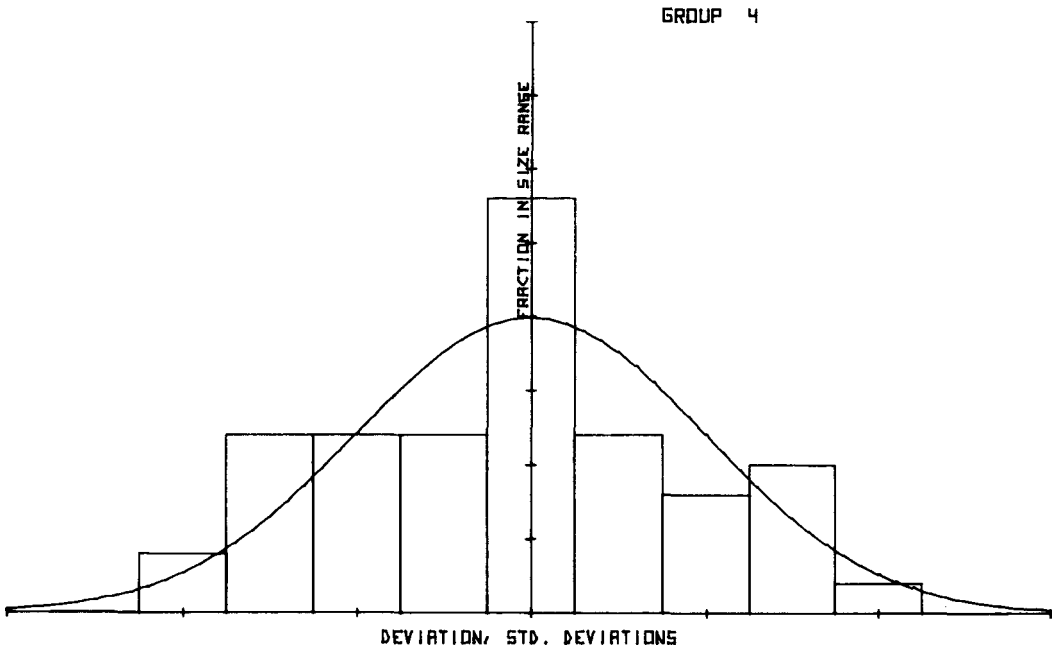

Figure E.4. Precracked Charpy Histogram Distribution for Temperature Group 4

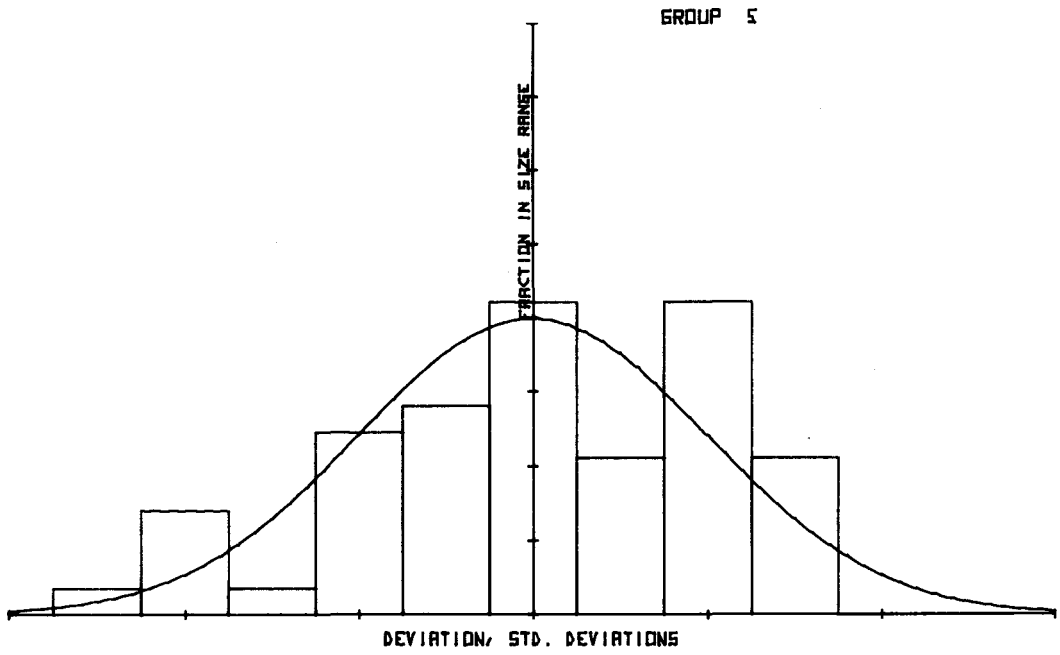

Figure E.5. Precracked Charpy Histogram Distribution for Temperature Group 5

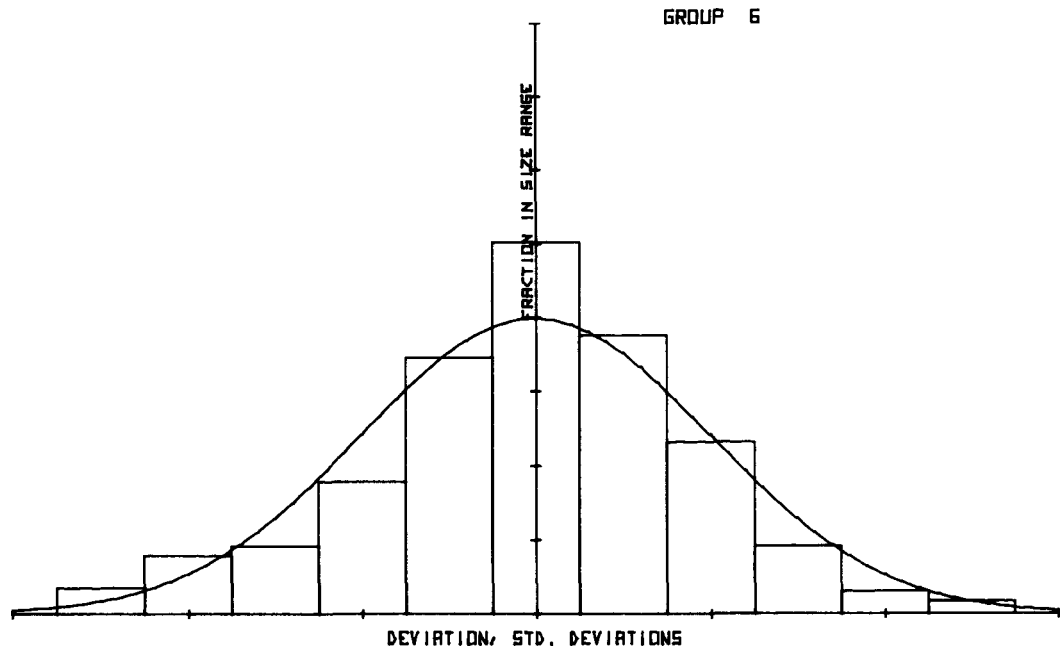

Figure E.6. Precracked Charpy Histogram Distribution for Temperature Group 6

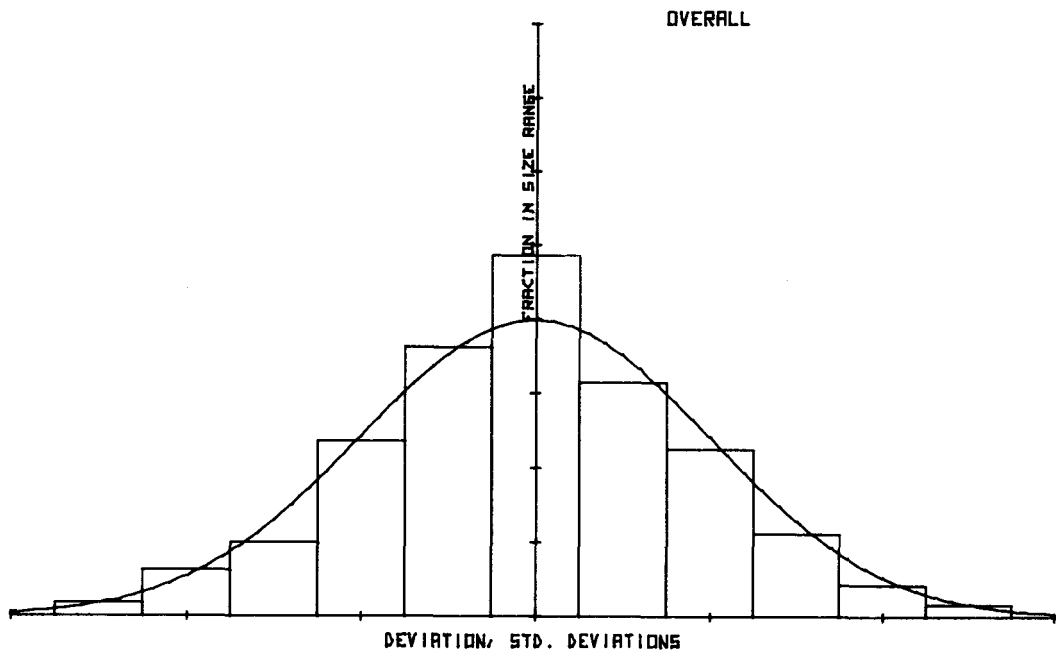

Figure E.7. Precracked Charpy Histogram Distribution for All Temperature Groups

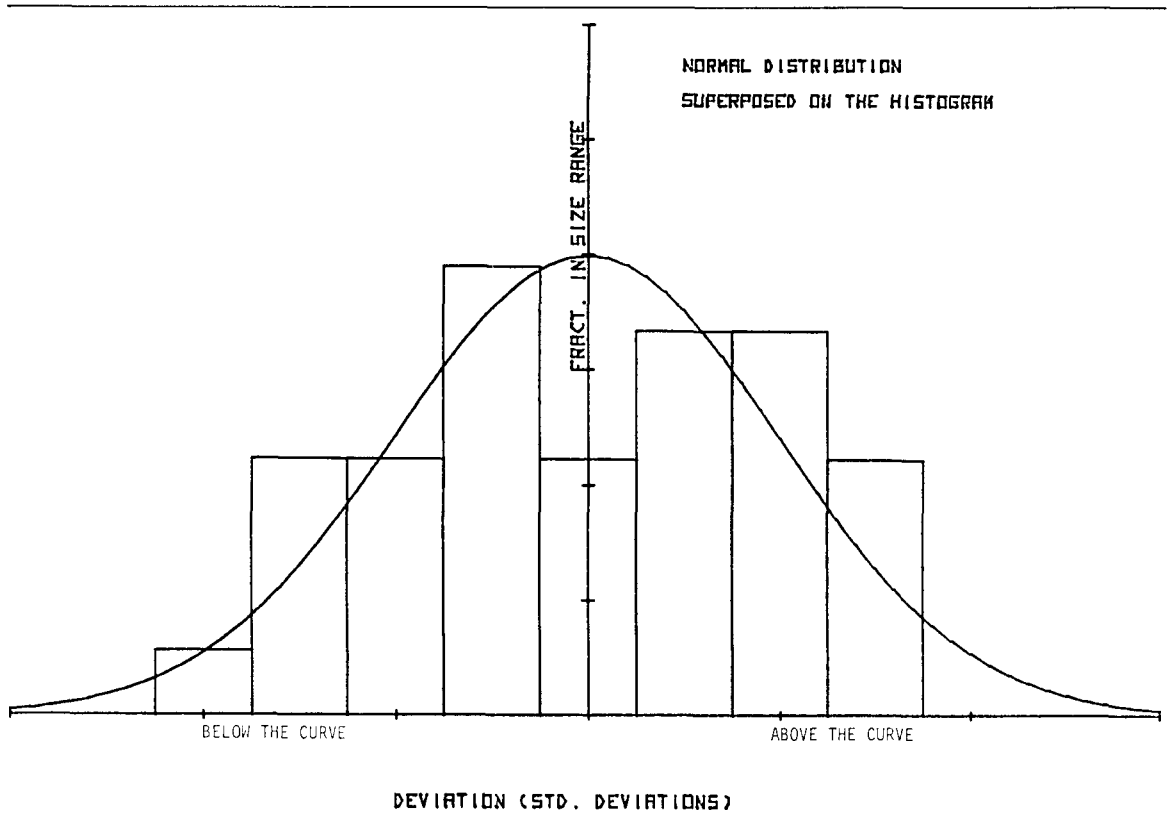

Figure E.8. Precracked Charpy Histogram Distribution for Overall Round Robin Data[9]

Overall the results can be reviewed by examining the distribution of outliers, in Table E.2. These outliers were entirely from the skewed groups, groups 1 and 6, and they confirm the analysis above (group 1 were almost all high, but while material 6 group 6 were high, the others from group 6 were low). The total number of outliers, 14, from 1025 tests, is close to the 13 which would be predicted to be outside the ± 2.5 σ limits of the Normal distribuiton. The similarity between the distribution of this data and the Normal distribution is confirmed by the histogram, Figure E.7. In contrast, the overall round robin data was platikurtosic (see Figure E.8).

Static Compact Tests

The static compact fracture specimen data were normalized by means of the precracked Charpy impact test results to allow combination of all heats of each material. The results are summarized in Table E.4 and in Figures E.9 - E.15.

There was only one point outside the ± (2.5 standard deviation) range at 2.9 σ above the mean for group 1 material 1, suggesting that the distribution generally had short tails (platikurtosis).

The results of a comparison of the statistics shown in Table E.4 with the probability tables shown in Table E.3 revealed that some of the data did not conform to the Normal distribution. These results are summarized in Table E.5. Only those results are shown in which there were enough data to perform the appropriate significance test, and for which there was a positive result. For other groups for which there were enough data values, no significant difference between the data and the Normal distribution could be asserted. The analysis shows clearly that the use of the Normal distribution to describe data of this sort is a conservative assumption in that fewer results than predicted would lie outside lower bounds set on such a basis. There were really too few data values to develop a more accurate description of the probability distribution from the test data than that given by the Normal distribution.

Table E.4. Static Compact Fracture Toughness Distribution Statistics

MATERIAL 1

GP	A VALUE	ROOT B1	B2	
1	0.7578	1.3779	4.2413	30
2	0.8342	0.5723	2.3144	7
3	0.8222	-1.4810	2.3617	6
4	0.7502	0.2901	2.9490	14
5	0.8337	0.4656	2.3491	11
6	0.7937	-0.9696	2.4331	12

MATERIAL 2

GP	A VALUE	ROOT B1	B2	
1	0.7520	1.5453	2.8330	11
2	0.9808	1.0554	1.1462	2
3	0.8964	1.2487	1.6316	2
4	0.9610	1.1048	1.2730	3
6	0.7801	-1.3714	3.3435	7

MATERIAL 3

GP	A VALUE	ROOT B1	B2	
1	0.5554	1.9838	3.9580	4
3	1.0000	1.0000	1.0000	1
6	0.7750	-0.2717	3.0901	19

MATERIAL 5

GP	A VALUE	ROOT B1	B2	
1	0.8225	0.6435	3.3650	16
2	0.9541	0.8451	1.3269	2
3	0.8613	0.8702	1.4776	4
4	0.8372	-1.2348	1.5377	3
5	0.9931	0.5456	1.0588	3
6	0.8920	-0.0023	1.5742	14

Table E.4. (continued)

MATERIAL 6

GP	A VALUE	ROOT B1	B2	
1	0.8444	1.2918	2.9074	7
2	0.9440	-0.9180	1.3881	2
3	0.9902	0.4141	1.0767	2
4	1.0000	-1.0000	1.0000	1
5	1.0000	1.0000	1.0000	1
6	0.7920	0.8678	3.0865	12

MATERIAL 7

GP	A VALUE	ROOT B1	B2	
1	0.8508	0.8306	2.3222	11
2	0.8117	-1.4402	2.6947	4
3	0.9570	-0.8213	1.3682	2
4	0.8631	1.3146	1.8312	3
5	0.9248	-0.0916	1.2965	7
6	0.9406	-0.7016	1.5051	3

MATERIAL 8

GP	A VALUE	ROOT B1	B2	
1	0.8864	0.4639	1.7302	8
4	0.8834	-1.2000	1.6855	2
6	0.8933	-0.1139	1.8047	16

OVERALL

GP	A VALUE	ROOT B1	B2	
1	0.7903	1.1317	3.3082	87
2	0.8732	0.0126	2.0413	17
3	0.8862	-0.1601	1.9243	17
4	0.8175	0.1621	2.2916	26
5	0.8920	0.3235	1.7769	22
6	0.8201	-0.2403	2.4529	83

Table E.5. Static Compact Outlying Trends

Material	Group	Kurtosis	Skewness
1	1		***H
5	6	*P	
8	6	**P	
overall	1		***H
	2	*P	
	3	**P	
	5	**P	

P = platikurtosis
H = skewed high

* = 90% significance level
** = 95% significance level
*** = 99% significance level

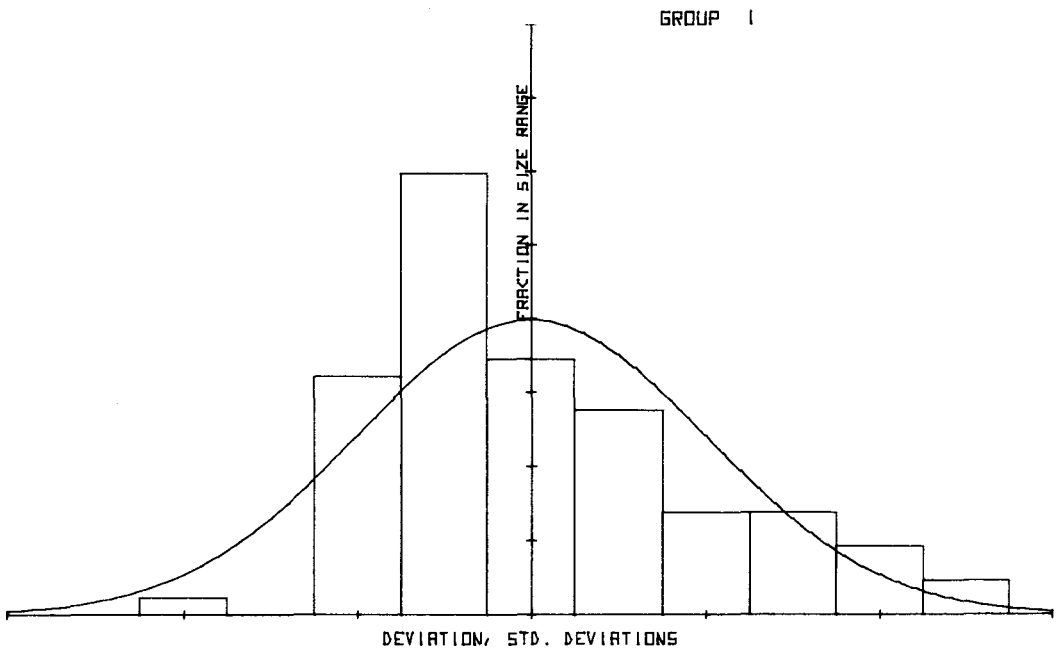

Figure E.9. Static Compact Histogram Distribution for Temperature Group 1

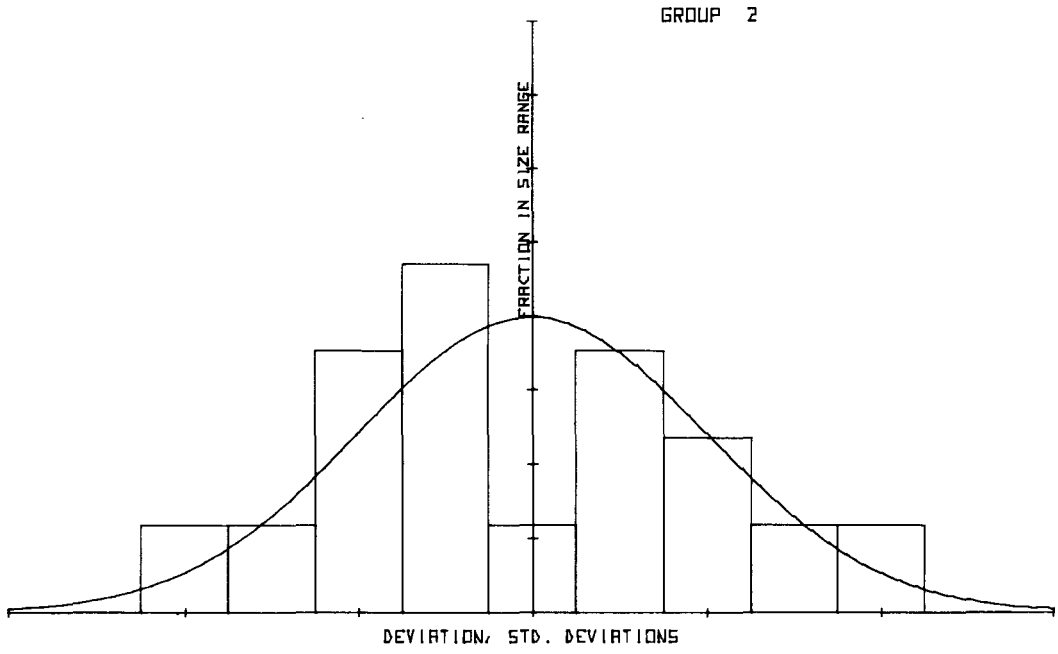

Figure E.10. Static Compact Histogram Distribution for Temperature Group 2

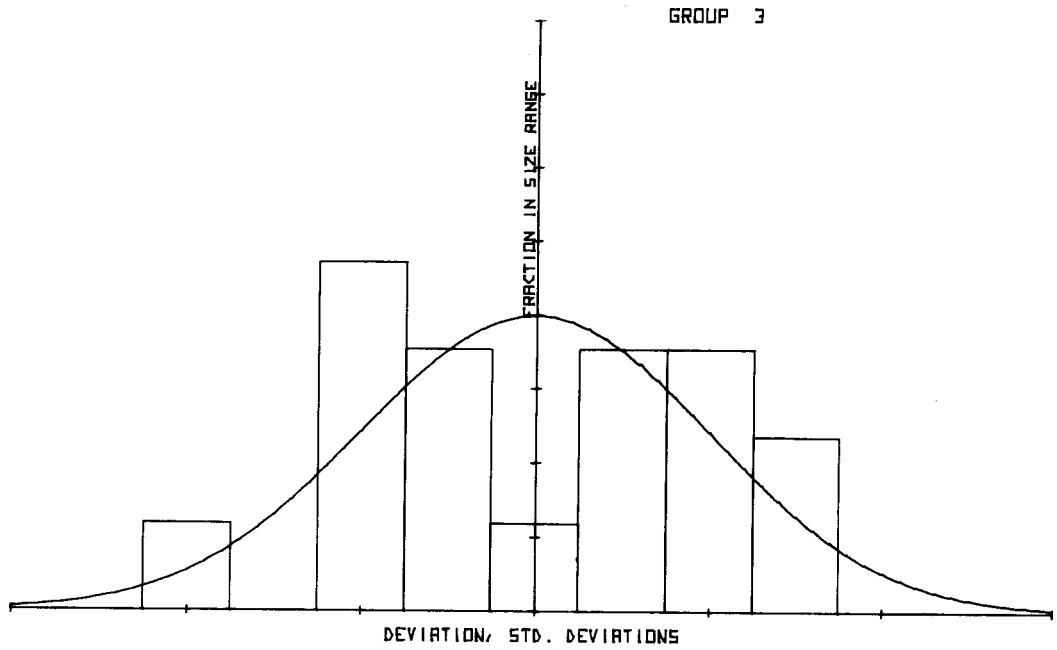

Figure E.11. Static Compact Histogram Distribution for Temperature Group 3

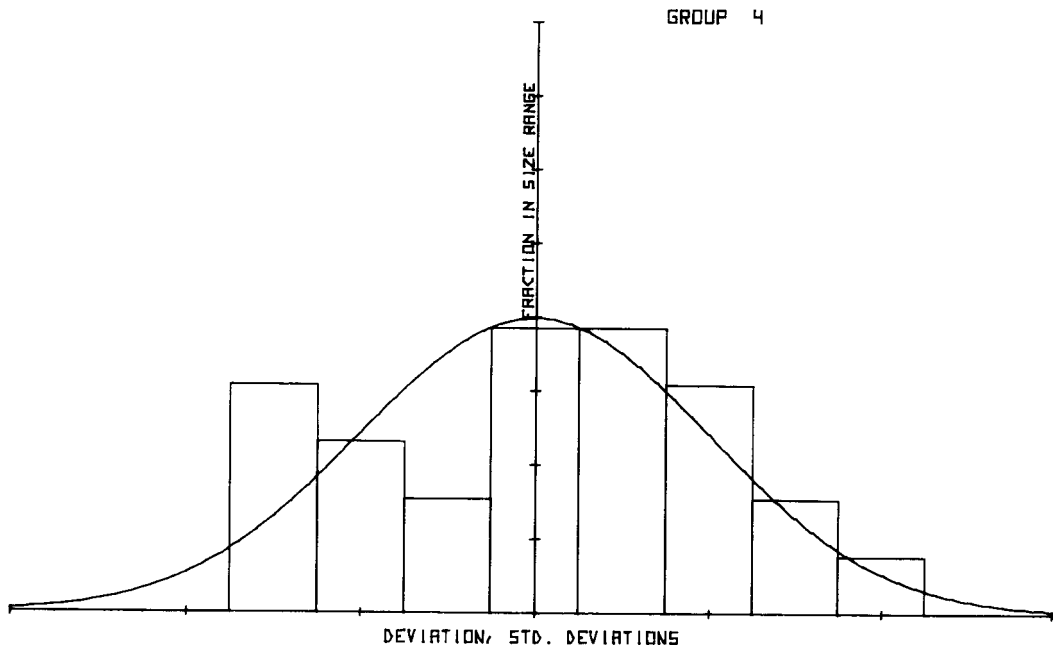

Figure E.12. Static Compact Histogram Distribution for Temperature Group 4

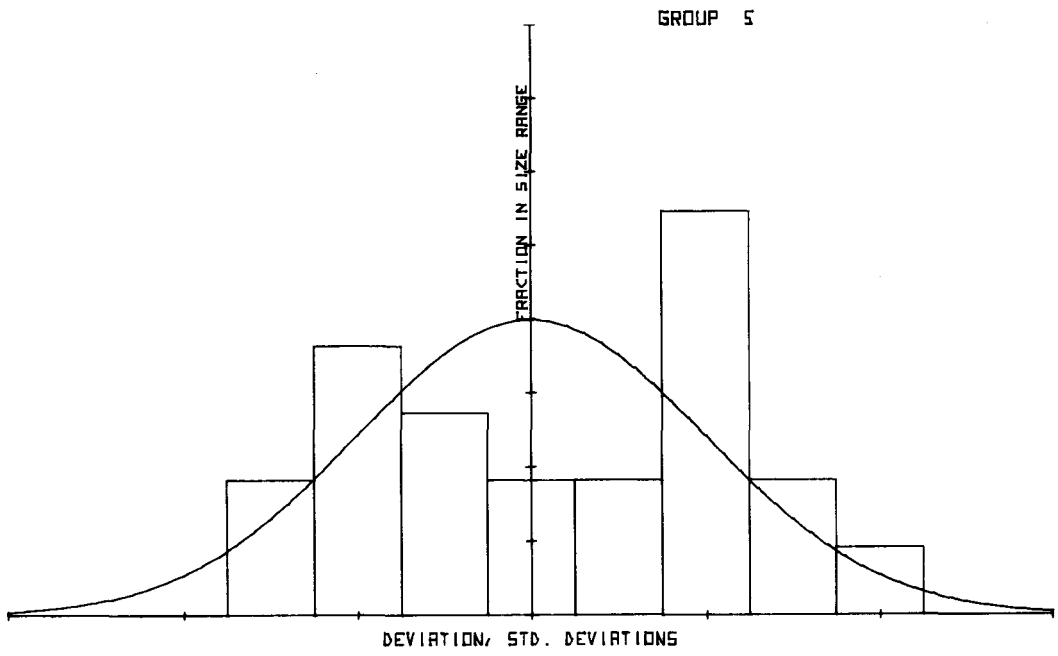

Figure E.13. Static Compact Histogram Distribution for Temperature Group 5

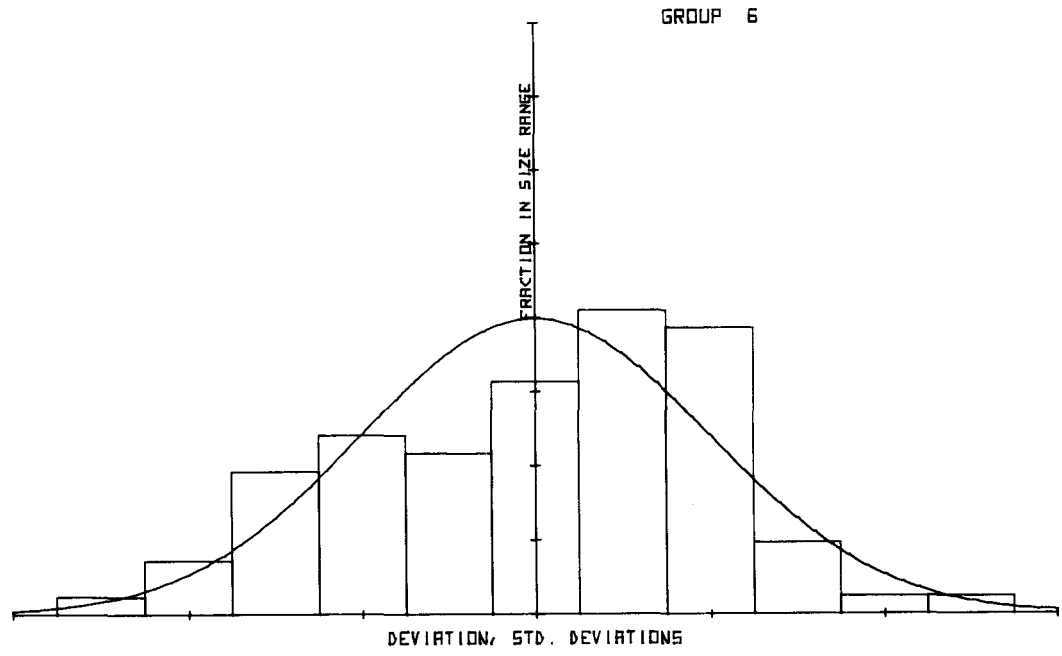

Figure E.14. Static Compact Histogram Distribution for Temperature Group 6

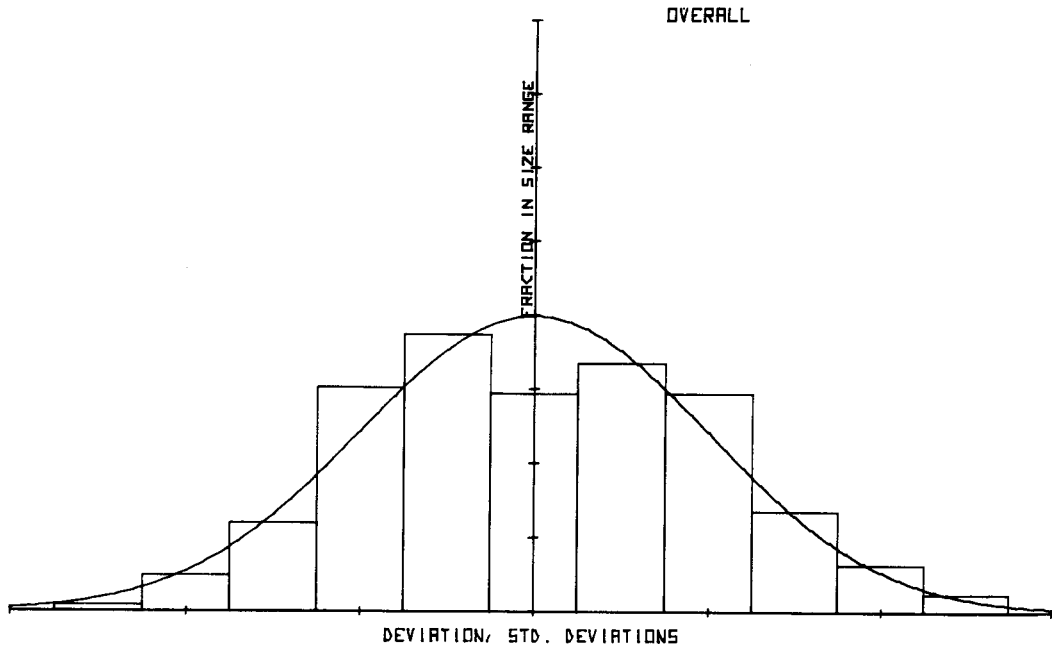

Figure E.15. Static Compact Histogram Distribution for All Temperature Groups

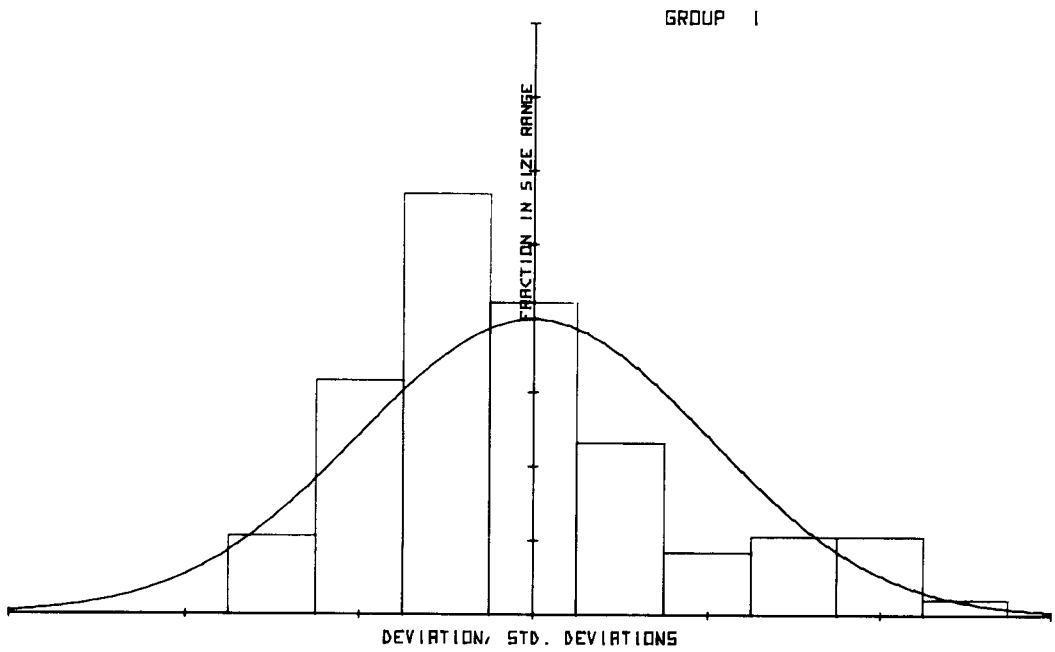

Figure E.16. Dynamic Compact Histogram Distribution for Temperature Group 1

Dynamic Compact Tests

There was only one point lying outside the range $\pm$ (2.5 standard deviations) out of over 200 data points. This result was for group 1, material 6, and lay about 3σ above the curve. (The expectation is that 1-2 results will be beyond the 2.5σ range by chance if the data were Normally distributed.)

The results of the analysis are summarized in Table E.6, and shown in histogram form in Figures E.16-E.22. The statistics shown in Table E.6 were compared to the tabulated values of the a and $\sqrt{b_1}$ functions (Table E.3). The results of the comparison are summarized in Table E.7. The analysis again shows that the Normal distribution is a conservative approach to the prediction of a lower bound, with the possible exception of data near the upper shelf, which tend to have low values. The tendency was slight, and it is not likely to present a major difficulty, as can be seen by examining Figure E.21.

Dynamic Bend Tests

The dynamic bend test (test type 6) was performed by ETI on materials 1 and 3. There were too few data points to permit a detailed analysis as shown by the summary in Table E.8.

Only group 1 for material 1 showed any meaningful statistic. The a statistic shows platykurtosis at the possibly significant (90% confidence) level. While overall, group 1 was skewed high, there was insufficient data to indicate a significant trend (see Figure E.23). The overall data set also appears to have a skew high, as shown by the histogram in Figure E.24.

Table E.6. Dynamic Compact Fracture Toughness Distribution Statistics

MATERIAL 1

GP	A VALUE	ROOT B1	B2	
1	0.6868	1.5222	4.6244	23
2	0.9878	-1.1132	1.9196	9
3	0.8690	-0.7453	1.7449	8
4	0.9436	0.5580	1.4064	6
5	0.8621	-0.0303	1.4795	3

MATERIAL 2

GP	A VALUE	ROOT B1	B2	
1	0.7837	0.9301	2.8185	14
2	0.8829	0.6607	1.8620	4
4	0.8491	-1.3230	1.8048	2
6	0.7789	-0.3237	2.4306	10

MATERIAL 3

GP	A VALUE	ROOT B1	B2	
1	0.9284	0.6281	1.7332	5
2	0.8834	-0.6037	1.7570	4
3	1.0000	1.0000	1.0000	1
4	0.9997	-0.0678	1.0020	2
6	0.7402	-1.4533	3.8524	14

MATERIAL 5

GP	A VALUE	ROOT B1	B2	
1	0.8618	0.7304	2.1067	12
2	0.7572	1.6281	3.0267	4
3	0.9849	-1.0438	1.1163	3
4	1.0000	1.0000	1.0000	1
5	0.9783	0.6034	1.1641	2
6	0.9997	0.0679	1.0021	2

Table E.6. (continued)

MATERIAL 6

GP	A VALUE	ROOT B1	B2	
1	0.6707	2.1369	7.2736	16
2	1.0000	1.0000	1.0000	1
3	1.0000	-1.0000	1.0000	1
4	0.9975	0.2119	1.0200	2
5	0.8314	1.4594	2.2826	3
6	0.8993	-0.7842	1.7625	7

MATERIAL 7

GP	A VALUE	ROOT B1	B2	
1	0.7333	1.3812	4.1823	9
2	0.8833	0.3947	1.8288	6
3	0.9232	-0.0430	1.4266	11
4	0.7510	0.7336	2.5085	5
6	1.0000	-1.0000	1.0000	1

MATERIAL 8

GP	A VALUE	ROOT B1	B2	
1	0.8726	0.1570	1.8822	16
2	1.0000	1.0000	1.0000	1
3	0.7095	1.6383	3.2270	4
4	0.7974	-1.3782	1.9262	2
6	0.8461	-0.2516	1.9863	7

OVERALL

GP	A VALUE	ROOT B1	B2	
1	0.7689	1.1481	3.8306	95
2	0.8753	0.0376	1.9597	29
3	0.8893	-0.1076	1.7110	28
4	0.8852	0.1451	1.6743	20
5	0.8796	0.6868	1.7018	8
6	0.8139	-0.7731	2.6216	41

Table E.7. Dynamic Compact Outlying Trends

Material	Group	Kurtosis	Skewness
1	1	***L	***H
3	6	*L	
6	1	***L	*H
6	1	*L	
7	3	**P	
overall	1	*L	***H
	2	**P	
	3	**P	
	4	**P	
	6		**L

L = leptokurtosis
P = platikurtosis
H = skewed high

* = 90% significance level
** = 95% significance level
*** = 99% significance level

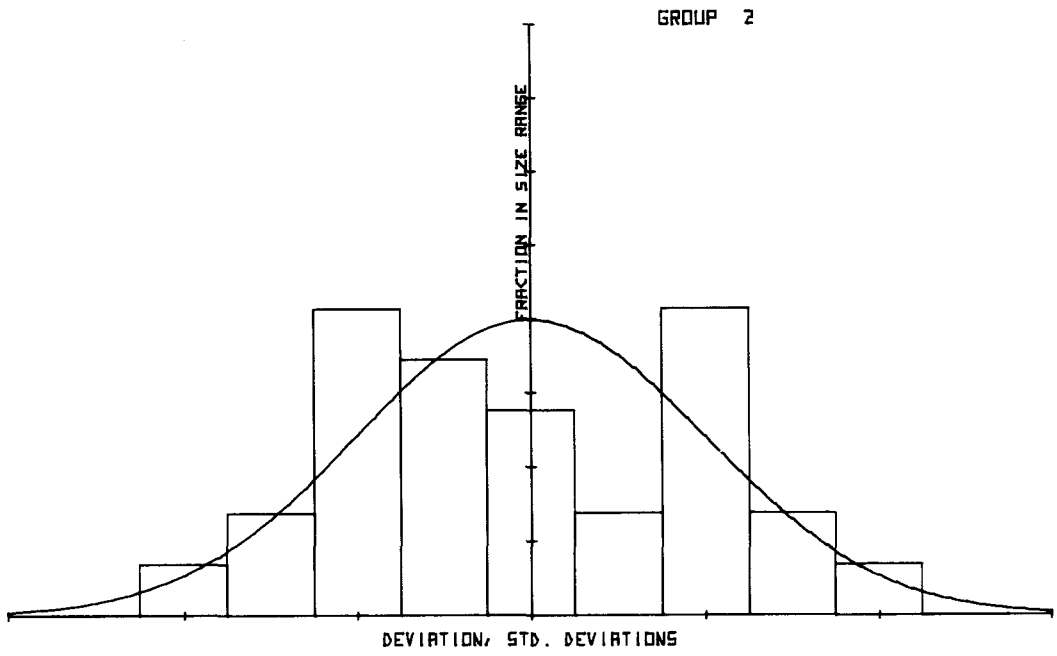

Figures E.17. Dynamic Compact Histogram Distribution for Temperature Group 2

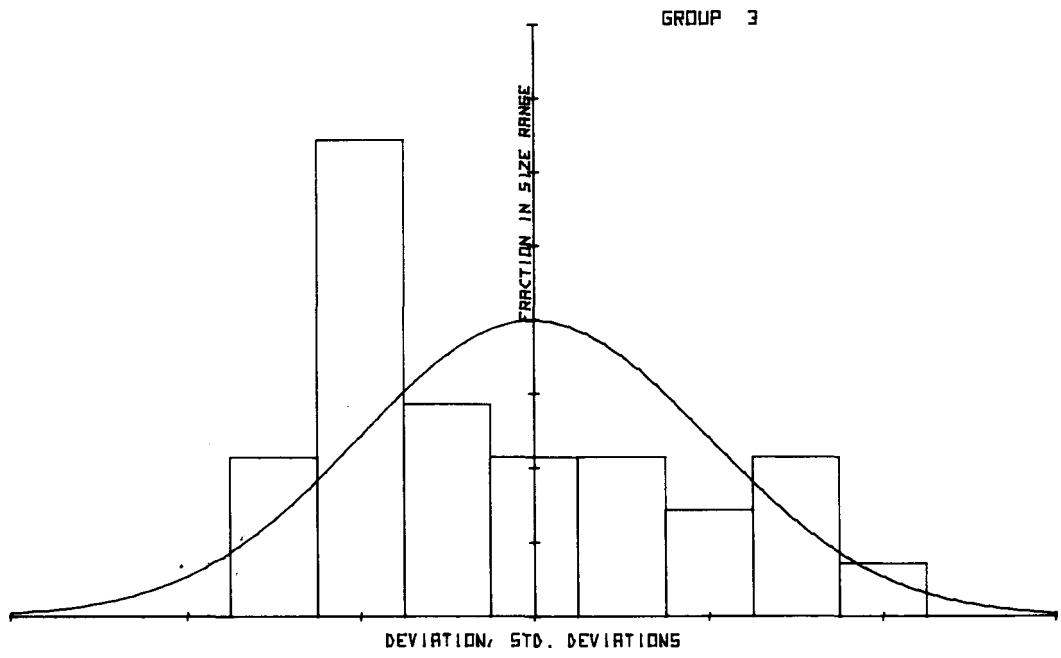

Figure E.18. Dynamic Compact Histogram Distribution for Temperature Group 3

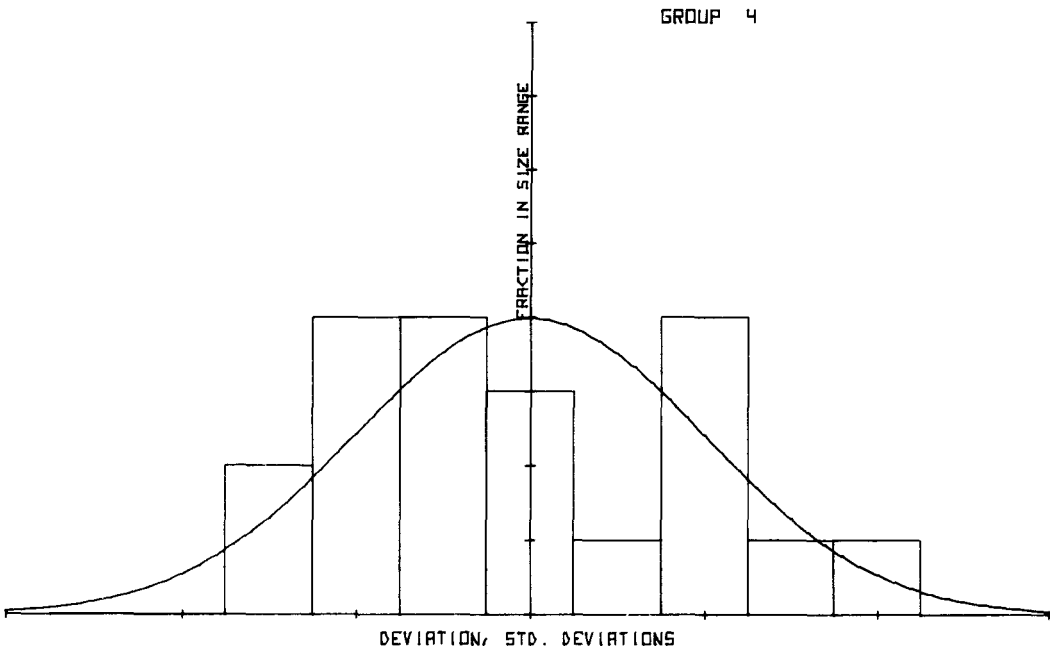

Figure E.19. Dynamic Compact Histogram Distribution for Temperature Group 4

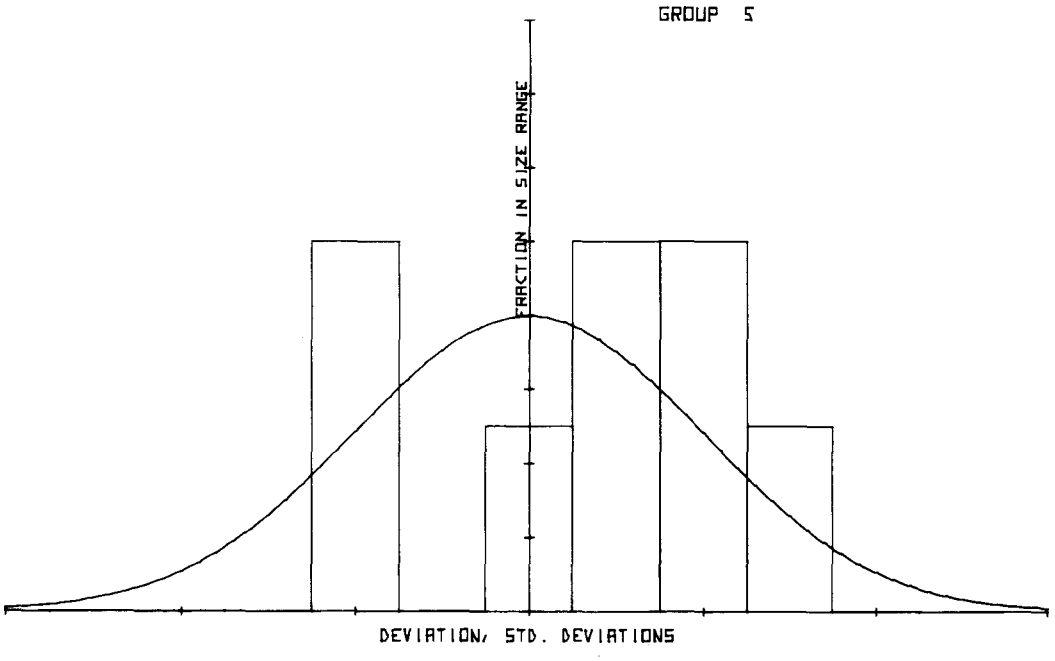

Figure E.20. Dynamic Compact Histogram Distribution for Temperature Group 5

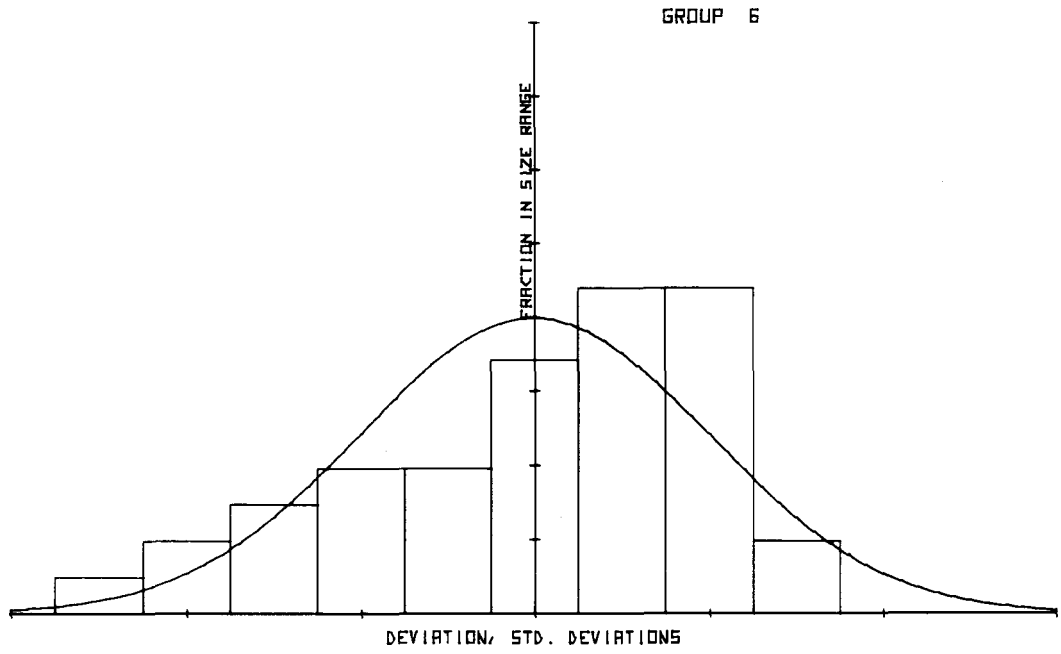

Figure E.21. Dynamic Compact Histogram Distribution for Temperature Group 6

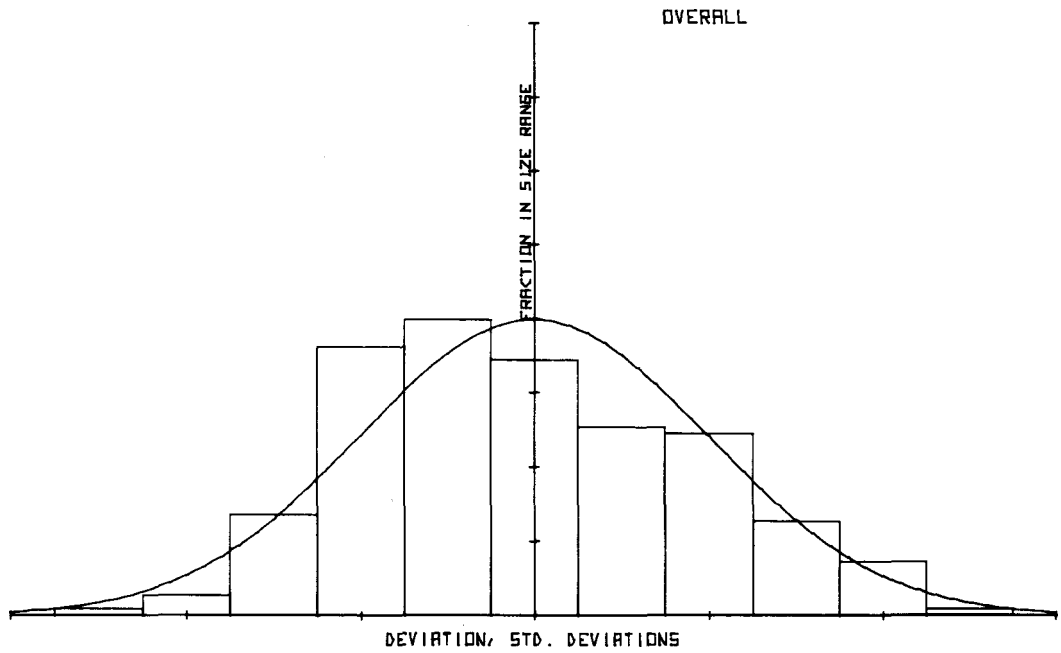

Figure E.22. Dynamic Compact Histogram Distribution for All Temperature Groups

Table E.8. Dynamic Bend Test Fracture Toughness Test Distribution Statistics

MATERIAL 1

GP	A VALUE	ROOT B1	B2	#
1	0.8761	0.4668	1.8093	16
2	0.9295	-1.0614	1.6521	7
3	0.8490	0.8866	2.4024	9
4	0.9819	-0.1909	1.1157	4
5	0.8970	0.3693	1.4847	3
6	0.9025	0.1192	1.6038	5

MATERIAL 5

GP	A VALUE	ROOT B1	B2	#
1	0.8108	0.5688	2.5908	12
2	0.8414	-1.3329	1.8271	2
4	1.0000	-1.0000	1.0000	1
6	0.9168	-0.1996	1.5127	4

OVERALL

GP	A VALUE	ROOT B1	B2	#
1	0.8481	0.5185	2.1442	28
2	0.9099	-1.1217	1.6910	9
3	0.8490	0.8866	2.4024	9
4	0.9855	-0.3527	1.0926	5
5	0.8970	0.3693	1.4847	3
6	0.9089	-0.0225	1.5633	9

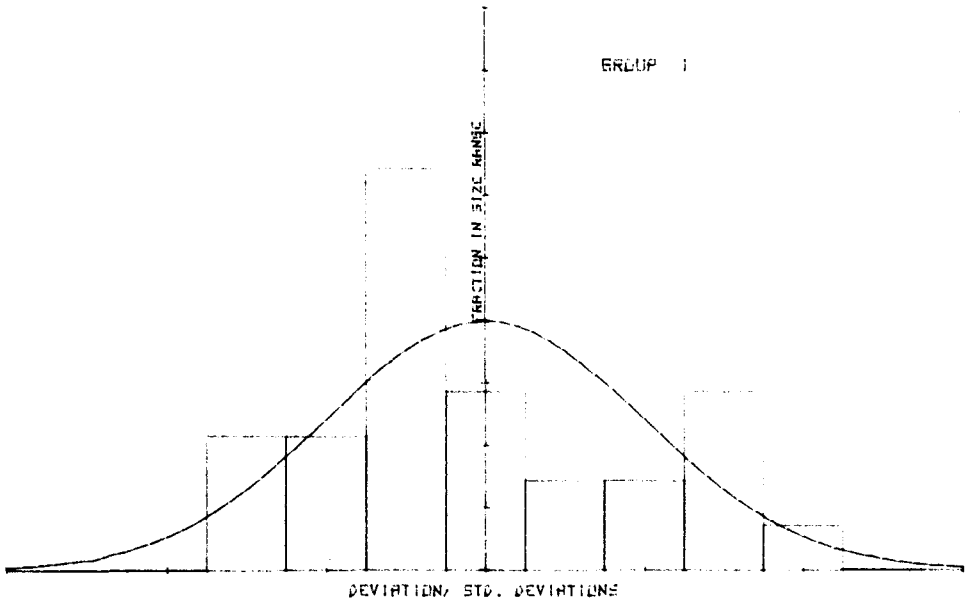

Figure E.23. Dynamic Bend Histogram Distribution for Temperature Group 1

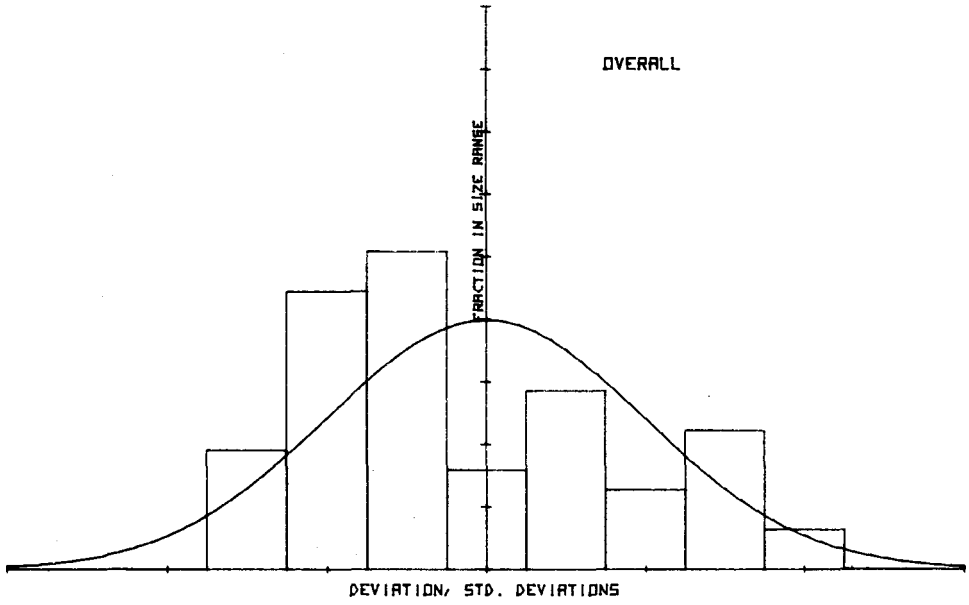

Figure E.24. Dynamic Bend Histogram Distribution for All Temperature Groups

REFERENCES

1e. Pearson, E.S. and H.O. Hartley, Editors, Biometrika Tables for Statistics, Vol. 1, Third Edition, Cambridge University Press, 1970.

This page left intentionally blank for notes